BIOMATERIAL-BASED MODELS OF THE ENDOMETRIUM AND TROPHOBLAST INVASION TO INVESTIGATE EARLY PREGNANCY

BY

SAMANTHA G. ZAMBUTO

DISSERTATION

Submitted in partial fulfillment of the requirements
for the degree of Doctor of Philosophy in Bioengineering
in the Graduate College of the
University of Illinois Urbana-Champaign, 2022

Urbana, Illinois

Doctoral Committee:

Robert W. Schaefer Professor Brendan A.C. Harley, Chair
Associate Professor Kathryn B.H. Clancy
Associate Professor Gregory H. Underhill
Professor Romana A. Nowak

ABSTRACT

Pregnancy is established once an invading blastocyst successfully implants into the lining of the uterus known as the endometrium. Cellular crosstalk between endometrial cells and trophoblast cells from the blastocyst coordinate the extent of invasion into the endometrium and defects in this crosstalk can lead to a spectrum of pregnancy conditions; however, implantation occurs 6-12 days into pregnancy which provides a difficult challenge to studying this process in humans. Initial blastocyst implantation into the endometrium has never been observed in humans and what we currently know is inferred from rare histological specimens. With complex, three-dimensional in vitro model systems, we have the unique opportunity to develop platforms to study this process in systems that replicate the in vivo tissue microenvironment. We demonstrated that methacrylamide-functionalized gelatin (GelMA) hydrogels are adaptable for studying dynamic endometrial processes, including vascular formation, hormone responsiveness, epithelial monolayer formation, and trophoblast invasion. We create and characterize a library of GelMA hydrogels with mechanical properties similar to the native endometrium and placenta, support the culture of an endometrial perivascular niche to study endometrial angiogenesis, provide biochemical cues to hormone-responsive cells (e.g., decidualization of endometrial stromal cells), establish epithelial monolayers overlaying GelMA hydrogels and have employed the GelMA platform for trophoblast invasion assays. These tools allow us to answer the following questions: How does cortisol influence endometrial function? How do biomolecular signals from stress influence trophoblast invasion?

ACKNOWLEDGMENTS

We stand on the shoulders of giants. Completion of this thesis is an amalgamation of not only my work but the work of many others before and after me. I thank and acknowledge everyone I have encountered who grew and nurtured my love of science, women's health, and helping others. I thank the generous individuals who donated their cells and tissues for science so that I could pursue this work.

This thesis is for my son Charles who was my very first "in vivo" pregnancy "experiment." You continue to inspire me each and every day from the moment I knew of your existence to now.

I'd like to thank my best friends who made my days in Chambana so much better by loving and supporting me: Ishita Jain, Alec Tiffany, and Marley Dewey. Thank you to all my other friends I made along the way as well—you know who you are! I'd like to thank my partner Zach for his love and support of me and my career. Thank you to my cat Stewart for all your snuggles.

Finally, I would like to thank my advisor Brendan who has offered me unwavering support with not only my science but also other challenging aspects of my life. You have helped me grow into an independent scientist and I'm so grateful and thankful to have been a part of your lab. Thank you for believing in me and this work.

Research reported was supported by the National Institutes of Diabetes and Digestive and Kidney Diseases of the National Institutes of Health under Award Numbers R01 DK0099528 (B.A.C.H) and R01 DK125471 (G.H.U), the National Cancer Institute of the National Institutes

of Health under Award Number R01 CA256481 (B.A.C.H), the National Institute of Biomedical Imaging and Bioengineering of the National Institutes of Health under Award Numbers T32 EB019944 (**S.G.Z**) and R21 EB018481 (B.A.C.H), and the National Institute of Allergy and Infectious Diseases under Award Number Al1290918 (G.D).

TABLE OF CONTENTS

CHAPTER 1: INTRODUCTION[1]

1.1 Dissertation Overview

The objective of this dissertation is to develop a biomaterial-based model of the endometrium to study aspects of endometrial function and trophoblast invasion. The endometrium is the lining of the uterus and site of blastocyst implantation during pregnancy. Despite the importance of the endometrium in the context of reproduction and female reproductive health, few models of the endometrium exist and those that do lack critical aspects of the complexity of the native endometrial microenvironment. The development of tissue engineering models of the endometrium suggests opportunities to create tunable model systems to probe questions relating to female reproductive health and pregnancy. Such model systems provide a framework to incorporate central elements associated with endometrial function, including recapitulation of tissue biophysical properties, stratification of an epithelium overlaying a perivascular component, and ability to replicate dynamic hormonal properties. Furthermore, such models may also be used in the context of trophoblast invasion in order to understand early pregnancy. Indeed, endometrial model platforms offer the potential to address questions relating to reproduction but also begin to develop a deeper understanding of female reproductive physiology on the cellular level.

Chapter One of this dissertation provides context and motivation for the development of engineering tools for understanding reproductive physiology. Chapter Two introduces engineering techniques for developing endometrial and trophoblast model systems. Chapter

[1] This work will be submitted as a standalone review article.

Three explores the role of extracellular matrix biomolecules on endometrial epithelial cell attachment and cytokeratin 18 expression on methacrylamide-functionalized gelatin hydrogels. Chapter Four determines how endometrial stromal cell decidualization affects aspects of the endometrial perivascular niche, including vessel network complexity, soluble factor secretion, and matrix remodeling. Chapter Five describes the development of three-dimensional trophoblast motility assays and begins to probe how cues from the maternal-fetal interface influence motility. Chapter Six continues development of these motility models and asks how pregnancy-specific glycoproteins impact motility. Chapter Seven provides a conclusion for these works and poses future opportunities.

1.2 Chapter Overview

In this chapter, we describe the current climate of maternal health in the United States and introduce certain factors that impact maternal health, including psychosocial stress. We then describe the endometrium and its role in reproduction, subsequently discussing the role of trophoblast in this process. Next, we describe examples of three-dimensional models of the endometrium.

1.3. Maternal Health in the United States

Although the number of women who die from pregnancy-related complications has decreased from 1990 to 2015, the average annual decline in maternal mortality is only 2.3% (1). Today, global maternal mortality is 216 maternal deaths per 100,000 live births (2). In the U.S., pregnancy-related mortality rates have been steadily increasing (3), with pregnancy-related maternal deaths increasing from 7.2 to as high as 26.4 maternal deaths per 100,000 live births

from 1987 to 2015 (3, 4). The current maternal mortality rate in the U.S. (14 deaths per 100,000 live births) is higher than the average maternal mortality rates in developed countries (12 deaths per 100,000 live births) (1).

1.4. Racial Disparities in Maternal Health

Although the reasons for high maternal mortality in the U.S. are largely unknown, racial disparity in pregnancy is a significant contributor (5-11). In the U.S. from 2006-2010, pregnancy-related deaths were 12.0 deaths per 100,000 live births for white women, 38.9 deaths per 100,000 black women, and 14.2 deaths per 100,000 live births for women of other races (12). The causes of racial disparities in pregnancy transcend socioeconomic status and education level and are largely unknown; however, recent research has suggested that high levels of psychosocial stress, defined as stress relating to interpersonal relations (e.g., discrimination, anxiety, depression), experienced by non-White women may contribute to these disparities (13-20). The effects of stress on pregnancy outcomes may not be possible to study in humans or animals due to the complexity of the stress response; however, models of early implantation will allow us to study how stress affects pregnancy on a cellular level.

1.5 Stress and Reproduction

Glucocorticoids, such as cortisol, are steroid hormones produced in response to stress and are synthesized by the adrenal cortex in response to adrenocorticotropic hormone (ACTH) production from the pituitary gland (21). While ACTH cannot cross the placenta, maternal glucocorticoids, including cortisol, can cross the placenta and cause detrimental effects on the fetus (22). Placental hydroxysteroid 11β dehydrogenase 2 (11β-HSD2) is an enzyme responsible for converting cortisol into its inactive form, cortisone, and protects the fetus from high maternal

cortisol levels (23); however, increased maternal glucocorticoid levels can lead to increased fetal exposure and may alter the activity of 11β-HSD2 (22). Reduced activity of 11β-HSD2 has been implicated in prematurity in preeclampsia (24).

Glucocorticoids have been shown to have a detrimental effect on embryo implantation, pregnancy outcomes, and fetal health (24-30). Glucocorticoids can regulate the hormonal actions of estrogen and progesterone in the uterus by blocking estrogen-mediated uterine growth and differentiation and embryo implantation (23). Previous studies have also demonstrated that there is an association between high cortisol levels and increased miscarriage risk (26), as well as insulin resistance, associated with hypertension and endothelial dysfunction typically seen in preeclampsia (24). Cortisol has previously been shown to reduce endothelial cell tube formation and trophoblast invasion in two-dimensional assays (25, 31, 32); however, much remains unknown regarding the effects of cortisol on early events in pregnancy. Defining how cortisol affects pregnancy may lead to improvements in maternal and fetal outcomes and also offers exciting potential to incorporate a new class of biomolecular signal into tissue engineering models of the endometrium and trophoblast invasion. One goal of this thesis is to develop endometrial models to allow study of the influence of cortisol on trophoblast invasion to better understand how cues pertaining to stress may relate to pregnancy disorders.

1.6 The Endometrium

As the lining of the uterus and site of blastocyst implantation, the endometrium is a dynamic tissue that undergoes rapid cycles of growth and breakdown over the course of the menstrual cycle (33). The endometrium consists of the luminal epithelium supported by an underlying stromal layer containing endometrial glands and vasculature (34). Through coordination by

steroidal sex hormones, both the luminal epithelium and underlying stroma undergo differentiation during the menstrual cycle to prepare for blastocyst implantation and trophoblast invasion (34). Endometrial preparation leading up to the 4-day window of receptivity is critical for successful establishment of pregnancy. A key stage of this process is the differentiation of the endometrial stroma, or decidualization, marked by the transformation of endometrial stromal cells into specialized decidual cells that are both morphologically and functionally distinct from undifferentiated stromal cells (34, 35). This process occurs in the presence of progesterone during the secretory phase of the menstrual cycle and continues if pregnancy occurs (34). Defective decidualization has been shown to result in pregnancy disorders such as the hypertensive pregnancy disorder preeclampsia (36, 37). In addition to stromal differentiation, the endometrial epithelium must also undergo changes to permit blastocyst adhesion and attachment; however, much remains unknown regarding what molecules mediate this process (38). Developing physiologically relevant models of the endometrium that can recapitulate aspects of endometrial receptivity, including stromal and epithelial function, may provide an important experimental platform to examine early-stage complications in pregnancy related to trophoblast invasion.

1.7 Trophoblast Invasion

Implantation failure is estimated to account for 75% of failed pregnancies and may also result in adverse effects over the course of the pregnancy leading to poor outcomes (39). Improved understanding of cellular mechanisms relating to implantation failure in humans is needed; however, studies of embryo implantation are largely intractable. Trophoblast cells that form the outer layer of the blastocyst have numerous roles in pregnancy, including anchoring the placenta,

secreting hormones, modulating decidual angiogenesis, and remodeling the maternal spiral arteries (40). Remodeling of spiral arteries by trophoblast cells, initiated by plugging of spiral arteries and subsequent dilation, is necessary for providing blood flow to the placenta to provide nutrients and oxygen to the developing fetus (40). Insufficient trophoblast invasion of the spiral arteries results in poor vascular remodeling, leading to placental and endothelial cell damage (41). Despite the importance of these early events for the establishment of a successful pregnancy, initial blastocyst adhesion to the endometrial epithelium has never been observed in humans and other integral processes have been observed only from single specimens (42). Understanding critical factors in pregnancy, including what drives trophoblast invasion and endometrial vascular remodeling, has significant value in improving our understanding of human reproduction; therefore, strategies to monitor mechanisms associated with early trophoblast invasion and vascular remodeling in the endometrium are urgently required to understand normal and pathological pregnancy.

1.8 Three-Dimensional Model Systems

Although animal models provide complexity of the in vivo environment, physiological differences in placentation between humans and animals call into question the relevance of such models for studying human pregnancy (43, 44). Another common strategy is to use human cell models (45); however, traditional two-dimensional (2D) cell models do not provide an opportunity to investigate the role of endometrial cell-cell interactions or the role of cell-extracellular matrix interactions in three-dimension (3D). Few studies have investigated trophoblast invasion in 3D and for the studies that did, trophoblast interaction was monitored with maternal vasculature (46) or with the endometrial epithelium and stroma (47-49) but none investigated the roles of the vasculature, epithelium, and stroma together. Microphysiological

models have been recently shown to be a new avenue to investigate mechanistic processes associated with cell and matrix interactions with vascular structures (45, 50-52). Most commonly, these approaches use immortalized endothelial and stromal cell lines, combining them in a biomaterial matrix to facilitate the formation of vascular networks. More recently, some efforts have begun to use tissue-specific cell sources (45, 50-52).

This thesis aims to adapt microphysiological systems to create endometrial-specific hydrogel models. This approach may reveal a powerful capability to study trophoblast invasion in the presence of the endometrial stroma, vasculature, and epithelium in combination. Such tissue engineering methods may allow us to rigorously define the degree of biomaterial complexity required to gain functional insight into processes associated with the influence of biomolecular signals, matrix biophysical cues, and heterotypic cell-cell interaction in trophoblast invasion. Such approaches have the potential to advance studies in female reproductive health, a significantly understudied and underfunded field (53). Future efforts that extend from the development of increasingly complex endometrial models will allow us to study other endometrial processes and diseases, including the menstrual cycle and endometriosis. To do this, we use an adaptable biomaterial platform that allows us to increase complexity by integrating additional signals from the native tissue microenvironment of the endometrium (matrix biophysical properties; inclusion of a hormone-responsive endometrial tri-culture; stress biomolecules). Extending beyond endometrial physiology, this approach may also provide insight into how stress molecules affect angiogenesis and invasion, processes relevant to diseases such as cancer where angiogenesis and invasion of tumor cells impact malignancy and disease progression. Three-dimensional, stratified endometrial models such as these described herein

provide platforms to dissect cell-cell interactions relevant to a wide range of diseases and cellular processes.

CHAPTER 2: A GELATIN HYDROGEL TO STUDY ENDOMETRIAL ANGIOGENESIS AND TROPHOBLAST INVASION[2]

2.1 Chapter Overview

The endometrium is the lining of the uterus and site of blastocyst implantation. Each menstrual cycle, the endometrium cycles through rapid phases of growth, remodeling, and breakdown. Significant vascular remodeling is also driven by trophoblast cells that form the outer layer of the blastocyst. Trophoblast invasion and remodeling enhance blood flow to the embryo ahead of placentation. Understanding mechanisms of endometrial vascular remodeling and trophoblast invasion would provide key insights into endometrial physiology and cellular interactions critical for establishment of pregnancy. The objective for this study was to develop a tissue engineering platform to investigate processes of endometrial angiogenesis and trophoblast invasion in a 3D environment. We report adaptation of a methacrylamide-functionalized gelatin hydrogel that presents matrix stiffness in the range of the native tissue, supports the formation of endometrial endothelial cell networks with human umbilical vein endothelial cells and human endometrial stromal cells as an artificial endometrial perivascular niche and the culture of an endometrial epithelial cell layer, enables culture of a hormone-responsive stromal compartment, and provides the capacity to monitor the kinetics of trophoblast invasion. With these studies, we provide a series of techniques that will instruct researchers in the development of endometrial models of increasing complexity.

[2] This chapter is adapted from the following publication: **Zambuto SG**, Clancy KBH, Harley BAC. A gelatin hydrogel to study endometrial angiogenesis and trophoblast invasion. Interface Focus. 2019;9(5). doi: 10.1098/rsfs.2019.0016.

2.2 Introduction

As the lining of the uterus and site of blastocyst implantation, the endometrium is a dynamic tissue that undergoes rapid cycles of growth and breakdown over the course of the menstrual cycle (33). The endometrium consists of the luminal epithelium supported by an underlying stromal layer containing endometrial glands and vasculature (34). Both the luminal epithelium and underlying stroma undergo differentiation during the menstrual cycle to prepare for blastocyst implantation and trophoblast invasion (34). Endometrial preparation leading up to the window of receptivity is critical for successful establishment of pregnancy. A key stage of this process is the differentiation of the endometrial stroma, or decidualization, marked by the transformation of endometrial stromal cells into specialized decidual cells that are both morphologically and functionally distinct from undifferentiated stromal cells (34, 35). This process occurs in the presence of progesterone during the secretory phase of the menstrual cycle and continues if pregnancy occurs (34).

The endometrium is one of the only adult human tissues where non-pathological angiogenesis occurs regularly to rebuild the vascular bed (54, 55). Further, significant vascular remodeling is driven by trophoblast cells that form the outer layer of the blastocyst in order to enhance blood flow to the embryo ahead of placentation (40, 55, 56). Trophoblast cells play numerous roles during pregnancy, including adhesion of the blastocyst, invasion into the endometrium, anchoring the placenta, secreting hormones, modulating decidual angiogenesis, and remodeling the maternal uterine spiral arteries (40, 42). Mutations in trophoblast function can harm maternal and fetal health. For example, insufficient endometrial vascular remodeling by trophoblast cells is believed to be a risk factor for preeclampsia, a hypertensive pregnancy disorder characterized by high maternal blood pressure and the presence of proteins in urine (41, 57-59). Additionally,

excessive trophoblast invasion can lead to a spectrum of placental disorders, including placenta accreta, a condition in which the placenta attaches too deeply into the uterine wall (42). Despite the importance of these early events for the establishment of a successful pregnancy, initial blastocyst adhesion to the endometrial epithelium has never been observed in humans and other integral processes have been observed only from single specimens (42). Understanding critical factors in pregnancy, including what drives trophoblast invasion and endometrial vascular remodeling, has significant value in improving our understanding of human reproduction. Therefore, strategies to monitor mechanisms associated with early trophoblast invasion and vascular remodeling in the endometrium are required to understand normal and pathological pregnancy.

Few models of the endometrium have the complexity necessary to recapitulate features of the endometrial microenvironment relevant to implantation and trophoblast invasion. These include biophysical properties, ability to monitor dynamic processes such as angiogenic events and trophoblast invasion, inclusion of a structure similar to the native tissue, and selective presentation of hormonal cues. Although animal models provide the complexity of the *in vivo* environment, physiological differences in placentation between humans and animals call into question the relevance of such models for studying human pregnancy (43, 44). For example, rodents lack the deep invasion of trophoblast cells into the endometrium that occurs in humans (43) and blastocyst location in the uterus and the lack of interstitial trophoblast cells differ between humans and non-human primates (44). While more common, traditional two-dimensional (2D) culture models do not provide the flexibility to examine endometrial cell-cell interactions in three-dimensions (3D) as they occur in the body and although 3D models could

facilitate analysis of angiogenesis and trophoblast invasion, few studies to date have investigated trophoblast invasion in 3D. Further, while recent efforts have monitored trophoblast interaction with maternal vasculature (46) or the endometrial epithelium and stroma (47-49), none have developed a platform to examine the roles of the vasculature, epithelium, and stroma together. Biomaterial platforms can facilitate extended culture of cells in defined 3D microenvironments that present biophysical and biochemical properties inspired by the native tissue. Such tools are increasingly being considered to study a variety of processes relevant for endometrial physiology, including angiogenesis and invasion (52, 60-63). Advanced tissue engineering platforms offer the potential to enhance our understanding of core processes that influence endometrial vascular formation and trophoblast invasion through the development of increasingly complex models.

In this project, we seek to develop tissue engineering platforms to explore the relationship between biophysical, biochemical, and cellular signals from the endometrium at the maternal-fetal interface between endometrial cells and trophoblast cells. Design criteria for such a system require integration of: (i) a hydrogel environment containing matrix stiffness relevant to the *in vivo* environment; (ii) the ability to monitor endometrial angiogenesis via culture of an endometrial perivascular niche; (iii) spatial structure similar to the endometrium luminal epithelium; (iv) capacity to vary the temporal presentation of hormonal cues (e.g. estradiol and progesterone); and (v) capability to examine trophoblast invasion in 3D (**Figure 1*a-b***). Here, we describe adaptation of endometrial biomaterial platforms to study endometrial angiogenesis and trophoblast invasion in 3D gelatin hydrogels that incorporate the key features listed above. We validated this model by quantifying endometrial angiogenesis metrics, stromal cell

decidualization status, and trophoblast invasion in gelatin hydrogels as well as analyzing various phenotypic markers pertaining to endometrial cell function. This model will provide critical insight into the cellular mechanisms of endometrial vascular remodeling and trophoblast invasion.

2.3 Materials and Methods

Hydrogel Fabrication and Characterization

Methacrylamide-Functionalized Gelatin (GelMA) Synthesis

GelMA was synthesized as described by Shirahama et al. (64). Briefly, gelatin (Sigma G2500) was dissolved in 10% (w/v) in carbonate buffer (Thermo Fisher 28382) at 50°C. Subsequently, 0.04 mL/g gelatin methacrylic anhydride (Sigma-Aldrich 276685) was added dropwise while stirring. The reaction was allowed to proceed for 1 hour and then was stopped by adding 40 mL/g gelatin of warm DI water. The pH of the reaction was adjusted to pH 6-7. The solution was transferred to dialysis membranes (12,000 - 14,000 molecular weight cutoff, Fisher Scientific 21-152-8), dialyzed for one week against DI water to remove salts and excess methacrylic acid, and subsequently lyophilized. Methacrylate degree of functionalization (DOF) was quantified via ^{1}H NMR as described previously by comparing the ratio of the integrated intensity of the aromatic region (7.24 ppm) to the integrated intensity of the double bond region (5.40 and 5.64 ppm) on MestReNova (Mestrelab Research) and was determined to be approximately 66% (65, 66).

Hydrogel Fabrication

5 wt% and 7 wt% hydrogels were prepared by dissolving lyophilized GelMA in phosphate buffered saline (PBS). After the addition of 0.1% w/v lithium acylphosphinate photoinitiator (LAP PI), prepolymer solution was cast into custom circular Teflon molds (1 mm height, 5 mm

diameter) and photopolymerized for 30 s under UV light (λ=365 nm, 5.69 mW/cm^2, AccuCure Spot System ULM-3-365).

Compression Testing

Elastic modulus was determined by compression testing as described previously (65, 67). Hydrogels were hydrated for 2 hours in PBS at 37°C and then subjected to unconfined compression using an Instron 5943 mechanical tester with a 5N load cell. Hydrogels were compressed with a preload of 0.5 mm/min and an extension rate of 0.1 mm/min until 30% strain was reached. Elastic modulus was determined from the slope of the linear regime (0-10% strain) of the stress-strain curve.

Mass Swelling Ratio

5 wt% and 7 wt% hydrogels were hydrated in PBS at 37°C overnight. Swollen hydrogels were weighed, subsequently lyophilized to determine dry mass, and weighed once more. Mass swelling ratio was determined by calculating the ratio of wet polymer mass to dry polymer mass (68, 69).

Cell Culture

Cell Maintenance

Human umbilical vein endothelial cells (HUVECs, Lonza C2517A, used experimentally before passage 6) were maintained in Endothelial Cell Growth Medium 2 (EGM) (PromoCell C-22211) supplemented with a SupplementPack (Promocell C-39211). Human endometrial stromal cells (HESCs, ATCC® CRL-4003, used experimentally before 6 passages after purchase), normal

primary human endometrial epithelial cells (EECs, LifeLine Cell Technology FC-0078, used experimentally before passage 6), and HTR-8/SVneo trophoblast cells (ATCC® CRL-3271, used experimentally before passage 6 after purchase) were maintained as per the manufacturer's instructions. HUVEC, HESC, and HTR-8/SVneo growth media were supplemented with 1% penicillin/streptomycin (Thermo Fisher 15140122). All cells were cultured in 5% CO_2 incubators at 37°C.

HUVEC-HESC Co-cultures

Endothelial cell networks were formed using previously described techniques by encapsulating HUVECs and HESCs in GelMA hydrogels in 2:1 and 5:1 ratios (HUVEC:HESC) with a total cell encapsulation density of 3 x 10^6 cells/mL (67, 70). Briefly, cells were resuspended in prepolymer solution, pipetted into Teflon molds, and polymerized under UV light. Hydrogels were maintained in 48 well plates for 7 days with daily media changes. Hydrogels were maintained in phenol red-free EGM (PromoCell C-22216) supplemented with a SupplementPack and 1% penicillin/streptomycin. The fetal calf serum was replaced with charcoal-stripped fetal bovine serum (Sigma-Aldrich F6765) to reduce sex steroid hormone concentrations. The vascular endothelial growth factor (VEGF) concentration in this medium was 0.5 ng/mL.

HESC Decidualization

Decidualization was induced by culturing HESCs in the presence of 1 μM medroxyprogesterone acetate (MPA; Sigma-Aldrich M1629) and 0.5 mM 8-Bromoadenosine 3',5'-cyclic monophosphate (8-Br-cAMP; Sigma-Aldrich B5386) in EGM for 6 days (71-75). For assays of decidualization in conventional 2D culture, HESCs were seeded in 6 well tissue culture plates at

an initial seeding density of 36,000 cells/well. For assays of decidualization in 3D hydrogel culture, HESCs were embedded in 5 wt% GelMA hydrogels at a seeding density of 1 x 10^6 cells/mL (approximately 20,000 cells/hydrogel). Decidualization was initiated when HESCs reached confluence for 2D culture and decidualization in hydrogels was initiated 1 day after seeding (n=3 samples for both 2D and 3D assays were imaged and analyzed). Endothelial cell growth medium (EGM) was employed as the base medium for all decidualization experiments as this medium was required for HUVEC-HESC co-culture experiments used to examine endothelial network formation (described above). Medium was replaced every 2 days and was collected for enzyme-linked immunosorbent assays (ELISAs) by centrifuging the media at 1,500 rpm for 10 minutes, aliquoting the supernatant, and storing it at -80°C until use. Human Prolactin DuoSet ELISAs (R&D DY682) and Human IGFBP-1 (insulin-like growth factor binding protein 1) DuoSet ELISAs (R&D DY871) were performed as per the manufacturer's instructions. Samples were tested in duplicate and optical density measurements were taken at 450 nm and 540 nm using a BioTek Synergy HT Plate Reader and Gen5 software (BioTek Instruments, Inc.). Optical density was determined by subtracting the optical density at 540 nm from the optical density at 450 nm, averaging sample duplicates, and subtracting the optical density of the average of duplicate blanks (reagent diluent). OriginPro 2018b (Origin Lab) was used to fit the standard curve to a four parameter logistic curve and optical density data was inputted into the equation to extrapolate sample concentration. Cumulative release of prolactin and IGFBP-1 was calculated by adding the total concentrations from previous time points. Control data are not shown because the prolactin and IGFBP-1 concentrations in these samples fell below the detection limit of the ELISA kits.

Epithelial Monolayer Formation

EECs were grown to confluence, passaged, and seeded at a density of 1, 2, or 4 x 10^5 cells/cm^2 on 5 wt% GelMA hydrogels cast in ibidi µ-Slides Angiogenesis (76). Cells growing on hydrogels were imaged in brightfield daily for 7 days using a Leica DMI 4000 B microscope (Leica Microsystems). Cell medium was replaced daily. For cytokeratin 18 staining, cells were allowed to attach for 6 hours and then hydrogels were washed once with cell growth medium to remove any unattached cells. Cells were fixed 6 hours and 3 days after seeding and stored in PBS until staining and imaging. These time points were chosen so that cytokeratin 18 expression could be evaluated after seeding and half-way through the 7 day experiment before the epithelial layers began to lose stability.

Trophoblast Invasion Assay

A trophoblast invasion assay was developed by embedding individual spheroids into GelMA hydrogels and observing invasion of cells into the surrounding gel matrix (77, 78), adapting methods previously described by our lab to investigate cancer cell invasion (79-81). 2,000, 4,000, 6,000, and 8,000 HTR-8/SVneo cells were seeded into round bottom plates (Corning 4515) for 48 hours in CO_2 incubators to create spheroids. Individual spheroids were pipetted onto prepolymer solution cast into Teflon molds. Prepolymer solution was polymerized under UV light. 8,000 cell spheroids were chosen for subsequent invasion assays due to ease of handling. Hydrogels embedded with spheroids were maintained in cell growth medium for 7 days and imaged daily. Medium was replaced on Day 3.

Imaging Techniques

Immunofluorescent Staining

Immunofluorescent staining was used to visualize endothelial cell networks as described previously (67). Briefly, hydrogels were fixed in formalin (Sigma-Aldrich HT501128) and washed 3 times with PBS. All subsequent steps were performed at room temperature on a shaker unless otherwise noted. Cells were permeabilized for 15 minutes in a 0.5% Tween 20 (Fisher Scientific BP337) solution in PBS, blocked for 1 hour in a 2% bovine serum albumin (Sigma-Aldrich A4503) and 0.1% Tween 20 solution in PBS. Hydrogels were incubated in a 1:100 dilution mouse anti-human CD31 primary antibody (Agilent IS61030-2) overnight at 4°C. Hydrogels were subsequently washed in a 0.1% Tween 20 solution in PBS for 20 minutes 4 times and incubated in a 1:500 dilution of goat anti-mouse secondary antibody (Thermo Fisher A-11001) while protected from light overnight at 4°C. Hydrogels were washed in a 0.1% Tween 20 solution in PBS for 20 minutes 4 times, incubated for 30 minutes with a 1:2000 dilution of Hoechst (Thermo Fisher H3570) in PBS, and washed with the 0.1% Tween 20 solution in PBS. Samples were stored in 0.1% Tween 20 solution in PBS at 4°C until imaged.

Immunofluorescent staining was also used to visualize cytokeratin 18 expression in EECs (76). The protocol described above was used with the exception of shortening wash steps in 0.1% Tween 20 solution in PBS to 5 minutes 3 times since cells were not encapsulated within the gel. Dilutions of antibodies were as follows: 1:250 dilution of rabbit anti-human cytokeratin 18 primary antibody (Abcam ab52948) overnight at 4°C and 1:500 dilution of goat anti-rabbit secondary antibody (Thermo Fisher A-11008) overnight at 4°C. Samples were imaged using a DMi8 Yokogawa W1 spinning disk confocal microscope outfitted with a Hamamatsu EM-CCD

digital camera (Leica Microsystems). A total of three 50 μm z-stacks with a 5 μm step size were taken for each hydrogel. Maximum intensity projections of the images were created in Fiji.

Analysis of Endothelial Network Complexity

Endothelial cell network images were acquired using a DMi8 Yokogawa W1 spinning disk confocal microscope outfitted with a Hamamatsu EM-CCD digital camera (Leica Microsystems). A total of 6 250 μm z-stacks with a 10 μm step size were taken for each hydrogel. As described previously (67), TubeAnalyst (IRB Barcelona), a macro available for Fiji (82), was used to quantify total vessel length, total number of junctions, total number of branches, and average branch length in 3D z-stacks. Total number of junctions and branches and total vessel length were normalized to the image volume. TubeAnalyst results were visualized using Volume Viewer and were compared manually to maximum intensity projections of each image. Regions of the skeleton that corresponded to endothelial cell sheets or image artifacts were removed.

Analysis of Trophoblast Invasion

HTR-8/SVneo spheroids were imaged daily using a Leica DMI 4000 B microscope (Leica Microsystems). To quantify initial spheroid diameter at the day of embedding (day 0), each spheroid was manually traced using Fiji and measured using the measure tool. The perimeter values for each spheroid were measured a total of 3 times and averaged. The spheroids were assumed to be circular and radius and diameter were estimated using the equation for the perimeter of a circle. Initial spheroid area was calculated using the equation for the area of a circle. For total outgrowth area measurements, the area of each outgrowing spheroid was

measured via manual tracing on Fiji (78, 83). 3 area measurements were made for each spheroid and averaged. Fold change was calculated by comparing total spheroid outgrowth area at days 3 and 7 to the initial spheroid area at day 0.

Statistics

Statistical analysis was performed using OriginPro 2018b (Origin Lab). Hydrogel elastic modulus and mass swelling ratio data were analyzed using a two-sample Student's t-test. Endothelial cell network data were analyzed using a two-sample Student's t-test (total vessel length/mm^3 and average branch length) or two-sample Welch's t-test (total number of junctions and branches/mm^3). Decidualization ELISA data and spheroid outgrowth area were analyzed via one-way ANOVA. Outgrowth area fold change was analyzed via a paired t-test. Normality was determined via the Shapiro-Wilkes test. For t-test data, equality of variance was assessed using an F-test. If the sample variances were significantly different, Welch's correction was applied. For ANOVA data, equality of variance was determined via Levene's test. Compression testing experiments had n=18 hydrogels per condition. Mass swelling ratio was determined for n=6 hydrogels of each condition. Analysis of endothelial cell networks was performed for n=3-6 regions imaged per hydrogel for n=3 hydrogels per experimental group. For decidualization experiments, n=3 control and n=3 treated samples were imaged and analyzed via ELISA. For spheroid invasion, n=3-6 hydrogels were measured for diameter measurements. For spheroid area outgrowth, n=6 hydrogels were imaged and measured. Outlier identification and removal was performed only on endothelial cell network data for the 2:1 HUVEC:HESC ratio using Rosner's generalized extreme Studentized deviate test in R, assuming 3 suspected outliers and α=0.05 (84). A total of two outliers were removed from the total number of junctions/mm^3, one

outlier was removed from total number branches/mm^3, and three outliers were removed from total vessel length/mm^3 (**Figure 8**). Significance was set as $p<0.05$. Results are reported as mean ± standard deviation unless otherwise noted.

2.4 Results

GelMA hydrogel biophysical properties and their relevance to the in vivo environment

GelMA hydrogels demonstrated a range of mechanical properties that varied with weight percent. Hydrogel elastic moduli increased significantly ($p=4.77\text{x}10^{-4}$) from 5 wt% (8.97 ± 4.17 kPa) to 7 wt% (15.5 ± 5.83 kPa), respectively (**Figure 2*b***). Hydrogel mass swelling ratios were also significantly different between groups ($p=0.0096$), decreasing from 33.0 ± 10.9 to 17.4 ± 4.9 for 5 and 7 wt% variants, respectively (**Figure 2*c***). 5 wt% hydrogels were used for all subsequent cell studies as its stiffness was in a similar range as the native endometrium (85, 86).

Endometrial angiogenesis via culture of an endometrial perivascular niche

As an artificial endometrial perivascular niche, we created co-cultures of HUVECs with HESCs that formed endothelial cell networks by 7 days. The endothelial cell to stromal cell ratio of cells encapsulated within the GelMA hydrogel influenced the complexity of resultant endothelial cell networks (**Figure 3*a-b***). A 2:1 HUVEC:HESC ratio led to significantly ($p=8.79\text{x}10^{-4}$) increased total number of branches/mm^3 (204 ± 107) compared to a 5:1 HUVEC:HESC ratio (96 ± 42). Further, samples with a 2:1 HUVEC:HESC ratio had significantly ($p=0.00149$) increased total number of junctions/mm^3 (65 ± 35 vs. 30 ± 15) as well as significantly ($p=0.00167$) increased total vessel length/mm^3 (12.39 ± 5.18 mm vs. 7.13 ± 3.55 mm). Average branch length was not significantly different ($p=0.946$) between the 2:1 (0.0735 ± 0.0145 mm) and 5:1 (0.0732 ± 0.0106 mm) groups. These results suggest that the ratio of endothelial to stromal cells affects

endothelial cell network complexity and the ratio can be optimized to better replicate endothelial cell networks in the endometrium.

Endometrial epithelial cells overlaying GelMA hydrogels

The formation of epithelial cell monolayers overlaying GelMA hydrogels was explored as a function of time and cell seeding density. Primary endometrial epithelial cells adhered to GelMA hydrogels by 6 hours after seeding and remained attached to the hydrogel surface for 7 days (**Figure 4a**). Although the cells remained attached to the hydrogel surface for 7 days, the cells began to aggregate toward the edge of the hydrogel over time, most noticeably in the highest initial cell seeding density (4×10^5 cells/cm^2), which suggests that monolayer stability decreases over time in culture. Furthermore, the cells did not form a monolayer at any seeding density and instead formed cellular aggregates non-uniformly over the hydrogel surface. Minimal spreading was observed over time and the cells retained a round morphology. Cytokeratin 18 expression was also examined at 6 hours and 3 days in culture. Cytokeratin 18 is a keratin commonly expressed in epithelial tissues and anchors cytoskeletal structures to the underlying basement membrane (76). At 6 hours and 3 days after seeding, epithelial cells stained positive for cytokeratin 18 (**Figure 4b**), indicating cell anchoring to the hydrogel surface. Cytokeratin 18 staining appeared more prevalently at the perimeter of the cells at 3 days in culture compared to 6 hours after seeding where cytokeratin 18 staining appeared more diffuse. These results demonstrate the feasibility of creating and retaining epithelial cell cultures overlaying GelMA hydrogels and suggest that monolayer formation likely is dependent on a variety of factors, including cell seeding density and time in culture.

Presentation of hormonal cues and the decidual response of endometrial stromal cells

HESC decidualization was monitored in conventional 2D cultures and 3D 5 wt% GelMA hydrogel cultures following exposure to 1 μM MPA and 0.5 mM 8-Br-cAMP. In both conventional 2D and 3D hydrogel cultures, HESCs showed characteristic rounded morphologies by 2 days that persisted for 6 days of hormonal stimulation (**Figure 5*a***). In addition, the cumulative secretion of two decidual proteins, prolactin and IGFBP-1, increased significantly (p<0.05) over the course of 6 days of hormonal stimulation (**Figure 5*b***) as indicated by one-way ANOVA analysis of ELISA data (Prolactin 2D: $F(2,6)=389.9$, $p=4.45\text{x}10^{-7}$); Prolactin 3D: $F(2,6)=10.3$, $p=0.011$; IGFBP-1 2D: $F(2,6)=88.6$; $p=3.51\text{x}10^{-5}$); IGFBP-1 3D: $F(2,6)=75.9$, $p=5.49\text{x}10^{-5}$). Tukey post hoc comparisons indicated that prolactin cumulative secretion in 2D cultures significantly (p<0.05) differed between days 2 and 4 ($p=4.66\text{x}10^{-4}$), days 2 and 6 ($p=3.60\text{x}10^{-7}$), and days 4 and 6 ($p=3.26\text{x}10^{-6}$). In 3D hydrogel cultures, prolactin cumulative secretion increased significantly (p<0.05) between days 2 and 6 (p=0.00963), but not between days 2 and 4 and 4 and 6. In 2D cultures, IGFBP-1 cumulative secretion significantly (p<0.05) differed between days 2 and 4 (p=0.0029), days 2 and 6 ($p=2.80\text{x}10^{-5}$), and days 4 and 6 ($p=7.02\text{x}10^{-4}$). In 3D hydrogel cultures, IGFBP-1 cumulative secretion significantly (p<0.05) differed between days 2 and 4 ($p=7.14\text{x}10^{-4}$), days 2 and 6 ($p=4.52\text{x}10^{-5}$), and days 4 and 6 (p=0.0077). Unstimulated HESCs retained their elongated morphology over the course of 6 days in culture and did not express prolactin and IGFBP-1 proteins above the detection limits of the ELISA assays used to quantify secretion. Interestingly, prolactin secretion in cell culture medium measured at each timepoint increased over time in both 2D and 3D cultures. However, while IGFBP-1 secretion increased at each timepoint in 2D cultures, secretion levels decreased over time for 3D hydrogels cultures despite the overall increase in cumulative secretion. HESCs

maintained good viability over the course of the study, as indicated by live/dead staining, and no obvious differences were observed in viability for HESCs cultured in HESC growth medium or EGM (**Figure 7**). Taken together, these results demonstrate that decidualization of endometrial stromal cells can be induced via hormonal stimulation in 3D cultures in a manner consistent with the established 2D decidualization assays (71-75).

Examination of trophoblast invasion in GelMA hydrogels

A library of HTR-8/SVneo spheroids containing 2,000, 4,000, 6,000, or 8,000 cells/spheroid displayed spheroid diameters that increased with cell density (**Table 1**). 8,000 cell spheroids were selected for invasion assays in 5 wt% GelMA hydrogels due to ease of manipulability and imaging. Trophoblast invasion into the surrounding hydrogel matrix was monitored for up to 7 days *in vitro* via serial imaging. A one-way ANOVA indicated that total outgrowth area increased significantly ($p<0.05$) over time ($F(2,15)=33.7$, $p=2.81\text{x}10^{-6}$) (**Figure 6*b***). Tukey post hoc comparisons indicated that mean outgrowth area increased significantly ($p=2.88\text{x}10^{-6}$, day 0-7; $p=7.48\text{x}10^{-5}$, day 3-7) from day 0 (0.0834 ± 0.00682 mm^2) or day 3 (0.353 ± 0.165 mm^2) to day 7 (1.18 ± 0.385 mm^2). No significant difference in outgrowth was observed between days 0 and 3. Fold change in outgrowth area was subsequently calculated by comparing outgrowth areas on days 3 and 7 to initial spheroid area (Day 0, **Figure 6*c***). Fold change in outgrowth area differed significantly ($p=6.46\text{x}10^{-4}$) from day 3 (3.33 ± 2.23) to day 7 (13.4 ± 5.26). These results demonstrate the feasibility of monitoring trophoblast invasion in GelMA hydrogels over time.

2.5 Discussion

The objective of this study was to develop a hydrogel platform to support future mechanistic investigations of endometrial angiogenesis and trophoblast invasion. We have described a gelatin hydrogel model system that provides: (i) mechanical properties similar to native tissue; (ii) a platform to monitor endometrial angiogenesis; (iii) support of the culture of an epithelial layer; (iv) capability to selectively induce endometrial stromal cell decidualization via hormonal cues; and (v) ability to perform quantitative trophoblast invasion assays. Such a platform is critical for enhancing our understanding of endometrial processes and trophoblast invasion metrics.

GelMA is an attractive material for the study of endometrial angiogenesis and trophoblast invasion for multiple reasons. Gelatin is denatured collagen that retains Arg-Gly-Asp (RGD) cell binding motifs and matrix metalloproteinase (MMP)-sensitive degradation sites that ultimately allow for cell attachment and matrix remodeling (65, 69, 87, 88). The addition of methacrylamide groups allows gelatin to be UV-light polymerized and hence, stable at 37ºC and relatively homogeneous in terms of structure and composition (65, 69, 87, 88). Further, the biophysical properties of GelMA can be tuned to more closely mimic the properties of native tissue. In the body, the endometrium has a stiffness ranging from 5 to 12 kPa (85, 86). These biophysical properties informed our creation of a library of gelatin hydrogels for our model. The library we created for these studies had compressive moduli that fell within this stiffness range. We further characterized our library of hydrogels by quantifying the mass swelling ratio, an indication of the degree of crosslinking in the hydrogel (68, 88). Mass swelling ratio decreased with hydrogel polymer weight percent, indicating that crosslinking density increased with polymer weight percent, consistent with results from other studies (68, 69, 88).

The endometrium undergoes dynamic tissue changes over the course of the menstrual cycle and during pregnancy, including vascular remodeling and angiogenesis (34, 54-56, 89). The ability to study dynamic processes of endometrial angiogenesis would provide insight into endometrial function and vascular remodeling. Our lab (67, 70), along with other labs (90, 91), has successfully created endothelial cell networks in gelatin hydrogels by co-culturing endothelial cells with stromal cells. Here, as an artificial endometrial perivascular niche, HUVECs and HESCs were encapsulated in 5 wt% GelMA hydrogels. Encapsulating endothelial and stromal cells in gelatin hydrogels resulted in vessel-like endothelial cell network formation in 3D. The native endometrium contains a vessel length per branch point ranging from approximately 100 - 200 μm over the course of the menstrual cycle (34, 54, 92). We report endothelial networks formed within the hydrogel that had average branch lengths of approximately 70 μm. While values reported here are similar to physiological levels, future efforts will exploit technologies we have previously reported to incorporate covalently-immobilized VEGF into the GelMA hydrogel to alter the complexity of perivascular networks to study of brain cancer cell invasion (67). Such techniques, as well as other methods to generate GelMA hydrogels containing spatial-gradients in immobilized biomolecules (93), may provide the ability to further optimize or spatially manipulate average branch length within the range of 100 and 200 μm. Additionally, this adaptable platform offers the opportunity to demonstrate an endometrial perivascular niche with increasing complexity as we further define the endometrial tissue microenvironment *in vitro*. Although the perivascular niche has been defined in the context of tumor microenvironments and stem cell niches (94-96), there exists an opportunity to define the perivascular niche in the context of the endometrium. Endometrial stem/progenitor cells have

been considered to be a part of the endometrial perivascular niche (97-101). However, no studies to date have attempted to define the microenvironment of the endometrial perivascular niche in the context of other relevant cell types known to interact with endometrial vasculature, including endometrial stromal cells and trophoblasts. In this paper, we explored using HUVECs and HESCs in co-culture as a model of the endometrial perivascular niche.

Blastocyst adhesion onto and invasion into the endometrium have never been observed in humans thus, our knowledge of these early stages of implantation come from rare, histological specimens (34). The establishment of an epithelial monolayer overlaying an endometrial perivascular niche would provide a tool important for studying trophoblast attachment and invasion. A benefit to the GelMA system described in this study is that gelatin natively presents cell binding motifs in its backbone, enabling us to add cells directly to the material without having to incorporate additional cell adhesion peptides (76). We observed that primary endometrial epithelial cells seeded onto GelMA hydrogels adhered to the hydrogel surface by 6 hours and remained adhered for 7 days. We observed fast (6 hour) attachment of cells to hydrogels which resulted in the formation of cell clusters stacked on top of each other. The cells remained attached for 7 days in culture; however, the stability of the epithelial cultures decreased over time as indicated by cellular aggregation toward the edge of the hydrogels. Epithelial cells stained positive for cytokeratin 18 after seeding and after 3 days in culture, indicating that they were anchored to the hydrogel surface. Over time we expected to observe epithelial cell spreading along the surface of the hydrogel as well as the formation of a monolayer; however, we observed only minimal spreading of cells along the surface and most cells retained a round morphology for 7 days in culture. Previous studies have indicated that the crosslinking density,

basement membrane deposition, and donor-to-donor heterogeneity affect the ability of epithelial cells to form functional monolayers on gels (76). Higher crosslinking of the gel matrix may inhibit cells from accessing RGD cell binding motifs and MMP-sensitive degradation sites which may affect their ability to move along the gel surface (76). Future studies should consider how specific features (e.g. degree of functionalization, polymer weight percent, swelling ratio) of the biomaterial affect the ability of epithelial cells to form functional monolayers. Furthermore, the addition of a basement membrane layer onto the hydrogel may increase the uniformity of cell seeding along the hydrogel surface. The basement membrane of the endometrium includes extracellular matrix components such as laminin, type IV collagen, fibronectin, and heparan sulfate proteoglycans (76, 102-104). The addition of these matrix components onto the gel surface may facilitate epithelial cell surface adhesion and promote cellular deposition of additional basement membrane (76). Finally, Cook et al. report differences in epithelial monolayer formation from donor-derived epithelial cells (76). The cell seeding density required for epithelial monolayer formation varied donor-to-donor and lower densities (1.5×10^5 cells/cm^2) were ineffective at forming monolayers and resulted in incomplete coverage of the hydrogel surface (76). In this paper, we observed incomplete coverage of our hydrogel surface at lower cell seeding densities ($1 – 2 \times 10^5$ cells/cm^2) and some sparsely covered regions at a high cell seeding density (4×10^5 cells/cm^2) as well. This suggests that the cell seeding density necessary for monolayer formation must be optimized for this donor and might require an even higher initial cell seeding density. Future in-depth characterization of epithelial monolayers include immunostaining for characteristic markers of epithelial sheets, including E-cadherin, and detailed studies of monolayer functionality, including transepithelial electrical resistance measurements (76, 105, 106).

Models of trophoblast invasion will require an endometrial model that recapitulates the endometrial microenvironment during the window of receptivity. Endometrial stromal cell decidualization, modulated by steroidal sex hormones and cyclic AMP, must occur for human embryo implantation (34, 35). Decidualized endometrial stromal cells show a characteristic morphological rounding as well as a characteristic increase in prolactin and IGFBP-1 secretion (34, 35). We demonstrated that the GelMA hydrogel is capable of supporting endometrial stromal cell differentiation for at least 6 days in response to hormonal cues of 1 μM MPA and 0.5 mM 8-Br-cAMP. This decidualization protocol has been used extensively in literature primarily for 2D cultures (71-73, 76), though some success has been reported inducing stromal differentiation with hormonal cues in 3D environments formed from thermally gelled collagen or crosslinked polyethylene glycol macromers (49, 71, 76, 107, 108). In our study, stromal cells encapsulated in GelMA hydrogels maintained a decidual phenotype for 6 days in culture, as indicated by their rounded morphology as well as increased secretion of characteristic decidual markers prolactin and IGFBP-1. Further characterization and establishment of hormone responsive hydrogel endometrial models would provide critical insights into endometrial function over the course of the entire menstrual cycle.

Monitoring early processes of trophoblast invasion in pregnancy is essential for understanding what drives successful embryo implantation and pregnancy pathologies associated with mutations in implantation. Although trophoblast invasion and endometrial remodeling are critical for the establishment of a successful pregnancy, much is still unknown regarding what drives trophoblast invasion (40, 109). Our goal was to demonstrate a 3D trophoblast invasion assay

developed using a GelMA hydrogel platform. As existing models of invasion in 2D lack the complexity necessary to provide insights into cellular crosstalk and interactions in native 3D environments, 3D models of trophoblast invasion are becoming increasingly a focus for development (47-49, 110, 111). Here, we seeded 8,000 HTR-8/SVneo cell spheroids into GelMA hydrogels and quantified their invasiveness over the course of 7 days. HTR-8/SVneo cells invaded the GelMA hydrogel matrix over the course of 7 days of culture without exogenous stimulation from various biochemical cues. Studies of this nature provide insight into trophoblast invasion in 3D and allow us to develop invasion assays of increased complexity. We will incorporate promotors (e.g. human chorionic gonadotrophin) and inhibitors (e.g. the transforming growth factor β family) into the cultures and quantify changes in invasion distance in future studies (112-115). We also intend to explore trophoblast invasion as a function of endometrial stromal cell decidualization status and the presence of an endometrial epithelium. We expect that trophoblast adhesion to the epithelium and invasion into the underlying stroma requires hormonal preparation. The proposed model has the potential to investigate processes of trophoblast invasion as it relates to hormonal activation of endometrial cells. A limitation of this first-generation model is the exclusion of the endometrial epithelium and perivascular niche in trophoblast invasion assays. For future work, we intend to incorporate these key features into a 3D invasion platform to determine how each of these factors alone and in combination affect trophoblast adhesion and invasion. Additionally, with continued development of advanced image processing techniques to quantify invasive phenotype of cell cohorts in three-dimensions (116-118), we expect future efforts will be able to parse full three-dimensional invasion metrics.

Finally, the efforts reported here used established cell lines, with the exception of the primary endometrial epithelial cells derived from healthy female donors and HUVECs. The use of cell lines for the establishment of this model reduced the cost of the cell sources and provided reproducibility in our studies. Although cell lines provide reproducibility and insight into biological function, primary cells derived from donors would provide the most accurate depiction of endometrial function. HUVECs were used as an endothelial cell source because HUVECs are one of the most widely used cell sources for microphysiological angiogenesis models (119-121). Interestingly, when using HUVECs in co-culture with endometrial stromal cells we observed less endothelial network formation compared to studies using HUVECs in co-culture with stromal cells derived from other tissues, such as normal lung fibroblasts (67). This suggests that cellular crosstalk between HUVECs and HESCs might affect endothelial network complexity. Other labs have demonstrated that although a stromal component featuring stromal cells or other support cells (pericytes, astrocytes, etc.) is necessary for the establishment of stable endothelial networks, specific stromal features, including their tissue source, expression of soluble factors, and mechanical activity, can inhibit or promote vascularization (122-124). While increasing local presentation of VEGF within the GelMA hydrogel could increase the extent of the endothelial cell network formation, there is also potential to utilize endometrial-specific endothelial cells to create a tissue-specific model of endometrial angiogenesis and alter stromal cell decidualization status to determine the effects of stromal differentiation on endothelial network complexity.

2.6 Conclusions

We report a gelatin hydrogel platform that replicates features of the endometrial microenvironment in GelMA hydrogels. Studies of this nature provide insight into endometrial function and will enable us to study other relevant diseases and processes that occur in the endometrium and during pregnancy. Such tissue engineering methods allow us to rigorously define the degree of biomaterial complexity required to gain functional insight into processes associated with the influence of biomolecular signals, matrix biophysical cues, and heterotypic cell-cell interaction in endometrial physiology and trophoblast invasion. The 3D endometrial platform described here poses the ability to alter endometrial-relevant features, notably: (i) matrix stiffness, (ii) endometrial angiogenesis, (iii) hormonal stimulation of endometrial stromal cells (e.g. decidualization), (iv) epithelial cell culture overlaying hydrogels, and (v) trophoblast invasion through a matrix. With these studies, we provide a series of techniques to facilitate future development of endometrial models of increasing complexity. Development of such endometrial models will be transformative for studies pertaining to reproductive health.

2.7 Table

Table 1. Average HTR-8/SVneo spheroid diameter.

Spheroid Density	Mean Diameter (μm)	Standard Deviation (μm)	n
2,000	231.8	20.0	3
4,000	278.6	10.7	3
6,000	305.2	15.8	3
8,000	325.6	13.2	6

2.8 Figures

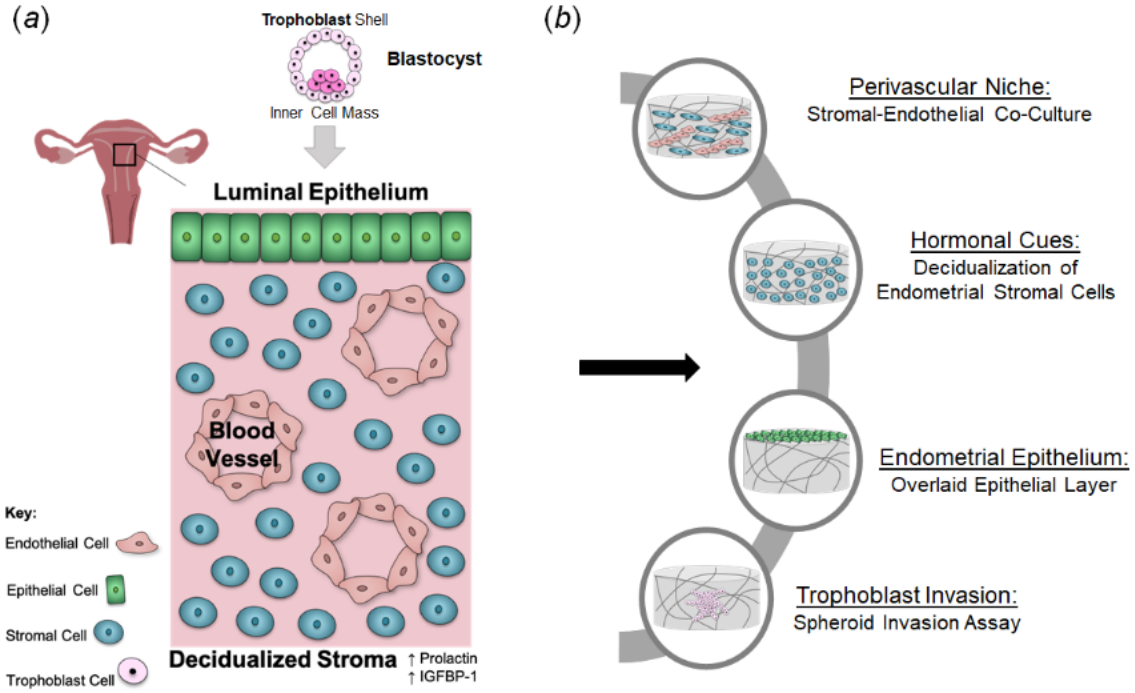

Figure 1. Development of a gelatin hydrogel model to recapitulate elements of the endometrial microenvironment to investigate trophoblast invasion. (*a*) *In vivo* endometrial microenvironment. (*b*) Key features to be incorporated into a gelatin hydrogel platform: endometrial perivascular niche, endometrial epithelium, hormonal stimulation, and trophoblast invasion.

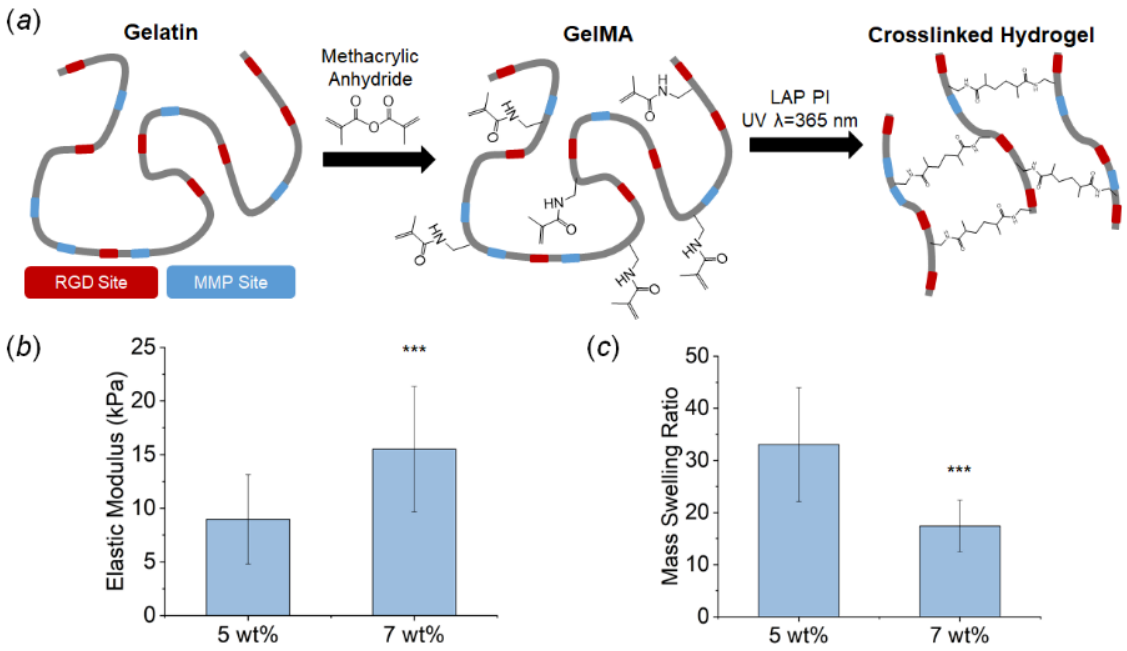

Figure 2. Mechanical and swelling properties of GelMA hydrogels. (*a*) Schematic of gelatin macromer, GelMA synthesis, and hydrogel formation. (*b*) Elastic moduli of 5 wt% and 7 wt% GelMA hydrogels (n=18). (*c*) Mass swelling ratio of 5 wt% and 7 wt% hydrogels (n=6). Data presented as mean ± standard deviation. ***: significant compared to 5 wt% (p<0.001). LAP PI: Lithium acylphosphinate photoinitiator.

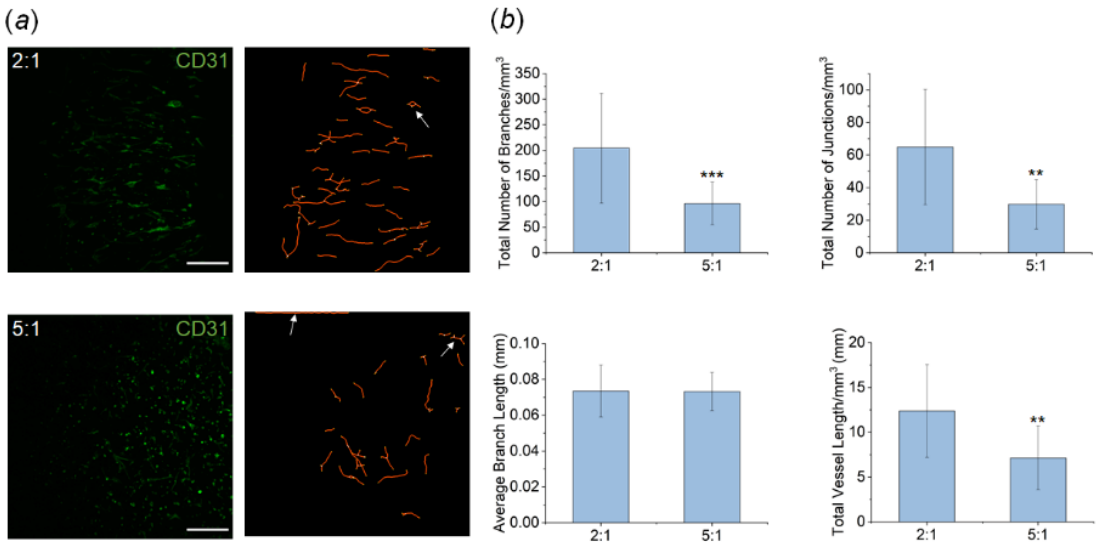

Figure 3. (*a*) Representative maximum intensity projection images of endothelial cell networks (green, CD31+) and corresponding skeletonized images of networks (red) in hydrogels with 2:1 and 5:1 HUVEC:HESC cell seeding ratios after 7 days in culture. Images were artificially brightened for this figure to better display cells but not for analysis of network architecture. White arrows: image artifacts or endothelial sheets removed from analysis. Scale bar: 250 μm. (*b*) Endothelial cell network metrics: total number of branches/mm^3, total number of junctions/mm^3, average branch length (mm), and total vessel length/mm^3. These metrics were calculated from original z-stack images of 6 regions of interest per hydrogel (n=3). Data presented as mean ± standard deviation. **: significant compared to 2:1 group (p<0.01). ***: significant compared to 2:1 group (p<0.001).

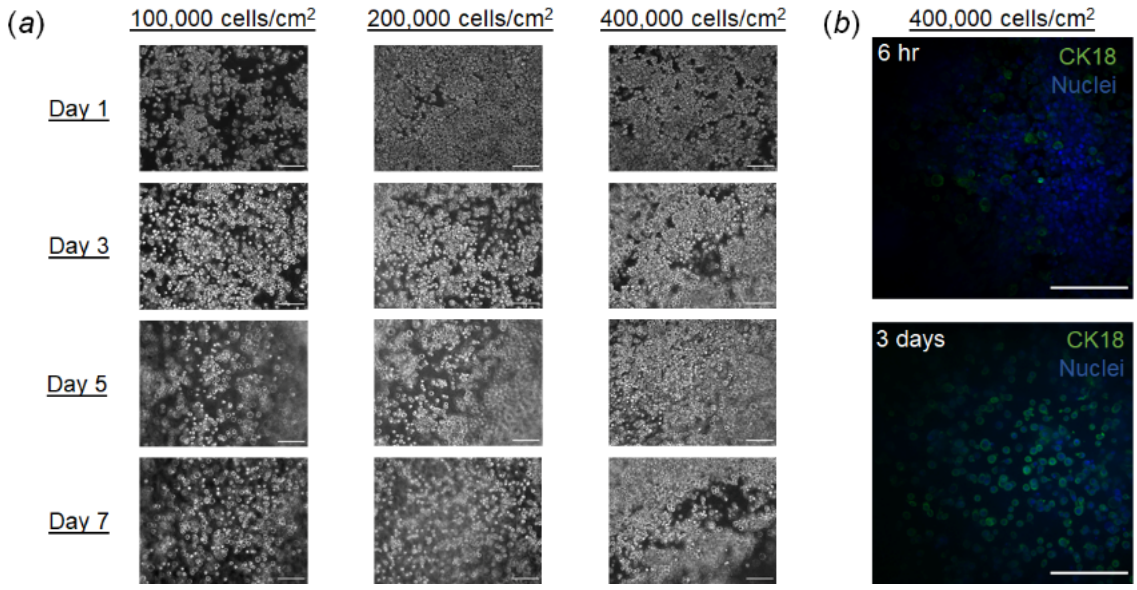

Figure 4. Primary endometrial epithelial cells seeded onto 5 wt% gelatin hydrogels cast in ibidi µ-Slides Angiogenesis. Cells were seeded onto hydrogels at an initial seeding density of 1, 2, or 4 x 10^5 cells/cm^2. (*a*) Representative bright field image of epithelial cells at days 1, 3, 5, and 7 in culture. (*b*) Representative maximum intensity projection images of epithelial cells stained with cytokeratin 18 (CK18) and Hoechst (nuclei) 6 hours and 3 days after seeding. Scale bars: 200 µm.

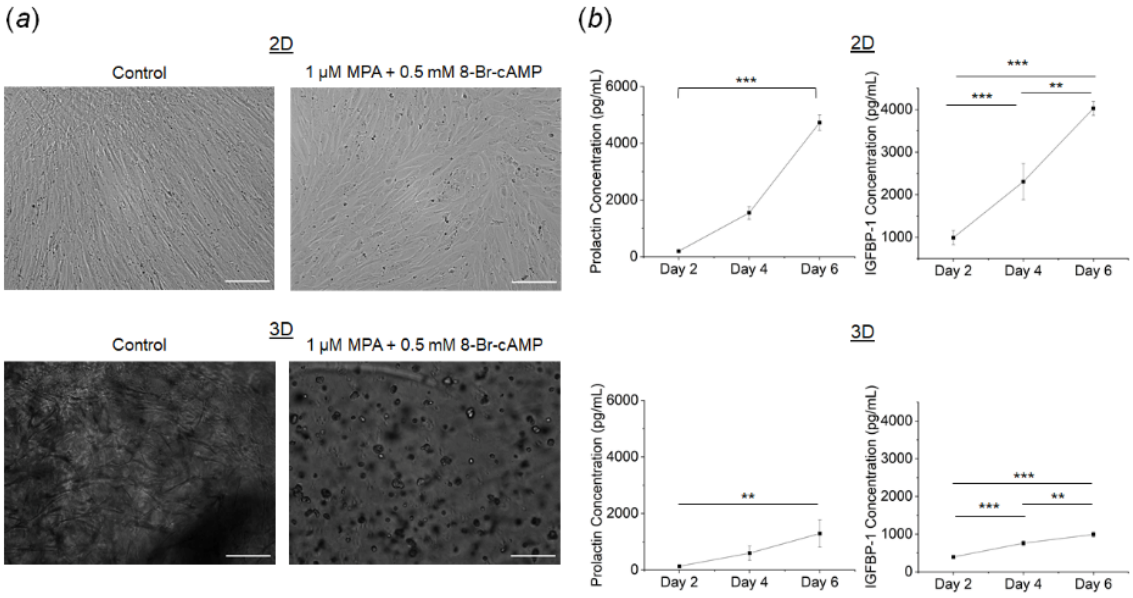

Figure 5. Endometrial stromal cell differentiation induced in 2D monolayers or for cells encapsulated in 5 wt% GelMA hydrogels via addition of 1 μM medroxyprogesterone acetate (MPA) and 0.5 mM 8-Bromo-cAMP at day 0. Medium was collected and replaced every two days for ELISA analysis. (*a*) Representative bright field images of control and treated cells in 2D or 3D hydrogel conditions at day 6 of exposure to decidualization factors. Scale bars: 200 μm. (*b*) Cumulative prolactin and IGFBP-1 concentrations for 2D and 3D cultures over 6 days. Data presented as mean ± standard deviation, n=3. **: significant (p<0.01); ***: significant (p<0.001).

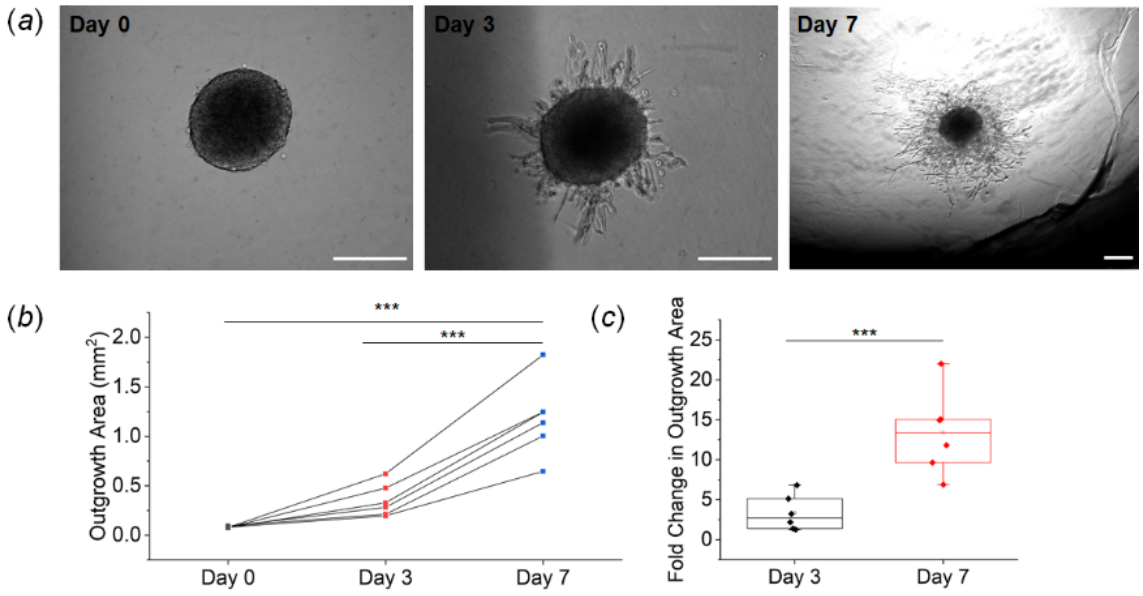

Figure 6. Kinetics of trophoblast invasion within a 5 wt% GelMA hydrogel. (*a*) Representative brightfield images of HTR-8/SVneo trophoblast spheroid invasion at days 0, 3, and 7. Scale bars: 250 µm. (*b*) Average outgrowth area of 8,000 HTR-8/SVneo cell spheroids at day 0, day 3, and day 7. Data presented as individual data points traced over time. (*c*) Fold change in spheroid outgrowth area at days 3 and 7. Data presented as individual data points traced over time, n=6. ***: significant (p<0.001).

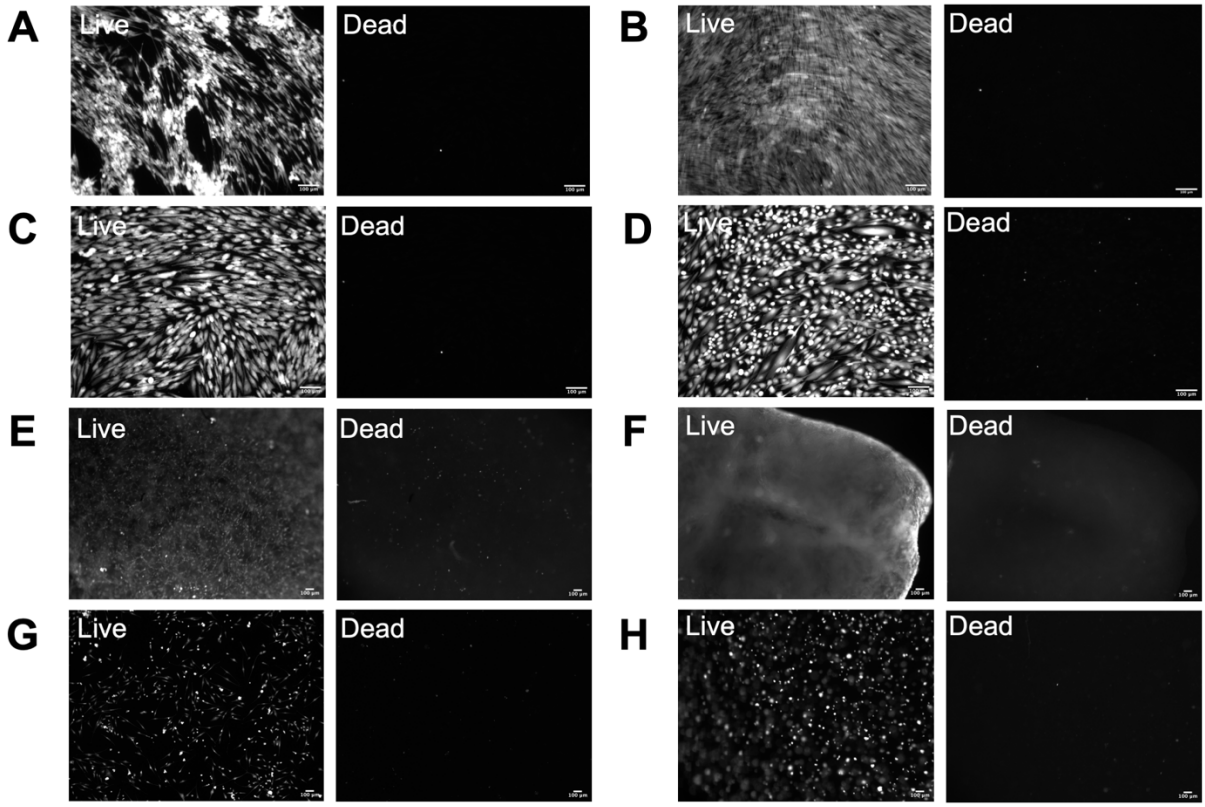

Figure 7. Representative live and dead images for 2D and 3D control and decidualized HESCs at day 6. HESCs were cultured in growth medium (HESC medium) or co-culture medium (EGM). (*a*-*d*) 2D samples on tissue culture wells: (*a)* Control HESCs cultured in HESC medium. (*b*) Control HESCs cultured in EGM. (*c*) Treated HESCs cultured in HESC medium. (*d*) Treated HESCs cultured in EGM medium. (*e*-*h*) HESCs seeded in hydrogels: (*e*) Control HESCs in a hydrogel cultured in HESC medium. (*f*) Control HESCs in a hydrogel cultured in EGM. (*g*) Treated HESCs in a hydrogel cultured in HESC medium. (*h*) Treated HESCs in a hydrogel cultured in EGM. Scale bars: 100 μm.

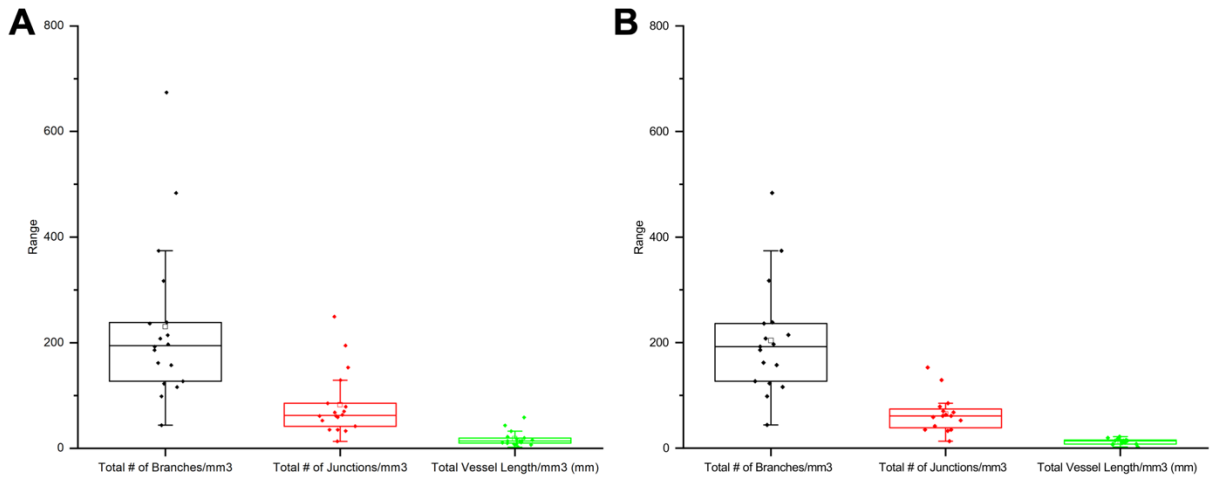

Figure 8. Boxplots of image analysis metrics for 2:1 HUVEC:HESC ratio samples. (*a*) All data including outliers. (*b*) Data with outliers removed. Outliers were identified and removed using Rosner's generalized extreme Studentized deviate test assuming 3 suspected outliers and with α set to 0.05. Outliers removed for total # of branches/mm^3: k=1. Outliers removed for total # of junctions/mm^3: k=2. Outliers removed for total vessel length/mm^3: k=3. □: mean.

CHAPTER 3: THE ROLE OF EXTRACELLULAR MATRIX BIOMOLECULES ON ENDOMETRIAL EPITHELIAL CELL ATTACHMENT AND CYTOKERATIN 18 EXPRESSION ON GELATIN HYDROGELS[3]

3.1 Chapter Overview

The endometrium undergoes profound changes in tissue architecture and composition, both during the menstrual cycle as well as in the context of pregnancy. Dynamic remodeling processes of the endometrial extracellular matrix (ECM) are a major element of endometrial homeostasis, including changes across the menstrual cycle. A critical element of this tissue microenvironment is the endometrial basement membrane, a specialized layer of proteins that separates the endometrial epithelium from the underlying endometrial ECM. Bioengineering models of the endometrial microenvironment that present an appropriate endometrial ECM and basement membrane may provide an improved environment to study endometrial epithelial cell (EEC) function. Here, we exploit a tiered approach using two-dimensional high throughput microarrays and three-dimensional gelatin hydrogels to define patterns of EEC attachment and cytokeratin 18 (CK18) expression in response to combinations of endometrial basement membrane proteins. We identify combinations (collagen IV + tenascin C; collagen I + collagen III; hyaluronic acid + tenascin C; collagen V; collagen V + hyaluronic acid; collagen III; collagen I) that facilitate increased EEC attachment, increased CK18 intensity, or both. We also identify significant EEC mediated remodeling of the GelMA matrix environment via analysis of nascent protein deposition. Together, we report efforts to tailor the localization of basement membrane-associated proteins and proteoglycans in order to investigate tissue engineered models of the endometrial microenvironment.

[3] This chapter is partially adapted from the following publication: **Zambuto SG**, Jain I, Clancy KBH, Underhill GH, Harley BAC. The role of extracellular matrix biomolecules on endometrial epithelial cell attachment and cytokeratin 18 expression on gelatin hydrogels. *In revision.*

3.2 Introduction

The endometrium is the lining of the uterus (34). The endometrium is stratified, with an epithelium overlaying a highly vascularized stromal compartment (34). The luminal epithelium is the location of critical cell-cell dialogue between endometrial cells and an implanting blastocyst (34). The luminal epithelium also remodels during each menstrual cycle phase to become more receptive to a potential pregnancy (34). A basement membrane layer connects the epithelial and stromal layers; although an expanding group of extracellular matrix and adhesion molecules have been identified as part of the basement membrane, much remains unknown regarding the dynamic remodeling processes that occur at its intersection with the endometrial epithelium (34, 38). The study of many of these processes is intractable *in vivo* due to our inability to study early pregnancy in humans and due to significant differences between pregnancy in humans and the most common animal models (39, 44, 125). *In vitro* endometrial model systems provide a framework to investigate physiological processes underlying endometrial activity. Two-dimensional models of the endometrial epithelium fail to recapitulate the native 3D tissue structure. Further, many existing endometrial epithelial models do not incorporate a basement membrane layer despite its importance in endometrial function and pregnancy (48, 49, 76). A critical opportunity exists to develop engineered systems to examine the role of ECM biomolecules on the dynamic nature of the endometrial epithelium and its basement membrane. Such a platform would provide an important framework to investigate the role of the basement membrane on endometrial epithelial cell attachment and phenotype.

First generation models of the endometrial basement microenvironment have included a range of conventional hydrogel models, notably Matrigel^{TM}, fibrin, alginate, and hyaluronic gels.

Matrigel™, a commonly used ECM mixture used to mimic the basement membrane, consists of a mixture of thousands of proteins, primarily type IV collagen, laminin, and nidogen, derived from Engelbrecht-Holm Swarm (EHS) murine sarcoma cells (126). However, lot variability and a heterogeneous protein composition, along with an inability to decouple biophysical and biochemical properties, render it difficult to examine matrix-templated endometrial cell activity (126-128). Despite the diversity of proteins explicitly linked to the endometrium, the majority of prior studies use generic basement membrane constituents such as fibronectin or collagen IV and laminin (76) and have not explored a wider range of combinations. As a result, we propose a systematic examination of combinations of known biomolecules within the endometrium to determine the roles they may play on epithelial cellular behavior.

We previously described a first generation stratified endometrial culture formed via seeding of primary endometrial epithelial cell (EEC) cultures on methacrylamide-functionalized gelatin (GelMA) hydrogels (129). Because gelatin contains RGD cell binding motifs (65), EECs attached to the GelMA hydrogel surface without any additional basement membrane layer; however, we observed that cells formed non-uniform layers on the gels that lost stability over time. Strategies to immobilize supplemental basement membrane proteins onto defined endometrial hydrogel formulations may allow for the inclusion of defined basement membrane layer analogs the provide the ability to locally control ligand density and protein/proteoglycan combinations to more faithfully replicate endometrial basement membrane function. Recent advances with microbial transglutaminase (mTg) suggest a route to enzymatically crosslink a layer of ECM proteins onto a gel surface (130), offering a strategy to decouple endometrial basement membrane properties from those of the underlying endometrial ECM-inspired hydrogel

environment. Furthermore, mTg is water-soluble, inexpensive, biocompatible, and stable long term which renders it an attractive method for producing coated GelMA hydrogels for long term cell culture (130).

The endometrial extracellular matrix exhibits dynamic changes in tissue composition and architecture during homeostasis, pregnancy, and in response to endometrial-associated pathologies (34). Previous studies have identified a wide range of ECM-associated proteins and proteoglycans in the endometrium and decidua whose expression changes markedly across the menstrual cycle or in response to steroidal sex hormones (34). For our study, we systematically investigated the influence of combinations of 10 extracellular matrix proteins and proteoglycans present in the endometrium on endometrial epithelial cell activity: collagens I, III, IV, V, decorin, fibronectin, hyaluronic acid, laminin, lumican, tenascin C. These biomolecules were chosen because of their functional significance in structural remodeling, tissue biomechanics, cell adhesion, cell proliferation, tissue differentiation, as well as other cellular processes crucial to endometrial remodeling during the menstrual cycle and pregnancy (34). Collagen I is most prevalent in the endometrium throughout the menstrual cycle as well as during pregnancy (34, 131) while collagen III is present during all menstrual cycle phases but less abundant than collagen I during the first trimester of pregnancy (34, 131). Collagen IV is present during the menstrual cycle (131) while collagen V increases during decidualization (34). Fibronectin is highly abundant in the endometrium and decidual ECM (34) while tenascin C is more localized near stromal cells surrounding proliferating or developing endometrium epithelia (34) and decorin is present in decidual ECM (34). Although primarily studied in the context of murine models, lumican is localized within the uterine stroma during pregnancy and may potentially be

important in human pregnancy as well (34). Laminin is present in the decidua and mediates trophoblast attachment and spreading (34) while hyaluronic acid likely influences elevated hydration during the mid-proliferative and mid-secretory phases in the human endometrium (34). The basement membrane plays an important role in mucosal barrier tissues, particularly the endometrium (34, 104, 126). In humans, the decidual basement membrane consists of laminin, collagens type IV, VII, XVII, and heparan sulfate proteoglycans (34). Because of the dynamic nature of the endometrial ECM and basement membrane, tissue engineering models offer a unique opportunity to examine the role of endometrial ECM and basement membrane factors in endometrial cell activity, remodeling, and processes associated with trophoblast invasion and placentation.

We report a tissue engineering approach to examine benchmarks of endometrial epithelial cell activity (e.g., cell attachment, phenotypic markers of attachment). We describe a high throughput microarray-based approach to investigate shifts in EEC attachment and epithelial maturation in response to 55 single and pairwise combinations of 10 ECM proteins and proteoglycans found in the endometrium ECM (collagens I, III, IV, V, decorin, fibronectin, hyaluronic acid, laminin, lumican, tenascin C). We track the degree of cell attachment as well as a biomarker of epithelial monolayer maturation (expression of cytokeratin 18, CK18) responsible for anchoring the endometrial epithelial cell cytoskeleton to the basement membrane (76). We identified ECM combinations that promote both high and moderate levels of cell attachment and CK18 intensity, combinations that promoted high cell attachment and median CK18 intensity, and combinations that promote median cell attachment and high CK18 intensity. We subsequently used microbial transglutaminase to immobilize a down-selected set of ECM combinations on three-dimensional

methacrylamide-functionalized gelatin (GelMA) hydrogels. We subsequently evaluate patterns of attachment, CK18 expression, and nascent protein deposition by EECs on GelMA hydrogels. This project describes a pipeline for creating and characterizing model basement membrane constructs as part of a larger tissue engineered strategy to replicate the stratified endometrium.

3.3 Materials and Methods

Cell Culture and Maintenance

We cultured primary human endometrial epithelial cells (EECs; LifeLine Cell Technology FC-0078) as per the manufacturer's instructions and used them experimentally at two passages from receipt. Cells were cultured in phenol red-free medium (LifeLine Cell Technology) and in 5% CO_2 incubators at 37°C. Cells were routinely tested for mycoplasma contamination using the MycoAlert™ Mycoplasma Detection Kit (Lonza).

Microarray Fabrication and Experimentation

Microarray Fabrication

We prepared polyacrylamide (PA) hydrogels following previous protocols (132-134). Briefly, 25×75 mm glass microscope slides were washed with 0.25% v/v Triton X-100 in dH_2O and placed on an orbital shaker for 30 minutes. After rinsing with dH_2O, slides were immersed in acetone and methanol for 30 minutes each on an orbital shaker. This was followed by etching the glass slide by immersing them 0.2 N NaOH for 1 hour on an orbital shaker and then rinsing with dH_2O. The slides were then air-dried and placed on a hot plate at 110°C until dry. For silanization, the cleaned slides were immersed in 2% v/v 3-(trimethoxysilyl)propyl methacrylate in ethanol and placed on the shaker for 30 minutes, followed by a wash in ethanol for 5 minutes. The silanized slides were air-dried, and again placed on the hot plate at 110°C until dry. For

fabrication of hydrogels with specific elastic moduli, prepolymer solution with 6% acrylamide (Sigma-Aldrich A3553-100G) and 0.45% bis-acrylamide (Sigma-Aldrich M7279-25G) was prepared to achieve elastic moduli of 6 kPa. The prepolymer solution was then mixed with Irgacure 2959 (BASF, Corp.) solution (20% w/v in methanol) at a final volumetric ratio of 9:1 (prepolymer:Irgacure). This working solution was then deposited onto slides (100 µL/slide) and covered with 22×60 mm cover glasses. The sandwiched working solution was transferred to a UV oven and exposed to 365 nm UV A for 10 min (240E3 µJ). After removing the cover glasses, the slides were immersed in dH_2O at room temperature for 3 days in order to remove excess reagents from the hydrogel substrates. Before microarray fabrication, hydrogel substrates were thoroughly dehydrated on a hot plate for ≥15 minutes at 50°C. Microarrays were fabricated as described previously (135-137). Extracellular matrix proteins for arraying were diluted in 2×growth factor buffer (38% v/v glycerol in 1× phosphate-buffered saline (PBS), 10.55 mg/mL sodium acetate, 3.72 mg/mL EDTA, 10 mg/mL CHAPS) to a final concentration of 250 µg/mL and loaded in a 384-well V-bottom microplate. List of all the ECM venders and part numbers can be found in Table 1. A robotic benchtop microarrayer (OmniGrid Micro, Digilab) loaded with SMPC Stealth microarray pins (ArrayIt) was used to microprint ECM combinations from the 384 microplate to polyacrylamide hydrogel substrate, resulting in ~600 µm diameter arrayed domains. Fabricated arrays were stored at room temperature and 65% RH overnight and left to dry under ambient conditions in the dark.

Microarray Cell Culture

We sterilized microarrays using a 1% penicillin/streptomycin (Thermo Fisher) solution for 20 minutes under UV light. EECs were then passaged and seeded at a density of 500,000 cells per

microarray in 4 mL cell growth medium. After seeding, microarrays were shaken by hand every 30 minutes for 2 hours and then rinsed with cell growth medium 6 hours after seeding. Microarrays were cultured in slide plates for 24 hours after seeding and cultured in 5% CO_2 incubators at 37°C. Three independent biological replicates were cultured and analyzed for these experiments with at least three technical replicates per experiment.

Microarray Staining

We fixed microarray cultures 24 hours after seeding using 4 mL of formalin (Sigma-Aldrich) followed by three PBS washes. Cultures were stored in PBS at 4°C until use. Microarrays were permeabilized in a 0.5% Tween20 (Fisher Scientific) solution for 15 minutes followed by three 5 minute washes in (PBST). Samples were blocked for 1 hour at room temperature in a 2% Abdil solution (bovine serum albumin; Sigma Aldrich, Tween20, PBS) and subsequently incubated in primary antibody (cytokeratin 18; 1:250; Abcam ab52948) overnight at 4°C. Samples were then washed three times with PBST and then cultured in secondary antibody (Alexafluor 488 goat anti-rabbit; 1:500; Thermo Fisher A-11008) overnight at 4°C. Three 5 minute PBST washes were performed and then slides were mounted with DAPI Fluoromount (Southern Biotechnology Associates, Inc.).

Microarray Imaging

We imaged the microarrays using Axioscan.Z1 Slide Scanner and 10X objective. A wide tile region was defined for the whole array region which was then stitched offline using Zen and exported into TIFF Images for each individual channel.

Microarray Image Analysis

We converted images of entire arrays to individual 8-bit TIFF files per channel (i.e., red, green, blue, and gray) by Fiji (ImageJ version 1.52p) (82). CellProfiler (version 4.0.0) was used obtain per cell measurement for each channel (138). The images were cropped in MATLAB (version R2018b) to separate each array in a single image. Positional information for each array was automatically calculated using their relative position from the positional dextran-rhodamine markers. Nuclei were identified using the DAPI channel image using IdentifyPrimaryObject module and cell boundary was identified using the CK18 stain around these nuclei using IdentifySecondaryObject module. The MeasureObjectIntensity module was used to quantify single-cell intensity. The data were exported to CSV files that were then imported in RStudio for data visualization.

Methacrylamide-Functionalized Gelatin (GelMA) Hydrogel Experimentation

Synthesis and Fabrication of GelMA Hydrogels

GelMA was synthesized as described previously and was found to have a degree of functionalization of 57%, determined via ^{1}H-NMR (65, 139). Prior to hydrogel fabrication, lyophilized GelMA was sterilized under UV light for 30 minutes. To fabricate hydrogels, a solution was created consisting of lyophilized GelMA (5 wt%) combined with 1% fluorescent beads (Fluospheres Polystyrene Microspheres 1.0 μm orange fluorescent beads; $1x10^{10}$ beads/mL; Invitrogen) and dissolved at 37°C in phosphate buffered saline (PBS; Lonza 17-516F). Microspheres were used to visualize hydrogels during imaging. 0.1% w/v lithium acylphosphinate (LAP) was added to this solution as a photoinitiator. 10 μL of the prepolymer solution was added to each well of Ibidi μ-Slides Angiogenesis Glass Bottom and was

polymerized under UV light (λ=365 nm, 7.14 mW cm^{-2}; AccuCure Spot System ULM-3-365) for 30 s.

Extracellular Matrix Coating of GelMA Hydrogels

We used microbial transglutaminase (mTg; Zedira T001, Lot 0920aT001) to coat polymerized GelMA hydrogels with extracellular matrix (ECM) proteins (130, 140, 141). A 1:1 ratio of 0.5 mg/mL mTg and 10 μg/mL ECM protein were combined and 20 μL of this solution was pipetted onto hydrogels. If two ECM proteins were used to coat gels, they were combined in a 1:1 ratio. Coated hydrogels were incubated for 1 hour in 5% CO_2 incubators at 37°C. A quick wash was performed using 20 μL of PBS. Information regarding ECM protein vendors and part numbers can be found in Table 1.

Visualization of ECM Coated Hydrogels

We evaluated the effectiveness of mTg-based matrix immobilization for Laminin-coated GelMA hydrogels. Immediately following laminin coating, hydrogels were blocked for 1 hour in 30 μL of a 2% Abdil solution (bovine serum albumin, Tween20, PBS). Samples were then stained with anti-laminin primary antibody (1:200, 30 μL; Abcam ab11575) at 4°C overnight. Three PBS washes were performed followed by incubation with secondary antibody (1:500, 30 μL; Alexafluor 488 goat anti-rabbit Thermo Fisher A-11008) for 2 hours at room temperature. Three additional PBS washes were performed and samples were stored in PBS at 4°C until imaged. Samples were imaged using a DMi8 Yokogawa W1 spinning disc confocal microscope outfitted with a Hamamatsu EM-CCD digital camera (Leica Microsystems). Two fluorescent Z-stacks

were taken per gel using the 10x objective, 10 μm step size, and 50-100 slices (3 hydrogels per condition). Maximum intensity image projections were created using FIJI.

Endometrial Epithelial Cell Hydrogel Cultures

Endometrial Epithelial Cell Hydrogels

We fabricated and coated hydrogels as described above, with EECs subsequently seeded at 200,000 cells/cm^2 onto the hydrogel surface. EECs were allowed to adhere to the hydrogels for 1 hour and were subsequently washed with 50 μL cell medium to remove unattached cells. Hydrogels were cultured for 3 days in 5% CO2 incubators at 37°C and culture medium was replaced daily.

Immunofluorescent Staining

Hydrogels were fixed on day 3 of culture using 4 mL of formalin (Sigma-Aldrich) followed by three PBS washes. Hydrogels were permeabilized in a 0.5% Tween20 (Fisher Scientific) solution for 15 minutes followed by three 5 minute washes in (PBST). Samples were blocked for 1 hour at room temperature in a 2% Abdil solution (bovine serum albumin; Sigma Aldrich, Tween20, PBS) and subsequently incubated in primary antibody (cytokeratin 18; 1:250; Abcam ab52948) overnight at 4°C. Hydrogels were washed 4 x 20 minutes with PBST and then cultured in secondary antibody (Alexafluor 488 goat anti-rabbit; 1:500; Thermo Fisher A-11008) overnight at 4°C. Hydrogels were washed 4 x 20 minutes with PBST and then incubated in Phalloidin-iFluor 633 Reagent (Abcam ab176758) as per the manufacturer's instructions for 90 minutes at room temperature. Cells were rinsed in PBS 4 x 20 minutes and then incubated in Hoechst

(1:2000; Thermo Fisher) for 30 minutes. One PBS wash was performed and samples were stored in PBS until imaged.

Hydrogel Confocal Imaging

We imaged hydrogels using a Zeiss LSM 710 Confocal Microscope and 10X objective. One image was taken per hydrogel (n=3 hydrogels) in a random region of interest. Maximum intensity image projections used for analysis were generated using ZEN (black edition; Zeiss).

Image Analysis

We used CellProfiler (version 4.0.0) to analyze CK18 intensity from maximum intensity projection images of cells seeded onto hydrogels (138). Nuclei were identified using the DAPI channel image using IdentifyPrimaryObject module and cell boundary was identified using the CK18 stain around these nuclei using IdentifySecondaryObject module. The MeasureObjectIntensity module was used to quantify single-cell intensity. The data were exported to CSV files that were then imported in RStudio for data visualization.

Nascent Protein Deposition

Nascent Protein Staining

Following the protocols developed by Loebel et al. (142, 143), we performed metabolic labeling to visualize nascent protein deposition. Briefly, epithelial hydrogel cultures were cultured as described above. On day 3 of culture, hydrogels were washed once with Hanks' Balanced Salt Solution (HBSS) and incubated in HBSS for 30 minutes to deplete the cells of any remaining methionine. The HBSS was removed and cells were then incubated at 37°C in HBSS containing

the methionine analog azidohomoalanine (Click-iT AHA; Invitrogen, C10102; 100 μM) for 1 hour. Following incubation, two HBSS washes were performed and hydrogels were then incubated in AFDye 488 DBCO (Click Chemistry Tools, 1278-1; 30 μM) for 40 minutes at 37°C, washed three times with PBS, fixed for 15 minutes followed by three PBS washes, and stored at 4°C in PBS until staining. Hydrogels were incubated in CellMask™ Deep Red Plasma Membrane Stain (1:1000; Invitrogen, C10046) for 40 minutes at 37°C followed by three PBS washes. Samples were then incubated in Hoechst at room temperature for 30 minutes (1:2000) followed by one PBS wash. Samples were stored at 4°C in PBS until imaged.

Nascent Protein Intensity Quantification

We used CellProfiler to analyze nascent protein intensity from maximum intensity projection images. Hydrogels were imaged using a Zeiss LSM 710 Confocal Microscope and 10X objective. One image was taken per hydrogel (n=3 hydrogels) in a random region of interest. Maximum intensity image projections used for analysis were generated using ZEN (black edition; Zeiss). These images were uploaded to CellProfiler and analyzed as described above.

Statistics

We used RStudio for our statistical analyses. Normality was determined using the Shapiro-Wilkes test and homoscedasticity was determined via Bartlett's test for normal data or Levene's test for non-normal data. Data were analyzed using a one-way analysis of variance (ANOVA) and Tukey post hoc test (normal, homoscedastic), Welch's ANOVA and Games-Howell post hoc test (normal, heteroscedastic), Kruskall-Wallis ANOVA and Dunn's post hoc test (non-normal, homoscedastic), or Welch's Heteroscedastic F Test with Trimmed Means and Winsorized

Variances and Games-Howell post hoc test (non-normal, heteroscedastic). Significance was defined as $p<0.05$ and data are presented as box plots unless otherwise described.

3.4 Results

High throughput microarray analysis reveals differential epithelial cell attachment and CK18 expression in response to endometrial ECM biomolecule combinations

Epithelial cell attachment and CK18 expression was quantified in response to 55 single and pairwise combinations of 10 ECM proteins and proteoglycans microarrayed onto slides (Fig. 9A). EECs were analyzed 24 hours after seeding onto arrays to assess cell behavior at early culture timepoints. From this experiment, we observed differential attachment and CK18 expression in EECs based on the ECM proteins on which the cells were cultured. For subsequent analysis, we chose combinations of ECM biomolecules with the highest number of cells attached (Fig. 9B,C; Collagen IV + Tenascin C; Collagen I + Collagen III), or the highest value for CK18 intensity (Fig. 1D,E; Hyaluronic Acid + Tenascin C; Collagen V). We also selected combinations with median (~15^{th} position out of 55 rank ordered samples) levels of cell attachment and CK18 intensity (Fig. 1B-F; Collagen I + Hyaluronic Acid; Collagen V + Hyaluronic Acid) as well as combinations that displayed high cell attachment but median CK18 intensity (Fig. 1B-F; Collagen 1) or high CK18 intensity but median cell attachment (Fig. 9B-F; Collagen III).

GelMA hydrogels can be coated with ECM biomolecules using microbial transglutaminase

Microbial transglutaminase (mTg) was used to coat GelMA hydrogels with proteins/proteoglycan combinations identified via high throughput screen to subsequently investigate EEC attachment and CK18 expression on GelMA hydrogels with functionalized

basement membrane layers (Fig. 10A). To confirm biomolecule attachment, GelMA hydrogels were functionalized with laminin, a commonly used ECM protein for cell attachment. Immunofluorescent staining showed that while simple addition of laminin to GelMA hydrogels without mTG resulted in limited laminin adhesion, laminin adhered to GelMA hydrogels via mTg produced a strong laminin signal (Fig. 10B).

Epithelial cells cultured on ECM biomolecule combinations show variation in cell attachment and CK18 intensity

We subsequently assessed EEC attachment and CK18 expression on GelMA hydrogels coated with mTg-immobilized ECM proteins and proteoglycans to evaluate whether combinations down-selected from the microarray experiments would facilitate improved EEC attachment or CK18 expression. EEC attachment and CK18 expression were evaluated relative to control GelMA hydrogels as well as GelMA hydrogels coated with fibronectin or collagen IV + laminin factors previously used in the literature as endometrial basement membrane mimics (76). We first examined cell attachment at CK18 expression using hits with highest cell adhesion in 2D microarray experiments (C4+TC: Collagen IV + Tenascin C; C1+C3: Collagen 1 + Collagen 3). Although overall analysis of the number of adhered cells suggested significant differences between conditions (Welch's ANOVA, p=0.018), post hoc analysis showed no differences between experimental (Collagen IV + Tenascin C; Collagen I + Collagen III) and controls (Fig. 11A). CK18 intensity was not found to differ between groups (Fig. 11B; One-way ANOVA, p=0.88). We then examined the role of ECM combinations that resulted in the highest CK18 intensity in 2D microarray experiments (HA+TC: Hyaluronic Acid + Tenascin C; C5: Collagen V), finding no differences in the number of cells attached (Fig. 12A; One-way ANOVA, p=0.77)

or in CK18 intensity (Fig. 12B; One-way ANOVA, p=0.31) on functionalized GelMA hydrogels. Finally, comparing ECM combinations with median cell attachment and CK18 intensity in 2D microarray experiments (C1+HA: Collagen I + Hyaluronic Acid; C5+HA: Collagen V + Hyaluronic Acid), high cell attachment and median CK18 intensity (C1: Collagen I), or median cell attachment and high CK18 intensity (C3: Collagen III), we observed no significant differences in cell attachment (Fig. 13A; Welch's ANOVA, p=0.17). However, CK18 intensity was statistically significantly different between groups (Fig. 13B; Welch's ANOVA, p=4.8×10^{-4}), with post hoc analysis revealing significantly increased CK18 intensity in collagen I versus fibronectin coatings.

Epithelial cells deposit nascent proteins onto GelMA hydrogels

We evaluated the potential for EECS to significantly remodel their basement membrane environment on 3D GelMA hydrogels, examining nascent protein deposition in response to ECM combinations that increased cell attachment in microarray experiments (C4+TC: Collagen IV + Tenascin C; C1+C3: Collagen I + Collagen III). Within 1 hour, EECs deposited observable levels of nascent proteins onto hydrogels in all conditions (Fig. 14A), with analysis of the intensity of nascent protein deposition revealed no difference between groups (Fig. 14B; One-way ANOVA, p=0.24).

3.5 Discussion

Dynamic changes in the endometrial ECM plays a key role in homeostasis, pregnancy, and endometrial-associated pathologies (34). Previous studies have identified a wide range of ECM-associated proteins and proteoglycans in the endometrium and decidua whose expression

changes markedly across the menstrual cycle or in response to steroidal sex hormones (34). Nevertheless, developing a deeper understanding of the role of the endometrial basement membrane and extracellular matrix on endometrial epithelial cell behavior may provide critical information on cell attachment phenotype (e.g., cytokeratin expression). Understanding endometrial epithelial cell attachment behavior to the basement membrane would also provide crucial information on how trophectoderm signaling and alterations to the basement membrane may facilitate blastocyst adhesion, disruption, breach, and resealing of the endometrial epithelium. Our goal was to identify ECM combinations that facilitate improved endometrial epithelial cell attachment and CK18 expression in order to support the development of tissue engineering systems that more appropriately mimic the endometrial ECM.

We have previously described overlaid cultures of endometrial epithelial cells on GelMA hydrogels (139); however, we observed instability of the epithelial cultures over time and inability of the cultures to form a confluent monolayer. We hypothesized that an appropriate basement membrane layer on the surface of the GelMA hydrogel may be required to form a consistent, confluent monolayer. To determine whether a broader set of ECM biomolecule combinations inspired by the composition of the native endometrium may impact the stability of the epithelial layers, we performed high throughput experiments using microarrays to assess the effect of 55 single and pairwise combinations of 10 ECM biomolecules found in the endometrium (collagens I, III, IV, V, decorin, fibronectin, hyaluronic acid, laminin, lumican, and tenascin C) on endometrial epithelial cell attachment and CK18 expression.

We found collagen IV + tenascin C and collagen I + collagen III combinations resulted in the highest number of EECs attached while hyaluronic acid + tenascin C and collagen V had the highest values for CK18 intensity. Further, collagen I + hyaluronic acid and collagen V + hyaluronic acid had values for cell attachment and CK18 intensity around the 15th position from the highest values, while collagen I promoted high cell attachment and median CK18 intensity, while collagen III promoted median cell attachment and high CK18 intensity. These results identified combinations of key ECM proteins and proteoglycans found in the endometrium that affect EEC attachment and CK18 expression. For example, collagens I, III, and V are all present in the endometrium but collagen I is most prevalent during the proliferative and secretory phases, collagen III is present during all phases, and collagen V increases during decidualization (34). Tenascin C is present near stromal cells surrounding proliferating or developing endometrial epithelia (34). Logically, tenascin C would be relevant to these studies because EECs would likely be proliferating and developing in these cultures. Finally, hyaluronic acid may influence hydration of the tissue during the mid-proliferative and mid-secretory phases (34). Interestingly, our microarray data did not identify fibronectin or collagen IV + laminin as combinations that resulted in high cell attachment or CK18 expression, despite many studies utilizing these as basement membrane mimics based on their prevalence in the endometrial basement membrane (34, 76). Future efforts looking at a larger screen of metrics of EEC bioactivity may be required to understand the role of these biomolecules on endometrial epithelial cell activity.

We used these data to identify a set of biomolecules to immobilize on the surface of three-dimensional GelMA hydrogels to assess epithelial cell attachment and CK18 expression. We adapted a recently reported microbial transglutaminase (mTg) biomolecule immobilization

strategy (130) to covalently bind biomolecules to GelMA hydrogels. This approach enables attachment of ECM combinations using a relatively simple protocol with immobilized biomolecules showing extended stability (28 days) in culture (130). We then quantified cell attachment and CK18 intensity on GelMA hydrogels coated with a range of endometrial-inspired matrix biomolecules. While the number of cells per island and CK18 expression levels varied for each set of selected ECM biomolecules, the statistical significance of the data was variable. Compared to controls (GelMA only, Fibronectin, Collagen IV + Laminin), matrix hits for adhesion Collagen IV + Tenascin C and Collagen I + Collagen III) had statistically different number of cells per island but not CK18 intensity. For combinations resulting in the highest CK18 intensity in microarray experiments (Hyaluronic Acid + Tenascin C and Collagen V), the numbers of cells attached and the CK18 intensity were not statistically significantly different between groups. Finally, for ECM combinations around the 15th position from the highest values of cell attachment and CK18 intensity (Collagen I + Hyaluronic Acid and Collagen V + Hyaluronic Acid), high cell attachment and median CK18 intensity (Collagen I), and median cell attachment and high CK18 intensity (Collagen III), we determined that the cells attached did not statistically differ between groups but, CK18 intensity was statistically significantly different between groups. Post hoc analysis revealed statistical significance between CK18 intensity between the fibronectin and collagen I conditions. These data demonstrated that there is variation in cell response based on ECM coating and that CK18 expression, a marker of endometrial cell phenotype, was more strongly affected that overall numbers of attached cells. Taken together, these data suggest that careful selection of basement membrane ECM combinations must be considered for tissue engineering constructs under development to replicate the stratified endometrium.

Finally, we demonstrated functional metrics of EEC-mediated remodeling of the engineered basement membrane environment by quantifying nascent protein deposition by EECs on GelMA hydrogels. We observed rapid (~1 h) protein deposition, demonstrating EECs rapidly deposit their own ECM onto the surface on which they are cultured and continue to deposit proteins throughout their culture period regardless of the ECM biomolecules on which they are growing. These results suggest significant opportunities to examine variations in the specific proteins being deposited as well as shifts in matrix deposition as a function of initial basement membrane content. Extending on our previous use of the GelMA hydrogel platform to evaluate endometrial stromal models (129), these findings suggest opportunities to evaluate crosstalk between endometrial epithelial layers and underlying endometrial perivascular models as well as the opportunity to evaluate the role of external stimuli such as steroidal sex hormones in a fully stratified endometrial culture platform. We also recognize some limitations and future opportunities for these studies. The cells used in these studies are primary endometrial epithelial cells derived from a single donor. What matrix the EECs prefer may have donor-to-donor variability and may depend on the menstrual cycle phase during which the cells were collected as well as donor-to-donor cell preferences. For example, *Cook et al*. previously identified differences in epithelial cell behavior that was dependent on cell donors (76). These results suggest that the basement membrane and ECM biomolecule combinations may vary between individuals and underlie the need for an adaptable tissue engineering approach such as the 2D microarray to 3D biomaterial pipeline described here, to help identify how this variability affects uterine function and health. Future studies that incorporate cells from multiple donors collected

at various points in the menstrual cycle may provide insight in donor-to-donor and cycle-dependent variability in cell response to different ECM components.

3.6 Conclusions

The endometrium is a highly dynamic tissue that suggests the need for a dynamic model system to replicate processes of growth, remodeling, and breakdown in order to properly recapitulate endometrial physiology. The ability to create an endometrial basement membrane mimic within a tissue engineered construct would provide opportunities to develop complex platforms that mimic not just a single menstrual cycle phase but also various points in the menstrual cycle. Here, we demonstrate differential response of EECs to ECM biomolecule combinations using a coordinated set of high-throughput two-dimensional microarrays and three-dimensional matrix-functionalized GelMA hydrogels. We report an approach to coat GelMA hydrogels with combinations of ECM proteins and proteoglycan to investigate the role of engineered basement membrane composition on endometrial epithelial cell attachment and phenotypic markers via immunostaining as well as evaluate endometrial epithelial cell mediated matrix remodeling via nascent protein deposition. Together, these results suggest an approach to replicate features of a stratified endometrial model, notably epithelial cell adhesion and remodeling via combinations of immobilized ECM biomolecules that can be tuned to match the changing endometrial microenvironment.

3.7 Table

Table 2. Microarray Biomolecule Information.

Biomolecule	Vendor	Catalog Number	Stock Concentration
Collagen 1	EMD Millipore	08-115MI	1 mg/mL
Collagen 3	EMD Millipore	CC054	1 mg/mL
Collagen 4	Abcam	ab7536	1 mg/mL
Collagen 5	Abcam	ab7530	1 mg/mL
Fibronectin	EMD Millipore	FC010-10MG	1 mg/mL
Decorin	R&D Systems	143-DE-100	0.5 mg/mL
Lumican	ACROBiosystems	LUM-H5227-100ug	0.5 mg/mL
Laminin	EMD Millipore	CC095	1 mg/mL
Hyaluronic Acid	Lifecore Biomedical	HA60k-1	1 mg/mL
Tenascin C	R&D Systems	3358-TC-050	0.5 mg/mL

3.8 Figures

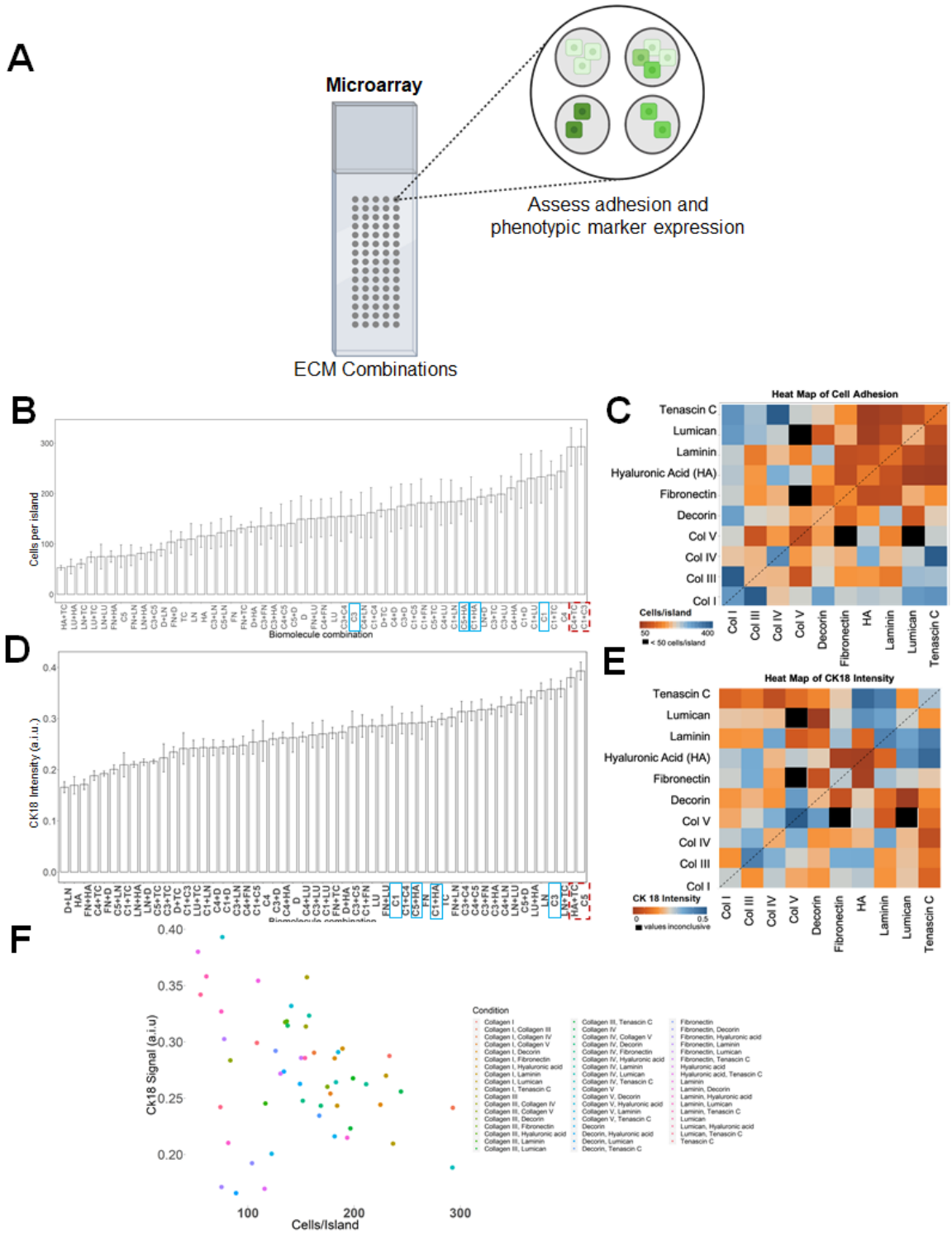

Figure 9. High throughout microarrays demonstrate differences in adhesion and cytokeratin 18 (CK18) intensity. Single and pairwise combinations of extracellular matrix

Figure 9 (cont), (ECM) biomolecules were arrayed onto polyacrylamide gels to determine adhesion patterns of primary endometrial epithelial cells. Epithelial cells were seeded at a density of 500,000 cells per microarray and cultured for 24 hours prior to fixation and staining. **(A)** Experimental summary. Created with BioRender.com. **(B)** Average number of cells per island on various ECM combinations. Red, dotted box: highest cells per island. Blue boxes: median values of CK18 and adhesion. Data expressed as average ± standard deviation. **(C)** Heat map of cell adhesion based on ECM combinations. **(D)** Average CK18 intensity on various ECM combinations. Red, dotted box: highest CK18 intensity. Blue boxes: median values of CK18 and adhesion. Data expressed as average ± standard deviation. **(E)** Heat map of CK18 intensity based on ECM combinations. **(F)** Scatterplot of average cell adhesion values vs. average CK18 intensity based on ECM combinations.

Key: C1: Collagen 1; C2: Collagen 2; C3: Collagen 3; C4: Collagen 4; C5: Collagen 5; D: Decorin; FN: Fibronectin; HA: Hyaluronic Acid; LN: Laminin; LU: Lumican; TC: Tenascin C.

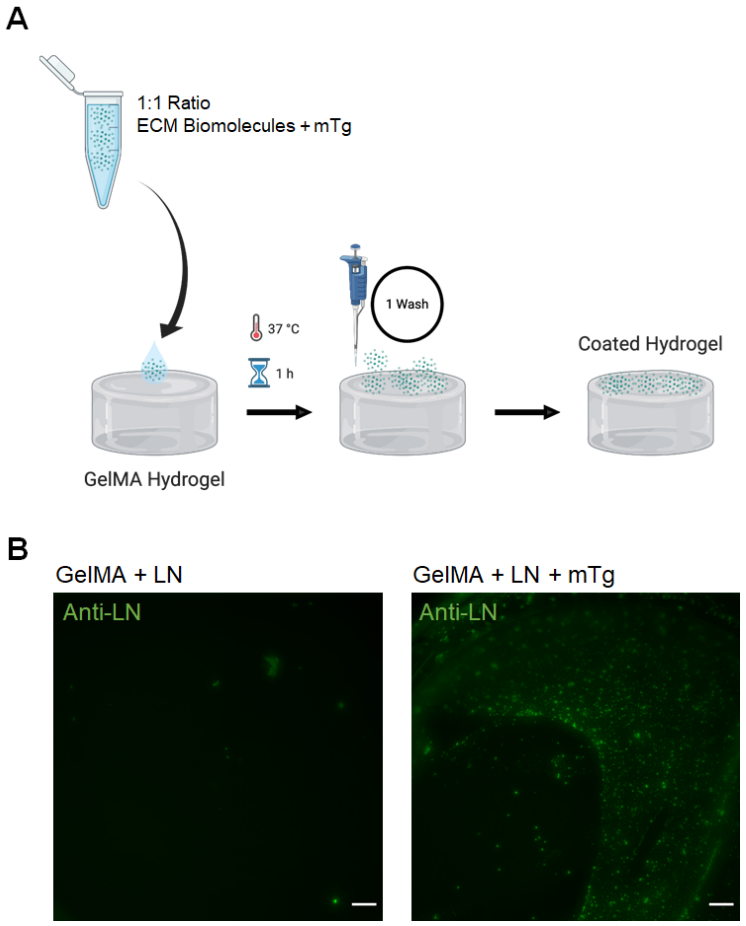

Figure 10. Methacrylamide-functionalized gelatin (GelMA) hydrogels are coated with extracellular matrix (ECM) biomolecules using microbial transglutaminase (mTg). (A) Experimental procedure for coating hydrogels. ECM biomolecules (10 µg/mL) and mTg (0.5 mg/mL) were mixed in a 1:1 ratio and pipetted onto GelMA hydrogels to coat the hydrogel surface. Created with BioRender.com. **(B)** GelMA hydrogels coated with laminin (LN) by adsorption or using the mTg protocol demonstrate significantly increased protein attachment using mTg. Green: laminin. Scale bar: 200 µm.

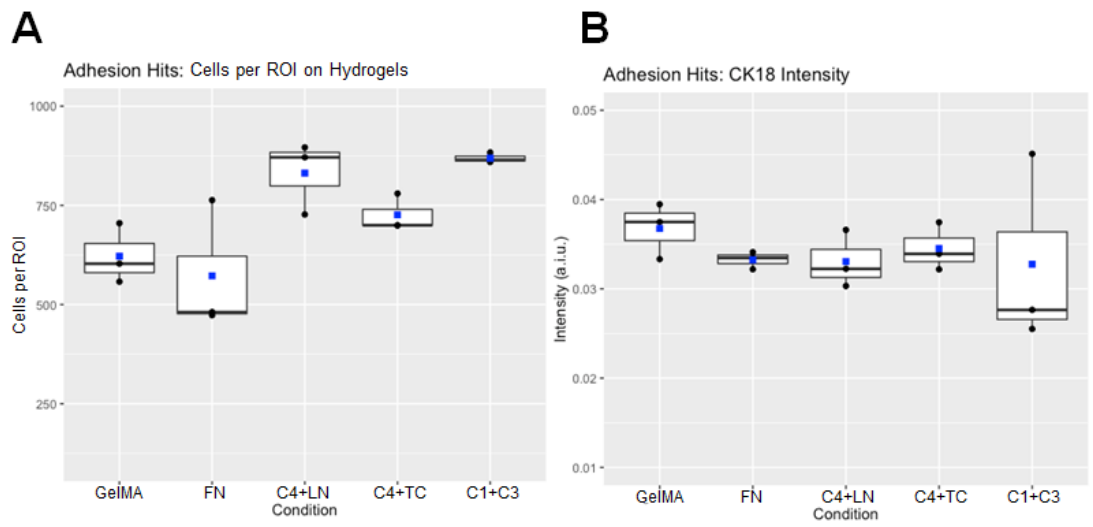

Figure 11. Cell attachment and cytokeratin 18 (CK18) intensity on methacrylamide-functionalized gelatin (GelMA) hydrogels coated with extracellular matrix combinations with highest adhesion in microarray experiments (C4+TC: Collagen IV + Tenascin C and C1+C3: Collagen 1 + Collagen 3). Control conditions consist of GelMA with no coating (GelMA) and coating conditions from literature (FN: Fibronectin and C4+LN: Collagen IV + Laminin). Data consists of n=3 hydrogels per condition (1 ROI per gel) with 1 maximum intensity confocal image analyzed per hydrogel. Data presented in box plots with blue squares representing the mean. **(A)** Average number of cells per ROI for each condition. Cells per ROI showed significant (Welch's ANOVA: p=0.018) differences between groups. **(B)** Average CK18 intensity of cells on hydrogels for each condition. CK18 intensity showed no differences between groups (One-way ANOVA: p=0.88).

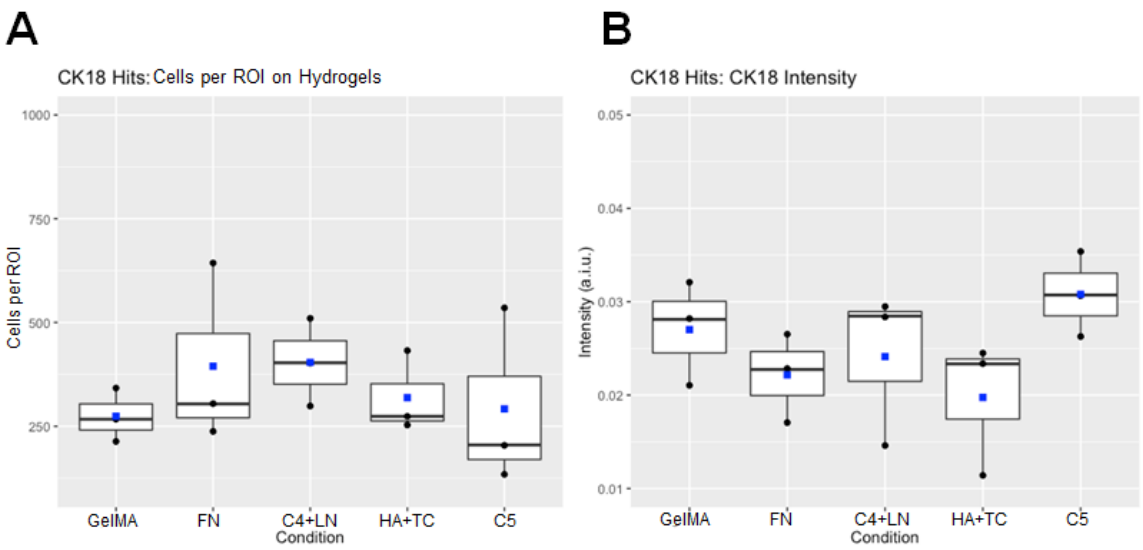

Figure 12. Cell attachment and cytokeratin 18 (CK18) intensity on methacrylamide-functionalized gelatin (GelMA) hydrogels coated with extracellular matrix combinations with highest CK18 intensity in microarray experiments (HA+TC: Hyaluronic Acid + Tenascin C and C5: Collagen 5). Control conditions consist of GelMA with no coating (GelMA) and coating conditions from literature (FN: Fibronectin and C4+LN: Collagen IV + Laminin). Data consists of n=3 hydrogels per condition (1 ROI per gel) with 1 maximum intensity confocal image analyzed per hydrogel. Data presented in box plots with blue squares representing the mean. **(A)** Average number of cells per ROI for each condition. Cells per ROI showed no differences between groups (Welch's ANOVA: p=0.77). **(B)** Average CK18 intensity of cells on hydrogels for each condition. CK18 intensity showed no differences between groups (One-way ANOVA: p=0.31).

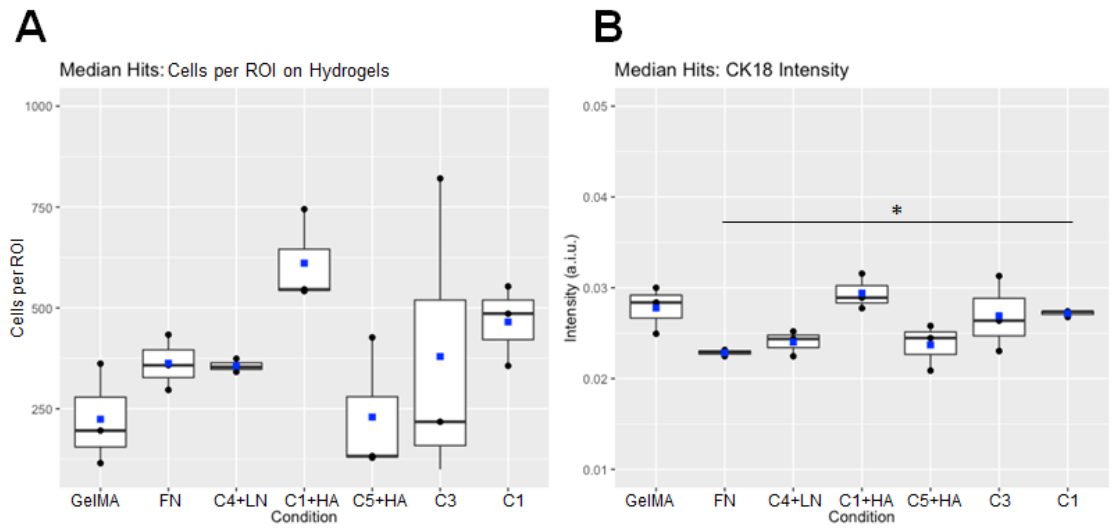

Figure 13. Cell attachment and cytokeratin 18 (CK18) intensity on methacrylamide-functionalized gelatin (GelMA) hydrogels coated with extracellular matrix combinations with median adhesion and CK18 intensity (C1+HA: Collagen I + Hyaluronic Acid and C5+HA: Collagen V + Hyaluronic Acid), high cell adhesion and median CK18 intensity (C1: Collagen I), and median cell adhesion and high CK18 intensity (C3: Collagen III) in microarray experiments. Control conditions consist of GelMA with no coating (GelMA) and coating conditions from literature (FN: Fibronectin and C4+LN: Collagen IV + Laminin). Data consists of n=3 hydrogels per condition (1 ROI per gel) with 1 maximum intensity confocal image analyzed per hydrogel. Data presented in box plots with blue squares representing the mean. **(A)** Average number of cells per ROI for each condition. Cells per ROI showed no differences between groups (Welch's ANOVA: p=0.17). **(B)** Average CK18 intensity of cells on hydrogels for each condition. CK18 intensity showed statistically significant differences between groups (Welch's ANOVA: p=4.8x10^{-4}) with post hoc analysis demonstrating that CK18 intensity was significantly increased for collagen I vs fibronectin conditions.

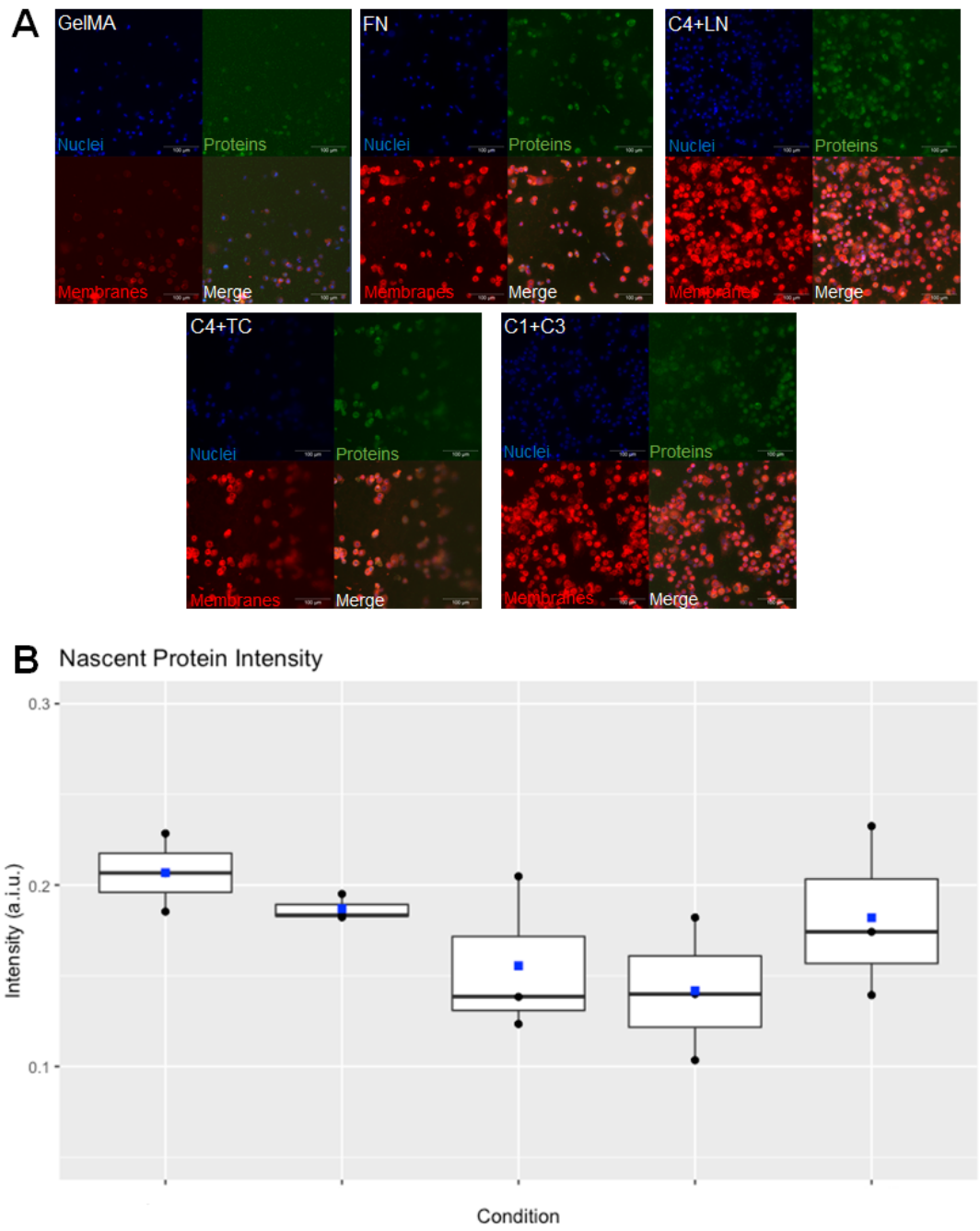

Figure 14. Primary endometrial epithelial cells deposit nascent proteins onto methacrylamide-functionalized gelatin (GelMA) hydrogels. (A) Nascent protein deposition after 1 hour on extracellular matrix (ECM) combinations highest adhesion in microarray experiments (C4+TC: Collagen IV + Tenascin C and C1+C3: Collagen 1 + Collagen 3). Control conditions consist of GelMA with no coating (GelMA) and coating conditions from literature

Figure 14 (cont), (FN: Fibronectin and C4+LN: Collagen IV + Laminin). Green: nascent proteins; Red: cell membranes; Blue: nuclei. Scale: 100 μm. **(B)** Nascent protein intensity for each condition (no significant differences; One-way ANOVA: p=0.24). Data consists of n=3 hydrogels per condition (1 ROI per gel) with 1 maximum intensity confocal image analyzed per hydrogel. Data presented in box plots with blue squares representing the mean.

CHAPTER 4: DECIDUALIZATION STATUS MODULATES ENDOMETRIAL PERIVASCULAR NICHE COMPLEXITY IN GELATIN HYDROGELS[4]

4.1 Chapter Overview

To support tissue regrowth during the menstrual cycle as well as significant remodeling during placentation, the lining of the uterus undergoes rapid cycles of vascular growth, remodeling, and breakdown. Steroidal sex hormones progesterone and estrogen play a central role in modulating processes of endometrial angiogenesis and vascular remodeling by directly regulating an endometrial differentiation process known as decidualization. During decidualization, vessels sprout and lengthen, surface area of spiral arterioles increases, uterine glands undergo secretory transformation, and specialized uterine natural killer cells increase in number (144). Decidualization in the endometrium is critical for blastocyst implantation and defects in this process have been linked to a variety of pregnancy disorders such as preeclampsia, fetal growth restriction, and infertility. For example, in the hypertensive pregnancy disorder preeclampsia, studies have demonstrated that in patients with severe preeclampsia, defects in decidualization subsequently led to impaired trophoblast invasion (37). However, much remains unknown regarding the role of steroidal sex hormones on endometrial angiogenesis. Here, we develop and characterize models of an artificial endometrial perivascular niche embedded in GelMA hydrogels and culture them in the absence and presence of decidualization hormone cocktails. We quantify metrics of vessel network complexity, analyze soluble factor secretion of perivascular cultures, and assess matrix remodeling in the context of hormonal stimulation. We subsequently use these models to assess the role of secreted factors generated by decidualized

[4] This chapter is partially adapted from the following publication: **Zambuto SG**, Theriault H, Jain I, Crosby C, Pintescu, IP, Chiou, N, Zoldan J, Clancy KBH, Underhill GH, Harley BAC. Decidualization status modulates endometrial perivascular niche complexity in gelatin hydrogels. *In preparation.*

perivascular structures on trophoblast motility. Finally, we demonstrate an artificial endometrial triculture consisting of a stratified epithelial monolayer overlaying embedded perivascular networks. This artificial perivascular niche replicates aspects replicates aspect of the *in vivo* perivascular environment but shows potential to investigate dynamic changes in endometrial angiogenesis in response to a variety of endometrial states.

4.2 Introduction

To support tissue regrowth during the menstrual cycle and significant remodeling during pregnancy, the lining of the uterus undergoes rapid cycles of vascular growth, remodeling, and breakdown. This tissue known as the endometrium is one of the only adult human tissues to undergo non-pathological angiogenesis (55). Angiogenesis is defined as the development of new vessels from existing blood vessels via elongation, intussusception, or sprouting by endothelial cells (55, 145). During the menstrual cycle, angiogenesis occurs during three distinct phases: the proliferative phase, the secretory phase, and the menstrual phase (55, 144). The proliferative phase is characterized by initiation of vessel growth (55, 144) and the secretory phase is characterized by branching, lengthening, and vessel maturation (55, 144). Menstruation then induces vessel degeneration and endometrial shedding (144). After menstruation, angiogenic processes work to repair the superficial layer of the basal endometrium in preparation for the subsequent menstrual cycle (55). Rapid angiogenesis also occurs immediately after trophoblast implantation but ahead of the formation of a placenta during pregnancy due to significant demands to support a growing placenta and fetus (144). Angiogenesis is critical for successful pregnancy because adequate blood flow, placental perfusion, and vascular responsiveness to the growing fetus are all necessary to support the placenta and fetus (144).

Steroidal sex hormones progesterone and estrogen modulate endometrial angiogenesis as well as vascular remodeling (144). Progesterone controls vessel elongation, growth and coiling of spiral arterioles, and maturation of the subepithelial capillary plexus whereas estrogen plays a key role in concert with the VEGF (vascular endothelial growth factor) family to control vascular remodeling (144). Steroidal sex hormones also orchestrate an endometrial differentiation process known as decidualization. Decidualization is the process by which the endometrium prepares for a potential pregnancy by thickening and enhancing the tissue matrix for the incoming blastocyst (144). During decidualization, vessels sprout and lengthen, surface area of spiral arterioles increases, uterine glands undergo secretory transformation, and specialized uterine natural killer cells increase in number (144). Successful endometrial decidualization enables the endometrium to enter a period of receptivity that occurs during the late secretory phase of the menstrual cycle and lasts approximately four days (144). During this window, the blastocyst will attach to the endometrial epithelium and subsequently invade the underlying stroma and vasculature (144). Crosstalk between endometrial cells and trophoblast cells from the invading blastocyst are believed to modulate processes of invasion and also dynamic remodeling of the tissue microenvironment including vascular networks (144). Decidualization in the endometrium is critical for blastocyst implantation and defects in this process have been linked to a variety of pregnancy disorders such as preeclampsia, fetal growth restriction, and infertility (144). For example, in the hypertensive pregnancy disorder preeclampsia, studies have demonstrated that in patients with severe preeclampsia, defects in decidualization subsequently led to impaired trophoblast invasion (37). However, much remains unknown regarding the role of steroidal sex hormones on endometrial angiogenesis and vice versa.

Few models of the endometrial vasculature exist. Most models of the endometrial vasculature either cannot recapitulate tissue biophysical properties (stiffness), do not use relevant human cell types in heterogenous cell cultures, or cannot be cultured long term for 20+ days (46, 146-149). Creation of tissue engineered vasculature models have demonstrated promising results in mimicking vasculature *in vitro*. For example, Offendu et al. and Haase et al. have demonstrated perfusable vasculature in microphysiological microfluidic devices for quantifying transportation though the endothelium and flow-mediated vessel remodeling (150-152). Such model systems have also been used to study pregnancy-related vascular disorders, including placental vasculopathies (151). Engineered vasculature models are unique tools that provide high throughput, tunable platforms for studying vessel function. Specifically, biomaterial-based platforms allow for three-dimensional culture of heterogeneous cell populations in systems that can also recapitulate tissue biophysical properties and have the potential for transplantation in the long-term future. Gelatin is an attractive platform for these types of studies for a variety of reasons. As a natural polymer derived from collagen, it contains cell adhesion and degradation sites which allow for matrix remodeling by cells and functionalization of gelatin by adding methacrylate groups to its amine-containing side groups results in the synthesis of methacrylamide-functionalized gelatin, GelMA, which offers enhanced mechanical features that can be tuned to mimic *in vivo* biophysical properties (90). Previous studies from our group and others have demonstrated that vessel networks can be cultured in GelMA hydrogels by encapsulating co-cultures of endothelial and stromal cells (67, 90).

Here, we develop and characterize models of an artificial endometrial perivascular niche embedded in GelMA hydrogels and cultured in the absence and presence of decidualization

hormone cocktails. We quantify shifts in vessel network complexity, analyze soluble factor secretion of perivascular cultures, and assess matrix remodeling via basement membrane protein deposition and tight junction formation. Subsequently, we assess the role of trophoblast cell secreted factors on perivascular network remodeling as well as the role of perivascular secreted factors on trophoblast motility. Finally, we demonstrate a three-dimensional, stratified model of the endometrium consisting of an epithelial culture overlaying an embedded perivascular niche. This artificial perivascular niche replicates aspect of the *in vivo* perivascular environment and suggests a platform to study endometrial angiogenesis in a variety of endometrial states.

4.3 Materials and Methods

Cell Culture and Maintenance

Human Endometrial Microvascular Endothelial Cell Culture

Human endometrial microvascular endothelial cells (HEMEC; ScienCell #7010) were maintained as per the manufacturer's instructions in phenol red-free Endothelial Cell Medium (ECM; ScienCell #1001-prf) supplemented with an endothelial cell growth supplement (ScienCell #1052), 5% charcoal-stripped fetal bovine serum (Sigma-Aldrich F6765), and 1% penicillin/streptomycin (ThermoFisher 15140122). Charcoal-stripped fetal bovine serum was used to reduce the steroid hormone concentrations in the cell medium. HEMECs were cultured on bovine plasma fibronectin (ScienCell #8248) coated vessels. HEMECs were used experimentally no more than 5 passages from purchase. HEMECs were cultured in 5% CO_2 incubators at 37°C. Routine mycoplasma testing was performed using a MycoAlert™ Mycoplasma Detection Kit (Lonza). Cell ancestry information (e.g., racial and ethnic

background, age, gender identity) was not provided by the vendor although the cell ancestry may affect cellular behavior and response (153, 154).

Human Endometrial Stromal Cell Culture

Human endometrial stromal cells (HESC; ATCC® CRL-4003) were maintained as per the manufacturer's instructions in custom phenol red-free DMEM/F-12 (based on Sigma #D 2906) supplemented with 1% ITS+ Premix (Corning 354352), 500 ng/mL puromycin (Millipore Sigma P8833), 10% charcoal stripped fetal bovine serum (Sigma-Aldrich F6765), and 1% penicillin/streptomycin. HESC were used experimentally no more than 5 passages from purchase. HESC were cultured in 5% CO_2 incubators at 37°C. Routine mycoplasma testing was performed using a MycoAlert™ Mycoplasma Detection Kit (Lonza). Cell ancestry information (e.g., racial and ethnic background, age, gender identity) was not provided by the vendor although the cell ancestry may affect cellular behavior and response (153, 154).

Primary Human Endometrial Epithelial Cell Culture

We cultured primary human endometrial epithelial cells (EECs; LifeLine Cell Technology FC-0078; Lot 03839; Caucasian Female Donor, 33 y.o., uterine prolapse) as per the manufacturer's instructions in phenol red-free medium (LifeLine Cell Technology) and in 5% CO2 incubators at 37°C. EECs were used experimentally at two passages from receipt. Cells were routinely tested for mycoplasma contamination using the MycoAlertTM Mycoplasma Detection Kit (Lonza).

2D Culture of Human Endometrial Microvascular Endothelial Cells

HEMEC cells were seeded into individual wells of a 6 well plate and cultured until confluent. Cells were then fixed in formalin (Sigma-Aldrich), permeabilized for 15 minutes in 0.5% Tween20 (Fisher Scientific BP337), washed 3x5 minutes with 0.1% Tween20 solution (PBST), blocked with 2% Abdil (2% bovine serum albumin; Sigma Aldrich A4503 + 0.1% Tween20) for 1 hour, and stained with primary antibodies (1:200 CD31; Dako IS610 or 2.5 μg/mL von Willebrand Factor viii; Invitrogen MA5-14029) overnight at 4°C. 5x5 minute PBST washes were performed followed by staining with secondary antibody (1:500 Alexafluor 488 goat anti-mouse; Thermo Fisher A-11001) overnight at 4°C. 5x5 minute PBST washes were performed followed by staining with Hoechst (1:2000; Thermo Fisher H3570) for 10 minutes at room temperature. One final PBST wash was performed and cells were stored in PBST until imaged. Wells were imaged using a Leica DMI 4000 B Microscope (Leica Microsystems).

Matrigel Tube Formation Assay

100 μL of phenol red-free Matrigel (1.35 mg protein/well; Corning 356237) was pipetted into each well of a 96 well plate and polymerized in the incubator. 10,000 HEMECs were added per well (n=8 wells). Each well was imaged at 6 hours and 12 hours after seeding using a Leica DMI 4000 B Microscope (Leica Microsystems).

Synthesis and Fabrication of Methacrylamide-Functionalized Gelatin (GelMA) Hydrogels

GelMA was synthesized, dialyzed, lyophilized, and was found to have a degree of functionalization of 57%, determined via ^{1}H-NMR (65, 139, 155). Prior to cell culture experiments, lyophilized GelMA was sterilized for 30 minutes under UV light. Hydrogels were fabricated using a solution consisting of lyophilized GelMA (5 wt%) dissolved at 37°C in

phosphate buffered saline (PBS; Lonza 17-516F) and combined with 0.1% w/v lithium acylphosphinate (LAP) as a photoinitiator. Hydrogels were polymerized under UV light (λ=365 nm, 7.14 mW cm^{-2}; AccuCure Spot System ULM-3-365) for 30 s.

Endometrial Perivascular Niche Hydrogel Co-Cultures

Co-culture Fabrication and Maintenance

HEMEC and HESC were passaged and encapsulated in GelMA hydrogels at 1:1, 1:2, and 2:1 endothelial:stromal cell ratios. The concentration of endothelial cells was kept consistent with each ratio at 500,000 HEMEC/mL and the concentration of stromal cells was calculated from this value and the ratios. Hydrogels were cultured in 48 well plates for 7 days and maintained in ECM with or without additional growth factors (± 100 ng/mL recombinant human $VEGF_{165}$; PeproTech 100-20) and hormones. The medium for hydrogel samples was replaced every 3 days (800 μL/well). The endogenous VEGF concentration in ECM was reported to be 2 ng/mL by the vendor (ScienCell). All experiments except those in Fig. 2, 3, and 4 used charcoal-stripped fetal bovine serum (Sigma-Aldrich F6765) instead of regular fetal bovine serum to decrease endogenous hormones in the base medium.

Co-culture Decidualization

Decidualization of endometrial stromal cells was induced by culturing hydrogels in the presence of the following decidualization hormone cocktails: 1 μM medroxyprogesterone acetate (MPA; Sigma-Aldrich M1629) + 0.5 mM 8-bromodenosine 3',5'-cyclic monophosphate (8-Br-cAMP; Sigma-Aldrich B5386) or 0.5 mM dibutyryl cyclic AMP (dcAMP; Millipore Sigma 28745) + estradiol (E2; Sigma-Aldrich E2758) + progesterone (P4; Sigma-Aldrich P8783). Control

samples had no hormones added to the medium. Medium was replaced every 3 days, collected at days 3 and 6, and stored at -80°C.

Characterization of Perivascular Niche Cultures

Immunofluorescent Staining

On day 7 of culture, hydrogel samples were fixed with formalin (Sigma-Aldrich) and washed three times with PBS. Hydrogels were permeabilized for 15 minutes in a 0.5% Tween20 (Fisher Scientific BP337) solution and washed 3x5 minutes in 0.1% Tween20 solution (PBST). Samples were blocked for 1 hour at room temperature in a 2% Abdil solution (2% bovine serum albumin; Sigma Aldrich A4503 + 0.1% Tween20) and subsequently incubated in primary antibody solution (1:200 CD31 Dako IS610 + 1:200 CD10 Invitrogen PA5-85875 or 1:200 anti-laminin Abcam ab11575 or 5 μg/mL ZO-1 Invitrogen #61-7300) overnight at 4°C. 4x20 minutes washes with PBST were performed and then cultured in secondary antibody (1:500 Alexafluor 555 goat anti-rabbit Thermo Fisher A-21428 and/or 1:500 Alexafluor 488 goat anti-mouse Thermo Fisher A-11001) overnight at 4°C. Hydrogels were washed 4x20 minutes with PBST and then incubated for 30 minutes in Hoechst (1:2000; Thermo Fisher H3570). Samples were washed a final time in PBST and were stored in PBST until imaged.

Microscopy Techniques

Hydrogels were imaged using glass bottom confocal (In Vitro Scientific, D29-20-1-N) dishes on a DMi8 Yokogawa W1 spinning disc confocal microscope outfitted with a Hamamatsu EM-CCD digital camera (Leica Microsystems). Three 100 μm z-stacks with a 5 μm step size were taken for each hydrogel for 3 regions of interest (ROI) except for time course experiments and

laminin/ZO-1 stained hydrogels (n=2-3 hydrogels; n=2 ROI per hydrogel). For day 14 and day 21 hydrogels, 1 ROI was imaged which captured roughly 80-100% of the entire gel area. Fluorescent images were artificially brightened for figures but not for analysis.

Image Analysis

Images were analyzed using a computational pipeline consisting of a FIJI macro and custom MATLAB algorithm (156). This pipeline allows for 3D quantification of vessel networks across image z-stacks. Briefly, individual images of each z-stack were blurred, filtered, and binarized using a FIJI macro. Then, the binarized images were analyzed using a custom MATLAB algorithm that quantified total branches + endpoints, branch points, number of vessels, and total network length from skeletonized images. Using Microsoft Excel, we then calculated the total network length / mm^3, average branch length (network length / number of vessels), number of branches, and number of vessels for each sample.

To compute the degree of overlap between CD31 signal and laminin/ZO-1 signal, CD31 and laminin/ZO-1 Z-stacks were binarized using the same FIJI macro listed above. Compressed copies of the Z-stacks were also created to match the size of the binarized images. Average pixel intensity was generated for both stains and the degree of overlap was then calculated by multiplying the binarized matrix of vessels by the binarized matrix of the proteins (Unpublished method from Victoria Barnhouse et al. *in preparation*).

Cytokine Array

A Proteome Profiler Human Angiogenesis Array (R&D Systems ARY007) was used to determine relative levels of 55 angiogenesis-related proteins. Medium was collected at days 3 and 6 of culture, stored at -80°C until use, and pooled for analysis. 500 μL of medium was used for each day (1 mL total per cytokine array; n=3 samples per condition). The array was run as per the manufacturer's instructions and imaged (4 minute exposure) using an Amersham ImageQuant 800 Fluor system (Cytiva). Pixel density of each array spot was quantified using FIJI. The negative control spot averages were subtracted from the pixel density of each sample and then pixel density of each sample was normalized to the pixel density of positive control spots.

STRING Analysis

Statistical analysis was performed to determine which of the 55 angiogenesis-related proteins were statistically significantly different between groups. The resultant analysis revealed 14 significant proteins. These 14 proteins were entered into the STRING (Search Tool for the Retrieval of Interacting Genes/Proteins) Database to determine known and predicted protein-protein interactions (157-159). A network summary view was created using a medium confidence minimum required interaction score (0.400).

Trophoblast and Perivascular Niche Interactions

Perivascular Hydrogel Conditioned Media Effects on Trophoblast Motility

Control and decidualized perivascular hydrogels were cultured as described above. Media were collected during media changes on days 3 and 6 of culture, filtered, and stored at -20°C until use.

Unconditioned ECM was also collected for use as a control. Conditioned media from days 3 and 6 were pooled prior to adding to spheroid cultures. Spheroid motility assays were performed as described previously by our group (129, 139, 155). For these studies, we used Swan 71 cells derived from a 7-week first trimester placenta; however, no additional donor information was provided (160). Swan71 at passage one from receipt were cultured in growth medium consisting of phenol red-free DMEM (SCS Cell Media Facility, UIUC) supplemented with 10% charcoal-stripped fetal bovine serum, 1% penicillin/streptomycin, and 500 ng/mL puromycin. Once passaged for experiments, the cells were cultured in phenol red-free DMEM, 2% charcoal-stripped fetal bovine serum, and 1% penicillin/streptomycin (Swan71 motility medium). Cells were cultured in flasks until 80-90% confluence and added to round bottom plates (Corning 4515; 4,000 cells/well) for at least 48 hours on a shaker (60 rpm) in the incubator until spheroids formed. Individual spheroids were encapsulated in GelMA hydrogels and maintained in 800 µL of medium (Swan71 motility medium, 50:50 Swan71 motility medium:ECM, or 50:50 Swan71 motility medium:PVN-conditioned medium) for 3 days. Each encapsulated spheroid was imaged daily on a Leica DMI 4000 B microscope (Leica Microsystems). Total outgrowth area was calculated using the measure tool in FIJI by averaging three traced measurements of the outgrowth area. Fold change was calculated by normalizing outgrowth area to initial spheroid area (day 0).

Trophoblast Conditioned Media Effects on Perivascular Hydrogels

Swan71 at passage one from receipt were cultured in growth medium consisting of phenol red-free DMEM (SCS Cell Media Facility, UIUC) supplemented with 10% charcoal-stripped fetal bovine serum, 1% penicillin/streptomycin, and 500 ng/mL puromycin. Swan71 cells were

cultured in a T75 culture flask and medium was collected at confluence, syringe filtered, and stored at -20°C until use. Unconditioned growth medium was also collected for use as a control. Co-culture hydrogels were fabricated and cultured as described above in ECM (control), a 50:50 ratio of ECM to unconditioned Swan71 growth medium (media control), or 50:50 ratio ECM to Swan71 conditioned medium. Hydrogels were stained, imaged, and analyzed as described above.

Triculture of Endometrial Endothelial, Stromal, and Epithelial Cells.

Perivascular hydrogel cultures were prepared as described above and cast into Ibidi µ-Slides Angiogenesis (10 µL prepolymer solution; Ibidi 81506). Polymerized gels were then coated with Collagen 1 (EMD Millipore 08-115MI) and Collagen 3 (EMD Millipore CC054) using microbial transglutaminase (mTg; Zedira T001) (140, 141, 161). A 1:1 ratio of 0.5 mg/mL mTg and 10 µg/mL ECM protein (1:1 ratio Collagen 1 and Collagen 3) were combined and 20 µL of this solution was pipetted onto hydrogels. Coated hydrogels were incubated for 1 hour in 5% CO2 incubators at 37°C. A quick wash was performed using 20 µL of PBS. After the wash step, we seeded 200,000 EEC/cm^2 onto hydrogels. We cultured tricultures for 7 days and subsequently stained them with CD31 and phalloidin (7 µL per 1000 µL solution) or cytokeratin 18 (CK18; 1:250, Cell Signaling 24E10) using the protocol described above. We then took Z-stack images of each gel from the top of the gel as far down as we could visualize. We took 1 Z-stack per gel (n=2 gels per condition).

Statistics

OriginLab 2021b and RStudio were used for statistical analyses. Normality was determined via Shapiro-Wilkes and homoscedasticity was determined via Levene's test. Data were analyzed

using a one-way analysis of variance (ANOVA) and Tukey post hoc test (normal, homoscedastic), Welch's ANOVA and Games-Howell post hoc test (normal, heteroscedastic), Kruskall-Wallis ANOVA and Dunn's post hoc test (non-normal, homoscedastic), or Welch's Heteroscedastic F Test with Trimmed Means and Winsorized Variances and Games-Howell post hoc test (non-normal, heteroscedastic). Significance was set as $p<0.05$ and data are presented as mean ± standard deviation unless otherwise described. Each quantitative experiment used n=3-6 hydrogels unless otherwise noted. Plots were generated using OriginLab.

4.4 Results

Human endometrial microvascular endothelial cells (HEMEC) demonstrate angiogenic potential.

We first assessed characteristic phenotypic markers of endothelial cells and the ability of HEMEC to form vessel structures. HEMEC plated on 2D plates expressed CD31 (Fig. 16A) and von Willebrand factor (Fig. 16B). HEMECs plated on Matrigel formed tubes transiently that then fell apart in less than 24 hours (Fig. 16C). Taken together, these results demonstrate that HEMECs express characteristic endothelial cell markers and they have the potential to form vessel-like structures in culture.

Endometrial perivascular niche hydrogels can be cultured long term.

To assess longevity and stability of endometrial perivascular niche cultures (PVNs), we cultured PVNs created using 3 different endothelial to stromal cell ratios for 28 days. All conditions contained a constant number of endothelial cells (500,000 cells/mL) but varied in the amount of added stromal cells in 2:1, 1:1, and 1:2 endothelial:stromal ratios (250,000 cells/mL, 500,000

cells/mL, or 1,000,000 cells/mL, respectively). Notably, the ability to form stable perivascular models was tightly tied to the ratio of perivascular cells. For the 1:1 endothelial:stromal cell ratio, total network length, branches, and vessels all increased from days 7 to 14 but branch length decreased (Fig. 17B-E) and by day 21, all 1:1 hydrogels had disintegrated. Increasing the number of stromal cells (1:2 ratio) did not improve perivascular niche stability. For the 1:2 endothelial:stromal cell ratio, total network length, branches, and vessels all increased from days 7 to 14 but then decreased from days 14 to 21 (Fig. 17B-E). Branch length decreased between days 7 and 14 but increased between days 14 and 21. The 2:1 endothelial:stromal ratio contained the least amount of stromal cells but was most stable over time. The 2:1 endothelial:stromal ratio showed increasing metrics of total network length, branches, and vessels from days 7 to 21 while branch length appeared to remain consistent across all days with only a slight decrease over time (Fig. 17B-E). Unfortunately, none of the cultures remained stable through 28 days: hydrogels for all 3 variants were completely disintegrated.

Ratio of endothelial to stromal cells affects vessel complexity more so than addition of VEGF. Soluble VEGF was added to culture media to determine if additional exogenous proangiogenic factors would affect vessel complexity. We observed no significant differences in trends of metrics of perivascular network complexity as a result of VEGF inclusion (Fig. 18B-E), so we concluded that the endometrial PVNs do not need supplementation with additional proangiogenic factors. Based on these results and the results of the time course experiment, we selected the 2:1 ratio for all subsequent experiments because this condition resulted in the most consistent, stable networks over time.

PVN cultures deposit laminin and express tight junction marker ZO-1.

We then assessed metrics of basement membrane protein deposition and expression of tight junction proteins. Immunofluorescent staining demonstrated laminin, a common basement membrane protein, deposition by both cell types (Fig. 19B). Additionally, we confirmed ZO-1 expression with immunofluorescent staining, indicating tight junction expression in our cultures (Fig. 19C). We then quantified the degree of overlap between vessels (CD31+) and laminin/ZO-1 (Fig. 19D-E). Laminin and CD31 had a 31.3% average overlap. ZO-1 had a 26.9% overlap. These results suggest that laminin and ZO-1 are expressed in close proximity to the endometrial perivascular networks formed within gelatin hydrogels.

Endometrial stromal cell decidualization status modulates endometrial PVN complexity.

We subsequently examined decidualization processes within the engineering endometrial perivascular networks using two common decidualization protocols. The first used the synthetic progestin medroxyprogesterone acetate (MPA) while the other used progesterone (P4). Shifts in perivascular network parameters in response to decidualization factors were compared to each other as well as to the control condition (no decidualization hormones). Total network length, branches, and vessels were greater for the MPA decidualization condition compared to control (Fig. 20B-E). Branch length was lower compared to the control for the MPA and P4 groups (Fig. 20D). Total number of vessels increased for both decidualization conditions, with the MPA decidualization condition having the largest total number of vessels (Fig. 20E). Total network length and branches were not different between control and P4 decidualization conditions (Fig. 20B-C). Total network length and average branch length were not different between MPA and P4 groups but total branches were increased in the MPA group compared to the P4 group (Fig.

20B-E). Taken together, these results suggest decidualization status as well as choice of decidualization hormone cocktail strongly influence vessel network complexity in gelatin hydrogels.

Decidualization status strongly influences endometrial PVN secretome.

We subsequently used a cytokine array was used to detect qualitative differences in secretion by perivascular cultures across the three conditions (control, decidualized-MPA, decidualized-P4). We quantified the average mean pixel density of cytokine spots and normalized it to the positive control spots (Fig. 21B). We compared secretion of characteristic decidual markers prolactin and IGFBP-1 (insulin-like growth factor binding protein 1) in decidualized conditions compared to control (Fig. 21C). We observed an increase in prolactin and IGFBP-1 in decidualized conditions compared to control, strongly indicating that the stromal cells were decidualized in the presence of decidualization hormones. Subsequently, we performed statistical analysis across the 55 proteins to assess which were statistically significantly different across groups. We identified 14 proteins with significantly different levels: activin A, angiogenin, angiopoietin-1, amphiregulin, endoglin, endostatin/collagen XVIII, endothelin-1, FGF-1 (FGF acidic), IGFBP-2, Pentraxin 3 (PTX3), PDGF-AA, Platelet Factor 4 (PF4), Prolactin, and Serpin F1 (Fig. 21D; Table 1). P-values for statistical analysis can be found in Supplemental Information Figure 2. We then used STRING to generate a network summary of predicted protein associations between the 14 proteins (Fig. 21E). The STRING network contained 14 nodes, 25 edges, 3.57 average node degree with an average local clustering coefficient of 0.495 and PPI enrichment p-value < $1.0x10^{-16}$. STRING analysis demonstrated numerous interactions between these factors, except for PF4, Prolactin, and Amphiregulin. Gene ontology analysis from STRING suggests that these

cytokines play numerous roles, notably in blood vessel development and branching, regulation of endothelial cell proliferation, and branch elongation of an epithelium. The molecular functions of these cytokines include activin, growth factor, and glycosaminoglycan binding and receptor ligand activity. Most of these cytokines are associated with the basement membrane, ECM, extracellular space, and cytoplasmic vesicles.

Perivascular niche secreted factors influence trophoblast invasion, but trophoblast secreted factors do not affect vessel network complexity.

We then examined whether reciprocal crosstalk between endometrial perivascular cells and trophoblast cells influences cell activity. We first examined how perivascular niche secreted factors affect trophoblast motility. We then assessed whether and how trophoblast secreted factors influenced perivascular niche complexity. We quantified Swan71 trophoblast outgrowth area for 3 days after treatment with conditioned media from control and decidualized perivascular niche hydrogel cultures (Fig. 22). We found that outgrowth area after encapsulation had no difference between groups (Fig. 22B); however, by day 3, we observed significant (p=3.8x10^{-5}) differences across groups for outgrowth area and fold change in outgrowth area compared to day 0 (Fig. 22C). Dunn's post hoc analysis revealed four significant differences between outgrowth area groups: conditioned media (control-not decidualized) and conditioned media (MPA-decidualized) (p=4.35x10^{-5}), conditioned media (control-not decidualized) and control (p=0.016), conditioned media (MPA-decidualized) and conditioned media (P4-decidualized) (p=0.036), and conditioned media (MPA-decidualized) and media control (p=0.011). Fold change was then calculated by normalizing initial spheroid outgrowth area to

outgrowth area on day 3. This trend was also observed in fold change in outgrowth area, with p=3.69x10^{-5}, p=0.016, p=0.046, and p=0.011, respectively.

Next, we quantified metrics of vessel network complexity in the presence an absence of conditioned medium from Swan71 trophoblast cells (Fig. 23). We observed no differences in total network length/mm^3, total number of branches, and total number of vessels in the presence of conditioned media from Swan71 cells (Fig. 23B,C,E); however, branch length was decreased between the media control (50:50 media ratio) and control (Swan71 invasion media) conditions (Fig. 23D), likely due to increased serum content that was not depleted by cells.

Demonstration of a stratified endometrial epithelial culture overlaying a perivascular niche

Finally, we fabricated an endometrial triculture model to replicate the stratified structure of the *in vivo* endometrium by overlaying primary endometrial epithelial cells over the embedded perivascular culture (Fig. 24). This resulted in a model consisting of two stratified components: an epithelial culture and an embedded perivascular culture. Using Volume Viewer in FIJI, we observed an epithelial layer overlaying our perivascular compartment (Fig. 24B). Then, to assess epithelial cell morphology and phenotype, we stained our cultures with CK18 which is also a marker of epithelial cell attachment (Fig. 24C). We observed regions of epithelial monolayers that positively express CK18 which demonstrates that the epithelial cells are attached to the gel.

4.5 Discussion

Understanding endometrial angiogenesis is important for a variety of reasons. Angiogenesis and vessel remodeling in the endometrium occurs during the menstrual cycle as the tissue is rebuilt and differentiates to prepare for potential pregnancy. Subsequently, if successful implantation occurs, trophoblast cells from the blastocyst will remodel the existing vasculature to provide blood flow to the growing fetus and placenta. Here, we demonstrate the creation of a three-dimensional artificial endometrial perivascular niche embedded in gelatin hydrogels. We demonstrate hormone-responsiveness of the perivascular cultures in the presence of decidualization hormones and quantify variation in network complexity and soluble factor secretion across conditions. We then use these cultures to determine how crosstalk between the perivascular niche and trophoblast cells affect trophoblast motility and network complexity. Finally, we demonstrate the creation of an endometrial model consisting of primary endometrial epithelial cells overlaying the perivascular cultures. Taken together, we have defined elements of a stratified endometrial model system that offers significant potential to gain mechanistic insight into endometrial remodeling and changes in endometrial vascular networks in response to decidualization factors.

Most existing *in vitro* models of vasculature utilize human umbilical vein endothelial cells (HUVECs) as their endothelial cell source due to their wide availability, capacity to be passaged numerous times, and excellent ability to form vessels *in vitro* (162). However, HUVECs are derived from umbilical cords and are not tissue-specific which calls into question the use of such cells for the development of tissue-specific vasculature models. Here, we utilize HEMECs as an endothelial cell source to create an endometrial-specific model of the endometrial perivascular

niche. We also used HESCs as an endometrial stromal cell source. The addition of a stromal population to endothelial cells encourages and supports formation of endothelial networks for long-term culture (163-165). Without stromal cells, endothelial cells form endothelial structures that last only transiently and fall apart over time, consistent with our results from our tube formation assay. To determine the best ratio of endothelial to stromal cells for our perivascular cultures, we tested 3 ratios of cells (1:1, 1:2, and 2:1). From these experiments, we determined that a 2:1 ratio of endothelial to stromal cells was best because this ratio allowed for 20+ days of perivascular culture and was most consistent over time. Our studies suggest that less stromal cells are conducive to perivascular stability over time. Our observations suggest that this is because stromal cells are highly contractile and contract the gel matrix over time. More stromal cells result in more gel contraction which tends to increasingly shrink gels over time and lead to disintegration.

We then demonstrate that endometrial perivascular cultures do not need exogenous pro-angiogenic factors (VEGF) added to media to promote network formation. Further, these cultures express markers of vessel network maturity such as basement membrane protein deposition and tight junction markers. Our artificial perivascular cultures demonstrate some similarities to the native endometrium. The average vessel length per branch point was determined to be approximately 100-200 μm across the menstrual cycle and this value varies depending on cycle phase (92). Although our average branch values were less than these *in vivo* values, we observed significant differences in network complexity with the addition of hormones. This indicates that perivascular cultures formed *in vitro* from endometrial derived endothelial and stromal cells are hormone responsive. Given emerging literature seeking to better define population variation in

hormone concentration across the menstrual cycle, an engineered endometrial perivascular network may provide the opportunity to quantify shifts in vessel complexity in response to exogenous hormone signals representative of discrete menstrual cycle phases. Future work to assess lumen formation and patent vessels would allow for the creation of perfusable networks to assess molecule transport and vessel perfusion in the context of pregnancy.

We subsequently sought to determine how decidualization status of stromal cells affects the perivascular niche. Decidualization is necessary and critical to prepare the endometrium for a potential pregnancy (144). Recapitulating such a process may be important for an endometrial model system used to study implantation events. For these studies, we chose two decidualization protocols commonly used in the literature (72, 107, 108, 166-168). One employs the synthetic progestin medroxyprogesterone acetate (MPA) and the other uses progesterone (P4). Across our studies, we observed differences in the effects of these two protocols in our perivascular cultures, notably the effects of the P4-decidualized condition did not seem to increase total network length/mm^3, total vessels, and total branches as much as the MPA-decidualized condition and we also observed differences in the soluble factor secretion between these decidualization conditions as well. This indicates that the mode of decidualization affects network complexity and soluble factor secretion so choice of decidualization protocol may impact cellular behavior. Analysis of our perivascular cultures in the absence and presence of decidualization hormones revealed an increasing trend for total network length/mm^3, total number of branches, and total number of vessels with the addition of hormones; however, the mode of decidualization affected these results. On the other hand, branch length significantly decreased with the addition of hormones. Observations from human specimens demonstrate that the endometrial spiral arterioles grow,

lengthen, and coil during the secretory phase of the menstrual cycle (phase when decidualization occurs) (55). These data are consistent with our observations, further demonstrating that this model system captures endometrial physiologic responses *in vitro*.

Next, we analyzed the secretome of our control and decidualized cultures to determine differences in secreted factors. Our analysis of the perivascular secreted factors detected 14 cytokines with statistically significant differences between the conditions: Activin A (Gene ID 3624), Amphiregulin (AR; Gene ID 374), Angiogenin (ANG; Gene ID 283), Angiopoeitin-1 (Ang-1; Gene ID 284), Endoglin (ENG; CD105; Gene ID 2022), Endostatin/Collagen XVIII (Gene ID 80781), Endothelin-1 (ET-1; Gene ID 1906), FGF acidic (FGF-1; Gene ID 2246), IGFBP-2 (Gene ID 3485), PDGF-AA (Gene ID 5154), Pentraxin 3 (PTX3; TSG-14; Gene ID 5806), Platelet Factor 4 (PF4; CXCL4; Gene ID 5196), Prolactin (Gene ID 5617), and Serpin F1 (PEDF; Gene ID 5176). These 14 proteins can be broadly characterized into proteins associated with angiogenesis, vessel stabilization, and vessel maturation (Angiogenin, Angiopoietin-1, Endostatin/Collagen XVIII, FGF-1, PDGF, PTX3, Serpin F1), proteins relevant to endometrial function and receptivity (Amphiregulin, Endoglin, Endothelin-1, IGFBP-2, PF4), proteins relevant to decidualization and stromal cells (Activin A, Angiogenin, PDGF, Prolactin).

Angiogenin, Angiopoietin-1, Endostatin/Collagen XVIII, FGF-1, PDGF, PTX3, and Serpin F1 are related to angiogenesis, vessel stabilization, and vessel maturation. Angiogenin is a heparin-binding protein found to induce angiogenesis (169). In the context of endometrial function, Western Blot analysis indicated that angiogenin expression is enhanced in the decidualized endometrium (169). Endometrial stromal cells treated with progesterone did not show

differences in angiogenin concentrations until after 14 days of culture which may explain why we did not observed increased angiogenin levels compared to the control after only 6 days of culture (169). Dibutyryl cAMP was also found to increase angiogenin concentrations but the shorter timeframe for our experiments could explain why we did not see a significant increase in our samples (169). Ang-1 plays a role in maintaining vessel integrity and vascular remodeling (145). In concert with VEGF-A, Ang-1 increases vessel diameter and vascular network maturation (145). Low levels of Ang-1 are found in endometrial stromal fibroblasts and this decreases over the menstrual cycle (170). We observed a significant decrease in Ang-1 in one of the decidualization conditions compared to control. Although the second condition did not show a significant decrease, it did appear to be slightly lower than the control values. Endostatin is an inhibitor of angiogenesis but plays a role in maturation and stabilization of endothelial tubes (171). We observed slight increases in endostatin in decidualized cultures compared to the control which could indicated maturation and stabilization of cultures in the presence of hormones. FGF-1 is part of the fibroblast growth factor family and is a heparin-binding protein shown to promote angiogenesis (170, 172). FGF-1 is found in the endometrium but is more prevalent in endometrial epithelial cells compared to endometrial stromal cells (170). FGF-1 was increased in decidualized samples. Insulin-like growth factors (IGFs) are regulated in part by their binding proteins (IGFBPs) (173). PDGF-AA (the AA isoform of platelet-derived growth factor) is a growth factor shown to have roles in cell proliferation, angiogenesis, inflammation, and tissue repair (174). In the endometrium, PDGF is likely produced by endometrial stromal cells and also induces their proliferation, motility, and contractility (174). PDGF-AA was increased in decidualized samples which could indicate greater proliferation or motility of cells. PTX3 plays roles in immune response, angiogenesis, and extracellular matrix remodeling (175).

PTX3 has also been shown to play a key role in female fertility, specifically in mice studies (175). Studies have demonstrated that *Ptx3* null mutant mice had severe defects, including defective decidualization, that led to infertility (175). Furthermore, PTX3 expression was observed to be higher in the decidua in proximity to trophoblast and *PTX3* expression was shown to be upregulated by trophoblast conditioned medium (175). This suggests that PTX3 is likely important in stromal cell decidualization and implantation, although the mechanisms surrounding this remain unknown in humans. We observed decreased secretion of PTX3 in decidualized samples. Finally, Serpin F1 is part of the serine protease inhibitor (serpin) family but only structurally, not functionally (176). Serpin F1 is antiangiogenic and is shown to be increased by progesterone and decreased by estradiol (176). This contrasts with our results which showed that the E2+P4+dcAMP decidualization condition had significantly more Serpin F1 compared to control and MPA+8-Br-cAMP conditions.

Amphiregulin, Endoglin, Endothelin-1, IGFBP-2, PF4 are proteins relevant to endometrial function and receptivity. Amphiregulin is a member of the epidermal growth factor (EGF) family and has a role in uterine receptivity and blastocyst attachment (177). Amphiregulin has been found in the luminal epithelium at the site of blastocyst apposition and its expression is correlated with an increase in progesterone levels and blastocyst attachment (177). Our data also demonstrate this trend, with significantly increased levels of Amphiregulin in decidualized cultures. Endoglin is a TGFβ receptor and is expressed in uterine endothelial and stromal cells (178). In mice, endoglin expression was shown to increase during the receptive phase of the menstrual cycle (178). We did not observe this trend in our cultures. Endothelins have vascular effects including vasoconstriction and also play a role in myometrial contraction (144, 179).

These roles are crucial for menstruation as well as pregnancy. Endothelin was increased in decidualized samples. IGFBP-2 in particular has been shown to be localized to the endometrial stroma and more abundant in the secretory phase according to Northern Blot analysis of endometrial mRNA (180). These observations contrast with our observations. We observed significantly more IGFBP-2 levels in control samples compared to the decidualized samples. CXCL4 is part of the CXC family and plays a role in chemotaxis of neutrophils and monocytes as well as inducing differentiation of peripheral blood monocytes (181). P4, also called CXCL4, inhibits endothelial cell proliferation and has been detected at high concentrations at regions of vascular injury, suggesting it may have a role in repair (181). In the endometrium, *CXCL4* mRNA was detected in human biopsy samples through the menstrual cycle and immunohistochemistry data showed increased staining intensity during the secretory and menstrual phases (181). CXCL4 is regulated by progesterone withdrawal which suggests it likely has a role in endometrial repair following menses (181). Our results were consistent with these data: CXCL4 secretion was increased in decidualized samples.

Activin A, Angiogenin, PDGF, Prolactin are proteins relevant to decidualization and stromal cells. Activin A is a member of the TGFβ family and has been found to play roles in tissue remodeling and stimulation of follicle-stimulating hormone (FSH) (182). Activin A is produced in high concentrations by decidualized stromal cells and interacts with matrix metalloproteinases (MMPs) to promote matrix remodeling in the decidual response (182, 183). Our data were consistent with these previous observations: we observed significantly increased levels of Activin A in decidualized perivascular hydrogels compared to control.

Although much of our data are consistent with the literature, differences could be due to donor variability or the use of cell lines instead of primary cells (76, 153, 154). For example, previous data using endometrial epithelial cells noted donor to donor differences in epithelial cell behavior so we would suspect to see potential differences in the use of donor-derived HEMECs as well (76). This could be further explored using additional cells from more donors. Furthermore, signaling from other cells in the endometrium (e.g., epithelial cells, natural killer cells, immune cells, etc.) could alter the secretome of stromal and endothelial cells which could account for some of these differences (97, 145, 184, 185). Expanded studies using additional endometrial cell types could begin to probe these differences and glean additional insights into the secretome of other endometrial cells.

We then assessed crosstalk between the endometrial perivascular niche and Swan 71 trophoblast cells. The conditioned media control condition (conditioned media from non-decidualized perivascular cultures) increased trophoblast motility the most compared to the other conditions. Interestingly, the two decidualization conditions (MPA- and P4-decidualized) induced differential responses regarding trophoblast motility. Interestingly, the P4-decidualized condition medium showed an increase in trophoblast motility compared to the control (Swan71 invasion medium); however, the MPA-decidualized condition did not and showed less outgrowth area compared to the control. Although conditioned media (MPA- and P4-decidualized) from decidualized perivascular networks only induced a moderate increase in trophoblast motility, this only represents a single condition of hormone stimulation targeting initial decidualization events. There is a significant opportunity for future efforts to examine how trophoblast motility change in response to a more complex, dynamic secretome based on hormone concentrations

representative of greater shifts across the menstrual cycle. Notably, treatment of perivascular cultures with Swan71 trophoblast conditioned medium did not change the majority of markers used to assess vessel complexity; however, we did observe decreased branch length in the media control condition (50:50 ratio Swan71 invasion medium and ECM medium) compared to the control condition (Swan71 invasion medium). This could be because the Swan71 unconditioned growth medium contains less proangiogenic factors compared to ECM.

Finally, we demonstrate the creation of an endometrial triculture consisting of an endometrial epithelial layer overlaying the embedded perivascular system. Our work herein demonstrates an endometrial model of increased complexity compared to existing models that incorporates three endometrial cell types in one model system. We chose collagen I and collagen III as the basement membrane layer because our previous work demonstrated that this combination of ECM biomolecules resulted in the best epithelial cell attachment (161). Our model expands upon existing stratified endometrial model systems because we have added additional complexity by not only including stromal cells but also endothelial cells to create an embedded vascular culture instead of only an embedded stroma (76). Future work consists of quantification of vessel network metrics for the triculture and further hormonal work to determine how decidualization affects not only the perivascular compartment but also the epithelial layer.

Future opportunities for these studies include development an endometrial perivascular niche using primary endometrial stromal cells. HESCs are the most widely used cell line for endometrial stromal cells; however, as hTERT-immortalized cells, they may not mimic endometrial stromal cells as closely as primary cells could. The use of patient-derived cells could

ameliorate this challenge and provide additional insights into endometrial perivascular function. Additionally, we report data from only one point in the menstrual cycle. We aim to quantify metrics of network formation across the entire menstrual cycle to assess cyclic vessel formation and remodeling. Furthermore, studies in humans have shown variation in menstrual cycle length and hormone profiles (33, 186). To capture patient variation in our model system, our future studies will incorporate different hormone profiles.

4.6 Conclusions

Here, we describe the creation of an artificial endometrial perivascular niche embedded in GelMA hydrogels. Engineered endometrial perivascular cultures display hormone-responsiveness in our cultures, including variation in network complexity and secretion of soluble factors. Perivascular network conditioned medium increased trophoblast motility in spheroid motility assays; however, trophoblast conditioned medium showed limited effect on perivascular niche complexity. Finally, we create a stratified endometrial model consisting of an endometrial epithelium overlaying an embedded perivascular niche. Tissue engineering models such as these not only provide novel platforms for assessing endometrial function but also allow us to probe questions regarding implantation that are currently impossible to answer in humans due to ethical constraints, challenging time points, and lack of imaging modalities. With the creation of these platforms, we hope to provide researchers with novel technologies that can further the field of female reproductive health.

4.7 Table

Table 3. Relevance of cytokines to endometrial function.

Protein	Relevance	References
Activin A	Expressed in decidualized stromal cells	(182, 183)
Amphiregulin	Role in receptivity and blastocyst attachment	(177)
Angiogenin	Angiogenesis; Decidualization	(169)
Angiopoetin-1	Maintains vessel integrity and vascular remodeling	(145, 170)
Endoglin	Endometrial receptivity	(178)
Endostatin/Collagen XVIII	Maturation and stabilization of vessels	(171)
Endothelin-1	Vasoconstriction; Myometrial contraction	(144, 179)
FGF-1	Angiogenesis	(170, 172)
IGFBP-2	Found in stroma; Abundant in secretory phase	(173, 180)
PDGF	Angiogenesis; Stromal cell motility and proliferation	(174)
Pentraxin 3	Angiogenesis; Matrix Remodeling; Inflammation; Decidualization	(175)
Platelet Factor 4	Repair following menses	(181)
Prolactin	Decidualization	(35)
Serpin F1	Regulation of angiogenesis	(176)

4.8 Figures

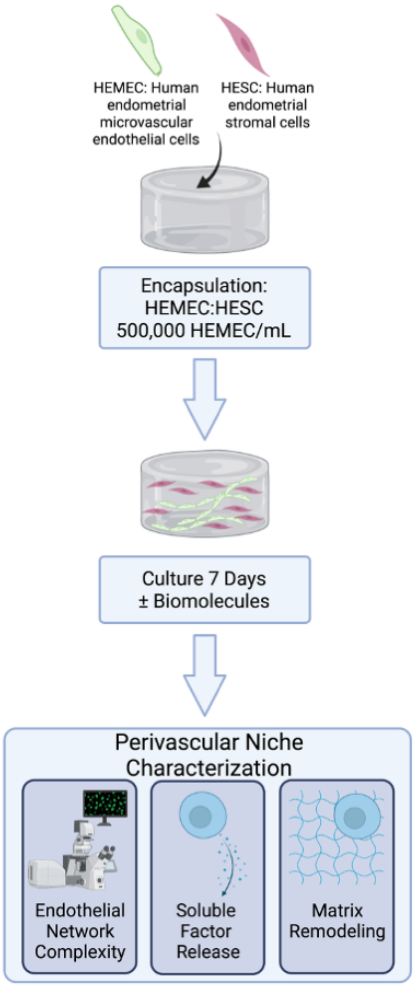

Figure 15. Development and characterization of an artificial endometrial perivascular niche model. Encapsulated endometrial endothelial and stromal cells are co-cultured in methacrylamide-functionalized gelatin hydrogels for 7 days and are subsequently analyzed for vessel network complexity, soluble factor secretion, and matrix remodeling. Created with Biorender.com.

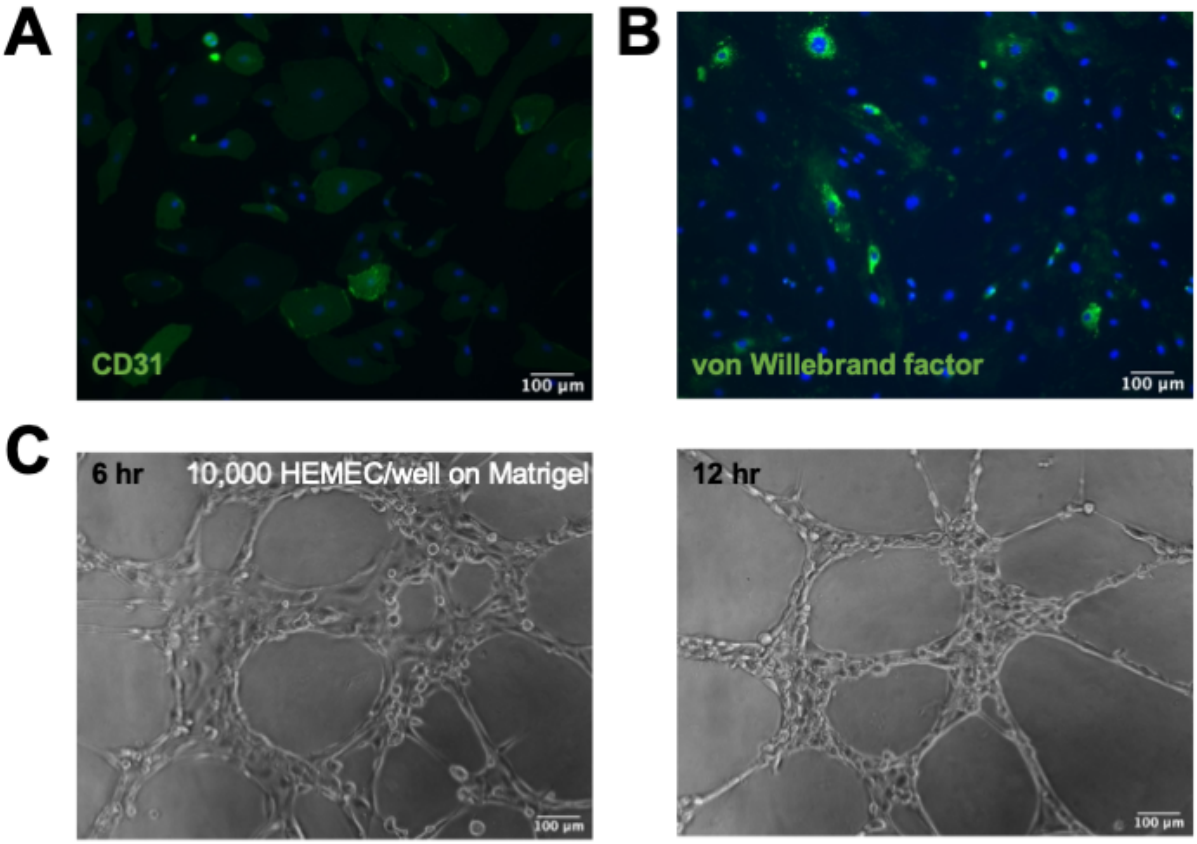

Figure 16. Angiogeneic potential of human endometrial microvascular endothelial cells (HEMEC). HEMEC cultured on well plates express characteristic endothelial cell markers such as **(A)** CD31 (cluster of differentiation 31) and **(B)** von Willebrand factor. **(C)** HEMEC demonstrate the ability to form tubes on Matrigel that form transiently and fall apart in less than 24 hours. Scale bar: 100 µm.

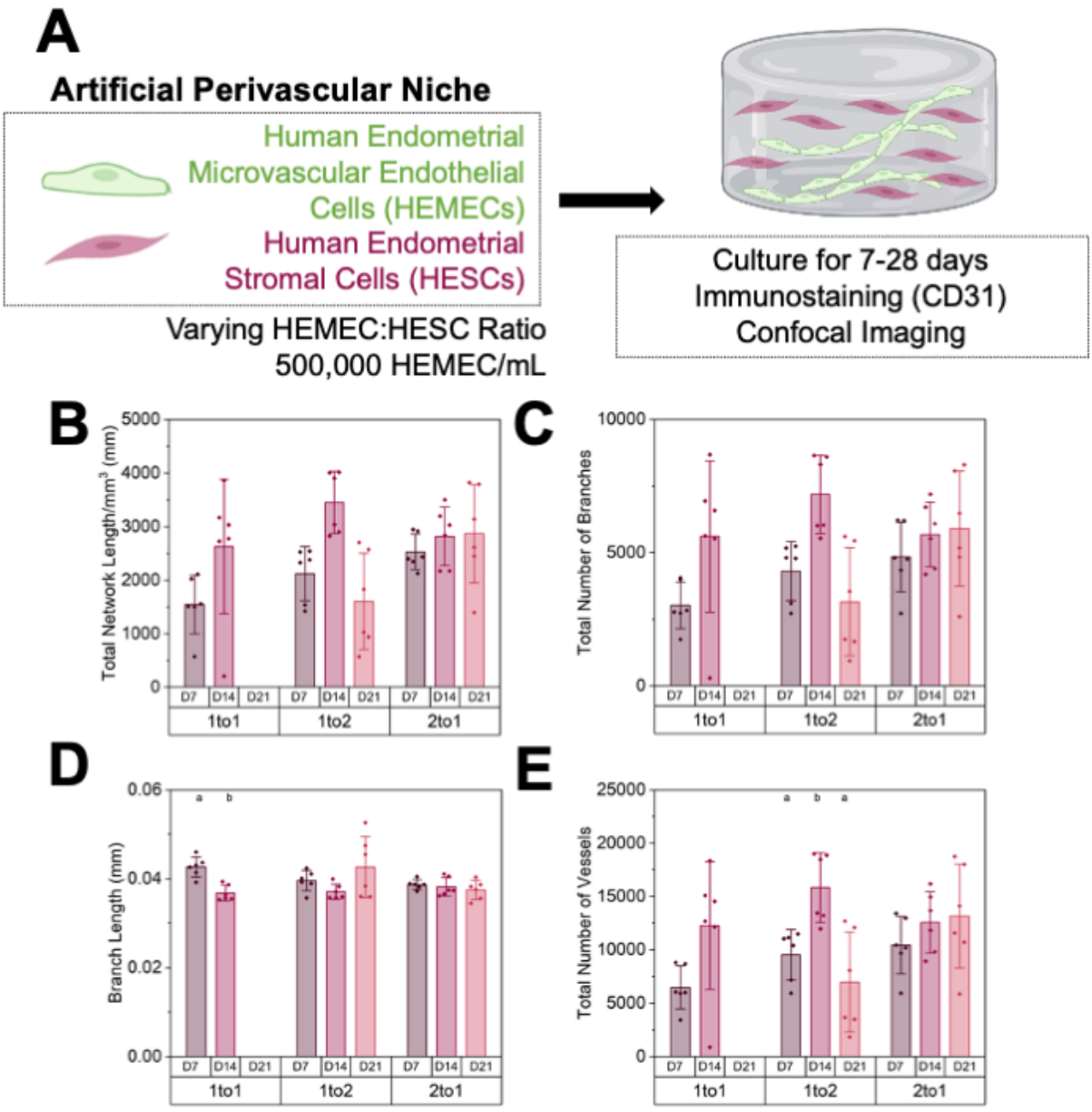

Figure 17. 28-day culture of an artificial endometrial perivascular niche. (A) Experimental summary. **(B)** Quantification of total vessel length per mm^3 , **(C)** total number of branches, **(D)** average branch length, and **(E)** total number of vessels at days 7, 14, and 21 (n=6 hydrogels per condition; 3 ROI imaged per gel and averaged) of varying endothelial to stromal cell ratios.

Figure 17 (cont), Groups with different letters are statistically significantly different from each other. Data presented as mean ± standard deviation. Created with Biorender.com.

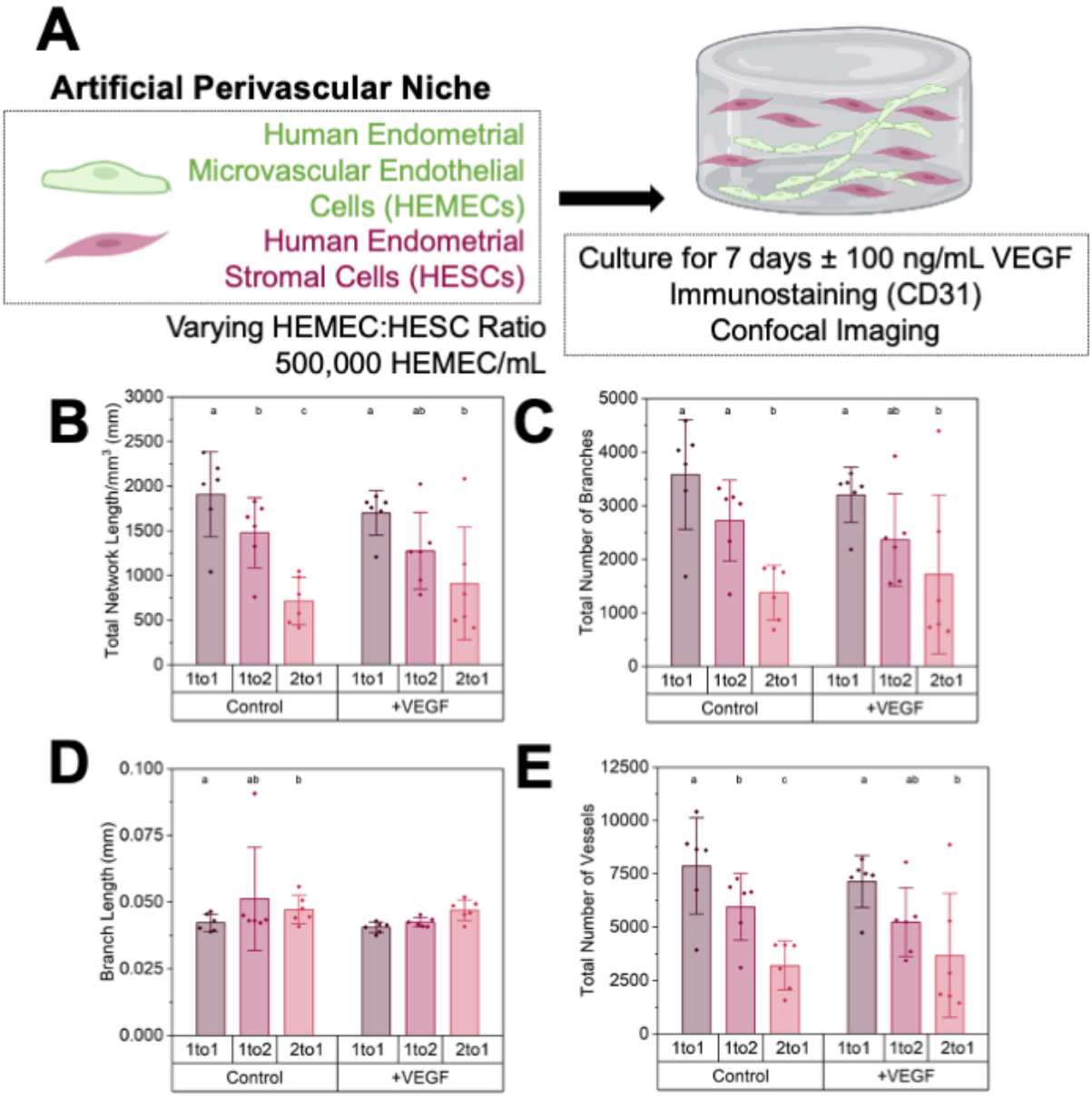

Figure 18. Optimization of an artificial endometrial perivascular niche. (A) Experimental summary. **(B)** Quantification of total vessel length per mm^3 , **(C)** total number of branches, **(D)** average branch length, and **(E)** total number of vessels for control and vascular endothelial growth factor (VEGF) samples (n=6 hydrogels per condition; 3 ROI imaged per gel and averaged) of varying endothelial to stromal cell ratios. Groups with different letters are

Figure 18 (cont), statistically significantly different from each other. Data presented as mean ± standard deviation. Created with Biorender.com.

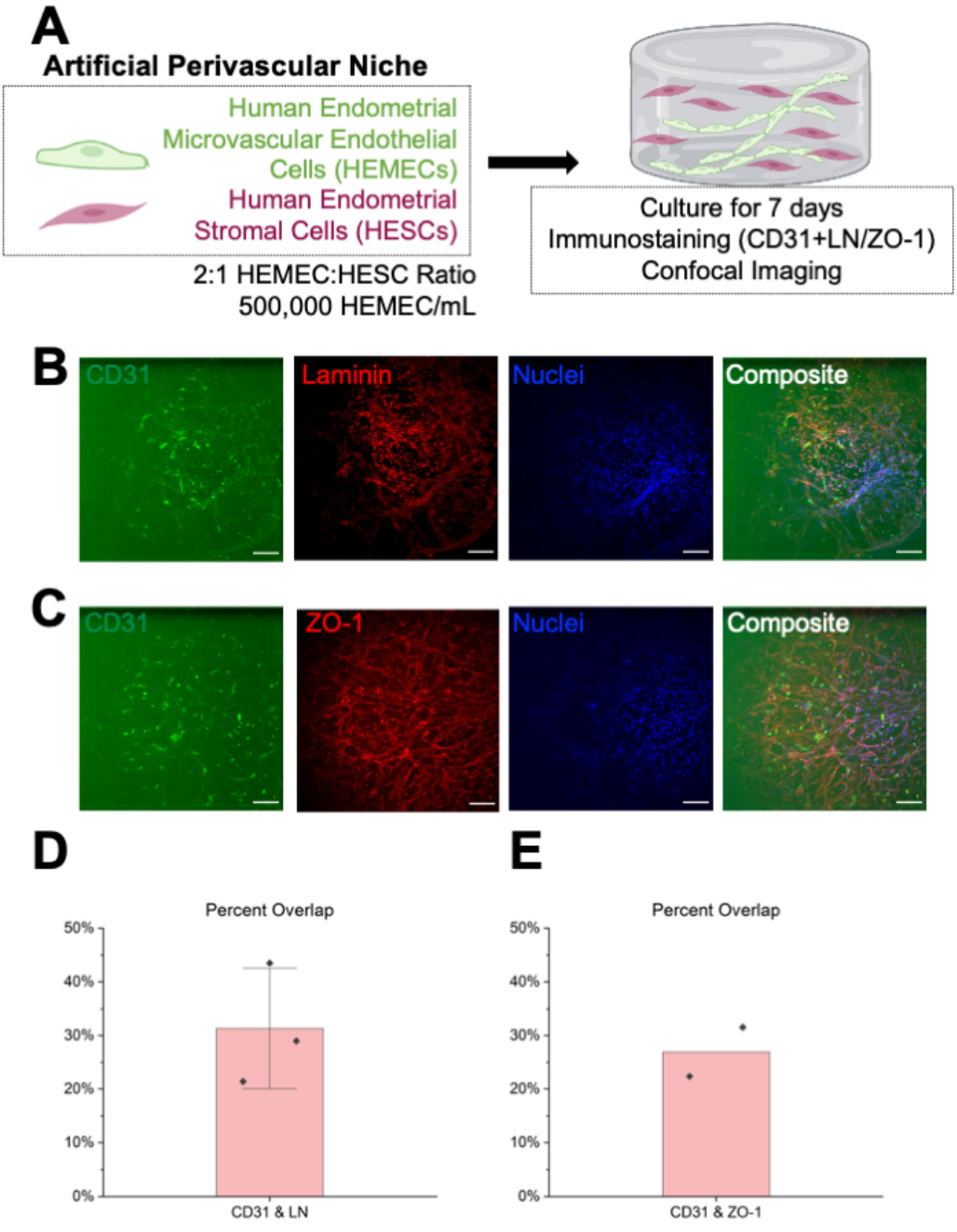

Figure 19. Characterization of extracellular matrix deposition and tight junction expression in perivascular cultures. (A) Experimental summary. Maximum intensity

Figure 19 (cont), projections of Z-stacks of artificial endometrial perivascular niche hydrogel cultures stained for CD31 (HEMEC-endothelial cells) and **(B)** laminin **(C)** and ZO-1. Green-CD31; Red-Laminin or ZO-1; Blue-Nuclei. Percent overlap was calculated between CD31 signal and **(D)** laminin and **(E)** ZO-1. n=2-3 hydrogels per condition. Data presented as mean ± standard deviation. 2 ROI imaged per gel. Scale bars: 100 μm. Images artificially brightened for visualization using FIJI. Created with Biorender.com.

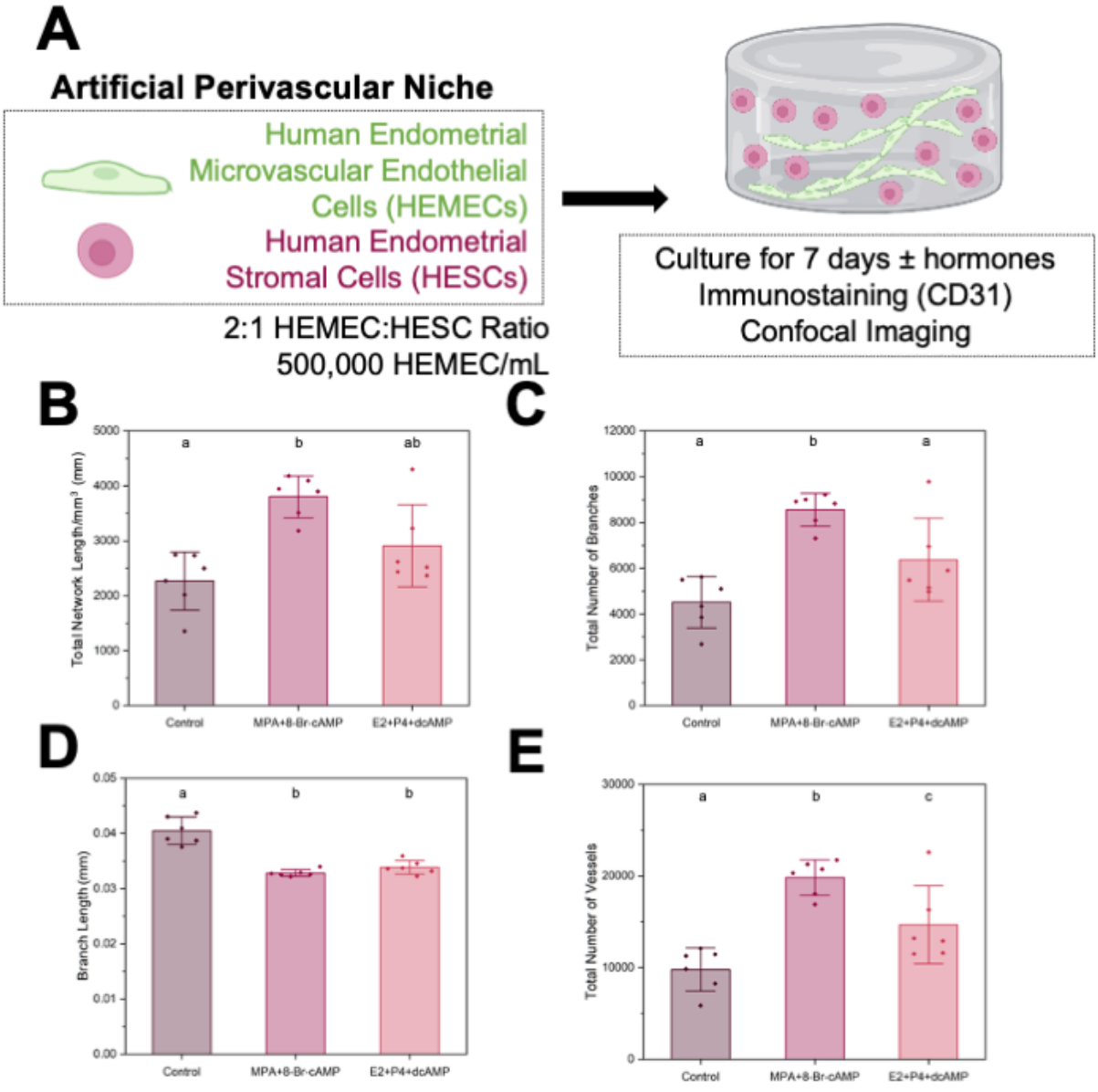

Figure 20. Stromal cell decidualization in an artificial endometrial perivascular niche. (A) Experimental summary. **(B)** Quantification of total vessel length per mm^3 , **(C)** total number of branches, **(D)** average branch length, and **(E)** total number of vessels for control and decidualized samples (n=6 hydrogels per condition; 3 ROI imaged per gel and averaged). Two decidualization conditions were tested. Control condition contained no added decidualization hormones. Groups with different letters are statistically significantly different from each other. Data presented as

Figure 20 (cont), mean ± standard deviation. MPA: medroxyprogesterone acetate, Br-cAMP: bromoadenosine cyclic AMP, E2: estradiol, P4: progesterone, dcAMP: dibutyryl cyclic AMP. Created with Biorender.com.

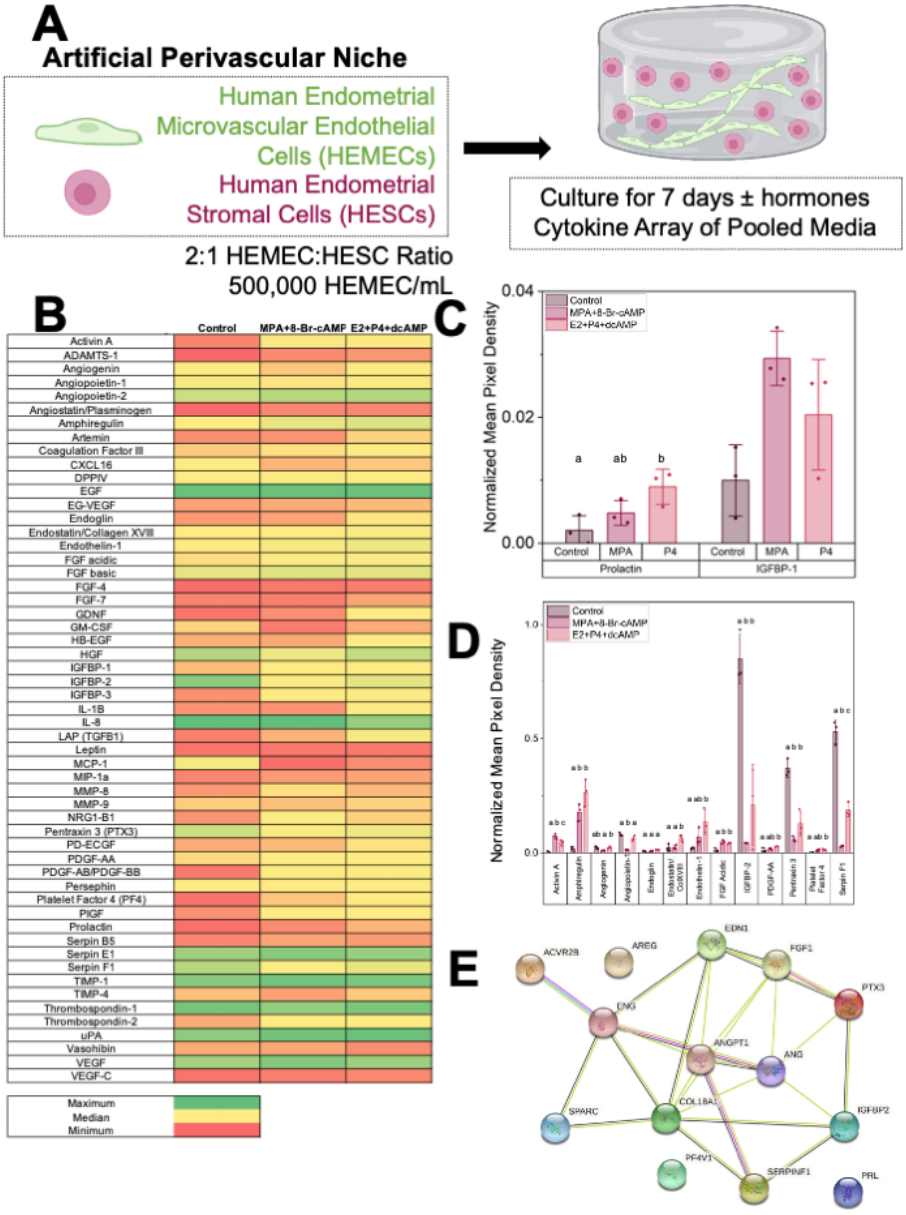

Figure 21. Cytokine secretion across control and decidualized artificial perivascular niche samples. (A) Experimental summary. **(B)** Cytokine array normalized mean pixel density results. **(C)** Normalized mean pixel density for characteristic decidual proteins Prolactin and IGFBP-1

Figure 21 (cont), across groups. **(D)** Normalized mean pixel density for statistically significantly different cytokines across groups. Groups with different letters are statistically significantly different from each other. Data presented as mean ± standard deviation. MPA: medroxyprogesterone acetate, Br-cAMP: bromoadenosine cyclic AMP, E2: estradiol, P4: progesterone, dcAMP: dibutyryl cyclic AMP. N=3 hydrogels per condition. **(E)** STRING analysis of statistically significantly different cytokines in homo sapiens. Red line-fusion evidence. Green line-neighborhood evidence. Blue line-concurrence evidence. Purple line-experimental evidence. Yellow line-textmining evidence. Light blue line-database evidence. Black line-coexpression evidence. COL18A1-Collagen alpha-1 (XVIII). ANGPT1-Angiopoetin-1. FGF1-Fibroblast growth factor 1. AREG-Amphiregulin. PTX3-Pentaxin-related protein 3. EDN1-Endothelin-1. ENG-Endoglin. ANG-Angiogenin. PRL-Prolactin. ACVR2B-Activin receptor type-2B. PF4V1-Platelet factor 4 variant. IGFBP-2-Insulin-like growth factor binding protein 2. FGF1-Fibroblast growth factor 1. SERPINF1-Pigment epithelium derived factor. Created with Biorender.com.

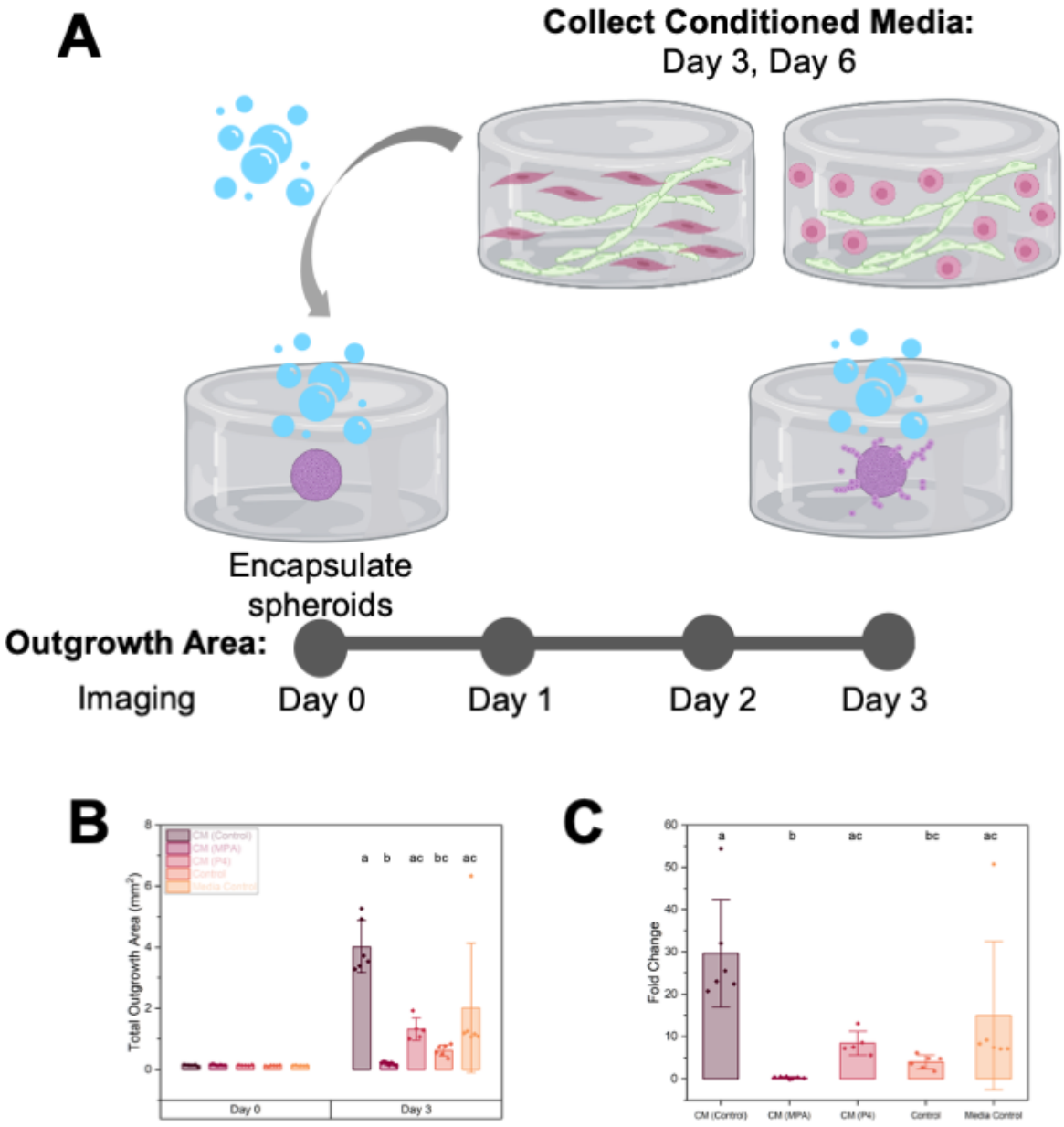

Figure 22. The effects of perivascular conditioned media on trophoblast motility. (A) Experimental summary. (B) Quantification of total outgrowth area (mm^2) and (C) fold change in outgrowth area at Day 3 compared to Day 0 (encapsulation). Groups with different letters are statistically significantly different from each other. Data presented as mean ± standard deviation. CM: Conditioned Media, MPA: medroxyprogesterone acetate, P4: progesterone. Created with Biorender.com.

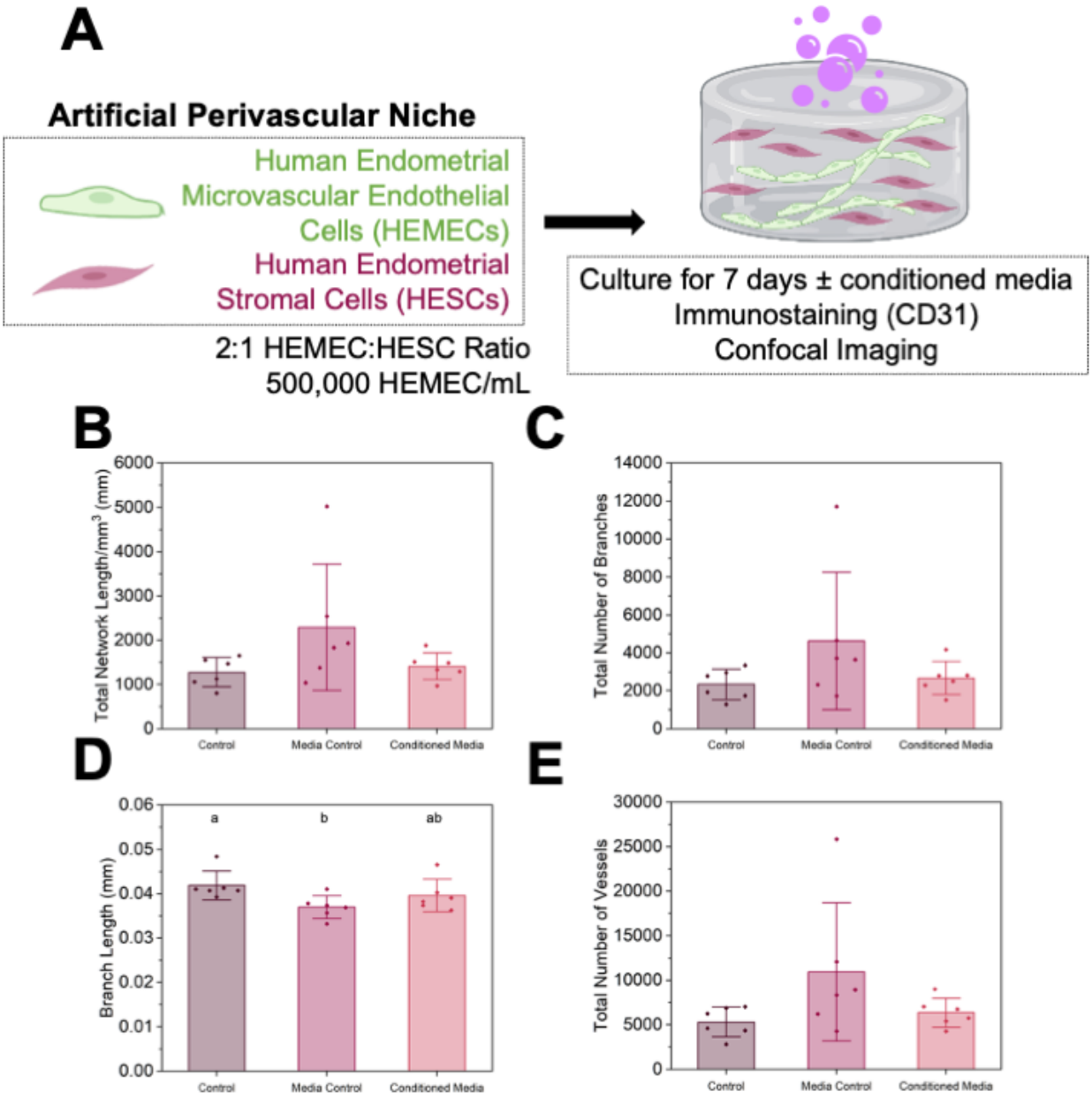

Figure 23. Effects of Swan71 trophoblast conditioned medium on endometrial perivascular niche complexity. (A) Experimental summary. **(B)** Quantification of total vessel length per mm^3, **(C)** total number of branches, **(D)** average branch length, and **(E)** total number of vessels for control, media control, and conditioned media samples (n=6 hydrogels per condition; 3 ROI imaged per gel and averaged). Groups with different letters are statistically significantly different from each other. Data presented as mean ± standard deviation. Created with Biorender.com.

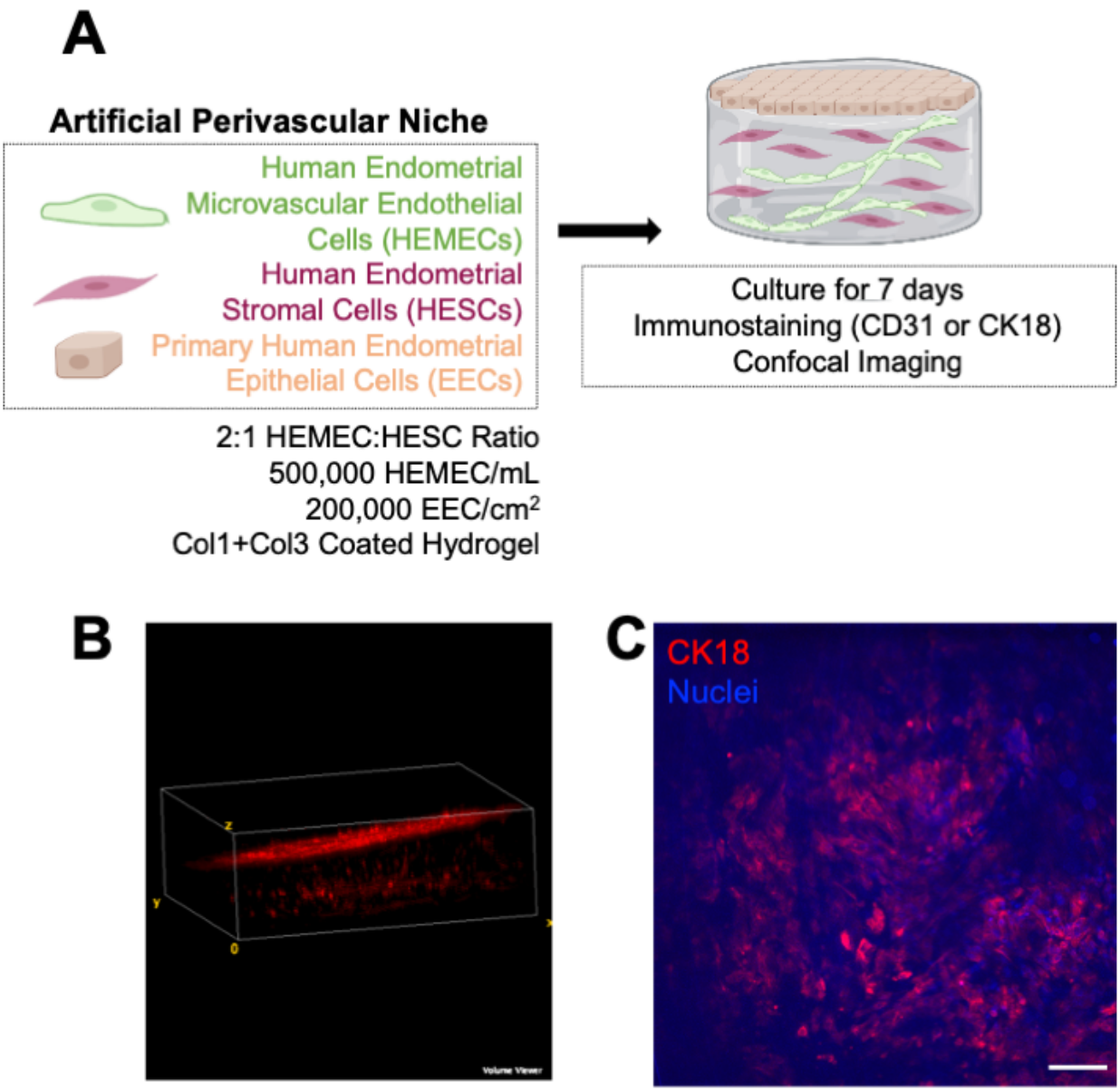

Figure 24. Fabrication of a stratified endometrial model. (A) Experimental summary. **(B)** FIJI Volume Viewer maximum intensity projection showing phalloidin-stained cells with EEC layer overlaying perivascular compartment. **(C)** Maximum intensity projections of Z-stacks of triculture hydrogel cultures stained for cytokeratin 18 (CK18). Scale bars: 100 μm. Created with Biorender.com.

CHAPTER 5: TUNING TROPHOBLAST MOTILITY IN A GELATIN HYDROGEL VIA SOLUBLE CUES FROM THE MATERNAL-FETAL INTERFACE[5]

5.1 Chapter Overview

Trophoblast cells play multiple critical roles in pregnancy, notably modulating blastocyst attachment to the endometrium as well as invading into and actively remodeling the endometrium to facilitate biotransport needs of the growing embryo. Despite the importance of trophoblast invasion for processes essential at early stages of pregnancy, much remains unknown regarding the balance of signaling molecules that may influence trophoblast invasion into the endometrium. The goal of this study was to use three-dimensional trophoblast spheroid motility assays to examine the effect of cues from the maternal-fetal interface on trophoblast motility. We report use of a methacrylamide-functionalized gelatin (GelMA) hydrogel to support quantitative analysis of trophoblast outgrowth area and cell viability. We show this multidimensional model of trophoblast motility can resolve quantifiable differences in outgrowth area and viability in the presence of a known invasion promoter, epidermal growth factor, and a known invasion inhibitor, transforming growth factor β1. We then investigate the sensitivity of trophoblast motility to cortisol, a hormone associated with exogenous stressors. Together, this approach provides a toolset to investigate the coordinated action of physiological and pathophysiological processes on early stages of trophoblast invasion.

[5] This chapter is adapted from the following publication: **Zambuto SG**, Clancy KBH, Harley BAC. Tuning Trophoblast Motility in a Gelatin Hydrogel via Soluble Cues from the Maternal-Fetal Interface. Tissue Eng Part A. 2020;27(15-16):1064-73. Epub 2020/11/21. doi: 10.1089/ten.tea.2020.0097. PubMed PMID: 33216701.

5.2 Introduction

Pregnancy is a complex biological process that involves molecular dialogue between trophoblast cells from the invading blastocyst and cells from the target of implantation, the endometrium. This dialogue coordinates the extent of trophoblast invasion into the endometrium. Although variations in trophoblast invasion are believed to impact the success of a pregnancy (39, 40, 42, 187), much remains unknown regarding pathological signaling processes that drive trophoblast invasion into the endometrium. Implantation occurs when the blastocyst establishes a stable connection with the endometrium (39, 42). In order for implantation to occur, the endometrium must undergo preparation via hormonal priming and enter what is known as the implantation window, a short 4-day window during the mid-secretory phase of a 28-day menstrual cycle (42, 188). Human implantation is thought to occur in three phases: apposition, adhesion, and invasion (39, 188). Apposition is defined as initial, unstable attachment of the blastocyst to the endometrial luminal epithelium (42, 188). Adhesion initiates physical interactions between trophoblast cells from the blastocyst and endometrial epithelium (42, 188). Finally, invasion occurs when trophoblast cells breach the endometrial epithelium and subsequently invade into the underlying stroma (42, 188). Perturbations in the implantation processes can result in a variety of pregnancy disorders. Implantation failure accounts for approximately 75% of failed pregnancies and represents a significant challenge to fertility (39, 42). Implantation failure is not clinically recognized as a pregnancy and defective implantation likely causes adverse effects that compound over the course of the pregnancy. These defects can result in poor pregnancy outcomes, including the hypertensive pregnancy disorder preeclampsia, intrauterine growth restriction, and recurrent pregnancy loss (39). Because implantation involves a highly coordinated molecular dialogue between endometrial cells and trophoblast cells, developing a

deeper understanding of the biological mechanisms surrounding implantation may provide critical insights into pregnancy and pregnancy disorders.

Implantation has never been observed in humans due to ethical concerns regarding studying pregnancy in humans as well as a lack of tools to study this process in the body (42, 189, 190). The blastocyst is fully embedded in the endometrial stroma by approximately 10 days post-conception which provides a unique challenge to obtaining direct mechanistic evidence regarding what influences trophoblast invasion into the endometrium (42). Rare histological specimens have allowed us to glean some information on implantation in human specimens; however, only a limited number of samples exist and these specimens cannot provide information on implantation in real time (42, 189). Additionally, inferring mechanistic processes from animal models may not be accurate due to significant differences between human and animal pregnancy, even amongst humans and non-human primates (190). Although we can use two-dimensional assays, including wound healing assays and Boyden chamber assays, to probe biological mechanisms of implantation, these traditional types of invasion assays cannot recapitulate the complexity necessary to capture dynamic processes associated with trophoblast invasion such as matrix remodeling. Tissue engineered models allow for mechanistic studies using rare populations of cells cultured for extended periods of time in three-dimensional environments. Such models can replicate relevant biophysical properties inspired by the native tissue, including matrix stiffness, extracellular matrix composition, and three-dimensional architecture. Advanced tissue engineered platforms have increasingly been utilized to study trophoblast invasion and migration in three-dimensional biomaterial platforms (85, 110, 111, 191); however, some limitations still remain with existing models. The use of three-dimensional

bioprinting (85, 191) and microfluidic technology (110) allows for tracking migration of trophoblast cells toward soluble factor gradients within biomaterials but these models quantify migration in dissociated cells and hence, do not recapitulate the native spherical structure of an invading blastocyst. Existing models that utilize embryos (111) utilize Matrigel which contains a heterogeneous combination of extracellular matrix proteins and exhibits significant lot to lot variability (127, 192). Further, these models did not quantify trophoblast invasion from the embryo. Adaptation of tissue engineered platforms of increasing complexity can address these issues by employing homogeneous, well-characterized materials and replicating native tissue structure and they can provide additional tools to study core processes associated with trophoblast invasion as they relate to pregnancy and pregnancy disorders.

The overall objective of this study was to use methacrylamide-functionalized gelatin (GelMA) hydrogels and advanced trophoblast spheroid motility assays to quantify trophoblast motility and cell viability in the presence of cues from the maternal-fetal interface. We show this multidimensional model can quantify trophoblast spheroid outgrowth area and viability using known promoters (epidermal growth factor; EGF) and inhibitors (transforming growth factor β1; TGFβ1) of trophoblast motility to demonstrate the relevance of our platform for such studies. EGF is a decidual factor which has been shown to stimulate trophoblast migration (85, 193, 194). Transforming growth factor β superfamily members are expressed in the endometrium, with TGFβ1 present in endometrial epithelial and stromal cells (115). Production and secretion of TGFβ by epithelial cells during the secretory phase suggest that it may play a role in implantation (115). Next, we investigate the effects of cortisol, a steroid hormone produced in response to stressors, on trophoblast motility and quantify trophoblast spheroid outgrowth area

and viability. Cortisol is a steroid hormone that increases as part of the physiological stress response. The overlap between the hypothalamic-pituitary-adrenal and hypothalamic-pituitary-ovarian axes make cortisol highly relevant to reproductive function and thus a variety of processes of pregnancy (26, 195). Psychosocial stressors during pregnancy can arise from poverty, intimate partner violence, lack of social support, and structural and interpersonal racism, have been associated with increased risk for certain pregnancy disorders, such as preterm birth, low birth weight, and preeclampsia (13, 28, 196, 197). Nonetheless, poorly understood processes of how psychosocial stressors affects early events in pregnancy such as trophoblast motility motivate our use of a tissue engineered platform to investigate the role of soluble cues from the maternal-fetal interface on trophoblast invasion.

5.3 Materials and Methods

Hydrogel Fabrication and Characterization

Methacrylamide-Functionalized Gelatin (GelMA) Synthesis and Hydrogel Fabrication

Methacrylamide-functionalized gelatin with 57% degree of functionalization, determined by ^{1}H-NMR, was synthesized as described previously using the one-pot method developed by Shirahama et al. (64, 129). Lyophilized GelMA (129) was dissolved in phosphate buffered saline (PBS; Lonza, 17-516F) at 37°C to make 5 wt% polymer solutions. 0.1% w/v lithium acylphosphinate (LAP) was used as a photoinitiator (93). Unless otherwise noted, 20 μL prepolymer solution was pipetted onto custom circular Teflon molds (5 mm diameter, 1 mm height). Hydrogels were polymerized under UV light (λ=365 nm, 7.14 mW cm^{-2}; AccuCure Spot System ULM-3-365) for 30 seconds.

Hydrogel Characterization

Hydrogel Young's modulus was determined via compression testing using an Instron 5943 mechanical tester with a 5N load cell (198). Hydrogel disks (10 mm diameter, 2 mm height, 100 μL prepolymer solution), fabricated to have approximately the same height as those made using the smaller molds, were submerged in PBS and allowed to swell for 2 hours at 37°C. Samples were compressed at a rate of 0.1 mm/min and moduli were quantified from the linear region of the stress-strain curve using a custom MATLAB code that calculates modulus from the linear regime at a load of 0.003 N and offset of 2.5% strain to ensure contact with the hydrogel surface (Figure 29). To calculate mass swelling ratio, hydrogels were fabricated using the smaller molds and were hydrated in PBS overnight at 37°C. Swollen hydrogels were weighed, lyophilized, and weighed once more to determine dry mass. Mass swelling ratio was calculated using the ratio of wet polymer mass to dry polymer mass as previously described (129).

HTR-8/SVneo Spheroid Invasion Assays

HTR-8/SVneo Cell Maintenance

HTR-8/SVneo trophoblast cells (ATCC® CRL-3271, used experimentally before passage 6 after purchase) were maintained as per the manufacturer's instructions in phenol red-free RPMI-1640 supplemented with 5% charcoal-stripped fetal bovine serum (Sigma-Aldrich, F6765) and 1% penicillin/streptomycin (Thermo Fisher, 15140122). All cultures were grown in 5% CO_2 incubators at 37°C. Routine mycoplasma testing was performed every 6 months to ensure cell quality using the MycoAlert™ Mycoplasma Detection Kit (Lonza).

Spheroid Motility Assays

Spheroid motility assays were performed as previously described by our group (129, 199). 4,000 HTR-8/SVneo cells were added to round bottom plates (Corning, 4515) and placed on a shaker for 48 hours to form spheroids. 4,000 cells/spheroid was selected because this generated spheroids with diameters similar to that of an invading blastocyst which ranges from approximately 100 – 200 μm (Figure 30) (200). Individual spheroids were pipetted onto the Teflon hydrogel molds. Prepolymer solution was added to the mold and spheroids were gently moved to the center of the mold using a pipette tip. Spheroids were moved to ensure they were fully embedded in the hydrogel (e.g., not on top of the hydrogel or attached to the glass slide) because otherwise, they would fall out of the hydrogel. Hydrogels were then polymerized and added to 48 well plates containing 500 μL of cell medium per well. Once all spheroids were encapsulated, spheroids were imaged and medium was replaced with 800 μL of medium with or without (control) biomolecules per well. Medium was not changed at any other times during the experiment unless otherwise noted. Spheroids and encapsulated spheroids were cultured in phenol red-free RPMI-1640 supplemented with 2% charcoal-stripped fetal bovine serum, 1% penicillin/streptomycin, and relevant biomolecules if applicable. No differences in cell growth or morphology were found for cells cultured in medium with 2% fetal bovine serum (Figure 31). Recombinant human transforming growth factor β1 (TGFβ1; R&D Systems, 240-B) and recombinant human epidermal growth factor (EGF; Sigma-Aldrich, E9644) were added to the medium at a concentration of 5 ng/mL. Cortisol (Sigma-Aldrich, H0888) was added to the medium at concentrations of 5, 20, 75, and 150 ng/mL. Control samples were incubated with no added biomolecules. Spheroids were imaged daily using a Leica DMI 4000 B microscope (Leica Microsystems). Total outgrowth area was calculated using the Measure tool in Fiji. Spheroids

were manually traced three times and outgrowth area was determined from the average of these three measurements. Image insets were created using the Zoom in Images and Stacks macro for ImageJ.

Viability Assay

The CellTiter-Glo® 3D Cell Viability Assay (Promega) was used to quantify spheroid viability on day 3. Samples were equilibrated to room temperature for at least 30 minutes prior to running the assay. A stock solution of 1:1 cell medium and CellTiter-Glo® was prepared, medium was removed from each sample well, and 400 µL of the stock solution was added to each sample. Samples were protected from light and incubated for 1 hour on a shaker at room temperature. 100 µL triplicates were added to an opaque plate and luminescence was read immediately using a plate reader (BioTek Synergy HT Plate Reader and Gen5 software; BioTek Instruments, Inc.). A blank was prepared using stock solution. Relative luminescence for each sample was calculated by subtracting the average luminescence value from the blank wells from the average luminescence values of each sample.

Imaging Techniques

Spheroid Staining

Spheroids were encapsulated in hydrogels and grown for 1 or 3 days. Samples were fixed in 4% formaldehyde in PBS for 15 minutes followed by 3 PBS washes. The following solutions were prepared: Permeabilizing Solution (0.1% Tween 20 (Fisher Scientific, BP337) in PBS) and Working Solution (1 µL Phalloidin-iFluor 488 Reagent (Abcam, ab176753) per 1 mL 1% bovine serum albumin (Sigma-Aldrich, A4503) in PBS). All subsequent steps were performed at room

temperature on a shaker. Samples were permeabilized in Permeabilizing Solution for 15 minutes. After permeabilization, 300 μL of Working Solution was added per well and samples were protected from light and incubated for 90 minutes. Staining was followed by 4x20 minute PBS washes. Samples were then stained with Hoechst (1:2000 in PBS; Thermo Fisher, H3570) for 30 minutes followed by a PBS wash. Samples were stored in PBS at 4°C until imaged. One Z-stack per spheroid was taken using a Zeiss LSM 710 Confocal Microscope. Maximum intensity projection images were generated using ZEN (blue edition; Zeiss) and Median filtering was used to smoothen images.

Two-Dimensional Immunofluorescent Staining

To determine glucocorticoid receptor expression in HTR-8/SVneo cells, HTR-8/SVneo cells were seeded on 6-well plates at a density of 3 x 10^4 cells/cm^2 and cultured in cell growth medium supplemented with 2% charcoal-stripped fetal bovine serum and 1% penicillin/streptomycin until approximately 80% confluence. Cells were fixed using 4% formaldehyde for 15 minutes followed by three PBS washes. Cells were permeabilized in 0.5% Tween 20 in PBS for 15 minutes followed by 3x5 minute washes in 0.1% Tween 20 solution in PBS, blocked in blocking solution (2% bovine serum albumin and 0.1% Tween 20 solution in PBS) for 1 hour at room temperature, and incubated in primary antibody solution (Abcam ab3578 rabbit polyclonal anti-glucocorticoid receptor antibody; 1:20) diluted in blocking solution overnight at 4°C. Following the overnight incubation, 5x5 minute washes in 0.1% Tween 20 solution in PBS were performed and samples were incubated in secondary antibody solution (Thermo Fisher A-21428 Goat Anti-Rabbit IgG (H+L) Cross-Adsorbed Secondary Antibody AlexaFluor 555; 1:500) diluted in blocking solution overnight 4°C while protected from light. 5x5 minute washes in 0.1% Tween

20 solution in PBS were performed followed by a 30-minute stain with Phalloidin-iFluor 488 Reagent diluted in Working Solution. 3x5 minute PBS washes were performed followed by a 10-minute Hoechst (1:2000) stain and a quick wash with 0.1% Tween 20 solution in PBS. Samples were stored in 0.1% Tween 20 solution in PBS at 4°C until imaged. Two images per well (n=3 wells each condition) were imaged using identical image settings on a DMi8 Yokogawa W1 spinning disk confocal microscope outfitted with a Hamamatsu EM-CCD digital camera (Leica Microsystems). Images were pseudo-colored and overlaid using Fiji.

Statistics

OriginPro 2019 (Origin Lab) and RStudio were used for statistical analysis. Normality was determined using the Shapiro-Wilkes test and homoscedasticity (equality of variance) was determined using Levene's test. For all quantitative data, n=4-6 spheroids were analyzed per sample group. For each experiment, outgrowth area was compared between groups on the same day. Normal, homoscedastic data was analyzed using a one-way ANOVA followed by post hoc Tukey Test. For data that violated the assumption of normality but maintained homoscedasticity, the Kruskal-Wallis Test was used to analyze data followed by Dunn's post hoc test. For normal, heteroscedastic data, Welch's ANOVA was used to analyze data followed by the Games-Howell post hoc test. For non-normal, heteroscedastic data, Welch's Heteroscedastic F Test with Trimmed Means and Winsorized Variances was used to analyze data followed by Games-Howell post hoc test. Significance was set as $p<0.05$. Outgrowth area results are reported as mean ± standard deviation and cell viability data are reported as box plots.

5.4 Results

The development of three-dimensional trophoblast spheroid motility assays allows for quantitative motility analysis

We cultured HTR-8/SVneo trophoblast spheroids in hydrogels with mechanical properties (Elastic modulus: 1.8±0.5 kPa; Mass Swelling Ratio: 46.5±6.4) similar to that of native tissue (Fig. 25), which was found to be approximately 1.25 kPa for the decidua basalis and 0.171 kPa for the decidua parietalis (201). We cultured spheroids for up to 3 days and observed cell migration into the surrounding hydrogel matrix over time (Fig. 26). These assays provide a platform to quantitatively analyze trophoblast motility in three-dimensions. We subsequently examined differences in motility and viability in response to exogenous soluble factors.

Epidermal growth factor and transforming growth factor β1 modulate trophoblast motility and viability

We quantified shifts in trophoblast motility and viability via the addition of soluble biomolecules in cell media. Control samples had a "thorn-like" migration pattern, with cells migrating away from the spheroid in thorn-like projections. Trophoblast spheroids showed increased motility and increased viability in the presence of known trophoblast motility promoter epidermal growth factor (EGF) and showed a "coronal" migration pattern. Trophoblast spheroids showed inhibited motility and decreased viability in the presence of known trophoblast motility inhibitor transforming growth factor β1 (TGFβ1) by day 2, but still showed a migration pattern of thorn-like projections (Fig. 27). Starting by day 1, the TGFβ1 condition was significantly different compared to control (Welch's ANOVA: p=0.00064; Games-Howell: p=0.001). By day 2, all conditions were significantly different (Welch's ANOVA: p=0.0023; Games-Howell: EGF-

control p=0.027, TGFβ1-control p=0.018, TGFβ1-EGF p=0.016) and the conditions were significantly different on day 3 as well (Welch's Heteroscedastic F Test with Trimmed Means and Winsorized Variances: p=0.036; Games-Howell: EGF-control p=0.023, TGFβ1-control p=0.031, TGFβ1-EGF p=0.012). Cell viability was significantly different across all three groups (One-way ANOVA: p=1.78x10^{-8}; Tukey Test: EGF-control p=1.05x10^{-5}, TGFβ1-control p=4.6x10^{-4}, TGFβ1-EGF p<1x10^{-8}).

Cortisol has no effect on outgrowth area or viability

We subsequently used immunofluorescence staining of HTR-8/SVneo cells in two-dimensional cell culture well plates to validate their expression of glucocorticoid receptors. Notably, HTR-8/SVneo cells positively express glucocorticoid receptors (Fig. 28A). Further, we observed no evidence of non-specific antibody binding (samples stained without primary antibody) and observed only minimal background fluorescence. We subsequently quantified trophoblast spheroid outgrowth area and viability in the presence of cortisol. Although sample outgrowth area in the presence of cortisol for lower and physiological concentrations showed a decreasing trend in outgrowth area by day 3 of culture, the effects were not significant. We observed no differences (p>0.05) in outgrowth area or viability (p=0.15) compared to control samples for lower (5 ng/mL and 20 ng/mL) concentrations at days 0 (p=0.88), 1 (p=0.23), 2 (p=0.08), and 3 (p=0.28) (Fig. 28B). Furthermore, for physiological (75 ng/mL and 150 ng/mL) concentrations of cortisol (Fig. 28C), we also observed no differences (p>0.05) in outgrowth area or viability at days 0 (p=0.52), 1 (p=0.83), 2 (p=0.06), and 3 (p=0.12) of culture.

5.5 Discussion

The objective of this study was to adapt a cell spheroid-based trophoblast motility assay to probe how biomolecules from the maternal-fetal interface influence trophoblast motility. Here, we demonstrate that trophoblast motility can be modulated through the use of known promoters and inhibitors of invasion. We then investigate the effects of exogenous cortisol and quantify outgrowth area and cell viability in the presence of this molecule.

For these studies, we employ methacrylamide-functionalized gelatin (GelMA) hydrogels. Gelatin is denatured collagen and hence retains cell binding motifs and degradation sites that allow for cell attachment and matrix remodeling, key processes relevant to invasion (65, 67, 129, 199, 202). The endometrium contains collagens I, III, IV, V, and VI, rendering gelatin relevant in terms of its extracellular matrix composition (34, 131). Additionally, the biophysical properties of GelMA can be adjusted to fall within the regime of tissue stiffness. Recently, *Abbas et al.* used atomic force microscopy to demonstrate that the stiffness of the nonpregnant endometrium and placenta have an order of magnitude of 10^2 Pa, whereas the decidua basalis, the region of the endometrium directly under the placenta that is invaded by trophoblast cells, exhibited an average stiffness on the order of 10^3 Pa (201). Our hydrogel formulation falls within this range and replicates relevant mechanical properties of the tissue through which trophoblast cells will invade. Nevertheless, the ability to tune the biophysical and biochemical properties of GelMA provides a unique opportunity to modulate hydrogel properties to mimic aspects of disease and disorders that may relate to differences in endometrial and placental tissue variation. We have previously demonstrated that microenvironmental signals within GelMA hydrogels, including biophysical cues, bound and soluble biomolecules, and heterotypic cell-cell interactions can

influence cell behavior and phenotype (203). Microenvironmental tissue variation may relate to the onset and progression of pregnancy disorders and the ability to probe such questions in an adaptable platform would be crucial for understanding how spatial variation in tissues plays a role in disease. From *in vivo* studies using shear wave elastography, it was demonstrated that placental stiffness was significantly higher in women with preeclampsia compared to women with normal pregnancies (86). Preeclampsia is a hypertensive pregnancy disorder characterized by high maternal blood pressure and the presence of proteins in urine at or after 20 weeks gestation (204-207). It is hypothesized that insufficient trophoblast invasion in early pregnancy may be a defect related to the onset of preeclampsia (187, 204, 208). Using our advanced hydrogel systems, we can create spatially graded hydrogel systems that would allow us to create gradients of stiffness and matrix components to recapitulate biophysical and biochemical variation across endometrial tissue that would occur normally and in diseased states (203, 209). Although varying spatial hydrogel properties was beyond the scope of this study, there is potential to assess gradients across hydrogels to determine how the biophysical and biochemical tissue microenvironment plays a role in early pregnancy, implantation, and pregnancy-disorders.

Unlike traditional two-dimensional wound healing assays or Boyden chamber assays, spheroid motility assays in biomaterial platforms can replicate the three-dimensional structure of an invading blastocyst and provide a matrix through which cells can invade. We demonstrate reproducible spheroid formation using the HTR-8/SVneo cell line, resulting in spheroid size within the range of an invading blastocyst (200). We employ these trophoblast assays to interrogate differences in trophoblast outgrowth area and viability in the presence of biomolecules from the maternal-fetal interface. First, we selected known trophoblast motility

promoters and inhibitors: epidermal growth factor (EGF) and transforming growth factor β1 (TGFβ1) and observed quantifiable differences in trophoblast outgrowth area and cell viability. We show that soluble EGF stimulates trophoblast motility and viability at concentrations used previously in literature (85, 193, 194). Additionally, soluble TGFβ1 inhibited trophoblast motility and resulted in decreased viability, similar to what was reported previously in the literature (114, 210). Taken together, we show a multidimensional tissue engineering model can be used to quantify differences in motility and viability using a small number of cells. Further, this platform is able to resolve effects of other biomolecules from the maternal-fetal interface known to modulate trophoblast invasion.

Subsequently, we included an investigation of the role of cortisol on trophoblast motility. The physiological stress response is an acute phase response that, when activated repeatedly, can have chronic effects (13, 21). Significant psychosocial stressors during pregnancy can be induced by poverty, intimate partner violence, lack of social support, and both structural and interpersonal racism. The downstream effects of this constantly activated physiological stress response has been associated with increased risk for certain pregnancy disorders, including preterm birth, low birth weight, and preeclampsia (13, 28, 196, 197). However, much remains unknown regarding how psychosocial stressors affect early events in pregnancy, such as trophoblast invasion. A benefit to our model system is that although stress effects on pregnancy outcomes may not be possible to study in humans or animals due to the complexity of the stress response, models of early implantation could allow us to study how cortisol affects trophoblast invasion. Cortisol is a steroid hormone that elevates as part of the physiological stress response and is functionally significant in multiple processes of reproductive functioning, including during

pregnancy (26, 195). Previous studies have shown that natural and synthetic glucocorticoids reduce trophoblast motility and proliferation in two-dimensional cultures, wound healing assays, and Matrigel invasion assays (29, 32, 211).

We first investigated trophoblast motility in the presence of cortisol at concentrations from *in vitro* studies (5-20 ng/mL) (25). Outgrowth area showed a decreasing trend in the presence of cortisol, although not statistically significant, with no changes in viability between groups. We next selected physiological concentrations of cortisol (75-150 ng/mL) comparable to what would occur during early pregnancy (195). We observed a similar trend, with no statistical differences in outgrowth area or viability despite physiologically relevant cortisol concentrations. To our knowledge, no studies to date have quantified cortisol levels in pregnant individuals with high stress levels; therefore, our selected concentrations may be lower than the required threshold to significantly reduce trophoblast motility. Furthermore, 11β-HSD2 activity may have been able to convert these levels of cortisol into cortisone, which could explain why cortisol had a minimal effect on outgrowth area and viability (212). An investigation of 11β-HSD2 activity in the presence and absence of cortisol as well as a further exploration of cortisol dosages may provide additional insight. If no differences are found, it is possible that cortisol does not have an effect on trophoblast motility or proliferation as previously found in the literature. Our system is three-dimensional and captures not only the spherical structure similar to an invading blastocyst but also allows cells to invade and remodel a surrounding gel matrix. Our system may be more applicable to what occurs physiologically and may not have as profound of an effect on motility and proliferation as previously demonstrated in less complex models.

We recognize some limitations of our studies. These limitations provide exciting opportunities to improve our platforms to create models of increasing physiological relevance. We first acknowledge that the use of the HTR-8/SVneo cell line may contain a mixed population of cells and may not accurately mimic *in vivo* trophoblast behavior (213). For future investigations, the physiological relevance of our platform can be increased through the use of primary trophoblast cells. Secondly, we simplified an increased stress response to external stressors as equivalent to higher levels of cortisol. Although this strategy is easily testable in our platform, literature suggests that cortisol levels exhibit a dinural pattern and there is some individual variation in cortisol responsiveness based on mental health conditions, e.g., post-traumatic stress disorder (214-222). Future work on cortisol may be improved with temporal adjustments of cortisol concentrations to more appropriately mimic what occurs in the body.

5.6 Conclusions

Trophoblast invasion is a biological process essential to the establishment and success of a pregnancy. We employ GelMA hydrogels to perform advanced quantitative trophoblast motility assays and demonstrate quantifiable differences in trophoblast outgrowth area and viability in the presence of known promoters and inhibitors of trophoblast invasion (EGF and TGFβ1). Further, we begin to probe how cortisol may influence trophoblast motility. The platform proposed herein will provide researchers with a unique tool critical for understanding implantation and will aid researchers in understanding mechanisms that dictate the success or failure of implantation.

5.7 Figures

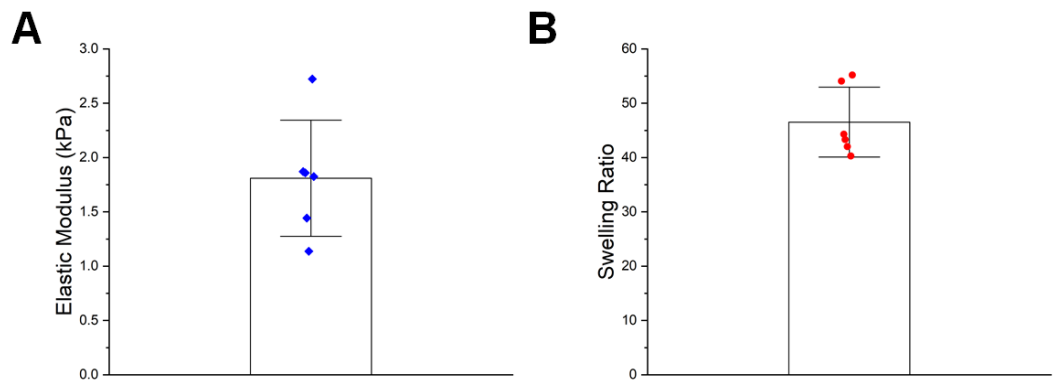

Figure 25. Mechanical characterization of 5 wt% GelMA hydrogels. A) Elastic modulus determined by compression testing (n=6 hydrogels). B) Mass swelling ratio determined by comparing swollen polymer mass to dry polymer mass (n=6 hydrogels). Data presented as mean ± standard deviation with individual data points shown.

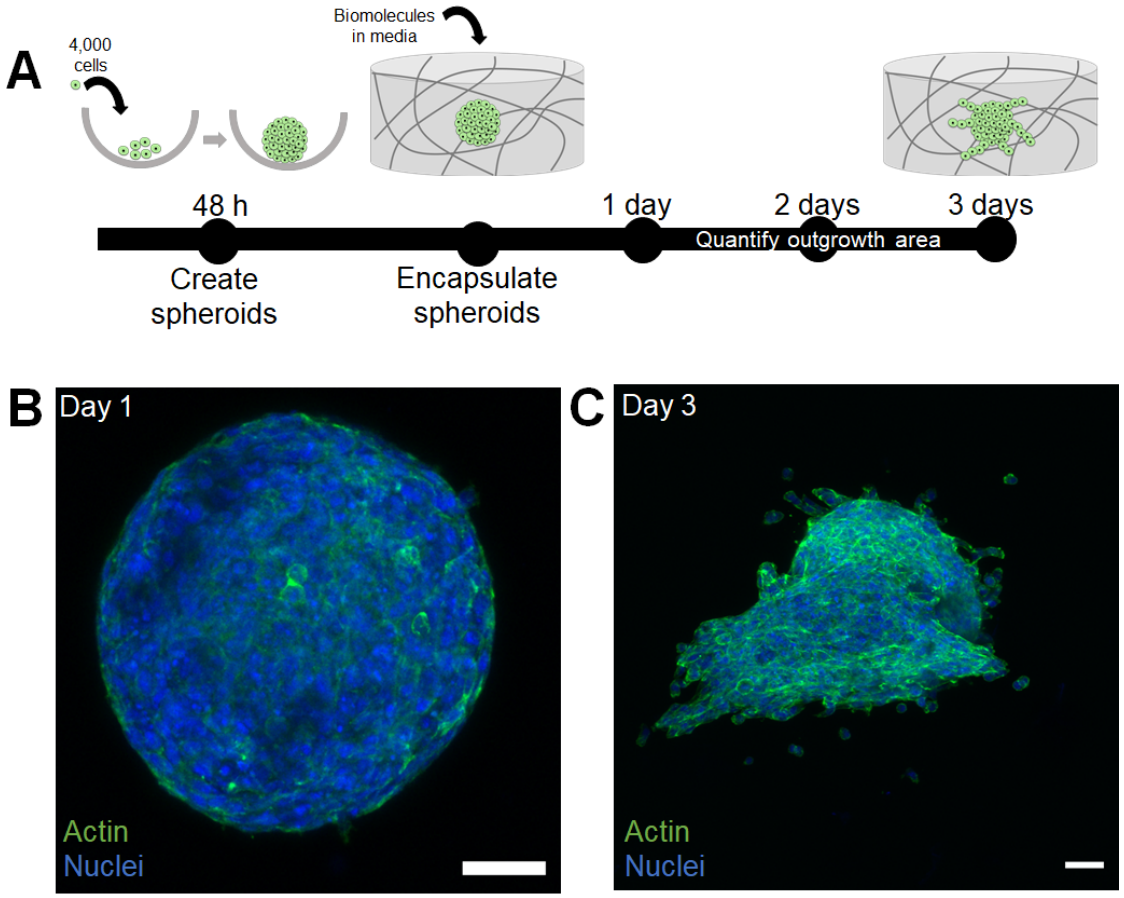

Figure 26. Three-dimensional trophoblast motility assays in methacrylamide-functionalized gelatin hydrogels. A) HTR-8/SVneo trophoblast cells were seeded into round bottom plates for 48 hours to create spheroids. Spheroids were then encapsulated in hydrogels and allowed to migrate into the surrounding hydrogel for up to 3 days in the presence of absence of soluble biomolecules in growth medium. B) Representative maximum intensity projection image of a spheroid in a hydrogel 1 day post-embedding. C) Representative maximum intensity projection image of a spheroid 3 days post-embedding. Green: Phalloidin (Actin). Blue: Hoechst (Nuclei). Scale: 200 μm.

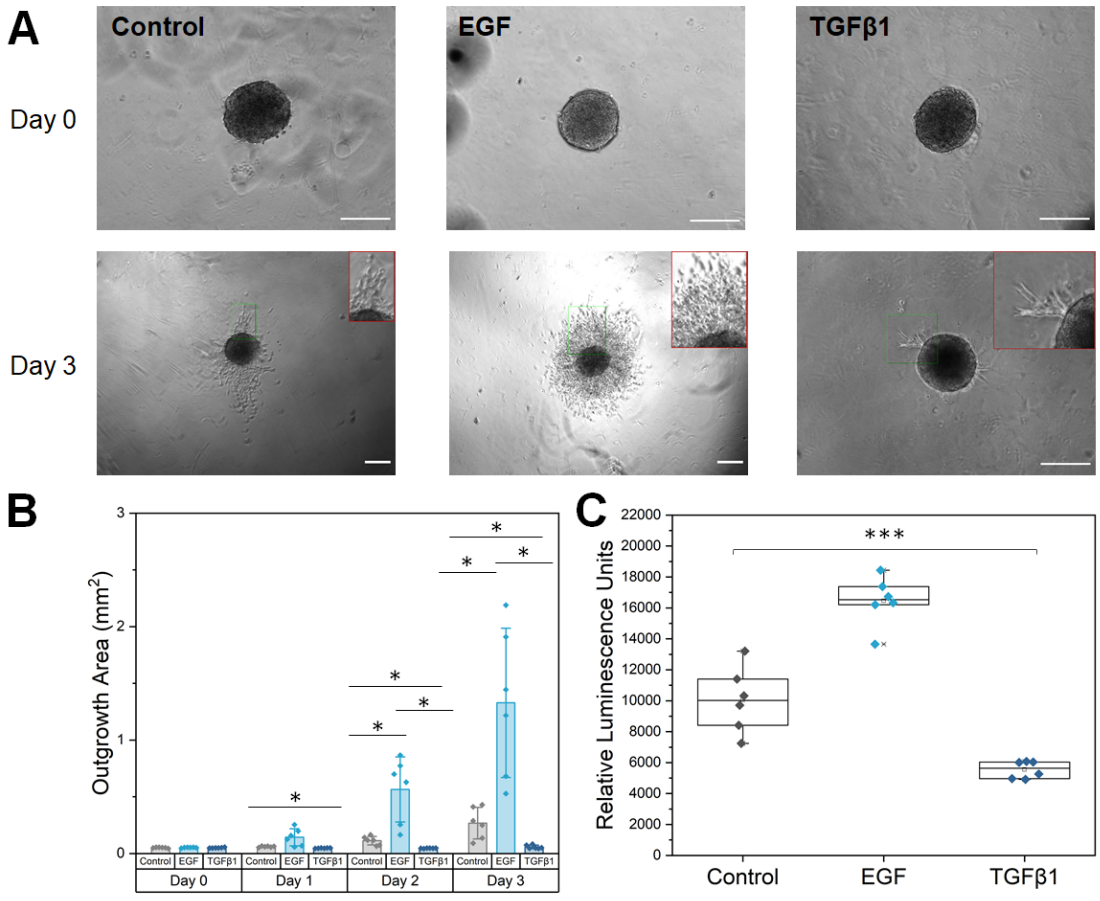

Figure 27. Epidermal growth factor (EGF) and transforming growth factor beta 1 (TGFβ1) modulate trophoblast outgrowth and viability. A) Representative phase images of individual HTR-8/SVneo trophoblast spheroids at days 0 and 3. Insets of invading cells are shown for day 3 in red. EGF and TGFβ1 were added to cell medium at day 0. Control samples contained no additional growth factors. B) Total spheroid outgrowth area at days 0-3 was quantified in Fiji and reported as averages for each condition. Data presented as mean ± standard deviation with individual data points shown. C) Cell viability data from CellTiter-Glo® 3D Cell Viability Assay measured in encapsulated spheroids on day 3. Data presented as box plots with individual data points shown. *: $p<0.05$. ***: $p<0.001$. n=6 samples per condition. Scale: 200 μm.

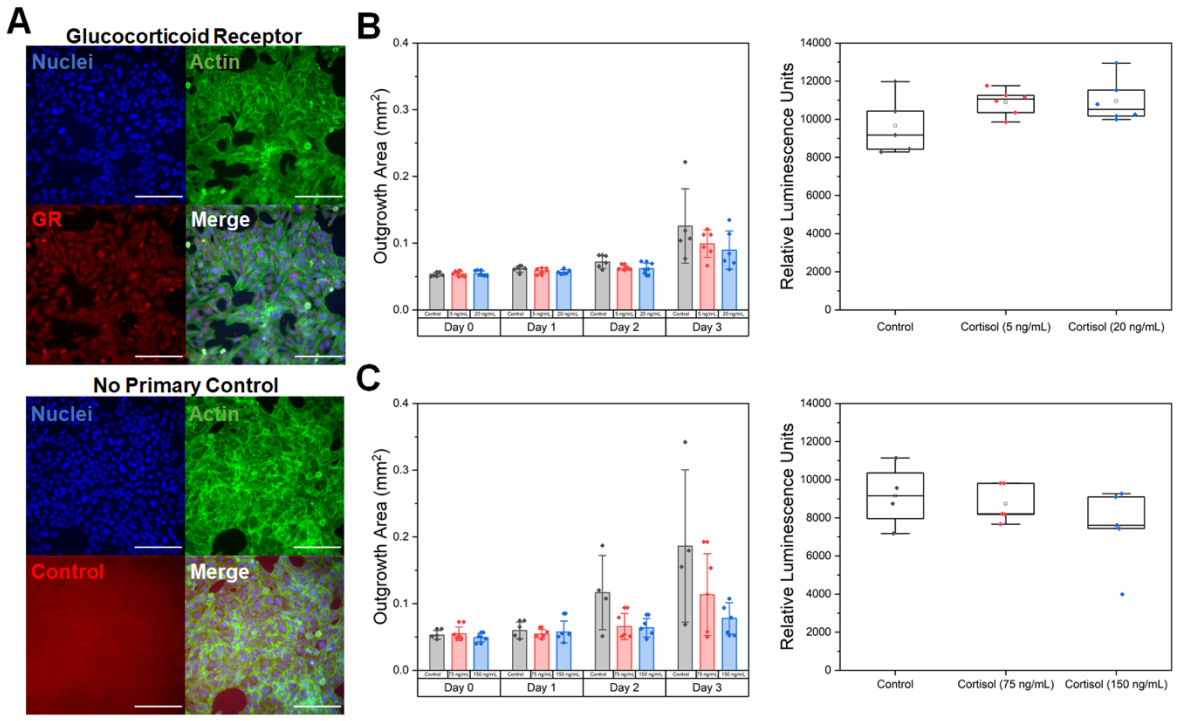

Figure 28. The effects of cortisol on trophoblast motility. A) Representative fluorescent images of HTR-8/SVneo trophoblast cells cultured in 6-well plates. HTR-8/SVneo trophoblast cells express glucocorticoid receptors with cytoplasmic staining. The no primary control showed only minimal background fluorescence with no indication of non-specific binding. Green: Phalloidin (Actin). Red: Anti-Glucocorticoid Receptor. Blue: Hoechst (Nuclei). B) Total outgrowth area at days 0-3 and cell viability at day 3 for control, 5 ng/mL cortisol, or 20 ng/mL cortisol. Data presented as mean ± standard deviation with individual data points shown. C) Total outgrowth area at days 0-3 and cell viability at day 3 for control, 75 ng/mL cortisol, or 150 ng/mL cortisol. Data presented as box plots with individual data points shown. n=4-6 samples per condition. Scale: 200 µm.

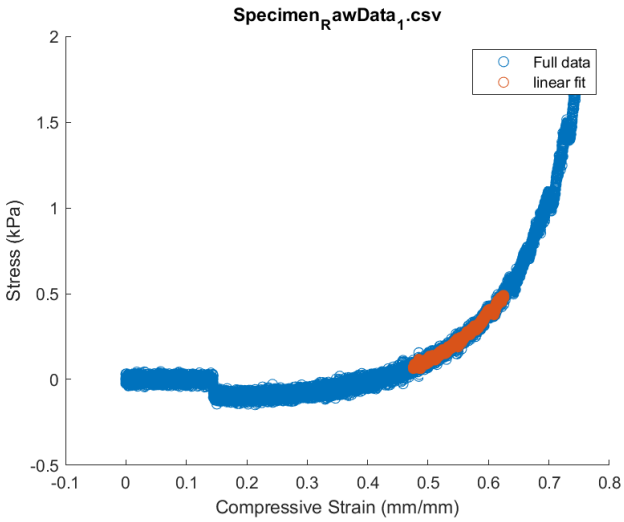

Figure 29. Representative stress-strain curve (blue) for a GelMA hydrogel and linear region chosen to calculate modulus (orange). R^2 value for the linear regime: 0.97.

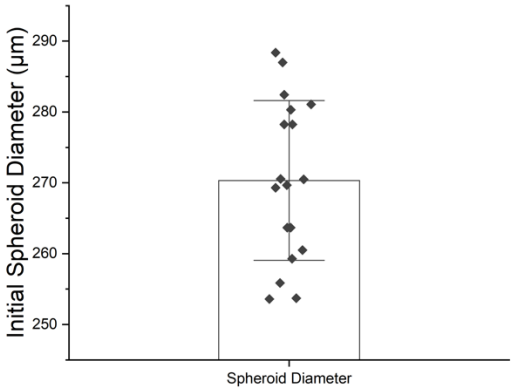

Figure 30. Initial spheroid diameter on day 0 (encapsulation) for n=18 spheroids. Data presented as mean ± standard deviation with individual data points shown.

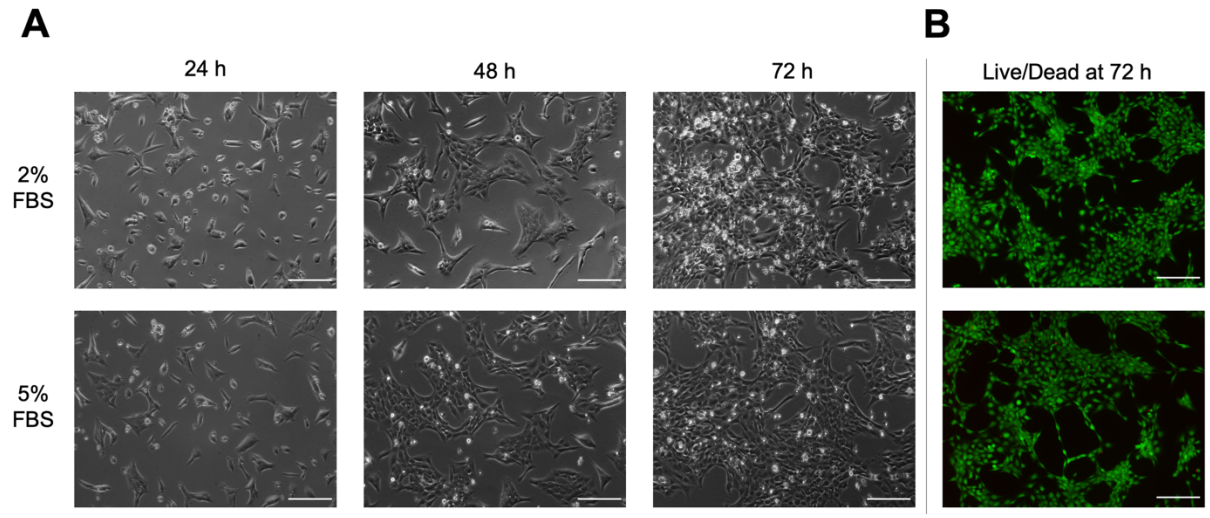

Figure 31. Control experiment to verify cell HTR-8/SVneo growth and viability in reduced serum concentrations. A) Representative phase images of HTR-8/SVneo cells grown in well plates at 24, 48, and 72 hours after seeding cultured in growth medium supplemented with 2% or 5% fetal bovine serum (FBS). B) Live/dead images of HTR-8/SVneo cells at 72 hours after seeding. Scale: 200 μm.

CHAPTER 6: THE ROLE OF PREGNANCY-SPECIFIC GLYCOPROTEINS ON TROPHOBLAST MOTILITY IN THREE-DIMENSIONAL GELATIN HYDROGELS[6]

6.1 Chapter Overview

Trophoblast invasion is a complex biological process necessary for establishment of pregnancy; however, much remains unknown regarding what signaling factors coordinate the extent of invasion. Pregnancy-specific glycoproteins (PSGs) are some of the most abundant circulating trophoblastic proteins in maternal blood during human pregnancy, with maternal serum concentrations rising to as high as 200-400 μg/mL at term. Here, we employ three-dimensional (3D) trophoblast motility assays consisting of trophoblast spheroids encapsulated in 3D gelatin hydrogels to quantify trophoblast outgrowth area, viability, and cytotoxicity in the presence of PSG1 and PSG9 as well as epidermal growth factor and Nodal. We show PSG9 reduces trophoblast motility whereas PSG1 increases motility. Further, we assess bulk nascent protein production by encapsulated spheroids to highlight the potential of this approach to assess trophoblast response (motility, remodeling) to soluble factors and extracellular matrix cues. Such models provide an important platform to develop a deeper understanding of early pregnancy.

6.2 Introduction

Pregnancy is an intricate biological process that involves a complex molecular dialogue between cells from the endometrium and trophoblast cells from the invading blastocyst; however, what orchestrates this cellular crosstalk remains poorly understood. Blastocyst implantation into the endometrium is thought to occur across three phases (39, 42, 188). Apposition is the initial,

[6] This chapter is adapted from the following publication: Zambuto SG, Rattila S, Dveksler G, Harley BAC. The role of pregnancy-specific glycoproteins on trophoblast motility in three-dimensional gelatin hydrogels. *Cellular and Molecular Bioengineering*. 2022. doi: 10.1007/s12195-021-00715-7.

unstable connection between the endometrium and the blastocyst. Adhesion establishes a more stable, physical connection between the endometrium and blastocyst. Finally, invasion occurs when trophoblasts breach the endometrial epithelium and embed the blastocyst within the endometrial stromal tissue. Ultimately, implantation is modulated by molecular signaling between cells from a hormonally-primed endometrium and trophoblast cells from a mature blastocyst (39, 42, 188). Although researchers have highlighted the importance of biological stimuli such as ovarian hormones estrogen and progesterone that modulate endometrial decidualization for successful implantation, much remains unknown regarding other factors expressed by maternal cells and trophoblast that coordinate the extent of invasion. Developing a deeper understanding of what biological cues influence invasion would provide clinical insights that may improve our ability to understand, prevent, and treat fertility disorders and early pregnancy loss.

Numerous challenges exist regarding studying early implantation in humans. Notably, this process occurs shortly after conception: the blastocyst is embedded within endometrial tissue by approximately 10 days post-conception which provides a significant challenge to directly studying this process within humans (39, 42, 188). As such, initial adhesion of the blastocyst to the endometrium has never been observed in humans and much of what we know regarding early pregnancy is inferred from rare histological specimens or from animal studies (39, 42, 188). Nevertheless, significant differences between human pregnancy and placentation compared to rodents and non-human primates calls into question the relevance of using such models to study mechanisms of early implantation in humans (39, 42, 188).

Three-dimensional (3D) models, such as organoid models and tissue engineered platforms, offer the unique opportunity to elucidate mechanistic processes associated with human implantation that are currently impossible to study in the body with current state of the art technologies. Unlike animal models which are complex and costly, these *in vitro* platforms offer controllability and scalability while providing an avenue to incorporate increasingly complex culture environments (e.g., cells, extracellular matrix, biomolecules) relevant to what occurs in the body (71, 76, 223). Here, we use methacrylamide-functionalized gelatin (GelMA) hydrogels to investigate the role of pregnancy-specific glycoproteins (PSGs) on trophoblast motility. Gelatin is an attractive platform for these studies because it is denatured collagen that retains relevant arginine-glycine-aspartic acid (RGD) cell binding motifs and matrix metalloproteinase-sensitive (MMP) degradation sites that ultimately allow for cellular adhesion and matrix remodeling which are critical processes in invasion (65). The addition of methacrylamide groups to gelatin's backbone allows for photopolymerization, which renders GelMA hydrogels stable under physiological temperatures and relatively homogeneous in terms of structure (65, 223). Compared to other materials, gelatin-based biomaterials have numerous advantages. For example, unlike Matrigel which contains a heterogeneous matrix composition that varies batch-to-batch, GelMA hydrogels have a defined matrix composition(127, 128). And unlike synthetic biomaterials such as polyethylene glycol (PEG), gelatin natively presents cell binding and degradation motifs that allow the material to be remodeled by cells. GelMA hydrogels offer the unique opportunity to study biomolecules in a defined material that offers not only simplicity but also tunability to match the native biophysical properties of the tissue of interest. Such models have previously been employed for quantifying trophoblast and cancer cell invasion in 3D (139, 199). Here, we adapted the technique to track cell migration away from cell spheroids embedded

within the hydrogel (79, 224, 225) to investigate the pattern of motility by Swan71 trophoblast cells in the presence of soluble factors present at the maternal-fetal interface. In contrast to 2D assays such as wound healing assays and Boyden chamber assays, these 3D motility strategies can replicate aspects of the *in vivo* environment, including tissue stiffness, 3D tissue architecture, and matrix composition.

In this work, we describe an approach to compare trophoblast motility patterns in response to soluble pregnancy-specific glycoproteins (PSGs). PSGs are some of the most abundant circulating trophoblastic proteins in maternal blood during human pregnancy (226-229). Over the course of pregnancy, the maternal serum level of PSGs increases to approximately 200-400 μg/mL at term (227). There are 10 coding *PSG* genes in humans, *PSG1-PSG9* and *PSG11*, and one non-coding pseudogene *PSG10* (226, 227). At the end of the first trimester, *PSG1* and *PSG3* account for the bulk majority of expression and by term, *PSG1, PSG3, PSG4, PSG5*, and *PSG6* are equally expressed with low expression of the other *PSGs* (227). PSGs are expressed by extravillous trophoblasts and syncytiotrophoblasts (226, 230). Lower serum concentrations of PSGs have been associated with pregnancy disorders and pathologies, such as fetal growth restriction and preeclampsia (PE) (226, 227). Using a specific enzyme-linked immunosorbent assay (ELISA), we found that the PSG1 concentration was significantly lower in African American women diagnosed with early-onset (EO) and late-onset PE compared to their respective controls (226). Due to the lack of specific antibodies, the concentration of the other PSGs in normal pregnancy and in pregnancy pathologies has not been explored but results using other techniques suggest that PSG9 is upregulated rather than down-regulated in EOPE. A label-free selected reaction monitoring workflow proteomic study identified PSG9 upregulation as a

potential predictive biomarker of EOPE(231). Because PSG1 and PSG9 concentrations may be predictive of EOPE, we chose to determine the effects of PSG1 and PSG9 on trophoblast motility. This study quantified the differences in trophoblast outgrowth area, fold change in outgrowth area, viability, and cytotoxicity after addition of PSG1 or PSG9 to the cell media. We report differences in outgrowth area and viability/cytotoxicity based on the addition of certain factors and investigate whether encapsulated trophoblast cells exhibit hallmarks of extracellular matrix remodeling within the hydrogels (232). Our work demonstrates GelMA hydrogels present a defined yet tunable matrix environment similar to the native tissue that can be used to study the influence of soluble factors on cell motility and matrix remodeling.

6.3 Materials and Methods

Methacrylamide-Functionalized Gelatin (GelMA) Synthesis and Hydrogel Fabrication

Methacrylamide-functionalized gelatin was synthesized as described previously using a method developed by Shirahama et al. (64). GelMA was fabricated from porcine gelatin (gel strength 300, Type A; Sigma G2500). GelMA was determined to have a 57% degree of functionalization as determined by ^{1}H-NMR and a stiffness of approximately 2 kPa as previously determined by compression testing (139). 5 wt% polymer solutions were created by dissolving lyophilized GelMA in phosphate buffered saline (PBS; Lonza, 17-516F) at 37°C, adding 0.1% w/v lithium acylphosphinate (LAP) as photoinitiator, and polymerizing hydrogels under UV light for 30 seconds (λ=365 nm, 7.14 mW cm^{-2}; AccuCure Spot System ULM-3-365). Each hydrogel was fabricated from 20 μL prepolymer solution pipetted into custom circular Teflon molds (5 mm diameter, 1 mm height).

Generation of Recombinant PSG1 and PSG9 and Fc Control Proteins

PSG1-His was harvested from the supernatant of a stably transfected CHO-K1 single-cell clone established in our laboratory and grown in a hollow fiber cartridge (FiberCell Systems, MD, USA) as previously described (233). The Fc fusion proteins were generated by cloning the PSG1a cDNA (UniProt KB-P11464) and PSG9 cDNA (NM_002784) into the pFuse-IgG1e3-Fc1 vector (InvivoGen, San Diego, CA). The Fc control protein was derived from the pFuse-IgG1e3-Fc2 (InvivoGen). For the generation of full length PSG1-Fc and PSG9-Fc, the plasmids were transfected into ExpiCHO cells (Thermo Fisher Scientific, Waltham, MA, USA) following the manufacturer's recommendations and the supernatants were collected 6 days post-transfection. Proteins were purified from the clarified supernatants on an anti-PSG1 mAb#4 column (for PSG1-His) and protein A columns (for PSG1-Fc, PSG9-Fc, Fc control) in an AKTA pure chromatography system (Cytiva, Marlborough, MA). All proteins were eluted with 0.1 M glycine buffer pH 2.7, followed by immediate neutralization with 1 M Tris-HCl pH 8 (Thermo Fisher Scientific). Following elution from the column, the fractions containing the proteins were pooled, concentrated, and buffer-exchanged with phosphate-buffered saline (PBS) using an Amicon Ultra centrifugal filter unit with a 10 kDa cutoff membrane (Millipore, Burlington, MA). To determine the protein concentration, the purified proteins were separated on 4–12% NuPAGE BisTris gels (Thermo Fisher Scientific) at different dilutions alongside known concentrations of BSA used as standards. The gels were stained with GelCode Blue (Thermo Fisher Scientific), and the proteins were quantitated by densitometry using a BioRad Gel Doc EZ Imager.

Swan71 Spheroid Motility Assays

Swan71 Cell Culture and Maintenance

The telomerase immortalized first trimester trophoblast cell line Swan71 was provided by Dr. Gabriela Dveksler. Cells were maintained in DMEM (Gibco, 11995-065) supplemented with 10% fetal bovine serum (FBS; R&D Systems, S11150H), 1% penicillin/streptomycin (Thermo Fisher, 15140122), and 500 ng/mL puromycin (Sigma-Aldrich, P8833). Medium was replaced every other day of culture. All cultures were grown in a humidified incubator at 37°C with 5% CO_2. Cells were routinely tested for mycoplasma every 6 months to ensure cell quality (MycoAlert™ Mycoplasma Detection Kit; Lonza).

Spheroid Motility Assays

Spheroid motility assays were performed as previously described by our group (139). Spheroids and encapsulated spheroids were cultured in DMEM supplemented with 2% FBS, and 1% penicillin/streptomycin. Briefly, 2,000, 4,000, or 6,000 Swan71 cells were added to each well of a round bottom plate (Corning, 4515). The plate was placed on a shaker at 60 rpm in a humidified incubator at 37°C with 5% CO_2 for 48 hours to allow spheroids to form. After 48 hours, individual spheroids were pipetted onto Teflon molds and 20 µL prepolymer solution was added to each mold well. Each spheroid was gently moved to the center of each hydrogel using a pipette tip. Hydrogels were then polymerized and added to 48 well plates containing 500 µL medium per well. Once all samples were fabricated, each hydrogel was imaged and then medium was replaced with 500 µL medium supplemented with relevant biomolecules. Recombinant human epidermal growth factor (EGF, 5 ng/mL; Sigma-Aldrich, E9644) was used as an invasion promoter and recombinant human nodal (250 ng/mL; R&D Systems, 3218-ND-025/CF) was

used as an invasion inhibitor. PSG variants and controls were used at 60 μg/mL as we previously showed that both PSG1-Fc and PSG9-Fc resulted in robust biological responses at this concentration, including their ability to activate TGF-□ and increase endothelial tubulogenesis (226, 227, 234). Additional control samples were cultured in medium without biomolecules. Encapsulated spheroids were imaged daily using a Leica DMI 4000 B microscope (Leica Microsystems). Total outgrowth area was calculated using the measure tool in Fiji by manually tracing spheroids three times and taking the average of these three measurements. Fold change was calculated for each hydrogel from average outgrowth area by comparing average outgrowth area on days 1, 2, and 3 to average area on day 0 (day of encapsulation) using Eq. 1.

Equation 1. $Fold\ Change_{Day\ X} = \frac{Area\ Day_x - Area\ Day_0}{Area\ Day_0}$

CellTiter-Glo® 3D Viability Assay

Viability was quantified using the CellTiter-Glo® 3D Viability Assay (Promega) as described previously using the manufacturer's instructions (139). Briefly, samples and reagents were equilibrated to room temperature for at least 30 minutes prior to completing the assay. Medium was removed from each hydrogel and 400 μL of a 1:1 solution of CellTiter-Glo® and medium was added to each hydrogel. Samples were incubated for 1 hour at room temperature on a shaker. Following incubation, 100 μL triplicates for each sample were added to an opaque, white-walled plate, including a blank consisting of only the stock solution. Plate luminescence was read immediately using a plate reader (BioTek Synergy HT Plate Reader and Gen5 Software, BioTek Instruments, Inc.). Relative luminescence for each sample was calculated by subtracting the average blank luminescence value from the average luminescence value for each sample.

LDH-Glo™ Cytotoxicity Assay

Cytotoxicity was quantified using the LDH-Glo™ (Promega, J2380) as described by the manufacturer's instructions. Briefly, samples were prepared by combining 4 µL of medium per hydrogel and diluting it in 96 µL LDH (lactate dehydrogenase) storage buffer (200 mM Tris-HCl (Roche, 10812846001), 10% glycerol (Promega, H5433), 1% bovine serum albumin (BSA; Sigma-Aldrich, A4503); filter sterilized and stored at 4°C). This dilution was calculated to fall within the linear regime of the assay (data not shown). Samples were used immediately or stored at -80°C until use. Prior to running the assay, all reagents were equilibrated to room temperature. Duplicate wells were prepared for each hydrogel by adding 50 µL of sample and 50 µL prepared LDH Detection Reagent per well in 96-well opaque, white-walled plates. Samples were protected from light and incubated at room temperature for 60 minutes. After 60 minutes, luminescence was read immediately using a plate reader with a 1 second integration time (BioTek Synergy HT Plate Reader and Gen5 Software, BioTek Instruments, Inc.). Relative luminescence for each sample was calculated by subtracting the luminescence from the sample blank (cell medium) from each hydrogel sample.

Spheroid Immunofluorescent Staining and Imaging

Encapsulated spheroids were stained as described previously (139). On days 1 and 3 of culture, encapsulated spheroids were fixed in 4% formaldehyde in PBS for 15 minutes followed by three PBS washes. All subsequent steps were performed on a shaker at room temperature unless otherwise noted. Samples were permeabilized for 15 minutes in a 0.1% Tween 20 (Fisher Scientific, BP337) in PBS. Following permeabilization, 300 µL of working solution was added to each sample (1 µL Phalloidin-iFluor 488 Reagent (Abcam, ab176753) per 1 mL 1% BSA in

PBS) for 90 minutes and samples were protected from light. After incubation, samples were washed in PBS 4x20 minutes. Samples were then stained with Hoechst (1:2000 in PBS; ThermoFisher, H3570) for 30 minutes followed by one PBS wash. Samples were stored at 4°C in PBS until imaged. Samples were imaged using a Zeiss LSM 710 Confocal Microscope and 20X objective. Two samples were imaged per day and one Z-stack was taken per sample. Maximum intensity projection images were generated using ZEN (black edition; Zeiss).

Nascent Protein Staining and Imaging

Nascent protein staining was performed as previously described by Loebel et al. (142, 143, 235). Starting on day 1 of culture, encapsulated spheroids were incubated with the methionine analog azidohomoalanine (Click-iT AHA; Invitrogen, C10102; 100 μM) in methionine-free DMEM (custom made; School of Chemical Sciences Cell Media Facility, University of Illinois at Urbana-Champaign) supplemented with 1% penicillin/streptomycin and 2% FBS. AHA was replenished daily. On day 3 of culture, live cells were washed two times with sterile PBS, incubated for 40 minutes in AFDye 488 DBCO (Click Chemistry Tools, 1278-1; 30 μM) at 37°C, washed three times with sterile PBS, and then fixed in 4% formaldehyde in PBS for 15 minutes followed by three PBS washes. Samples were stored at 4°C in PBS until stained. Samples were incubated in CellMask™ Deep Red Plasma Membrane Stain (1:1000; Invitrogen, C10046) for 40 minutes at 37°C followed by three PBS washes. Samples were then incubated in Hoechst at room temperature for 30 minutes (1:2000 dilution in PBS) followed by one PBS wash. Samples were stored at 4°C in PBS until imaged. Samples (n=3) were imaged using a Zeiss LSM 710 Confocal Microscope and 20X objective. One Z-stack was taken per sample and maximum intensity projection images were generated using ZEN (black edition; Zeiss).

Statistics

OriginPro 2020 (Origin Lab) and RStudio were used for statistical analysis. Underlying assumptions for each statistical test were tested prior to analyzing data. Normality was determined using the Shapiro-Wilkes test and homoscedasticity was determined using Levene's test. For each experiment, n=5-8 independent spheroids were analyzed per sample group. Normal, homoscedastic data were analyzed using a one-way analysis of variance (ANOVA) and post hoc Tukey Test. Normal, heteroscedastic data were analyzed using Welch's ANOVA and post hoc Games-Howell Test. Non-normal, homoscedastic data were analyzed using Kruskal-Wallis ANOVA and post hoc Dunn's Test. Non-normal, heteroscedastic data were analyzed using Welch's Heteroscedastic F Test with Trimmed Means and Winsorized Variances and post hoc Games-Howell Test. Significance was defined as $p<0.05$. Data are presented as mean ± standard deviation unless otherwise noted.

6.4 Results

Characterization of Swan71 Trophoblast Spheroid Motility Assays

A library of Swan71 spheroids was created with diameters that fall within the regime of invading blastocysts (200). Spheroids fabricated from 2,000, 4,000, or 6,000 cells/spheroid ranged in size from 360.4 ± 10.3 μm to 535.0 ± 11.1 μm in diameter and 0.11 ± 0.01 to 0.21 ± 0.03 mm^2 in projected area (Figure 33A-C). All spheroid densities were significantly different from each other in diameter (n=5 per condition; $p < 0.0001$) and area (n=5; 2,000 to 4,000 cells, p=0.0016; 2,000 to 6,000, $p=4.14 \times 10^{-6}$; 4,000 to 6,000 p=0.0037). Spheroids of 4,000 cells were selected for all subsequent studies because they had the lowest density possible to more closely mimic blastocyst size while maintaining feasible experimental procedures. Spheroids were encapsulated

in GelMA hydrogels for up to 3 days (Figure 33D). By day 3 of culture, trophoblast cells were observed to migrate into the surrounding hydrogel matrix away from the initial spheroid core (Figure 33E).

Swan71 Trophoblast Spheroids Are Capable of Matrix Deposition in 3D

Cell motility can be strongly influenced by dynamic remodeling of the extracellular matrix. We investigated bulk nascent protein production of encapsulated Swan71 trophoblast spheroids for days 1 through 3 of culture via a recently described metabolic labeling approach (utilizing cell media supplemented with the methionine-analog AHA) (143). We observed significant nascent protein production as well as accumulation in close proximity to trophoblast cells in three-dimensional hydrogels (Figure 34). These observations indicate that nascent protein deposition occurs relatively rapidly within hydrogels and likely occurs throughout the entirety of these experiments (3 days).

Epidermal Growth Factor Increases Trophoblast Motility and Viability Compared to Control and to Nodal

To demonstrate that soluble biomolecules significantly alter baseline motility patterns of Swan71 trophoblasts, we encapsulated Swan71 spheroids for 3 days in the presence of the known invasion promoter epidermal growth factor (EGF; 5 ng/mL) and known invasion inhibitor Nodal (250 ng/mL) (85, 194, 236). Over 3 days of culture, trophoblast cells migrated into the surrounding hydrogel matrix and we detected quantifiable differences in migration patterns and cell viability (Figure 35). By day 2, cells cultured in medium containing EGF had significantly higher outgrowth area (Figure 35B; n=6-7 per condition) compared to cells cultured in control

medium (p=0.022) or medium containing recombinant nodal (p=1.97x10^{-3}). By day 3, we observed robust differences (n=6-7) in outgrowth area in samples cultured with EGF compared to control and recombinant Nodal (p<0.0001). Differences in fold change in outgrowth area (Figure 35C) of samples compared to initial spheroid area on day 0 were discernable by day 1 for EGF samples compared to nodal samples (n=6-7, p=0.048). By days 2 and 3, EGF samples had significantly higher fold change compared to control and nodal samples (Day 2: n=6-7, EGF Control p=0.006, EGF Nodal p=0.004; Day 3: n=6-7, EGF Control p=4.22x10^{-5}, EGF Nodal p=1.76x10^{-5}). Although cell viability (Figure 35D) was increased for samples cultured with EGF compared to control samples (n=6-7, p=0.033) there were no statistically significant differences in cytotoxicity (Figure 35E) between the three groups by day 3 (n=5-7). Collectively, these data demonstrate that 3D spheroid motility assays provide an engineering platform that can be used to detect shifts in motility and viability/cytotoxicity patterns in response to soluble biomolecules.

The Addition of Soluble PSG9-Fc Decreases Trophoblast Motility

We subsequently quantified changes in trophoblast spheroid outgrowth area, viability, and cytotoxicity over 3 days of culture in response to 60 μg/mL soluble PSG9-Fc (Figure 36). By day 3 of culture, we observed a statistically significant decrease in outgrowth area (Figure 36B) in response to PSG9-Fc compared to both cell medium control and the Fc-treated control protein samples (n=8 per condition, Control PSG9-Fc p=7.13x10^{-6}, Fc-Control PSG9-Fc p=0.0066, Control Fc-Control p=0.020). The Fc-control was used as an additional control condition because PSG9-Fc has a Fc tag at the C-terminus; further, both PSG9-Fc and Fc-control were purified using the same procedure. Fold change (Figure 36C) in outgrowth area differed between control and PSG9-Fc samples on day 1 (n=8, p=0.019) and on day 3, fold change was significantly

different (n=8) in PSG9-Fc samples compared to control (p=9.60x10^{-6}) and Fc-control samples (p=0.0022). Notably, day 3 cell viability (CellTiter-Glo® 3D Viability Assay; Figure 36D) did not differ between groups, though cytotoxicity (LDH-Glo® Cytotoxicity Assay; Figure 36E) was statistically significantly lower in Fc-control samples versus control media (n=8, p=0.0018). Taken together, these data suggest that PSG9-Fc may have an inhibitory role on trophoblast invasion without influencing trophoblast viability or cytotoxicity.

PSG1-Fc, but not PSG1-His, Increases Trophoblast Motility

We examined the influence of PSG1 on trophoblast motility as insufficient trophoblast invasion has been associated with pre-eclampsia (205, 226). Previously, Swan71 migration was shown to increase in response to immobilized PSG1 in two-dimensional *in vitro* studies, but no differences were observed in transwell invasion assays (226). We quantified the role of soluble PSG1 on Swan71 trophoblast motility using a 3D motility assay. We compared patterns of migration and viability using two variants of PSG1 (Figure 37): PSG1-His and PSG1-Fc which differ based on their production and purification methods as previously described (237). By day 2 of culture, we observed higher outgrowth area (n=5-6 spheroids per condition) in samples cultured with PSG1-Fc compared to control (p=0.026), Fc-control (p=0.029), and PSG1-His samples (p=8.42x10^{-4}). On day 3 of culture, hydrogels cultured with PSG1-Fc had significantly higher (n=5-6) outgrowth compared to hydrogels cultured with PSG1-His (p=0.019). Fold change in outgrowth area did not differ on days 1 and 3 of culture; however, on day 2, fold change in outgrowth area was significantly higher in samples cultured with PSG1-Fc compared to samples cultured with PSG1-His (n=5-6, p=0.0078). Although we did not observe differences in cell viability between groups on day 3; however, cytotoxicity was found to be increased (n=5-6) in PSG1-Fc samples

compared to control (p=0.0082) and Fc-control samples (p=0.0071). Taken together, these results suggest that PSG1-Fc increases trophoblast motility.

6.5 Discussion

Many mechanisms driving early pregnancy and implantation remain unknown and poorly understood. Because of significant differences between animal and human pregnancy as well as the ethical concerns regarding studying early pregnancy in humans, *in vitro* models are often used to study mechanisms of human reproduction. Multidimensional *in vitro* models offer the opportunity to examine cellular mechanisms of early pregnancy using human-derived cells in controlled, tunable microenvironments. The 3D nature of these models can be tuned to recapitulate biophysical properties from the native tissue microenvironment such as architecture, stiffness, and inclusion of heterogeneous cohorts of cells, each offering increased biofidelity compared to existing 2D models. Recent 3D models of trophoblast migration have used biomaterials as a matrix around invading trophoblast cells as a means of replicating trophoblast invasion through tissue (47-49, 85, 111, 191, 238). For example, Buck et al. mixed trophoblast spheroids and epithelial spheroids in Matrigel as a model of trophoblast invasion of endometrial glands (47). Chang et al. embedded morulas in Matrigel and quantified outgrowth, proliferationn, and degradation over time (111). Others, such as Wang et al. created stratified cultures encapsulated in fibrin-agarose consisting of epithelial and stromal compartments through which trophoblast spheroids invade (48, 49). Nonetheless, many of these models often employ biomaterials such as Matrigel that have limitations. For example, Matrigel has been found to have significant batch-to-batch variations in biomechanical properties, extracellular matrix content, and protein content (127, 128, 239). These limitations highlight the need for more

controllable materials to analyze trophoblast invasion through a matrix. The GelMA hydrogel system used in this work offers a number of potential advantages specific for investigating trophoblast activity. The gelatin macromer used to create the GelMA hydrogel contains RGD cell binding motifs and MMP sites which allows for cell binding and matrix remodeling (69, 87, 88). The use of photoinitiator allows for photopolymerization of GelMA under UV light, which covalently crosslinks the hydrogels and renders the hydrogels relatively homogenous in structure (69, 87, 88, 93, 240). The biophysical properties of GelMA, including stiffness and crosslinking density, can be tuned by manipulating the degree of methacrylamide functionalization along the gelatin macromer during GelMA synthesis or via crosslinking intensity (69, 87, 88, 203). This makes the GelMA system amenable to creating libraries of monolithic environments or spatially-graded hydrogels containing a linear gradient of embossed stiffness or matrix-bound proteins to locally influence cell behavior (93, 203, 209). Other groups have used microfabrication techniques such as photopatterning, micromolding, self-assembly, and 3D printing to further customize the three-dimensional environment (69, 88). Although this study used unmodified GelMA hydrogels this versatility of the GelMA system provides exciting opportunities to examine trophoblast motility in increasingly complex, bioengineered systems.

We report Swan71 trophoblast motility in response to two different members of the human PSG family. We demonstrate reproducible, consistent methodology, as indicated by similar values in outgrowth area, fold change in outgrowth area, and viability for control samples across multiple experiments. We also quantify cytotoxicity of spheroids; however, this assay system has limitations compared to the viability assay system. We observed variability across experiments for cytotoxicity measurements even though the viability was similar, which has previously been

found to be a limitation for the LDH assay and should be addressed in future studies by reducing serum concentrations and adjusting the signal-to-noise ratio for the assay (241).

We next demonstrate the three-dimensional trophoblast motility assay also provides an avenue to explore trophoblast mediated matrix deposition. Remodeling and matrix deposition are powerful forces central to successful trophoblast invasion. We have previously used the GelMA hydrogel as a well-characterized platform to examine processes of cell mediated degradative and biosynthetic remodeling via assessments of stiffness, gene expression, and secreted biomolecules (242). Here, we adapted a recently described metabolic labeling approach to examine qualitative nascent protein production by Swan71 spheroids. We stained cells for bulk nascent protein production after 3 days of culture. Spheroids of Swan 71 trophoblasts secrete proteins within the hydrogels in sufficient quantities that their local accumulation can be visualized. Matrix remodeling plays a key role in trophoblast invasion so methods such as these will enable researchers to probe questions relating to the role of the extracellular matrix on trophoblast cell migration (39, 40, 42, 109). Future work will determine the specific proteins secreted by the cells to determine if matrix deposition plays a role on trophoblast motility.

To further validate our motility assay, we first examined trophoblast motility in response to a known promoter (EGF) and inhibitor (Nodal) of trophoblast invasion. Exogenously added EGF markedly increased trophoblast outgrowth area compared to control and Nodal samples and increased viability compared to control samples, consistent with previous reports in the literature that concentrate on the mechanistic role of EGF in trophoblast activity (85, 139, 194).

Interestingly, while samples cultured in the presence of Nodal showed no difference in outgrowth area and viability compared to control samples, Nodal did significantly reduce overall outgrowth area (as well as fold change in outgrowth area) compared to exogenous EGF addition as early as day 2 of culture. Nadeem et al. previously demonstrated that Nodal reduced trophoblast invasion in wound-healing assays, transwell assays, and first-trimester placental explant invasion when Nodal was overexpressed or added to culture media (236). However, there are also studies that saw opposite effects and acknowledge contrasting results (243, 244). This multidimensional hydrogel model offers significant opportunities for future studies to examine dose dependent effects as well as to incorporate additional soluble factors or inhibitor in order to mechanistically probe the differential role of Nodal vs. EGF on trophoblast motility and invasion.

PSGs are some of the most abundant circulating trophoblastic proteins in maternal blood during human pregnancy (226-229); however, much remains unknown regarding their role in early implantation and pregnancy disorders. Due to lack of specific antibodies that can distinguish the individual PSGs, temporal and expression levels have not been determined at the protein level; however, studies evaluating PSG expression at the mRNA level in the first and third trimesters indicated that PSG1 is expressed at much higher levels than PSG9, a finding confirmed by a different laboratory when examining expression of PSGs in villous cytotrophoblasts (245, 246).

The various PSGs that have been examined so far share identical functions; therefore, the expansion and rapid evolution of the human PSG family has been explained by selection for increased dosage of PSG proteins, rather than for diversification of function. Both PSG1 and PSG9

activate latent transforming growth factor β (TGF-β), bind to integrins αIIbβ3, and α5β1, induce endothelial tube formation by binding to heparan sulfate proteoglycans and also bind to galectin-1 in a glycan-dependent manner (226, 234, 246, 247). Interestingly, although we have not found differences in PSG1 and PSG9 receptor utilization, our previous studies with members of the murine PSG family showed that murine PSGs (designated as psg16-32) may not all share the same function as they bind to different receptors. Although murine psg17 and psg19 bind to the tetraspanin CD9, we found no evidence of interaction of CD9 with psg22 and psg23 (248, 249). Therefore, as we observed with murine psgs, it is possible that receptor usage may vary between different members of the human PSG family. Additional studies are required to confirm the potential differences in PSG1 and PSG9 expression and its association with pregnancy pathologies, here, we studied the effect of exogenously added PSG1 and PSG9 in trophoblast motility with this newly developed protocol.

To this end, we cultured encapsulated Swan71 spheroids with PSG9-Fc and quantified outgrowth area, viability, and cytotoxicity after 3 days of culture. We found that compared to control and Fc-control samples, PSG9-Fc reduced the trophoblast outgrowth area. This study suggests that PSG9-Fc reduces trophoblast invasion; however, in order to fully understand the mechanism, additional studies must be performed. We subsequently examined the influence of exogenous PSG1-Fc and PSG1-His on trophoblast motility. Previous studies showed staining of PSG1 in extravillous trophoblasts in distal placental areas, suggesting that there is likely increased expression of this PSG and potentially one or more of the other PSGs recognized by the monoclonal antibody utilized for the studies (PSG6, PSG7, and PSG8) in extravillous trophoblasts with an invasive phenotype (226). However, previous studies using two-

dimensional wound healing assays with Swan71 or transwell invasion assays using the HTR-8 SVneo extravillous trophoblast cell line did not identify shifts in cell invasion in response to soluble PSG1 (226). We employed our trophoblast motility assay to investigate the influence of two variants of PSG1 (PSG1-Fc and PSG1-His). These two proteins differ from each other by the tag fused to the PSG1 sequence, which results in a dimeric protein in the case of PSG1-Fc, and in the length of the carboxy-terminal end following the B2 domain (1a slice variant and 1d slice variant, respectively). Interestingly, we observed an increase in outgrowth area between control samples and samples incubated with PSG1-Fc on day 2 and day 3 of culture. Although we did not observe differences in outgrowth area between control samples and PSG1-His, we observed reduced cytotoxicity in response to PSG1-His versus control. We expected to observe similar results with PSG1-Fc and PSG1-His based on our prior results analyzing PSG1 binding to their binding partners; however, PSG1-His seems to cause a downward reduction in outgrowth area compared to control samples. Nevertheless, it is possible that PSG1-Fc and PSG1-His could have the same effects on trophoblast invasion and cell viability, but a limitation of these studies is that all proteins were utilized at a single concentration. Dose-response studies may provide additional insights into the differences in the activity of the proteins in the spheroid outgrowth assay. In addition, although we observed very low expression of PSG1 in the supernatant of Swan71 cells by ELISA (approximately 525 pg/mL secreted over a 48 h period after seeding 100,000 cells in a 6 well plate); transfection of the Swan 71 cells with the PSG1 and PSG9 rather than addition of the proteins to the media may provide additional valuable information on their activity as regulators of trophoblast motility.

6.6 Conclusions

In conclusion, multidimensional biomaterial platforms offer the opportunity to provide 3D tissue microenvironments to perform mechanistic studies to elucidate physiological and pathophysiological processes challenging to study *in vivo*. Our approach to recapitulate aspects of the endometrial microenvironment (e.g., tissue stiffness, spheroid culture, migration through a matrix) to probe questions relating to trophoblast invasion employs spheroids encapsulated in GelMA hydrogels to perform quantitative motility and viability assays. We used these assays to determine trophoblast response to soluble PSG9 and PSG1. Our results show that a spheroid-based motility has the sensitivity to rapidly (within 3 days) quantify differences in trophoblast invasion and further, these cells secrete significant new protein content that can be readily visualized. Notably, we find PSG9-Fc reduces trophoblast motility while PSG1-Fc increases trophoblast motility compared to control samples. Taken together, this 3D trophoblast motility model has the potential to allow us to better understand trophoblast interactions with the extracellular matrix through which they are migrating so we can develop a deeper understanding of the mechanisms associated with early implantation.

6.7 Figures

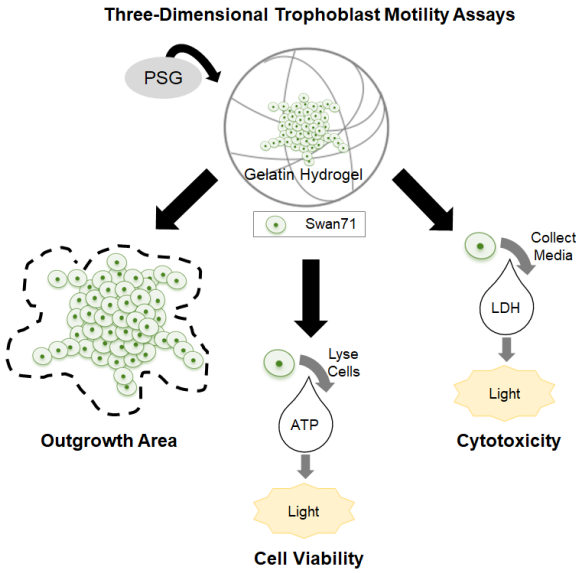

Figure 32. Table of contents graphic. Experimental work flow.

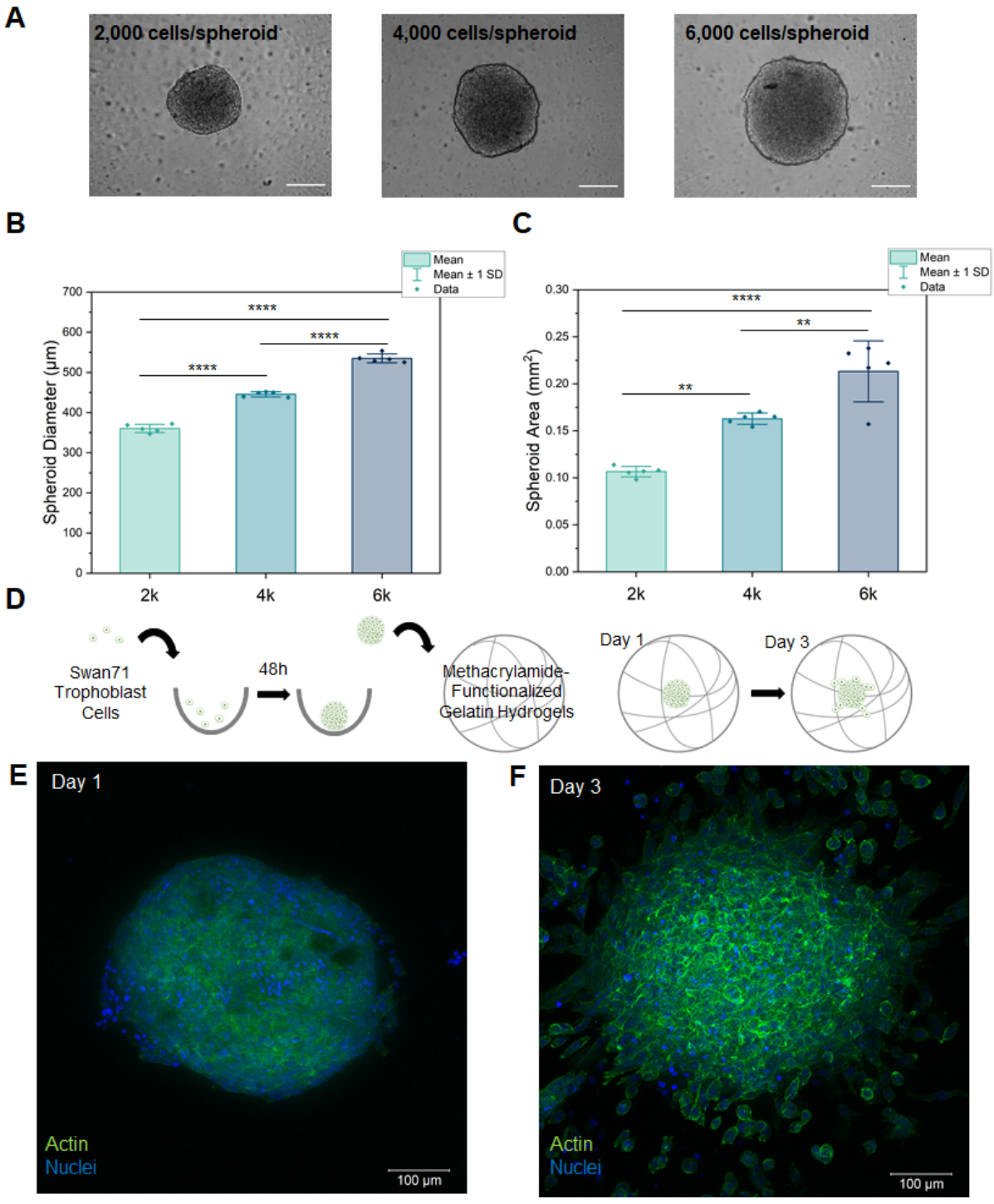

Figure 33. Three-Dimensional Swan71 Trophoblast Spheroid Assays. (A) Representative bright field images of Swan71 spheroids (2,000, 4,000, and 6,000 cells/spheroid). Scale bar, 200 µm. **(B)** Average spheroid diameter in round bottom plates. Data are displayed as individual data

Figure 33 (cont), points. Bar represents mean ± standard deviation. One-way ANOVA with Tukey post hoc analysis, **** $p < 0.0001$ (n=5 technical replicates per group). **(C)** Average spheroid area in round bottom plates. Data are displayed as individual data points. Bar represents mean ± standard deviation. One-way ANOVA with Tukey post hoc analysis, ** $p < 0.01$, **** $p < 0.0001$ (n=5 technical replicates per group). **(D)** Schematic of experimental procedure. **(E)** Representative maximum intensity projection of encapsulated Swan71 spheroid on day 1 of culture. Scale bar, 100 μm. **(F)** Representative maximum intensity projection of encapsulated Swan71 spheroid on day 3 of culture. Scale bar, 100 μm.

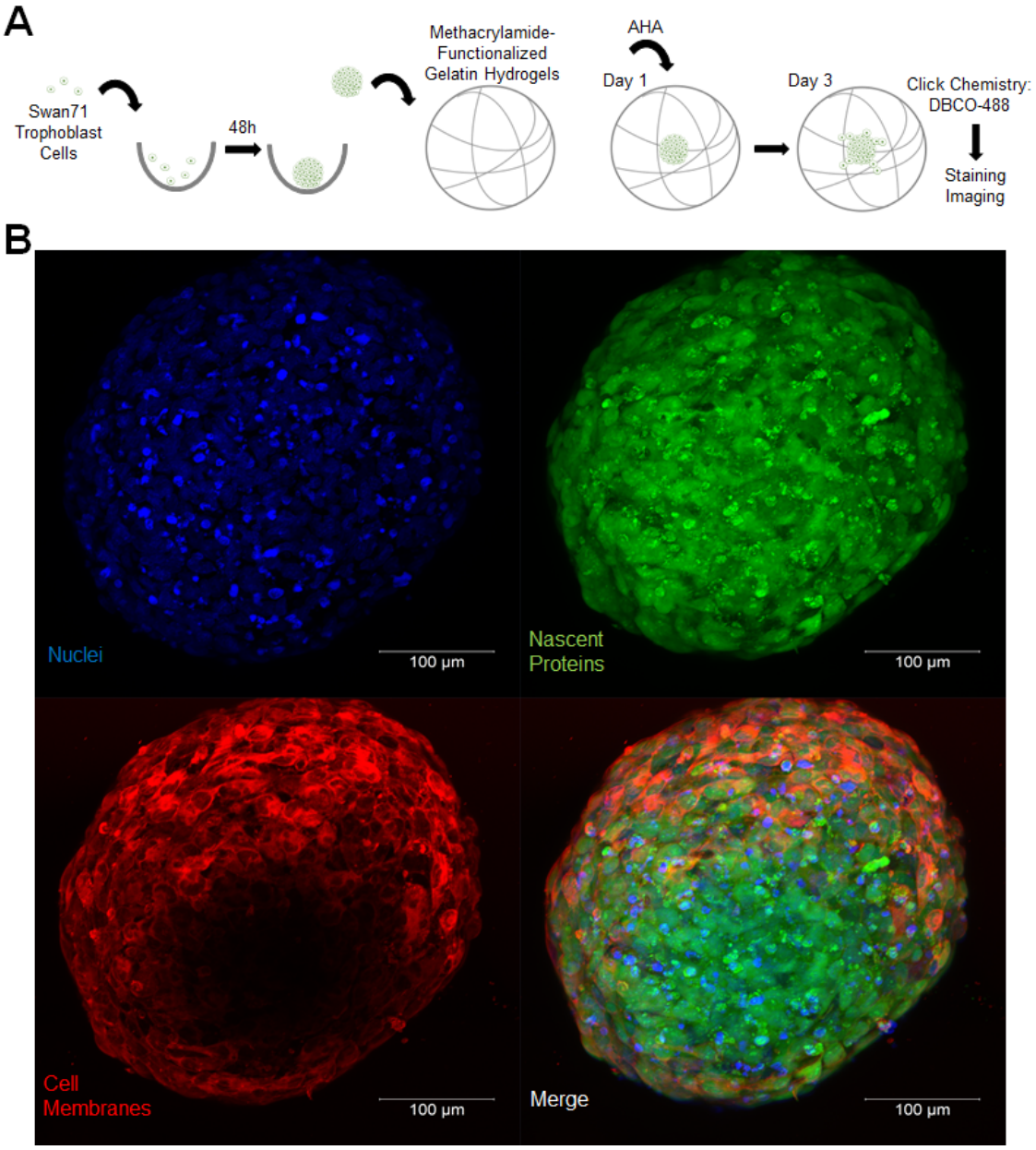

Figure 34. Matrix Remodeling by Encapsulated Swan71 Spheroids. (A) Schematic of experimental procedure. The methionine analog azidohomoalanine (AHA) was added to spheroids on day 1 of culture and replaced daily. On day 3, a click chemistry reaction was performed using DBCO-488, a fluorophore-conjugated cyclooctyne, to visualize nascent proteins. Staining was performed after the click chemistry reaction to visualize cells. **(B)**

Figure 34 (cont), Representative maximum intensity projection of encapsulated Swan71 spheroid on day 3 of culture stained for bulk nascent protein production.

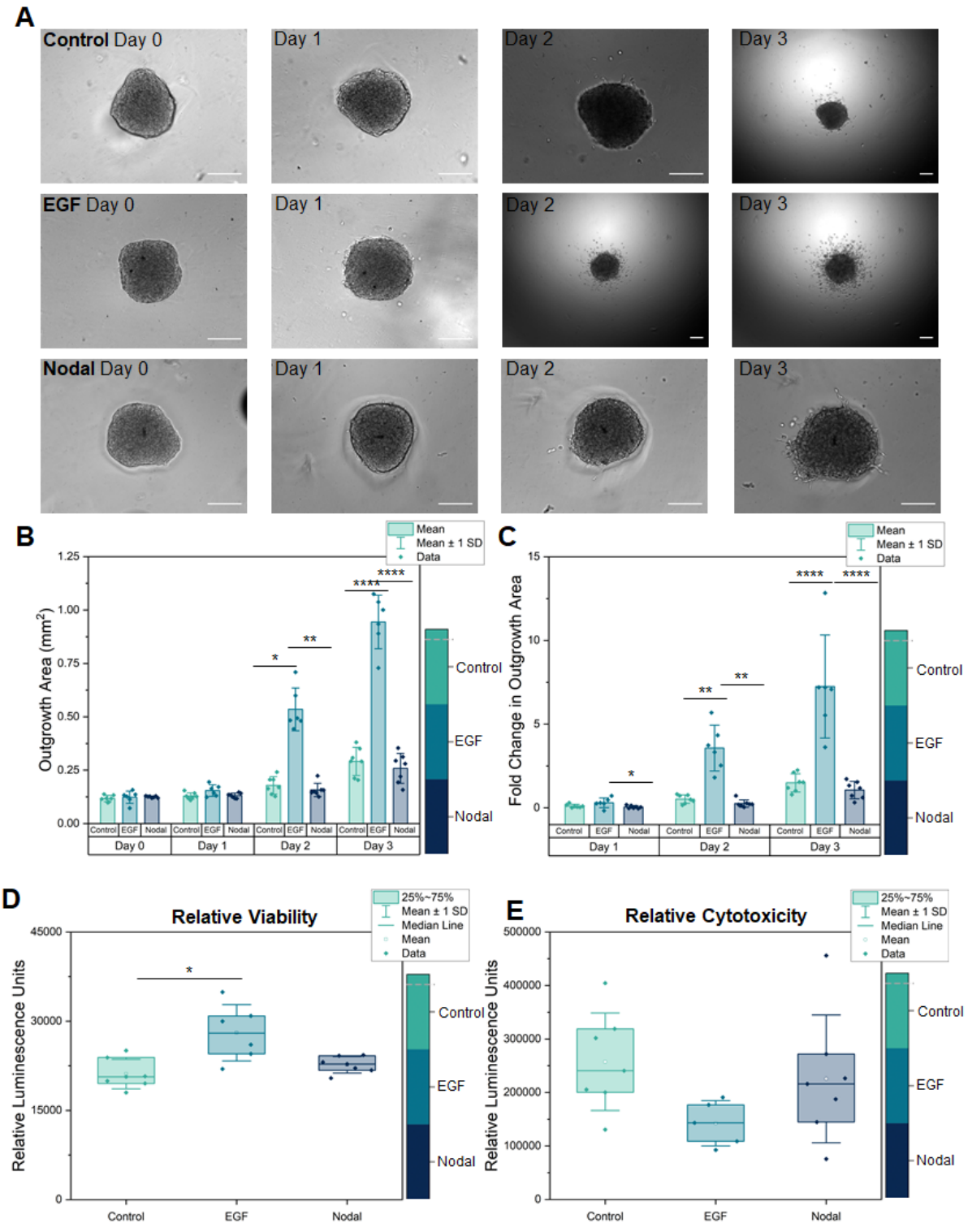

Figure 35. Invasion Pattern Analysis After the Addition of Exogenous Growth Factors Epidermal Growth Factor (EGF) and Nodal to Spheroids Encapsulated in

Figure 35 (cont), Methacrylamide-Functionalized Gelatin (GelMA) Hydrogels. (A) Representative bright field images of 4,000 cell spheroids encapsulated in GelMA hydrogels from day 0 (seeding) to day 3 for control and after addition of 5 ng/mL EGF or 250 ng/mL Nodal. Scale bar, 200 μm. **(B)** Average spheroid outgrowth area in GelMA hydrogels over 3 days. Data are displayed as individual data points. Bar represents mean ± standard deviation. Data were analyzed on each day between groups (Control n=7 technical replicates, EGF n=6 technical replicates, Nodal n=7 technical replicates). Day 0: One-way ANOVA with Tukey post hoc analysis, *** $p < 0.001$, **** $p < 0.0001$. Day 1: One-way ANOVA with Tukey post hoc analysis. Day 2: Kruskal-Wallis with Dunn's post hoc analysis, * $p < 0.05$, ** $p < 0.01$. Day 3: One-way ANOVA, **** $p < 0.0001$. **(C)** Spheroid outgrowth area fold change compared to initial area (day 0) over 3 days. Data are displayed as individual data points. Bar represents mean ± standard deviation. Data were analyzed on each day between groups (Control n=7 technical replicates, EGF n=6 technical replicates, Nodal n=7 technical replicates). Day 1: One-way ANOVA with Tukey post hoc analysis, * $p < 0.05$. Day 2: Welch's heteroscedastic F Test with Trimmed Means and Winsorized Variances with Games-Howell post hoc analysis, ** $p < 0.01$. Day 3: One-way ANOVA with Tukey post hoc analysis, **** $p < 0.0001$. **(D)** Relative viability of encapsulated spheroids at day 3 from CellTiter-Glo® 3D Viability Assay. Data are presented as individual data points overlaying box plots with the median denoted by a line, mean denoted by a square, and whiskers represent the mean ± standard deviation. Welch's ANOVA with Games-Howell post hoc analysis, * $p < 0.05$, Control n=7 technical replicates, EGF n=6 technical replicates, Nodal n=7 technical replicates. **(E)** Relative cytotoxicity of encapsulated spheroids at day 3 from measured from lactate dehydrogenase release via LDH-Glo® Cytotoxicity Assay. Data are presented as individual data points overlaying box plots with the

Figure 35 (cont), median denoted by a line, mean denoted by a square, and whiskers represent the mean ± standard deviation. One-way ANOVA with Tukey post hoc analysis, Control n=7 technical replicates, EGF n=5 technical replicates, Nodal n=7 technical replicates.

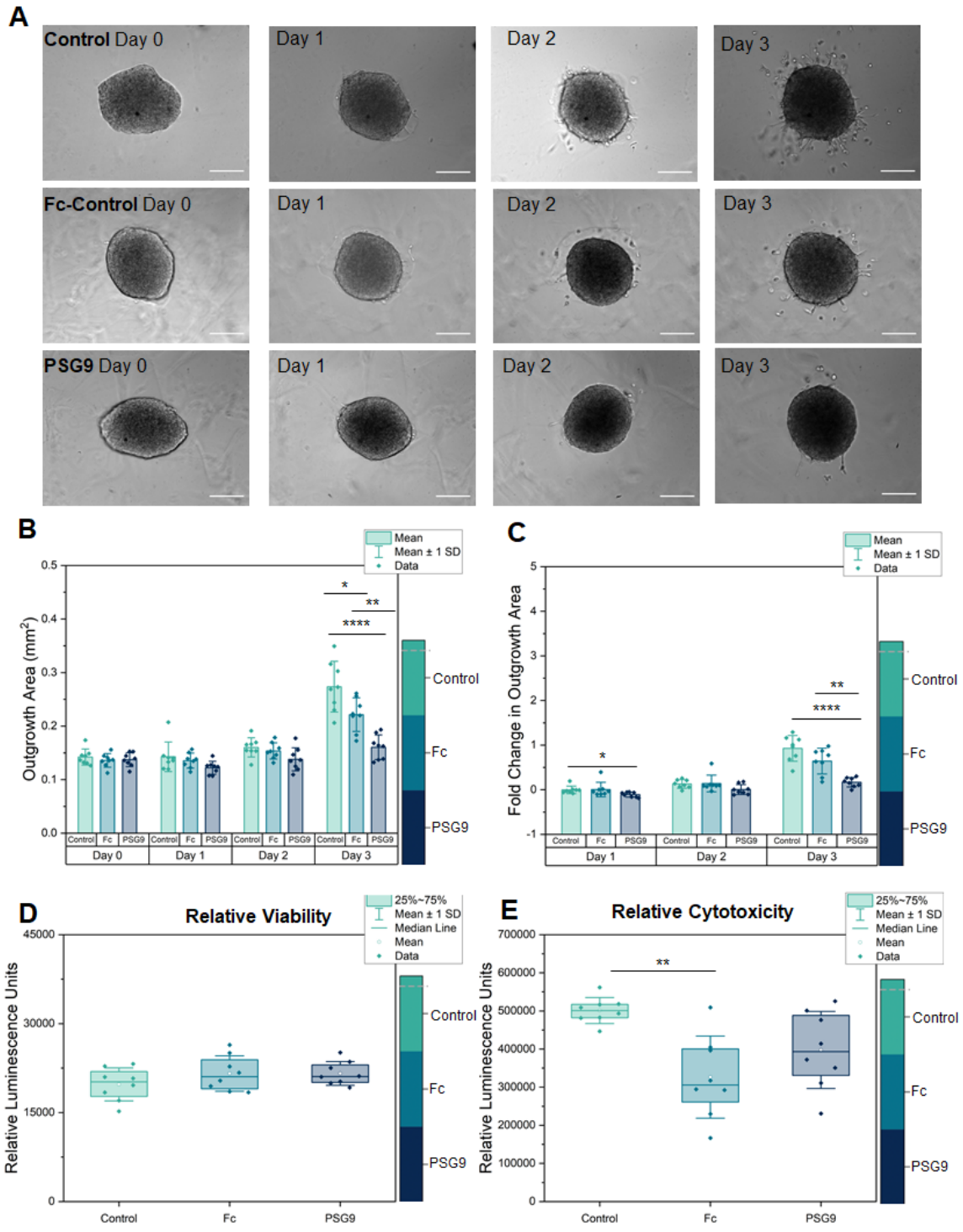

Figure 36. PSG9-Fc Inhibits Swan71 Spheroid Invasion in Methacrylamide-Functionalized Gelatin (GelMA) Hydrogels. (A) Representative bright field images of 4,000 cell spheroids

Figure 36 (cont), encapsulated in GelMA hydrogels from day 0 (seeding) to day 3 for Control samples, Fc-Control samples (60 μg/mL), and PSG9-Fc samples (60 μg/mL). Scale bar, 200 μm. **(B)** Average spheroid outgrowth area in GelMA hydrogels over 3 days. Data are displayed as individual data points. Bar represents mean ± standard deviation. Data were analyzed on each day between groups (Control n=8 technical replicates, Fc-control n=8 technical replicates, PSG9-Fc n=8 technical replicates). Day 0: One-way ANOVA. Day 1: Kruskal-Wallis ANOVA. Day 2: One-way ANOVA. Day 3: One-way ANOVA with Tukey post hoc analysis, * $p < 0.05$, ** $p < 0.01$, **** $p < 0.0001$. **(C)** Spheroid outgrowth area fold change compared to initial area (day 0) over 3 days. Data are displayed as individual data points. Bar represents mean ± standard deviation. Data were analyzed on each day between groups (Control n=8 technical replicates, Fc-control n=8 technical replicates, PSG9-Fc n=8 technical replicates). Day 1: Kruskal-Wallis ANOVA with Dunn's post hoc analysis, * $p < 0.05$. Day 2: Kruskal-Wallis ANOVA. Day 3: One-way ANOVA with Tukey post hoc analysis, ** $p < 0.01$, **** $p < 0.0001$. **(D)** Relative viability of encapsulated spheroids at day 3 from CellTiter-Glo® 3D Viability Assay. Data are presented as individual data points overlaying box plots with the median denoted by a line, mean denoted by a square, and whiskers represent the mean ± standard deviation. One-way ANOVA. Control n=8 technical replicates, Fc-control n=8 technical replicates, PSG9-Fc n=8 technical replicates. **(E)** Relative cytotoxicity of encapsulated spheroids at day 3 measured from lactate dehydrogenase release via LDH-Glo® Cytotoxicity Assay. Data are presented as individual data points overlaying box plots with the median denoted by a line, mean denoted by a square, and whiskers represent the mean ± standard deviation. One-way ANOVA with Tukey post hoc analysis. Control n=8 technical replicates, Fc-control n=8 technical replicates, PSG9-Fc n=8 technical replicates; ** $p < 0.01$.

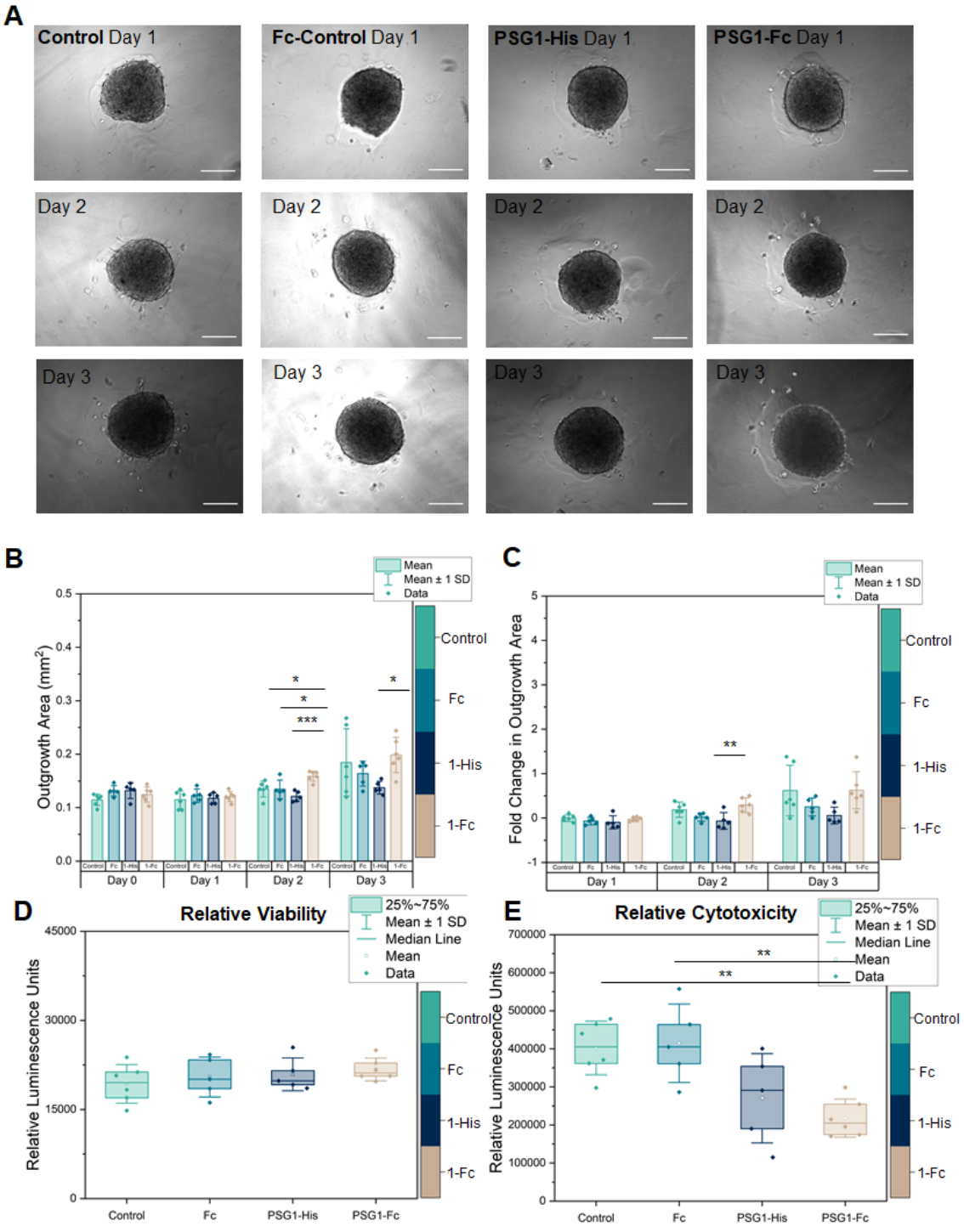

Figure 37. Invasion Pattern Analysis After the Addition of PSG1-Fc and PSG1-His to Swan71 Spheroids Encapsulated in Methacrylamide-Functionalized Gelatin (GelMA)

Figure 37 (cont), Hydrogels. (A) Representative bright field images of 4,000 cell spheroids encapsulated in GelMA hydrogels from day 1 to day 3 for Control samples, Fc-Control samples (60 μg/mL), PSG1-His samples (60 μg/ml), and PSG1-Fc samples (60 μg/mL). Scale bar, 200 μm. **(B)** Average spheroid outgrowth area in GelMA hydrogels over 3 days. Data are displayed as individual data points. Bar represents mean ± standard deviation. Data were analyzed on each day between groups (Control n=6 technical replicates, Fc-Control (Fc) n=5 technical replicates, PSG1-His (1-His) n=5 technical replicates, and PSG1-Fc (1-Fc) n=6 technical replicates). Day 0, 1: One-way ANOVA. Day 2: One-way ANOVA with Tukey post hoc analysis, * $p < 0.05$, *** $p < 0.001$. Day 3: Welch's ANOVA with Games-Howell post hoc analysis, * $p < 0.05$. **(C)** Spheroid outgrowth area fold change compared to initial area (day 0) over 3 days. Data are displayed as individual data points. Bar represents mean ± standard deviation. Data were analyzed on each day between groups (Control n=6 technical replicates, Fc-Control (Fc) n=5 technical replicates, PSG1-His (1-His) n=5 technical replicates, and PSG1-Fc (1-Fc) n=6 technical replicates). Day 1: Kruskal-Wallis ANOVA. Day 2: One-way ANOVA with Tukey post hoc analysis, ** $p < 0.01$. Day 3: One-way ANOVA. **(D)** Relative viability of encapsulated spheroids at day 3 from CellTiter-Glo® 3D Viability Assay. Data are presented as individual data points overlaying box plots with the median denoted by a line, mean denoted by a square, and whiskers represent the mean ± standard deviation. One-way ANOVA. Control n=6 technical replicates, Fc-Control (Fc) n=5 technical replicates, PSG1-His n=5 technical replicates, and PSG1-Fc n=6 technical replicates. **(E)** Relative cytotoxicity of encapsulated spheroids at day 3 from measured from lactate dehydrogenase release via LDH-Glo® Cytotoxicity Assay. Data are presented as individual data points overlaying box plots with the median denoted by a line, mean denoted by a square, and whiskers represent the mean ± standard deviation. One-way ANOVA

Figure 37 (cont), with Tukey post hoc analysis. Control n=6 technical replicates, Fc-Control (Fc) n=5 technical replicates, PSG1-His n=5 technical replicates, and PSG1-Fc n=6 technical replicates, ** $p < 0.01$.

CHAPTER 7: CONCLUDING REMARKS AND FUTURE OPPORTUNITIES

7.1 Conclusions

In this dissertation, we describe the creation of a stratified endometrial model platform to investigate trophoblast motility. This goal was inspired by high maternal mortality rates and poor pregnancy outcomes in the United States coupled with significant racial disparities in maternal and perinatal mortality for non-white people. We developed these platforms as tunable systems to probe questions surrounding defects in early implantation. We sought to develop platforms to begin to ask how aspects of stress (e.g., cortisol), experienced in higher amounts in people of color, impact aspects of endometrial function and trophoblast motility. Our central hypothesis was that stress molecules from the maternal-fetal interface (e.g., cortisol) negatively influence endometrial function and trophoblast invasion. Cortisol likely causes defects in cellular crosstalk at this interface that negatively influences the extent of trophoblast invasion, potentially resulting in defective implantation and pregnancy disorders.

We have demonstrated that GelMA hydrogel platforms are adaptable for studying dynamic endometrial processes, including vascular formation, hormone responsiveness, epithelial monolayer formation, and trophoblast invasion. We developed methods to create and characterize a library of GelMA with mechanical properties similar to the native endometrium and placenta (Chapter Two), support the culture of an endometrial perivascular niche to study endometrial angiogenesis (Chapter Four), provide biochemical cues to hormone-responsive cells (e.g., decidualization of endometrial stromal cells), establish epithelial monolayers overlaying GelMA hydrogels (Chapter Three), and have employed the GelMA platform for trophoblast invasion assays (Chapter Five and Chapter 6). These tools will now allow us to answer the

following questions: How does cortisol influence endometrial function? How do biomolecular signals from stress influence trophoblast invasion?

7.2 Future Opportunities

The work herein provides unique endometrial platforms that can be used to target other aspects of female reproductive health. We describe some future opportunities below.

Racial Disparities in Female Reproductive Health

Human cell lines are often necessary for bioengineering models due to the lack of primary donor cells as well as the expense and complicated protocols of isolating primary cells or differentiating human induced pluripotent stem cells. Unfortunately, human cell lines often lack diversity and do not provide crucial donor information such as race, sex, gender, and age. There has recently been a push to consider cell ancestry when developing bioengineering models so that we can capture racial/ethnic variation of populations to improve inclusion in our model systems (153, 154).

A contributing factor to poor maternal mortality rates in the United States compared to other developed nations stems from significant racial disparities in pregnancy. From 2011-2015, pregnancy-related deaths in the United States were 13.0 deaths per 100,000 live births for White women, 42.8 deaths per 100,000 Black women (5-11). The causes of racial disparities in pregnancy transcend socioeconomic status and education level: recent research has suggested that psychosocial stressors such as discrimination and microaggressions experienced by non-white women likely contribute to these disparities. With our tunable endometrial model system,

there is an opportunity to use patient-derived cells to develop endometrial model systems to begin to probe differences in endometrial physiology across groups. This may elucidate additional possible reasons why considerable racial disparities exist in pregnancy-related mortality.

Variation in Menstrual Cycle Dynamics

Menstruation is defined as the shedding of blood and tissue from the endometrium. Menstruation can be highly variable between cycles for individuals but also between individuals (33, 186, 250). As such, the menstrual cycle itself has significant variability that should be considered in endometrial models. The menstrual cycle is typically described as a 28-day cycle; however, there is significant variation between individuals from age of menarche, cycle length, and endometrial thickness (33, 186, 250). Our studies modeled only the decidualization phase of the menstrual cycle but did not consider other menstrual cycle phases. Furthermore, we utilized only two hormone cocktails previously described in the literature; however, altering the mode of delivery and bolus of delivery of hormones may help address variation in menstrual cycle dynamics.

Exploration of Other Female Reproductive Health Disorders

Although we focused on early implantation events, there are numerous endometrial disorders that can be studied using our model systems. For example, endometriosis is the presence of endometrial tissue outside of the uterus (251). Endometriosis is a heterogeneous disease but symptoms can include chronic pain and infertility (251). A deeper understanding of endometrial physiology may provide insights into how and why endometrial tissue implants in other regions of the body. Ongoing work continuing in our laboratory is seeking to adapt approaches

developed here to model aspects of endometrial cell invasion (spheroid invasion assays) in endometriotic cells, study interactions between extracellular matrix composition and lesion initiation (microarrays), and analyze the contribution of the perivascular niche on endometriosis development (perivascular hydrogels).

7.3 Final Remarks

As a historically understudied and underfunded field, female reproductive health has often lagged behind other more-studied fields. This has unfortunately led to disappointing prevention and treatment options for a variety of female reproductive disorders that not only impact the quality of life of females but also can extend into the lives of their children with poor perinatal outcomes. It is our hope that the platforms developed herein will provide engineering toolsets to address these issues to improve health outcomes for women.

REFERENCES

1. World Health Organization. Maternal Mortality 2016 [updated November 2016]. Available from: http://www.who.int/mediacentre/factsheets/fs348/en/.
2. Central Intelligence Agency. Maternal Mortality Ratio 2015. Available from: https://www.cia.gov/library/publications/the-world-factbook/fields/2223.html.
3. Centers for Disease Control and Prevention. Reproductive Health 2018 [updated January 10, 2018]. Available from: https://www.cdc.gov/reproductivehealth/index.html.
4. Collaborators MM. Global, regional, and national levels of maternal mortality, 1990-2015: a systematic analysis for the Global Burden of Disease Study 2015. Lancet. 2016;388:1775-812. doi: 10.1016/S0140-6736(16)31470-2.
5. Holdt Somer SJ, Sinkey RG, Bryant AS. Epidemiology of racial/ethnic disparities in severe maternal morbidity and mortality. Semin Perinatol. 2017;41(5):258-65. Epub 2017/09/11. doi: 10.1053/j.semperi.2017.04.001. PubMed PMID: 28888263.
6. Crawford S, Joshi N, Boulet SL, Bailey MA, Hood ME, Manning SE, McKane P, Kirby RS, Kissin DM, Jamieson DJ, States Monitoring Assisted Reproductive Technology C. Maternal Racial and Ethnic Disparities in Neonatal Birth Outcomes With and Without Assisted Reproduction. Obstet Gynecol. 2017;129(6):1022-30. Epub 2017/05/10. doi: 10.1097/AOG.0000000000002031. PubMed PMID: 28486370; PMCID: PMC5590368.
7. Goffman D, Madden RC, Harrison EA, Merkatz IR, Chazotte C. Predictors of maternal mortality and near-miss maternal morbidity. J Perinatol. 2007;27(10):597-601. doi: 10.1038/sj.jp.7211810. PubMed PMID: 17703181.
8. Metcalfe A, Wick J, Ronksley P. Racial disparities in comorbidity and severe maternal morbidity/mortality in the United States: an analysis of temporal trends. Acta Obstet Gynecol Scand. 2018;97(1):89-96. Epub 2017/10/17. doi: 10.1111/aogs.13245. PubMed PMID: 29030982.
9. Henry-Sanchez BL, Geronimus AT. Racial/Ethnic Disparities in Infant Mortality Among U.S. Latinos. Du Bois Review: Social Science Research on Race. 2013;10(1):205-31.
10. Singh GK, Siahpush M, Liu L, Allender M. Racial/Ethnic, Nativity, and Sociodemographic Disparities in Maternal Hypertension in the United States, 2014-2015. Int J Hypertens. 2018;2018:7897189. Epub 2018/06/12. doi: 10.1155/2018/7897189. PubMed PMID: 29887995; PMCID: PMC5985132.
11. Lorch SA, Enlow E. The role of social determinants in explaining racial/ethnic disparities in perinatal outcomes. Pediatr Res. 2016;79(1-2):141-7. Epub 2015/10/16. doi: 10.1038/pr.2015.199. PubMed PMID: 26466077.
12. Creanga AA, Berg CJ, Syverson C, Seed K, Bruce FC, Callaghan WM. Pregnancy-related mortality in the United States, 2006-2010. Obstet Gynecol. 2015;125(1):5-12. Epub 2015/01/07. doi: 10.1097/AOG.0000000000000564. PubMed PMID: 25560097.
13. Latendresse G. The interaction between chronic stress and pregnancy: preterm birth from a biobehavioral perspective. J Midwifery Womens Health. 2009;54(1):8-17. doi: 10.1016/j.jmwh.2008.08.001. PubMed PMID: 19114234; PMCID: PMC2651684.
14. Alhusen JL, Bower KM, Epstein E, Sharps P. Racial Discrimination and Adverse Birth Outcomes: An Integrative Review. J Midwifery Womens Health. 2016;61(6):707-20. Epub 2016/10/14. doi: 10.1111/jmwh.12490. PubMed PMID: 27737504; PMCID: PMC5206968.

15. Cozier Y, Palmer JR, Horton NJ, Fredman L, Wise LA, Rosenberg L. Racial discrimination and the incidence of hypertension in US black women. Ann Epidemiol. 2006;16(9):681-7. doi: 10.1016/j.annepidem.2005.11.008. PubMed PMID: 16458539.
16. Grobman WA, Parker CB, Willinger M, Wing DA, Silver RM, Wapner RJ, Simhan HN, Parry S, Mercer BM, Haas DM, Peaceman AM, Hunter S, Wadhwa P, Elovitz MA, Foroud T, Saade G, Reddy UM, Eunice Kennedy Shriver National Institute of Child H, Human Development Nulliparous Pregnancy Outcomes Study: Monitoring Mothers-to-Be N. Racial Disparities in Adverse Pregnancy Outcomes and Psychosocial Stress. Obstet Gynecol. 2018;131(2):328-35. Epub 2018/01/13. doi: 10.1097/AOG.0000000000002441. PubMed PMID: 29324613; PMCID: PMC5785441.
17. Paradies Y, Ben J, Denson N, Elias A, Priest N, Pieterse A, Gupta A, Kelaher M, Gee G. Racism as a Determinant of Health: A Systematic Review and Meta-Analysis. PLoS One. 2015;10(9):e0138511. doi: 10.1371/journal.pone.0138511. PubMed PMID: 26398658; PMCID: PMC4580597.
18. Slaughter-Acey JC, Sealy-Jefferson S, Helmkamp L, Caldwell CH, Osypuk TL, Platt RW, Straughen JK, Dailey-Okezie RK, Abeysekara P, Misra DP. Racism in the form of micro aggressions and the risk of preterm birth among black women. Ann Epidemiol. 2016;26(1):7-13 e1. doi: 10.1016/j.annepidem.2015.10.005. PubMed PMID: 26549132; PMCID: PMC4688115.
19. Mendez DD, Hogan VK, Culhane JF. Stress during pregnancy: the role of institutional racism. Stress Health. 2013;29(4):266-74. doi: 10.1002/smi.2462. PubMed PMID: 23055409.
20. Spruill TM. Chronic psychosocial stress and hypertension. Curr Hypertens Rep. 2010;12(1):10-6. doi: 10.1007/s11906-009-0084-8. PubMed PMID: 20425153; PMCID: PMC3694268.
21. McEwen BS. Central effects of stress hormones in health and disease: Understanding the protective and damaging effects of stress and stress mediators. Eur J Pharmacol. 2008;583(2-3):174-85. doi: 10.1016/j.ejphar.2007.11.071. PubMed PMID: 18282566; PMCID: PMC2474765.
22. Vrekoussis T, Kalantaridou SN, Mastorakos G, Zoumakis E, Makrigiannakis A, Syrrou M, Lavasidis LG, Relakis K, Chrousos GP. The role of stress in female reproduction and pregnancy: an update. Ann N Y Acad Sci. 2010;1205:69-75. doi: 10.1111/j.1749-6632.2010.05686.x. PubMed PMID: 20840255.
23. Whirledge S, Cidlowski JA. Glucocorticoids, Stress, and Fertility. Minerva Endocrinol. 2010;35(2):109-25.
24. Vianna P, Bauer ME, Dornfeld D, Chies JA. Distress conditions during pregnancy may lead to pre-eclampsia by increasing cortisol levels and altering lymphocyte sensitivity to glucocorticoids. Med Hypotheses. 2011;77(2):188-91. doi: 10.1016/j.mehy.2011.04.007. PubMed PMID: 21550175.
25. Smith A, Witte E, McGee D, Knott J, Narang K, Racicot K. Cortisol inhibits CSF2 and CSF3 via DNA methylation and inhibits invasion in first-trimester trophoblast cells. Am J Reprod Immunol. 2017;78(5). Epub 2017/08/29. doi: 10.1111/aji.12741. PubMed PMID: 28846166; PMCID: PMC5833927.
26. Nepomnaschy PA, Welch KB, McConnell DS, Low BS, Strassman BI, England BG. Cortisol levels and very early pregnancy loss in humans. Proc Natl Acad Sci U S A. 2006;103(10):3938-42.

27. Buss C, Davis EP, Shahbaba B, Pruessner JC, Head K, Sandmand CA. Maternal cortisol over the course of pregnancy and subsequent child amygdala and hippocampus volumes and affective problems. Proc Natl Acad Sci U S A. 2012;109(20):E1312-E9.
28. Aufdenblatten M, Baumann M, Raio L, Dick B, Frey BM, Schneider H, Surbek D, Hocher B, Mohaupt MG. Prematurity is related to high placental cortisol in preeclampsia. Pediatric Research. 2009;65(2):198-202.
29. Gennari-Moser C, Khankin EV, Schuller S, Escher G, Frey BM, Portmann CB, Baumann MU, Lehmann AD, Surbek D, Karumanchi SA, Frey FJ, Mohaupt MG. Regulation of placental growth by aldosterone and cortisol. Endocrinology. 2011;152(1):263-71. doi: 10.1210/en.2010-0525. PubMed PMID: 21068161.
30. Kalantaridou SN, Zoumakis E, Makrigiannakis A, Lavasidis LG, Vrekoussis T, Chrousos GP. Corticotropin-releasing hormone, stress and human reproduction: an update. J Reprod Immunol. 2010;85(1):33-9. doi: 10.1016/j.jri.2010.02.005. PubMed PMID: 20412987.
31. Rae M, Mohamad A, Price D, Hadoke PW, Walker BR, Mason JI, Hillier SG, Critchley HO. Cortisol inactivation by 11beta-hydroxysteroid dehydrogenase-2 may enhance endometrial angiogenesis via reduced thrombospondin-1 in heavy menstruation. J Clin Endocrinol Metab. 2009;94(4):1443-50. Epub 2009/01/23. doi: 10.1210/jc.2008-1879. PubMed PMID: 19158196.
32. Kisanga EP, Tang Z, Guller S, Whirledge S. Glucocorticoid signaling regulates cell invasion and migration in the human first-trimester trophoblast cell line Sw.71. Am J Reprod Immunol. 2018;80(1):e12974. Epub 2018/05/19. doi: 10.1111/aji.12974. PubMed PMID: 29774963.
33. Clancy KBH. Reproductive ecology and the endometrium: physiology, variation, and new directions. Yearbook of Physical Anthropology. 2009;52:137-54. doi: 10.1002/ajpa.21188. PubMed PMID: 19890864.
34. Aplin JD, Fazleabas AT, Glasser SR, Giudice LC. The Endometrium. Second ed. Gardner DK, Gerris J, Shoham Z, editors. United Kingdom: Informa Healthcare; 2008. 879 p.
35. Gellersen B, Brosens JJ. Cyclic decidualization of the human endometrium in reproductive health and failure. Endocr Rev. 2014;35(6):851-905. doi: 10.1210/er.2014-1045. PubMed PMID: 25141152.
36. Conrad KP, Rabaglino MB, Post Uiterweer ED. Emerging role for dysregulated decidualization in the genesis of preeclampsia. Placenta. 2017;60:119-29. doi: 10.1016/j.placenta.2017.06.005. PubMed PMID: 28693893; PMCID: PMC5718949.
37. Garrido-Gomez T, Dominguez F, Quinonero A, Diaz-Gimeno P, Kapidzic M, Gormley M, Ona K, Padilla-Iserte P, McMaster M, Genbacev O, Perales A, Fisher SJ, Simon C. Defective decidualization during and after severe preeclampsia reveals a possible maternal contribution to the etiology. Proc Natl Acad Sci U S A. 2017;114(40):E8468-E77. Epub 2017/09/20. doi: 10.1073/pnas.1706546114. PubMed PMID: 28923940; PMCID: PMC5635883.
38. Singh H, Aplin JD. Adhesion molecules in endometrial epithelium: tissue integrity and embryo implantation. J Anat. 2009;215(1):3-13. Epub 2009/05/21. doi: 10.1111/j.1469-7580.2008.01034.x. PubMed PMID: 19453302; PMCID: PMC2714633.
39. Cha J, Sun X, Dey SK. Mechanisms of implantation: strategies for successful pregnancy. Nat Med. 2012;18(12):1754-67. doi: 10.1038/nm.3012. PubMed PMID: 23223073.
40. Knofler M. Critical growth factors and signalling pathways controlling human trophoblast invasion. Int J Dev Biol. 2010;54(2-3):269-80. doi: 10.1387/ijdb.082769mk. PubMed PMID: 19876833; PMCID: PMC2974212.

41. Saito S, Nakashima A. A review of the mechanism for poor placentation in early-onset preeclampsia: the role of autophagy in trophoblast invasion and vascular remodeling. J Reprod Immunol. 2014;101-102:80-8. Epub 2013/08/24. doi: 10.1016/j.jri.2013.06.002. PubMed PMID: 23969229.
42. Norwitz ER, Schust DJ, Fisher SJ. Implantation and the Survival of Early Pregnancy. The New England Journal of Medicine. 2001;345(19):1400-8.
43. Orendi K, Kivity V, Sammar M, Grimpel Y, Gonen R, Meiri H, Lubzens E, Huppertz B. Placental and trophoblastic in vitro models to study preventive and therapeutic agents for preeclampsia. Placenta. 2011;32 Suppl:S49-54. doi: 10.1016/j.placenta.2010.11.023. PubMed PMID: 21257083.
44. Carter AM. Animal models of human placentation--a review. Placenta. 2007;28 Suppl A:S41-7. doi: 10.1016/j.placenta.2006.11.002. PubMed PMID: 17196252.
45. Fitzgerald HC, Schust DJ, Spencer TE. In vitro models of the human endometrium: evolution and application for women's health. Biol Reprod. 2021;104(2):282-93. Epub 2020/10/04. doi: 10.1093/biolre/ioaa183. PubMed PMID: 33009568; PMCID: PMC7876664.
46. Cartwright JE, Kenny LC, Dash PR, Crocker IP, Aplin JD, Baker PN, Whitley GS. Trophoblast invasion of spiral arteries: a novel in vitro model. Placenta. 2002;23(2-3):232-5. doi: 10.1053/plac.2001.0760. PubMed PMID: 11945091.
47. Buck VU, Gellersen B, Leube RE, Classen-Linke I. Interaction of human trophoblast cells with gland-like endometrial spheroids: a model system for trophoblast invasion. Hum Reprod. 2015;30(4):906-16. doi: 10.1093/humrep/dev011. PubMed PMID: 25662813.
48. Wang H, Pilla F, Anderson S, Martinez-Escribano S, Herrer I, Moreno-Moya JM, Musti S, Bocca S, Oehninger S, Horcajadas JA. A novel model of human implantation: 3D endometrium-like culture system to study attachment of human trophoblast (Jar) cell spheroids. Mol Hum Reprod. 2012;18(1):33-43. doi: 10.1093/molehr/gar064. PubMed PMID: 21989169.
49. Wang H, Bocca S, Anderson S, Yu L, Rhavi BS, Horcajadas J, Oehninger S. Sex steroids regulate epithelial-stromal cell cross talk and trophoblast attachment invasion in a three-dimensional human endometrial culture system. Tissue Eng Part C Methods. 2013;19(9):676-87. Epub 2013/01/17. doi: 10.1089/ten.TEC.2012.0616. PubMed PMID: 23320930.
50. Popovic M, Chuva de Sousa Lopes SM. Emerging in vitro platforms and omics technologies for studying the endometrium and early embryo-maternal interface in humans. Placenta. 2022. Epub 2022/01/27. doi: 10.1016/j.placenta.2022.01.006. PubMed PMID: 35078656.
51. Liu F, Hu S, Wang S, Cheng K. Cell and biomaterial-based approaches to uterus regeneration. Regenerative Biomaterials. 2019. doi: 10.1093/rb/rbz021.
52. Peng G, Liu H, Fan Y. Biomaterial Scaffolds for Reproductive Tissue Engineering. Ann Biomed Eng. 2017;45(7):1592-607. doi: 10.1007/s10439-016-1779-z. PubMed PMID: 28004214.
53. Fisk NM, Atun R. Systematic analysis of research underfunding in maternal and perinatal health. BJOG. 2009;116(3):347-56. doi: 10.1111/j.1471-0528.2008.02027.x. PubMed PMID: 19187366.
54. Girling JE, Rogers PA. Recent advances in endometrial angiogenesis research. Angiogenesis. 2005;8(2):89-99. doi: 10.1007/s10456-005-9006-9. PubMed PMID: 16211359.
55. Demir R, Yaba A, Huppertz B. Vasculogenesis and angiogenesis in the endometrium during menstrual cycle and implantation. Acta Histochem. 2010;112(3):203-14. doi: 10.1016/j.acthis.2009.04.004. PubMed PMID: 19481785.

56. Huppertz B, Peeters LL. Vascular biology in implantation and placentation. Angiogenesis. 2005;8(2):157-67. doi: 10.1007/s10456-005-9007-8. PubMed PMID: 16211358.
57. Possomato-Vieira JS, Khalil RA. Mechanisms of Endothelial Dysfunction in Hypertensive Pregnany and Preeclampsia. Advances in Pharmacology. 2016;77. doi: 10.1016/bs.apha.2016.04.008.
58. McNally R, Alqudah A, Obradovic D, McClements L. Elucidating the Pathogenesis of Pre-eclampsia Using In Vitro Models of Spiral Uterine Artery Remodelling. Curr Hypertens Rep. 2017;19(11):93. Epub 2017/10/25. doi: 10.1007/s11906-017-0786-2. PubMed PMID: 29063290; PMCID: PMC5653699.
59. Goulopoulou S, Davidge ST. Molecular mechanisms of maternal vascular dysfunction in preeclampsia. Trends Mol Med. 2015;21(2):88-97. Epub 2014/12/30. doi: 10.1016/j.molmed.2014.11.009. PubMed PMID: 25541377.
60. Campo H, Cervello I, Simon C. Bioengineering the Uterus: An Overview of Recent Advances and Future Perspectives in Reproductive Medicine. Ann Biomed Eng. 2017;45(7):1710-7. doi: 10.1007/s10439-016-1783-3. PubMed PMID: 28028711.
61. Novosel EC, Kleinhans C, Kluger PJ. Vascularization is the key challenge in tissue engineering. Adv Drug Deliv Rev. 2011;63(4-5):300-11. doi: 10.1016/j.addr.2011.03.004. PubMed PMID: 21396416.
62. Lovett M, Lee K, Edwards A, Kaplan DL. Vascularization Strategies for Tissue Engineering. Tissue Eng Part B. 2009;15(3):353-70.
63. Vats K, Benoit DS. Dynamic manipulation of hydrogels to control cell behavior: a review. Tissue Eng Part B Rev. 2013;19(6):455-69. Epub 2013/04/02. doi: 10.1089/ten.TEB.2012.0716. PubMed PMID: 23541134; PMCID: PMC3826471.
64. Shirahama H, Lee BH, Tan LP, Cho NJ. Precise Tuning of Facile One-Pot Gelatin Methacryloyl (GelMA) Synthesis. Sci Rep. 2016;6:31036. doi: 10.1038/srep31036. PubMed PMID: 27503340; PMCID: PMC4977492.
65. Pedron S, Harley BA. Impact of the biophysical features of a 3D gelatin microenvironment on glioblastoma malignancy. J Biomed Mater Res A. 2013;101(12):3404-15. doi: 10.1002/jbm.a.34637. PubMed PMID: 23559545.
66. Brinkman WT, Nagapudi K, Thomas BS, Chaikof EL. Photo-Cross-Linking of Type I Collagen Gels in the Presence of Smooth Muscle Cells: Mechanical Properties, Cell Viability, and Function. Biomacromolecules. 2003;4:890-5. doi: 10.1021/bm0257412.
67. Ngo MT, Harley BA. The Influence of Hyaluronic Acid and Glioblastoma Cell Coculture on the Formation of Endothelial Cell Networks in Gelatin Hydrogels. Advanced Healthcare Materials. 2017:1700687. doi: 10.1002/adhm.201700687.
68. Baier Leach J, Bivens KA, Patrick CW, Jr., Schmidt CE. Photocrosslinked hyaluronic acid hydrogels: natural, biodegradable tissue engineering scaffolds. Biotechnol Bioeng. 2003;82(5):578-89. Epub 2003/03/26. doi: 10.1002/bit.10605. PubMed PMID: 12652481.
69. Schuurman W, Levett PA, Pot MW, van Weeren PR, Dhert WJ, Hutmacher DW, Melchels FP, Klein TJ, Malda J. Gelatin-methacrylamide hydrogels as potential biomaterials for fabrication of tissue-engineered cartilage constructs. Macromol Biosci. 2013;13(5):551-61. Epub 2013/02/20. doi: 10.1002/mabi.201200471. PubMed PMID: 23420700.
70. Pence JC, Clancy KBH, Harley BAC. Proangiogenic Activity of Endometrial Epithelial and Stromal Cells in Response to Estradiol in Gelatin Hydrogels. Advanced Biosystems. 2017;1:1700056. doi: 10.1002/adbi.201700056.

71. Valdez J, Cook CD, Ahrens CC, Wang AJ, Brown A, Kumar M, Stockdale L, Rothenberg D, Renggli K, Gordon E, Lauffenburger D, White F, Griffith L. On-demand dissolution of modular, synthetic extracellular matrix reveals local epithelial-stromal communication networks. Biomaterials. 2017;130:90-103. doi: https://doi.org/10.1016/j.biomaterials.2017.03.030.
72. Huang JY, Yu PH, Li YC, Kuo PL. NLRP7 contributes to in vitro decidualization of endometrial stromal cells. Reprod Biol Endocrinol. 2017;15(1):66. doi: 10.1186/s12958-017-0286-x. PubMed PMID: 28810880; PMCID: PMC5558772.
73. Lynch VJ, Brayer K, Gellersen B, Wagner GP. HoxA-11 and FOXO1A cooperate to regulate decidual prolactin expression: towards inferring the core transcriptional regulators of decidual genes. PLoS One. 2009;4(9):e6845. doi: 10.1371/journal.pone.0006845. PubMed PMID: 19727442; PMCID: PMC2731163.
74. Pagani I, Ghezzi S, Ulisse A, Rubio A, Turrini F, Garavaglia E, Candiani M, Castilletti C, Ippolito G, Poli G, Broccoli V, Panina-Bordignon P, Vicenzi E. Human Endometrial Stromal Cells Are Highly Permissive To Productive Infection by Zika Virus. Sci Rep. 2017;7:44286. doi: 10.1038/srep44286. PubMed PMID: 28281680; PMCID: PMC5345097.
75. Mika KM, Li X, DeMayo FJ, Lynch VJ. An ancient fecundability-associated polymorphism creates a new GATA2 binding site in a distal enhancer of HLA-F. bioRxiv. 2018. doi: 10.1101/245043.
76. Cook CD, Hill AS, Guo M, Stockdale L, Papps JP, Isaacson KB, Lauffenburger DA, Griffith LG. Local remodeling of synthetic extracellular matrix microenvironments by co-cultured endometrial epithelial and stromal cells enables long-term dynamic physiological function. Integr Biol (Camb). 2017;9(4):271-89. doi: 10.1039/C6IB00245E.
77. Gerami-Naini B, Dovzhenko OV, Durning M, Wegner FH, Thomson JA, Golos TG. Trophoblast differentiation in embryoid bodies derived from human embryonic stem cells. Endocrinology. 2004;145(4):1517-24. doi: 10.1210/en.2003-1241. PubMed PMID: 14684604.
78. Wallace AE, Host AJ, Whitley GS, Cartwright JE. Decidual natural killer cell interactions with trophoblasts are impaired in pregnancies at increased risk of preeclampsia. Am J Pathol. 2013;183(6):1853-61. doi: 10.1016/j.ajpath.2013.08.023. PubMed PMID: 24103555; PMCID: PMC4188218.
79. Chen J-W, Blazek A, Lumibao J, Gaskins HR, Harley BAC. Hypoxia activates enhanced invasive potential and endogenous hyaluronic acid production by glioblastoma cells. Biomater Sci. 2018;6:854-62. doi: 10.1039/C7BM01195D; PMCID: PMC5869158.
80. Chen J-W, Pedron S, Shyu P, Hu Y, Sarkaria JN, Harley BAC. Influence of hyaluronic acid transitions in tumor microenvironment on glioblastoma malignancy and invasive behavior. bioRxiv. 2018. doi: 10.1101/291898.
81. Chen J-W, Pedron S, Harley BAC. The combined influence of hydrogel stiffness and matrix-bound hyaluronic acid content on glioblastoma invasion. Macromol Biosci. 2017;17(8):1700018. doi: 10.1002/mabi.201700018; PMCID: PMC5555785.
82. Schindelin J, Arganda-Carreras I, Frise E, Kaynig V, Longair M, Pietzsch T, Preibisch S, Rueden C, Saalfeld S, Schmid B, Tinevez JY, White DJ, Hartenstein V, Eliceiri K, Tomancak P, Cardona A. Fiji: an open-source platform for biological-image analysis. Nat Methods. 2012;9(7):676-82. Epub 2012/06/30. doi: 10.1038/nmeth.2019. PubMed PMID: 22743772; PMCID: PMC3855844.

83. Tsui KH, Li HY, Cheng JT, Sung YJ, Yen MS, Hsieh SL, Wang PH. The role of nitric oxide in the outgrowth of trophoblast cells on human umbilical vein endothelial cells. Taiwan J Obstet Gynecol. 2015;54(3):227-31. doi: 10.1016/j.tjog.2013.11.010. PubMed PMID: 26166331.
84. Millard SP. EnvStats An R Package for Environmental Statistics2013.
85. Kuo C-Y, Eranki A, Placone JK, Rhodes KR, Aranda-Espinoza H, Fernandes R, Fisher JP, Kim PCW. Development of a 3D Printed, Bioengineered Placenta Model to Evaluate the Role of Trophoblast Migration in Preeclampsia. ACS Biomaterials Science & Engineering. 2016;2(10):1817-26. doi: 10.1021/acsbiomaterials.6b00031.
86. Kilic F, Kayadibi Y, Yuksel MA, Adaletli I, Ustabasioglu FE, Oncul M, Madazli R, Yilmaz MH, Mihmanli I, Kantarci F. Shear wave elastography of placenta: in vivo quantitation of placental elasticity in preeclampsia. Diagn Interv Radiol. 2015;21(3):202-7. doi: 10.5152/dir.2014.14338. PubMed PMID: 25858523; PMCID: PMC4463268.
87. Loessner D, Meinert C, Kaemmerer E, Martine LC, Yue K, Levett PA, Klein TJ, Melchels FP, Khademhosseini A, Hutmacher DW. Functionalization, preparation and use of cell-laden gelatin methacryloyl-based hydrogels as modular tissue culture platforms. Nat Protoc. 2016;11(4):727-46. doi: 10.1038/nprot.2016.037. PubMed PMID: 26985572.
88. Yue K, Trujillo-de Santiago G, Alvarez MM, Tamayol A, Annabi N, Khademhosseini A. Synthesis, properties, and biomedical applications of gelatin methacryloyl (GelMA) hydrogels. Biomaterials. 2015;73:254-71. Epub 2015/09/29. doi: 10.1016/j.biomaterials.2015.08.045. PubMed PMID: 26414409; PMCID: PMC4610009.
89. Okada H, Tsuzuki T, Shindoh H, Nishigaki A, Yasuda K, Kanzaki H. Regulation of decidualization and angiogenesis in the human endometrium: mini review. J Obstet Gynaecol Res. 2014;40(5):1180-7. doi: 10.1111/jog.12392. PubMed PMID: 24754847.
90. Chen YC, Lin RZ, Qi H, Yang Y, Bae H, Melero-Martin JM, Khademhosseini A. Functional Human Vascular Network Generated in Photocrosslinkable Gelatin Methacrylate Hydrogels. Adv Funct Mater. 2012;22(10):2027-39. doi: 10.1002/adfm.201101662. PubMed PMID: 22907987; PMCID: PMC3422083.
91. Calderon GA, Thai P, Hsu CW, Grigoryan B, Gibson SM, Dickinson ME, Miller JS. Tubulogenesis of co-cultured human iPS-derived endothelial cells and human mesenchymal stem cells in fibrin and gelatin methacrylate gels. Biomater Sci. 2017;5(8):1652-60. doi: 10.1039/c7bm00223h. PubMed PMID: 28661522.
92. Gambino LS, Wreford NG, Bertram JF, Dockery P, Lederman F, Rogers PAW. Angiogenesis occurs by vessel elongation in proliferative phase human endometrium. Human Reproduction. 2002;17(5):1199-206.
93. Mahadik BP, Pedron Haba S, Skertich LJ, Harley BA. The use of covalently immobilized stem cell factor to selectively affect hematopoietic stem cell activity within a gelatin hydrogel. Biomaterials. 2015;67:297-307. doi: 10.1016/j.biomaterials.2015.07.042. PubMed PMID: 26232879; PMCID: PMC4550539.
94. Hambardzumyan D, Bergers G. Glioblastoma: Defining Tumor Niches. Trends Cancer. 2015;1(4):252-65. Epub 2016/04/19. doi: 10.1016/j.trecan.2015.10.009. PubMed PMID: 27088132; PMCID: PMC4831073.
95. Morrison SJ, Scadden DT. The bone marrow niche for haematopoietic stem cells. Nature. 2014;505(7483):327-34. Epub 2014/01/17. doi: 10.1038/nature12984. PubMed PMID: 24429631; PMCID: PMC4514480.
96. Carrion B, Huang CP, Ghajar CM, Kachgal S, Kniazeva E, Jeon NL, Putnam AJ. Recreating the perivascular niche ex vivo using a microfluidic approach. Biotechnol Bioeng.

2010;107(6):1020-8. Epub 2010/07/31. doi: 10.1002/bit.22891. PubMed PMID: 20672286; PMCID: PMC3367510.
97. Murakami K, Lee YH, Lucas ES, Chan YW, Durairaj RP, Takeda S, Moore JD, Tan BK, Quenby S, Chan JK, Gargett CE, Brosens JJ. Decidualization induces a secretome switch in perivascular niche cells of the human endometrium. Endocrinology. 2014;155(11):4542-53. Epub 2014/08/15. doi: 10.1210/en.2014-1370. PubMed PMID: 25116707.
98. Cousins FL, O DF, Gargett CE. Endometrial stem/progenitor cells and their role in the pathogenesis of endometriosis. Best Pract Res Clin Obstet Gynaecol. 2018;50:27-38. Epub 2018/03/06. doi: 10.1016/j.bpobgyn.2018.01.011. PubMed PMID: 29503126.
99. Gargett CE, Chan RW, Schwab KE. Hormone and growth factor signaling in endometrial renewal: role of stem/progenitor cells. Mol Cell Endocrinol. 2008;288(1-2):22-9. Epub 2008/04/12. doi: 10.1016/j.mce.2008.02.026. PubMed PMID: 18403104.
100. Kaitu'u-Lino TJ, Ye L, Salamonsen LA, Girling JE, Gargett CE. Identification of label-retaining perivascular cells in a mouse model of endometrial decidualization, breakdown, and repair. Biol Reprod. 2012;86(6):184. Epub 2012/03/10. doi: 10.1095/biolreprod.112.099309. PubMed PMID: 22402967.
101. Cervello I, Gil-Sanchis C, Santamaria X, Faus A, Vallve-Juanico J, Diaz-Gimeno P, Genolet O, Pellicer A, Simon C. Leucine-rich repeat-containing G-protein-coupled receptor 5-positive cells in the endometrial stem cell niche. Fertil Steril. 2017;107(2):510-9 e3. Epub 2016/11/27. doi: 10.1016/j.fertnstert.2016.10.021. PubMed PMID: 27887719.
102. Aplin JD, Charlton AK, Ayad S. An immunohistochemical study of human endometrial extracellular matrix during the menstrual cycle and first trimester of pregnancy. Cell and Tissue Research. 1988;253:231-40.
103. Bulletti C, Galassi A, Jasonni VM, Martinelli G, Tabanelli S, Flamigni C. Basement Membrane Components in Normal Hyperplastic and Neoplastic Endometrium. Cancer. 1988;62(1):142-9.
104. Yurchenco PD. Basement membranes: cell scaffoldings and signaling platforms. Cold Spring Harb Perspect Biol. 2011;3(2). Epub 2011/03/23. doi: 10.1101/cshperspect.a004911. PubMed PMID: 21421915; PMCID: PMC3039528.
105. Srinivasan B, Kolli AR, Esch MB, Abaci HE, Shuler ML, Hickman JJ. TEER measurement techniques for in vitro barrier model systems. J Lab Autom. 2015;20(2):107-26. Epub 2015/01/15. doi: 10.1177/2211068214561025. PubMed PMID: 25586998; PMCID: PMC4652793.
106. Arumugasaamy N, Ettehadieh LE, Kuo CY, Paquin-Proulx D, Kitchen SM, Santoro M, Placone JK, Silveira PP, Aguiar RS, Nixon DF, Fisher JP, Kim PCW. Biomimetic Placenta-Fetus Model Demonstrating Maternal-Fetal Transmission and Fetal Neural Toxicity of Zika Virus. Ann Biomed Eng. 2018. Epub 2018/07/14. doi: 10.1007/s10439-018-2090-y. PubMed PMID: 30003503.
107. Schutte SC, Taylor RN. A tissue-engineered human endometrial stroma that responds to cues for secretory differentiation, decidualization, and menstruation. Fertil Steril. 2012;97(4):997-1003. doi: 10.1016/j.fertnstert.2012.01.098. PubMed PMID: 22306710; PMCID: PMC3319234.
108. Schutte SC, James CO, Sidell N, Taylor RN. Tissue-engineered endometrial model for the study of cell-cell interactions. Reprod Sci. 2015;22(3):308-15. Epub 2014/07/18. doi: 10.1177/1933719114542008. PubMed PMID: 25031317; PMCID: PMC4352141.

109. Cohen M, Bischof P. Factors regulating trophoblast invasion. Gynecol Obstet Invest. 2007;64(3):126-30. doi: 10.1159/000101734. PubMed PMID: 17934306.
110. Abbas Y, Oefner CM, Polacheck WJ, Gardner L, Farrell L, Sharkey A, Kamm R, Moffett A, Oyen ML. A microfluidics assay to study invasion of human placental trophoblast cells. J R Soc Interface. 2017;14(130). doi: 10.1098/rsif.2017.0131. PubMed PMID: 28566515; PMCID: PMC5454302.
111. Chang TA, Bondarenko GI, Gerami-Naini B, Drenzek JG, Durning M, Garthwaite MA, Schmidt JK, Golos TG. Trophoblast differentiation, invasion and hormone secretion in a three-dimensional in vitro implantation model with rhesus monkey embryos. Reprod Biol Endocrinol. 2018;16(1):24. doi: 10.1186/s12958-018-0340-3. PubMed PMID: 29548332; PMCID: PMC5857108.
112. Korevaar TI, Steegers EA, de Rijke YB, Schalekamp-Timmermans S, Visser WE, Hofman A, Jaddoe VW, Tiemeier H, Visser TJ, Medici M, Peeters RP. Reference ranges and determinants of total hCG levels during pregnancy: the Generation R Study. Eur J Epidemiol. 2015;30(9):1057-66. doi: 10.1007/s10654-015-0039-0. PubMed PMID: 25963653; PMCID: PMC4584104.
113. Lee CL, Chiu PC, Hautala L, Salo T, Yeung WS, Stenman UH, Koistinen H. Human chorionic gonadotropin and its free beta-subunit stimulate trophoblast invasion independent of LH/hCG receptor. Mol Cell Endocrinol. 2013;375(1-2):43-52. doi: 10.1016/j.mce.2013.05.009. PubMed PMID: 23684886.
114. Lash GE, Otun HA, Innes BA, Bulmer JN, Searle RF, Robson SC. Inhibition of trophoblast cell invasion by TGFB1, 2, and 3 is associated with a decrease in active proteases. Biol Reprod. 2005;73(2):374-81. doi: 10.1095/biolreprod.105.040337. PubMed PMID: 15858216.
115. Jones RL, Stoikos C, Findlay JK, Salamonsen LA. TGF-beta superfamily expression and actions in the endometrium and placenta. Reproduction. 2006;132(2):217-32. doi: 10.1530/rep.1.01076. PubMed PMID: 16885531.
116. Mak M, Anderson S, McDonough MC, Spill F, Kim JE, Boussommier-Calleja A, Zaman MH, Kamm RD. Integrated analysis of intracellular dynamics of MenaINV cancer cells in a 3D matrix. Biophys J. 2017;112(9):1874-84. doi: 10.1016/j.bpj.2017.03.030. PubMed PMID: 28494958; PMCID: PMC5425400.
117. Reynolds DS, Tevis KM, Blessing WA, Colson YL, Zaman MH, Grinstaff MW. Breast cancer spheroids reveal a differential cancer stem cell response to chemotherapeutic treatment. Sci Rep. 2017;7(1):10382. doi: 10.1038/s41598-017-10863-4.
118. Mak M, Spill F, Kamm RD, Zaman MH. Single-cell migration in complex microenvironments: mechanics and signaling dynamics. J Biomech Eng. 2016;138(2):021004. doi: 10.1115/1.4032188. PubMed PMID: 26639083.
119. Adriani G, Ma D, Pavesi A, Kamm RD, Goh ELK. A 3D neurovascular microfluidic model consisting of neurons, astrocytes and cerebral endothelial cells as a blood–brain barrier. Lab on a Chip. 2017;17(3):448-59. doi: 10.1039/C6LC00638H.
120. Chen MB, Whisler JA, Jeon JS, Kamm RD. Mechanisms of tumor cell extravasation in an in vitro microvascular network platform. Integr Biol (Camb). 2013;5(10):1262-71. doi: 10.1039/c3ib40149a. PubMed PMID: 23995847; PMCID: PMC4038741.
121. Ehsan SM, Welch-Reardon KM, Waterman ML, Hughes CC, George SC. A three-dimensional in vitro model of tumor cell intravasation. Integr Biol (Camb). 2014;6(6):603-10. doi: 10.1039/c3ib40170g. PubMed PMID: 24763498; PMCID: 4046910.

122. Sewell-Loftin MK, Bayer SVH, Crist E, Hughes T, Joison SM, Longmore GD, George SC. Cancer-associated fibroblasts support vascular growth through mechanical force. Sci Rep. 2017;7(1):12574. Epub 2017/10/05. doi: 10.1038/s41598-017-13006-x. PubMed PMID: 28974764; PMCID: PMC5626692.
123. Kurokawa YK, Yin RT, Shang MR, Shirure VS, Moya ML, George SC. Human Induced Pluripotent Stem Cell-Derived Endothelial Cells for Three-Dimensional Microphysiological Systems. Tissue Eng Part C Methods. 2017;23(8):474-84. Epub 2017/06/18. doi: 10.1089/ten.TEC.2017.0133. PubMed PMID: 28622076; PMCID: PMC5567879.
124. Campisi M, Shin Y, Osaki T, Hajal C, Chiono V, Kamm RD. 3D self-organized microvascular model of the human blood-brain barrier with endothelial cells, pericytes and astrocytes. Biomaterials. 2018;180:117-29. doi: 10.1016/j.biomaterials.2018.07.014. PubMed PMID: 30032046.
125. Carter AM, Mess AM. Mammalian Placentation: Implications for Animal Models. Pathobiology of Human Disease2014. p. 2423-42.
126. Cruz-Acuna R, Garcia AJ. Synthetic hydrogels mimicking basement membrane matrices to promote cell-matrix interactions. Matrix Biol. 2017;57-58:324-33. Epub 2016/06/11. doi: 10.1016/j.matbio.2016.06.002. PubMed PMID: 27283894; PMCID: PMC5140848.
127. Hughes CS, Postovit LM, Lajoie GA. Matrigel: a complex protein mixture required for optimal growth of cell culture. Proteomics. 2010;10(9):1886-90. Epub 2010/02/18. doi: 10.1002/pmic.200900758. PubMed PMID: 20162561.
128. Aisenbrey EA, Murphy WL. Synthetic alternatives to Matrigel. Nature Reviews Materials. 2020;5(7):539-51. doi: 10.1038/s41578-020-0199-8.
129. Zambuto SG, Clancy KBH, Harley BAC. A gelatin hydrogel to study endometrial angiogenesis and trophoblast invasion. Interface Focus. 2019;9(5). doi: 10.1098/rsfs.2019.0016.
130. Besser RR, Bowles AC, Alassaf A, Carbonero D, Claure I, Jones E, Reda J, Wubker L, Batchelor W, Ziebarth N, Silvera R, Khan A, Maciel R, Saporta M, Agarwal A. Enzymatically crosslinked gelatin-laminin hydrogels for applications in neuromuscular tissue engineering. Biomater Sci. 2020;8(2):591-606. Epub 2019/12/21. doi: 10.1039/c9bm01430f. PubMed PMID: 31859298; PMCID: PMC7141910.
131. Oefner CM, Sharkey A, Gardner L, Critchley H, Oyen M, Moffett A. Collagen type IV at the fetal-maternal interface. Placenta. 2015;36(1):59-68. Epub 2014/12/04. doi: 10.1016/j.placenta.2014.10.012. PubMed PMID: 25465704; PMCID: PMC4302218.
132. Aratyn-Schaus Y, Oakes PW, Stricker J, Winter SP, Gardel ML. Preparation of Complaint Matrices for Quantifying Cellular Contraction. JoVE (Journal of Visualized Experiments). 2010;46.
133. Tse JR, Engler AJ. Preparation of hydrogel substrates with tunable mechanical properties. Current protocols in cell biology. 2010;47(1):10-6.
134. Wen JH, Vincent LG, Fuhrmann A, Choi YS, Hribar KC, Taylor-Weiner H, Chen S, Engler AJ. Interplay of matrix stiffness and protein tethering in stem cell differentiation. Nature Materials. 2014;13(10):979-87.
135. Flaim CJ, Chien JS, Bhatia SN. An extracellular matrix microarray for probing cellular differentiation. Nature Methods. 2005;2(2):119-25.
136. Brafman DA, Chien S, Willert K. Arrayed cellular microenvironments for identifying culture and differentiation conditions for stem, primary and rare cell populations. Nature Protocols. 2012;7(4):703-17.

137. Kaylan KB, Ermilova V, Yada RC, Underhill GH. Combinatorial microenvironmental regulation of liver progenitor differentiation by Notch ligands, TGFβ and extracellular matrix. Scientific Reports. 2016;6(1):1-15.
138. McQuin C, Goodman A, Chernyshev V, Kamentsky L, Cimini BA, Karhohs KW, Doan M, Ding L, Rafelski SM, Thirstrup D, Wiegraebe W, Singh S, Becker T, Caicedo JC, Carpenter AE. CellProfiler 3.0: Next-generation image processing for biology. PLoS Biol. 2018;16(7).
139. Zambuto SG, Clancy KBH, Harley BAC. Tuning Trophoblast Motility in a Gelatin Hydrogel via Soluble Cues from the Maternal-Fetal Interface. Tissue Eng Part A. 2020;27(15-16):1064-73. Epub 2020/11/21. doi: 10.1089/ten.tea.2020.0097. PubMed PMID: 33216701.
140. De Colli M, Massimi M, Barbetta A, Di Rosario BL, Nardecchia S, Conti Devirgiliis L, Dentini M. A biomimetic porous hydrogel of gelatin and glycosaminoglycans cross-linked with transglutaminase and its application in the culture of hepatocytes. Biomed Mater. 2012;7(5):055005. Epub 2012/07/27. doi: 10.1088/1748-6041/7/5/055005. PubMed PMID: 22832766.
141. Damodaran G, Collighan R, Griffin M, Pandit A. Tethering a laminin peptide to a crosslinked collagen scaffold for biofunctionality. J Biomed Mater Res A. 2009;89(4):1001-10. Epub 2008/05/15. doi: 10.1002/jbm.a.32045. PubMed PMID: 18478551.
142. Loebel C, Mauck RL, Burdick JA. Local nascent protein deposition and remodelling guide mesenchymal stromal cell mechanosensing and fate in three-dimensional hydrogels. Nat Mater. 2019;18(8):883-91. Epub 2019/03/20. doi: 10.1038/s41563-019-0307-6. PubMed PMID: 30886401; PMCID: PMC6650309.
143. Loebel C, Kwon MY, Wang C, Han L, Mauck RL, Burdick JA. Metabolic Labeling to Probe the Spatiotemporal Accumulation of Matrix at the Chondrocyte-Hydrogel Interface. Advanced Functional Materials. 2020. doi: 10.1002/adfm.201909802.
144. Fournier SB, D'Errico JN, Stapleton PA. Uterine Vascular Control Preconception and During Pregnancy. Compr Physiol. 2021;11(3):1871-93. Epub 2021/06/02. doi: 10.1002/cphy.c190015. PubMed PMID: 34061977; PMCID: PMC8485361.
145. Plaisier M. Decidualisation and angiogenesis. Best Pract Res Clin Obstet Gynaecol. 2011;25(3):259-71. Epub 2010/12/15. doi: 10.1016/j.bpobgyn.2010.10.011. PubMed PMID: 21144801.
146. Albrecht ED. Effect of estrogen on angiogenesis in co-cultures of human endometrial cells and microvascular endothelial cells. Human Reproduction. 2003;18(10):2039-47. doi: 10.1093/humrep/deg415.
147. Kapiteijn K, Koolwijk P, van der Weiden RM, van Nieuw Amerongen G, Plaisier M, van Hinsbergh VW, Helmerhorst FM. Human embryo-conditioned medium stimulates in vitro endometrial angiogenesis. Fertil Steril. 2006;85 Suppl 1:1232-9. doi: 10.1016/j.fertnstert.2005.11.029. PubMed PMID: 16616097.
148. Govindasamy N, Long H, Jeong HW, Raman R, Ozcifci B, Probst S, Arnold SJ, Riehemann K, Ranga A, Adams RH, Trappmann B, Bedzhov I. 3D biomimetic platform reveals the first interactions of the embryo and the maternal blood vessels. Dev Cell. 2021;56(23):3276-87 e8. Epub 2021/11/07. doi: 10.1016/j.devcel.2021.10.014. PubMed PMID: 34741805.
149. Lv B, Xu X, Zhang X, Qi L, He W, Wang L, Chen X, Peng L, Xue J, Ji Y, Xue Z. Activation of Blood Vessel Development in Endometrial Stromal Cells In Vitro Cocultured with Human Peri-Implantation Embryos Revealed by Single-Cell RNA-Seq. Life (Basel). 2021;11(5). Epub 2021/05/01. doi: 10.3390/life11050367. PubMed PMID: 33919335; PMCID: PMC8143346.

150. Offeddu GS, Possenti L, Loessberg-Zahl JT, Zunino P, Roberts J, Han X, Hickman D, Knutson CG, Kamm RD. Application of Transmural Flow Across In Vitro Microvasculature Enables Direct Sampling of Interstitial Therapeutic Molecule Distribution. Small. 2019;15(46):e1902393. Epub 2019/09/10. doi: 10.1002/smll.201902393. PubMed PMID: 31497931.
151. Haase K, Gillrie MR, Hajal C, Kamm RD. Pericytes Contribute to Dysfunction in a Human 3D Model of Placental Microvasculature through VEGF-Ang-Tie2 Signaling. Adv Sci (Weinh). 2019;6(23):1900878. Epub 2019/12/14. doi: 10.1002/advs.201900878. PubMed PMID: 31832308; PMCID: PMC6891921.
152. Haase K, Piatti F, Marcano M, Shin Y, Visone R, Redaelli A, Rasponi M, Kamm RD. Physiologic flow-conditioning limits vascular dysfunction in engineered human capillaries. biorxiv. 2021. doi: 10.1101/2021.03.03.433247.
153. Moore E, Allen JB, Mulligan CJ, Wayne EC. Ancestry of cells must be considered in bioengineering. Nature Reviews Materials. 2021;7(1):2-4. doi: 10.1038/s41578-021-00397-7.
154. Guerrero S, Lopez-Cortes A, Indacochea A, Garcia-Cardenas JM, Zambrano AK, Cabrera-Andrade A, Guevara-Ramirez P, Gonzalez DA, Leone PE, Paz YMC. Analysis of Racial/Ethnic Representation in Select Basic and Applied Cancer Research Studies. Sci Rep. 2018;8(1):13978. Epub 2018/09/20. doi: 10.1038/s41598-018-32264-x. PubMed PMID: 30228363; PMCID: PMC6143551.
155. Zambuto SG, Rattila S, Dveksler G, Harley BAC. Effects of Pregnancy-Specific Glycoproteins on Trophoblast Motility in Three-Dimensional Gelatin Hydrogels. Cellular and Molecular Bioengineering. 2022. doi: 10.1007/s12195-021-00715-7.
156. Crosby CO, Valliappan D, Shu D, Kumar S, Tu C, Deng W, Parekh SH, Zoldan J. Quantifying the vasculogenic potential of iPSC-derived endothelial progenitors in collagen hydrogels. Tissue Eng Part A. 2019. Epub 2019/01/09. doi: 10.1089/ten.TEA.2018.0274. PubMed PMID: 30618333.
157. Szklarczyk D, Gable AL, Nastou KC, Lyon D, Kirsch R, Pyysalo S, Doncheva NT, Legeay M, Fang T, Bork P, Jensen LJ, von Mering C. The STRING database in 2021: customizable protein-protein networks, and functional characterization of user-uploaded gene/measurement sets. Nucleic Acids Res. 2021;49(D1):D605-D12. Epub 2020/11/26. doi: 10.1093/nar/gkaa1074. PubMed PMID: 33237311; PMCID: PMC7779004.
158. von Mering C, Huynen M, Jaeggi D, Schmidt S, Bork P, Snel B. STRING: a database of predicted functional associations between proteins. Nucleic Acids Res. 2003;31(1):258-61. Epub 2003/01/10. doi: 10.1093/nar/gkg034. PubMed PMID: 12519996; PMCID: PMC165481.
159. von Mering C, Jensen LJ, Snel B, Hooper SD, Krupp M, Foglierini M, Jouffre N, Huynen MA, Bork P. STRING: known and predicted protein-protein associations, integrated and transferred across organisms. Nucleic Acids Res. 2005;33(Database issue):D433-7. Epub 2004/12/21. doi: 10.1093/nar/gki005. PubMed PMID: 15608232; PMCID: PMC539959.
160. Straszewski-Chavez SL, Abrahams VM, Alvero AB, Aldo PB, Ma Y, Guller S, Romero R, Mor G. The isolation and characterization of a novel telomerase immortalized first trimester trophoblast cell line, Swan 71. Placenta. 2009;30(11):939-48. Epub 2009/09/22. doi: 10.1016/j.placenta.2009.08.007. PubMed PMID: 19766308; PMCID: PMC2784169.
161. Zambuto SG, Jain I, Clancy KBH, Underhill GH, Harley BAC. The role of extracellular matrix biomolecules on endometrial epithelial cell attachment and cytokeratin 18 expression on gelatin hydrogels. bioRxiv. 2021:2021.10.24.465574. doi: 10.1101/2021.10.24.465574.

162. Bouïs D, Hospers GAP, Meijer C, Molema G, Mulder NH. Endothelium in vitro: a review of human vascular endothelial cell lines for blood vessel-related research. Angiogenesis. 2001;4:91-102.
163. Ehsan SM, George SC. Vessel network formation in response to intermittent hypoxia is frequency dependent. J Biosci Bioeng. 2015;120(3):347-50. doi: 10.1016/j.jbiosc.2015.01.017. PubMed PMID: 25735591; PMCID: PMC4527889.
164. Del Bufalo F, Manzo T, Hoyos V, Yagyu S, Caruana I, Jacot J, Benavides O, Rosen D, Brenner MK. 3D modeling of human cancer: A PEG-fibrin hydrogel system to study the role of tumor microenvironment and recapitulate the in vivo effect of oncolytic adenovirus. Biomaterials. 2016;84:76-85. Epub 2016/01/31. doi: 10.1016/j.biomaterials.2016.01.030. PubMed PMID: 26826297.
165. Nyga A, Loizidou M, Emberton M, Cheema U. A novel tissue engineered three-dimensional in vitro colorectal cancer model. Acta Biomater. 2013;9(8):7917-26. Epub 2013/04/30. doi: 10.1016/j.actbio.2013.04.028. PubMed PMID: 23624217; PMCID: PMC3711238.
166. Saleh L, Otti GR, Fiala C, Polheimer J, Knofler M. Evaluation of human first trimester decidual and telomerase-transformed endometrial stromal cells as model systems of in vitro decidualization. Reprod Biol Endocrinol. 2011;9(155):1-15.
167. Ahn JH, Park HR, Park CW, Park DW, Kwak-Kim J. Expression of TWIST in the first-trimester trophoblast and decidual tissue of women with recurrent pregnancy losses. Am J Reprod Immunol. 2017;78(2). doi: 10.1111/aji.12670. PubMed PMID: 28337825.
168. Yu J, Berga SL, Johnston-MacAnanny EB, Sidell N, Bagchi IC, Bagchi MK, Taylor RN. Endometrial Stromal Decidualization Responds Reversibly to Hormone Stimulation and Withdrawal. Endocrinology. 2016;157(6):2432-46. doi: 10.1210/en.2015-1942. PubMed PMID: 27035651; PMCID: PMC4891781.
169. Koga K, Osuga Y, Tsutsumi O, Yano T, Yoshino O, Takai Y, Matsumi H, Hiroi H, Kugu K, Momoeda M, Fujiwara T, Taketani Y. Demonstration of Angiogenin in Human Endometrium and Its Enhanced Expression in Endometrial Tissues in the Secretory Phase and the Decidua. J Clin Endocrinol Metab. 2001;86(11):5609.
170. Smith SK. Regulation of angiogenesis in the endometrium. Trends in Endocrinology & Metabolism. 2001;12(4):147-51.
171. Ergün S, Kilic N, Wurmbach J, Ebrahimnejad A, Fernando M, Sevinc S, Kilic E, Chalajour F, Fiedler W, Lauke H, Lamszus K, Hammerer P, Weil J, Herbst H, Folkman J. Endostatin inhibits angiogenesis by stabilization of newly formed endothelial tubes. Angiogenesis. 2001;4:193-206.
172. Hayrabedyan S, Kyurkchiev S, Kehayov I. FGF-1 and S100A13 possibly contribute to angiogenesis in endometriosis. J Reprod Immunol. 2005;67(1-2):87-101. Epub 2005/09/17. doi: 10.1016/j.jri.2005.07.001. PubMed PMID: 16165218.
173. Giudice LC, Lamson G, Rosenfeld RG, Irwin JC. Insulin-like Growth Factor-II (IGF-II) and IGF Binding Proteins in Human Endometrium. Annals New York Academy of Sciences. 1991:295-307.
174. Matsumoto H, Nasu K, Nishida M, Ito H, Bing S, Miyakawa I. Regulation of proliferation, motility, and contractility of human endometrial stromal cells by platelet-derived growth factor. J Clin Endocrinol Metab. 2005;90(6):3560-7. Epub 2005/03/10. doi: 10.1210/jc.2004-1918. PubMed PMID: 15755859.

175. Garlanda C, Maina V, Cotena A, Moalli F. The soluble pattern recognition receptor pentraxin-3 in innate immunity, inflammation and fertility. J Reprod Immunol. 2009;83(1-2):128-33. Epub 2009/11/11. doi: 10.1016/j.jri.2009.05.006. PubMed PMID: 19900712.
176. Daubriac J, Pandya UM, Huang KT, Pavlides SC, Gama P, Blank SV, Shukla P, Crawford SE, Gold LI. Hormonal and Growth Regulation of Epithelial and Stromal Cells From the Normal and Malignant Endometrium by Pigment Epithelium-Derived Factor. Endocrinology. 2017;158(9):2754-73. Epub 2017/09/16. doi: 10.1210/en.2017-00028. PubMed PMID: 28911166.
177. Massimiani M, Lacconi V, La Civita F, Ticconi C, Rago R, Campagnolo L. Molecular Signaling Regulating Endometrium-Blastocyst Crosstalk. Int J Mol Sci. 2019;21(1). Epub 2019/12/22. doi: 10.3390/ijms21010023. PubMed PMID: 31861484; PMCID: PMC6981505.
178. Chadchan SB, Kumar V, Maurya VK, Soni UK, Jha RK. Endoglin (CD105) coordinates the process of endometrial receptivity for embryo implantation. Mol Cell Endocrinol. 2016;425:69-83. Epub 2016/01/24. doi: 10.1016/j.mce.2016.01.014. PubMed PMID: 26802878.
179. Cameron IT, Bacon CR, Collett GP, Davenport AP. Endothelin Expression in the Uterus. J Steroid Biochem Mol Biol. 1995;53(1-6):209-14.
180. Zhou J, Dsupin BA, Giudice LC, Bondy CA. Insulin-Like Growth Factor System Gene Expression in Human Endometrium during the Menstrual Cycle. Journal of Clinical Endocrinology and Metabolism. 1994;79(6):1723-34.
181. Maybin JA, Thiruchelvam U, Madhra M, Saunders PTK, Critchley HOD. Steroids Regulate CXCL4 in the Human Endometrium During Menstruation to Enable Efficient Endometrial Repair. J Clin Endocrinol Metab. 2017;102(6):1851-60. Epub 2017/03/23. doi: 10.1210/jc.2016-3604. PubMed PMID: 28323919; PMCID: PMC5470763.
182. Jones RL, Findlay JK, Salamonsen LA. The role of activins during decidualisation of human endometrium. Aust N Z J Obstet Gynaecol. 2006;46(3):245-9. Epub 2006/05/18. doi: 10.1111/j.1479-828X.2006.00581.x. PubMed PMID: 16704482.
183. Jones RL, Salamonsen LA, Findlay JK. Activin A Promotes Human Endometrial Stromal Cell Decidualization In Vitro. J Clin Endocrinol Metab. 2002;87(8):4001-4.
184. Salamonsen LA, Hutchison JC, Gargett CE. Cyclical endometrial repair and regeneration. Development. 2021;148(17). Epub 2021/09/07. doi: 10.1242/dev.199577. PubMed PMID: 34486650.
185. Hess AP, Hamilton AE, Talbi S, Dosiou C, Nyegaard M, Nayak N, Genbecev-Krtolica O, Mavrogianis P, Ferrer K, Kruessel J, Fazleabas AT, Fisher SJ, Giudice LC. Decidual stromal cell response to paracrine signals from the trophoblast: amplification of immune and angiogenic modulators. Biol Reprod. 2007;76(1):102-17. doi: 10.1095/biolreprod.106.054791. PubMed PMID: 17021345.
186. Clancy KBH, Ellison PT, Jasienska G, Bribiescas RG. Endometrial thickness is not independent of luteal phase day in a rural Polish population. Anthropological Science. 2009;117(3):157-63. doi: 10.1537/ase.090130.
187. Goldman-Wohl D, Yagel S. Regulation of trophoblast invasion: from normal implantation to pre-eclampsia. Molecular and Cellular Endocrinology. 2002;187:233-8.
188. Su RW, Fazleabas AT. Implantation and Establishment of Pregnancy in Human and Nonhuman Primates. Adv Anat Embryol Cell Biol. 2015;216:189-213. Epub 2015/10/10. doi: 10.1007/978-3-319-15856-3_10. PubMed PMID: 26450500; PMCID: PMC5098399.

189. Moser G, Huppertz B. Implantation and extravillous trophoblast invasion: From rare archival specimens to modern biobanking. Placenta. 2017;56:19-26. Epub 2017/02/17. doi: 10.1016/j.placenta.2017.02.007. PubMed PMID: 28202182; PMCID: PMC5472199.
190. Cartwright JE, Whitley GS. Strategies for investigating the maternal-fetal interface in the first trimester of pregnancy: What can we learn about pathology? Placenta. 2017;60:145-9. doi: 10.1016/j.placenta.2017.05.003. PubMed PMID: 28506493; PMCID: PMC5730536.
191. Kuo CY, Guo T, Cabrera-Luque J, Arumugasaamy N, Bracaglia L, Garcia-Vivas A, Santoro M, Baker H, Fisher J, Kim P. Placental basement membrane proteins are required for effective cytotrophoblast invasion in a three-dimensional bioprinted placenta model. J Biomed Mater Res A. 2018;106(6):1476-87. doi: 10.1002/jbm.a.36350. PubMed PMID: 29368378; PMCID: PMC5924478.
192. Vukicevic S, Kleinman HK, Luyten FP, Roberts AB, Roche NS, Reddi AH. Identification of Multiple Active Growth Factors in Basement Membrane Matrigel Suggests Caution in Interpretation of Cellular Activity Related to Extracellular Matrix Components. Experimental Cell Research. 1992;202:1-8.
193. Cartwright JE, Fraser R, Leslie K, Wallace AE, James JL. Remodelling at the maternal-fetal interface: relevance to human pregnancy disorders. Reproduction. 2010;140(6):803-13. doi: 10.1530/REP-10-0294. PubMed PMID: 20837731.
194. Staun-Ram E, Goldman S, Gabarin D, Shalev E. Expression and importance of matrix metalloproteinase 2 and 9 (MMP-2 and -9) in human trophoblast invasion. Reprod Biol Endocrinol. 2004;2:59. doi: 10.1186/1477-7827-2-59. PubMed PMID: 15294019; PMCID: PMC516041.
195. Nepomnaschy PA, Salvante KG, Zeng L, Pyles C, Ma H, Blais JC, Wen L, Barha CK. Variation in maternal urinary cortisol profiles across the peri-conceptional period: a longitudinal description and evaluation of potential functions. Hum Reprod. 2015;30(6):1460-72. Epub 2015/04/24. doi: 10.1093/humrep/dev086. PubMed PMID: 25904636.
196. Dunkel Schetter C. Psychological science on pregnancy: stress processes, biopsychosocial models, and emerging research issues. Annu Rev Psychol. 2011;62:531-58. doi: 10.1146/annurev.psych.031809.130727. PubMed PMID: 21126184.
197. Yu Y, Zhang S, Wang G, Hong X, Mallow EB, Walker SO, Pearson C, Heffner L, Zuckerman B, Wang X. The combined association of psychosocial stress and chronic hypertension with preeclampsia. Am J Obstet Gynecol. 2013;209(5):438 e1- e12. doi: 10.1016/j.ajog.2013.07.003. PubMed PMID: 23850528; PMCID: PMC3825759.
198. Zambuto SG, Serrano JF, Vilbert AC, Lu Y, Harley BAC, Pedron S. Response of neuroglia to hypoxia-induced oxidative stress using enzymatically crosslinked hydrogels. MRS Communications. 2019:1-8. doi: 10.1557/mrc.2019.159.
199. Chen JE, Pedron S, Shyu P, Hu Y, Sarkaria JN, Harley BAC. Influence of Hyaluronic Acid Transitions in Tumor Microenvironment on Glioblastoma Malignancy and Invasive Behavior. Front Mater. 2018;5. Epub 2018/12/26. doi: 10.3389/fmats.2018.00039. PubMed PMID: 30581816; PMCID: PMC6300158.
200. Shapiro BS, Daneshmand ST, Garner FC, Aguirre M, Thomas S. Large blastocyst diameter, early blastulation, and low preovulatory serum progesterone are dominant predictors of clinical pregnancy in fresh autologous cycles. Fertil Steril. 2008;90(2):302-9. doi: 10.1016/j.fertnstert.2007.06.062. PubMed PMID: 17905239.
201. Abbas Y, Carnicer-Lombarte A, Gardner L, Thomas J, Brosens JJ, Moffett A, Sharkey AM, Franze K, Burton GJ, Oyen ML. Tissue stiffness at the human maternal-fetal interface.

Hum Reprod. 2019;34(10):1999-2008. Epub 2019/10/04. doi: 10.1093/humrep/dez139. PubMed PMID: 31579915; PMCID: PMC6809602.
202. Chen JE, Pedron S, Harley BAC. The Combined Influence of Hydrogel Stiffness and Matrix-Bound Hyaluronic Acid Content on Glioblastoma Invasion. Macromol Biosci. 2017;17(8). doi: 10.1002/mabi.201700018. PubMed PMID: 28379642; PMCID: PMC5555785.
203. Gilchrist AE, Lee S, Hu Y, Harley BAC. Soluble Signals and Remodeling in a Synthetic Gelatin-Based Hematopoietic Stem Cell Niche. Adv Healthc Mater. 2019;8(20):e1900751. Epub 2019/09/19. doi: 10.1002/adhm.201900751. PubMed PMID: 31532901; PMCID: PMC6813872.
204. Ananth CV, Keyes KM, Wapner RJ. Pre-eclampsia rates in the United States, 1980-2010: age-period-cohort analysis. BMJ. 2013;347:f6564. doi: 10.1136/bmj.f6564. PubMed PMID: 24201165; PMCID: PMC3898425.
205. Lala PK, Nandi P. Mechanisms of trophoblast migration, endometrial angiogenesis in preeclampsia: The role of decorin. Cell Adh Migr. 2016;10(1-2):111-25. doi: 10.1080/19336918.2015.1106669. PubMed PMID: 26745663; PMCID: PMC4853052.
206. Redman CW, Sargent IL. Latest Advances in Understanding Preeclampsia. Science. 2005;308(5728):1592-4.
207. Redman CW, Staff AC. Preeclampsia, biomarkers, syncytiotrophoblast stress, and placental capacity. Am J Obstet Gynecol. 2015;213(4 Suppl):S9 e1, S9-11. Epub 2015/10/03. doi: 10.1016/j.ajog.2015.08.003. PubMed PMID: 26428507.
208. Kaufmann P, Black S, Huppertz B. Endovascular trophoblast invasion: implications for the pathogenesis of intrauterine growth retardation and preeclampsia. Biol Reprod. 2003;69(1):1-7. Epub 2003/03/07. doi: 10.1095/biolreprod.102.014977. PubMed PMID: 12620937.
209. Pedron S, Pritchard AM, Vincil GA, Andrade B, Zimmerman SC, Harley BA. Patterning Three-Dimensional Hydrogel Microenvironments Using Hyperbranched Polyglycerols for Independent Control of Mesh Size and Stiffness. Biomacromolecules. 2017;18(4):1393-400. doi: 10.1021/acs.biomac.7b00118. PubMed PMID: 28245360; PMCID: PMC5444810.
210. Zhao MR, Qiu W, Li YX, Zhang ZB, Li D, Wang YL. Dual effect of transforming growth factor beta1 on cell adhesion and invasion in human placenta trophoblast cells. Reproduction. 2006;132(2):333-41. doi: 10.1530/rep.1.01112. PubMed PMID: 16885541.
211. Mandl M, Ghaffari-Tabrizi N, Haas J, Nohammer G, Desoye G. Differential glucocorticoid effects on proliferation and invasion of human trophoblast cell lines. Reproduction. 2006;132(1):159-67. Epub 2006/07/04. doi: 10.1530/rep.1.00976. PubMed PMID: 16816341.
212. Tomlinson JW, Stewart PM. Cortisol metabolism and the role of 11beta-hydroxysteroid dehydrogenase. Best Pract Res Clin Endocrinol Metab. 2001;15(1):61-78. Epub 2001/07/27. doi: 10.1053/beem.2000.0119. PubMed PMID: 11469811.
213. Abou-Kheir W, Barrak J, Hadadeh O, Daoud G. HTR-8/SVneo cell line contains a mixed population of cells. Placenta. 2017;50:1-7. doi: 10.1016/j.placenta.2016.12.007. PubMed PMID: 28161053.
214. Adam EK, Hawkley LC, Kudielka BM, Cacioppo JT. Day-to-day dynamics of experience--cortisol associations in a population-based sample of older adults. Proc Natl Acad Sci U S A. 2006;103(45):17058-63. Epub 2006/11/01. doi: 10.1073/pnas.0605053103. PubMed PMID: 17075058; PMCID: PMC1636578.
215. Adam EK, Quinn ME, Tavernier R, McQuillan MT, Dahlke KA, Gilbert KE. Diurnal cortisol slopes and mental and physical health outcomes: A systematic review and meta-analysis.

Psychoneuroendocrinology. 2017;83:25-41. Epub 2017/06/05. doi: 10.1016/j.psyneuen.2017.05.018. PubMed PMID: 28578301; PMCID: PMC5568897.
216. Bao AM, Ji YF, Van Someren EJ, Hofman MA, Liu RY, Zhou JN. Diurnal rhythms of free estradiol and cortisol during the normal menstrual cycle in women with major depression. Horm Behav. 2004;45(2):93-102. Epub 2004/03/17. doi: 10.1016/j.yhbeh.2003.09.004. PubMed PMID: 15019795.
217. Chida Y, Hamer M. Chronic psychosocial factors and acute physiological responses to laboratory-induced stress in healthy populations: a quantitative review of 30 years of investigations. Psychol Bull. 2008;134(6):829-85. Epub 2008/10/29. doi: 10.1037/a0013342. PubMed PMID: 18954159.
218. Chida Y, Steptoe A. Cortisol awakening response and psychosocial factors: a systematic review and meta-analysis. Biol Psychol. 2009;80(3):265-78. Epub 2008/11/22. doi: 10.1016/j.biopsycho.2008.10.004. PubMed PMID: 19022335.
219. Dahlgren A, Kecklund G, Theorell T, Akerstedt T. Day-to-day variation in saliva cortisol--relation with sleep, stress and self-rated health. Biol Psychol. 2009;82(2):149-55. Epub 2009/07/15. doi: 10.1016/j.biopsycho.2009.07.001. PubMed PMID: 19596045.
220. Dmitrieva NO, Almeida DM, Dmitrieva J, Loken E, Pieper CF. A day-centered approach to modeling cortisol: diurnal cortisol profiles and their associations among U.S. adults. Psychoneuroendocrinology. 2013;38(10):2354-65. Epub 2013/06/19. doi: 10.1016/j.psyneuen.2013.05.003. PubMed PMID: 23770247; PMCID: PMC3776005.
221. Heinrichs M, Baumgartner T, Kirschbaum C, Ehlert U. Social support and oxytocin interact to suppress cortisol and subjective responses to psychosocial stress. Biological Psychiatry. 2003;54(12):1389-98. doi: 10.1016/s0006-3223(03)00465-7.
222. Sin NL, Ong AD, Stawski RS, Almeida DM. Daily positive events and diurnal cortisol rhythms: Examination of between-person differences and within-person variation. Psychoneuroendocrinology. 2017;83:91-100. Epub 2017/06/12. doi: 10.1016/j.psyneuen.2017.06.001. PubMed PMID: 28601752; PMCID: PMC5541940.
223. Zambuto S, Clancy KBH, Harley BAC. A gelatin hydrogel to study endometrial angiogenesis and trophoblast invasion. Interface Focus. 2019;9(5):20190016. doi: doi:10.1098/rsfs.2019.0016; PMCID: PMC6710659.
224. Pedron S, Wolter GL, Chen J-WE, Laken SE, Sarkaria JN, Harley BAC. Hyaluronic acid-functionalized gelatin hydrogels reveal extracellular matrix signals temper the efficacy of erlotinib against patient-derived glioblastoma specimens. Biomaterials. 2019;219:119371. doi: https://doi.org/10.1016/j.biomaterials.2019.119371; PMCID: PMC6707069.
225. Chen J-WE, Pedron S, Shyu P, Hu Y, Sarkaria JN, Harley BAC. Influence of hyaluronic acid transitions in tumor microenvironment on glioblastoma malignancy and invasive behavior. Front Mater. 2018;5(39). doi: 10.3389/fmats.2018.00039; PMCID: PMC6300158.
226. Rattila S, Dunk CEE, Im M, Grichenko O, Zhou Y, Yanez-Mo M, Blois SM, Yamada KM, Erez O, Gomez-Lopez N, Lye SJ, Hinz B, Romero R, Cohen M, Dveksler G. Interaction of Pregnancy-Specific Glycoprotein 1 With Integrin Alpha5beta1 Is a Modulator of Extravillous Trophoblast Functions. Cells. 2019;8(11). Epub 2019/11/07. doi: 10.3390/cells8111369. PubMed PMID: 31683744; PMCID: PMC6912793.
227. Moore T, Dveksler GS. Pregnancy-specific glycoproteins: complex gene families regulating maternal-fetal interactions. Int J Dev Biol. 2014;58(2-4):273-80. Epub 2014/07/16. doi: 10.1387/ijdb.130329gd. PubMed PMID: 25023693.

228. Wurz H, Geiger HJ, Jabs-Lehmann A, Bohn H, Luben G. Radioimmunoassay of SP1 (Pregnancy-specific beta1-glycoprotein) in maternal blood and in amniotic fluid in normal and pathologic pregnancies. J Perinat Med. 1981;9:67-78.
229. Sorensen S. Pregnancy-"specific" beta 1-glycoprotein (SP1): purification, characterization, quantification and clinical application in malignancies (a review). Tumor Biol. 1984;5(6):275-302.
230. Zhou G-Q, Baranov V, Zimmermann W, Grunert F, Erhard B, Mincheva-Nilsson L, Hammarstrom S, Thompson J. Highly Specific Monoclonal Antibody Demonstrates that Pregnancy-specific Glycoprotein (PSG) is Limited to Syncytiotrophoblast in Human Early and Term Placenta. Placenta. 1997;18:491-501.
231. Blankley RT, Fisher C, Westwood M, North R, Baker PN, Walker MJ, Williamson A, Whetton AD, Lin W, McCowan L, Roberts CT, Cooper GJ, Unwin RD, Myers JE. A label-free SRM workflow identifies a subset of pregnancy specific glycoproteins as potential predictive markers of early-onset pre-eclampsia. Mol Cell Proteomics. 2013. Epub 2013/07/31. doi: 10.1074/mcp.M112.026872. PubMed PMID: 23897580.
232. Blankley RT, Fisher C, Westwood M, North R, Baker PN, Walker MJ, Williamson A, Whetton AD, Lin W, McCowan L, Roberts CT, Cooper GJ, Unwin RD, Myers JE. A label-free selected reaction monitoring workflow identifies a subset of pregnancy specific glycoproteins as potential predictive markers of early-onset pre-eclampsia. Mol Cell Proteomics. 2013;12(11):3148-59. Epub 2013/07/31. doi: 10.1074/mcp.M112.026872. PubMed PMID: 23897580; PMCID: PMC3820930.
233. Ballesteros A, Mentink-Kane MM, Warren J, Kaplan GG, Dveksler GS. Induction and activation of latent transforming growth factor-beta1 are carried out by two distinct domains of pregnancy-specific glycoprotein 1 (PSG1). J Biol Chem. 2015;290(7):4422-31. Epub 2014/12/31. doi: 10.1074/jbc.M114.597518. PubMed PMID: 25548275; PMCID: PMC4326847.
234. Jones K, Ballesteros A, Mentink-Kane M, Warren J, Rattila S, Malech H, Kang E, Dveksler G. PSG9 Stimulates Increase in FoxP3+ Regulatory T-Cells through the TGF-beta1 Pathway. PLoS One. 2016;11(7):e0158050. Epub 2016/07/09. doi: 10.1371/journal.pone.0158050. PubMed PMID: 27389696; PMCID: PMC4936685.
235. Dieterich DC, Lee JJ, Link AJ, Graumann J, Tirrell DA, Schuman EM. Labeling, detection and identification of newly synthesized proteomes with bioorthogonal non-canonical amino-acid tagging. Nat Protoc. 2007;2(3):532-40. Epub 2007/04/05. doi: 10.1038/nprot.2007.52. PubMed PMID: 17406607.
236. Nadeem L, Munir S, Fu G, Dunk C, Baczyk D, Caniggia I, Lye S, Peng C. Nodal signals through activin receptor-like kinase 7 to inhibit trophoblast migration and invasion: implication in the pathogenesis of preeclampsia. Am J Pathol. 2011;178(3):1177-89. Epub 2011/03/02. doi: 10.1016/j.ajpath.2010.11.066. PubMed PMID: 21356369; PMCID: PMC3069932.
237. Blois SM, Sulkowski G, Tirado-Gonzalez I, Warren J, Freitag N, Klapp BF, Rifkin D, Fuss I, Strober W, Dveksler GS. Pregnancy-specific glycoprotein 1 (PSG1) activates TGF-beta and prevents dextran sodium sulfate (DSS)-induced colitis in mice. Mucosal Immunol. 2014;7(2):348-58. Epub 2013/08/16. doi: 10.1038/mi.2013.53. PubMed PMID: 23945545; PMCID: PMC3844031.
238. Kuo CY, Shevchuk M, Opfermann J, Guo T, Santoro M, Fisher JP, Kim PC. Trophoblast-endothelium signaling involves angiogenesis and apoptosis in a dynamic bioprinted placenta model. Biotechnol Bioeng. 2019;116(1):181-92. Epub 2018/10/10. doi: 10.1002/bit.26850. PubMed PMID: 30298908; PMCID: PMC6289739.

239. Vukicevic S, Kleinman H, Luyten F, Roberts A, Roche N, Reddi A. Identification of Multiple Active Growth Factors in Basement Membrane Matrigel Suggests Caution in Interpretation of Cellular Activity Related to Extracellular Matrix Components. Experimental Cell Research. 1992;202:1-8.
240. Mahadik BP, Bharadwaj NA, Ewoldt RH, Harley BA. Regulating dynamic signaling between hematopoietic stem cells and niche cells via a hydrogel matrix. Biomaterials. 2017;125:54-64. doi: 10.1016/j.biomaterials.2017.02.013. PubMed PMID: 28231508; PMCID: PMC5444543.
241. Bopp SK, Lettieri T. Comparison of four different colorimetric and fluorometric cytotoxicity assays in a zebrafish liver cell line. BMC Pharmacol. 2008;8:8. Epub 2008/06/03. doi: 10.1186/1471-2210-8-8. PubMed PMID: 18513395; PMCID: PMC2438350.
242. Gilchrist AE, Lee S, Hu Y, Harley BAC. Soluble Signals and Remodeling in a Synthetic Gelatin-Based Hematopoietic Stem Cell Niche. Advanced healthcare materials. 2019;8(20):1900751. doi: 10.1002/adhm.201900751; PMCID: PMC6813872.
243. Law J, Zhang G, Dragan M, Postovit LM, Bhattacharya M. Nodal signals via beta-arrestins and RalGTPases to regulate trophoblast invasion. Cell Signal. 2014;26(9):1935-42. Epub 2014/05/28. doi: 10.1016/j.cellsig.2014.05.009. PubMed PMID: 24863882.
244. Quail DF, Siegers GM, Jewer M, Postovit LM. Nodal signalling in embryogenesis and tumourigenesis. Int J Biochem Cell Biol. 2013;45(4):885-98. Epub 2013/01/08. doi: 10.1016/j.biocel.2012.12.021. PubMed PMID: 23291354.
245. Camolotto S, Racca A, Rena V, Nores R, Patrito LC, Genti-Raimondi S, Panzetta-Dutari GM. Expression and transcriptional regulation of individual pregnancy-specific glycoprotein genes in differentiating trophoblast cells. Placenta. 2010;31(4):312-9. Epub 2010/02/02. doi: 10.1016/j.placenta.2010.01.004. PubMed PMID: 20116096.
246. Shanley DK, Kiely PA, Golla K, Allen S, Martin K, O'Riordan RT, Ball M, Aplin JD, Singer BB, Caplice N, Moran N, Moore T. Pregnancy-specific glycoproteins bind integrin alphaIIbbeta3 and inhibit the platelet-fibrinogen interaction. PLoS One. 2013;8(2):e57491. Epub 2013/03/08. doi: 10.1371/journal.pone.0057491. PubMed PMID: 23469002; PMCID: PMC3585349.
247. Warren J, Im M, Ballesteros A, Ha C, Moore T, Lambert F, Lucas S, Hinz B, Dveksler G. Activation of latent transforming growth factor-beta1, a conserved function for pregnancy-specific beta 1-glycoproteins. Mol Hum Reprod. 2018;24(12):602-12. Epub 2018/10/30. doi: 10.1093/molehr/gay044. PubMed PMID: 30371828; PMCID: PMC6262632.
248. Waterhouse R, Ha C, Dveksler GS. Murine CD9 is the receptor for pregnancy-specific glycoprotein 17. J Exp Med. 2002;195(2):277-82. PubMed PMID: 11805154.
249. Sulkowski GN, Warren J, Ha CT, Dveksler GS. Characterization of receptors for murine pregnancy specific glycoproteins 17 and 23. Placenta. 2011;32(8):603-10. Epub 2011/06/15. doi: S0143-4004(11)00199-8 [pii]
10.1016/j.placenta.2011.05.008. PubMed PMID: 21669460; PMCID: 3142296.
250. Clancy KB, Klein LD, Ziomkiewicz A, Nenko I, Jasienska G, Bribiescas RG. Relationships between biomarkers of inflammation, ovarian steroids, and age at menarche in a rural Polish sample. Am J Hum Biol. 2013;25(3):389-98. Epub 2013/04/23. doi: 10.1002/ajhb.22386. PubMed PMID: 23606228.
251. Eisenberg VH, Weil C, Chodick G, Shalev V. Epidemiology of endometriosis: a large population-based database study from a healthcare provider with 2 million members. BJOG. 2018;125(1):55-62. doi: 10.1111/1471-0528.14711.

APPENDIX A. CO-AUTHORED WORKS

A1. Response of neuroglia to hypoxia-induced oxidative stress using enzymatically crosslinked hydrogels

Citation
Zambuto SG*, Serrano JF*, Vilbert AC, Lu Y, Harley BAC, Pedron S. Response of neuroglia to hypoxia-induced oxidative stress using enzymatically crosslinked hydrogels. MRS Communications. 2019;10(1):83-90. doi: 10.1557/mrc.2019.159.

*These authors contributed equally to this work.

Abstract
Three-dimensional cultures have exciting potential to mimic aspects of healthy and diseased brain tissue to examine the role of physiological conditions on neural biomarkers, as well as disease onset and progression. Hypoxia is associated with oxidative stress, mitochondrial damage, and inflammation, key processes potentially involved in Alzheimer's and multiple sclerosis. We describe the use of an enzymatically-crosslinkable gelatin hydrogel system within a microfluidic device to explore the effects of hypoxia-induced oxidative stress on rat neuroglia, human astrocyte reactivity, and myelin production. This versatile platform offers new possibilities for drug discovery and modeling disease progression.

Contribution
Experimental work and manuscript preparation.

APPENDIX B. EXPERIMENTAL PROTOCOLS

B1. T Human Endometrial Stromal Cell Culture Protocol

All subsequent steps are to be performed in a biosafety cabinet using proper sterile technique.

T HESCs (ATCC CRL-4003, Fibroblast immortalized with hTERT)

- From non-malignant myomas
- Fibroblast-like morphology
- Expresses vimentin and fibroblast surface protein
- STR Profile:

Amelogenin: X

CSF1PO: 10,12

D13S317: 12,13

D16S539: 12,14

D5S818: 8

D7S820: 10

THO1: 7,8

TPOX: 9,11

vWA: 16,18

- Grows for a minimum of 15 population doublings
- Cite in manuscripts: T HESCs (ATCC® CRL-4003™)

Reagents

- Phenol red-free DMEM/F12 with 3.1 g/L glucose and 1 mM sodium pyruvate (based on Sigma Cat #D2906) supplemented with 1.5 g/L sodium bicarbonate (ordered from Cell Media Facility)
- ITS+ Premix (BD Cat# 354352, Fisher Scientific Cat# CB-40352)
- Puromycin (Sigma P8833)
    - 10 mg puromycin in 1 mL sterile cell culture water
    - Filter sterilize
- Charcoal-Stripped Fetal Bovine Serum (Sigma-Aldrich, F6765-500ML, Batch #16M289)
- 0.25% Trypsin-EDTA, Phenol Red-Free
    - 25 mL 0.5% Trypsin-EDTA, No Phenol Red (ThermoFisher, 15400054) and 25 mL PBS
- Cell Grade Water
- PBS without Ca^{2+} and Mg^{2+}
- DMSO
- Trypan Blue

Materials

- Pipettes and pipette tips
- T-25 or T-75 vented flasks, tissue culture treated
- Centrifuge tubes
- Microscope
- Hemocytometer

- 37ºC water bath
- Cell incubators
- Centrifuge
- Mr. Frosty
- Cryopreservation vials
- 0.22 micron filter

Media Preparation

As per manufacturer's instructions:

"A 1:1 mixture of Dulbecco's modified Eagle's medium and Ham's F-12 medium with 3.1 g/L glucose and 1mM sodium pyruvate and without phenol red (Sigma Cat# D 2906) supplemented with 1.5 g/L sodium bicarbonate, 1% ITS+ Premix (BD Cat# 354352), 500ng/mL puromycin, 90%; charcoal/dextran treated fetal bovine serum (HyClone Cat# SH30068.03), 10%"

Combine:

440 mL Media

50 mL CS-FBS

5 mL ITS+ Premix

25 µL Puromycin

5 mL penicillin/streptomycin

Filter sterilize. Store at 4ºC for up to one month.

Thawing Procedure

1. Thaw cell vial in 37ºC water bath by gentle agitation for approximately 2 minutes. Do not allow cap to touch water (contamination risk).
2. Transfer contents from vial into a centrifuge tube with 9 mL of complete culture medium.
3. Centrifuge cell suspension at 130 x g for 5 minutes.
4. Aspirate supernatant.
5. Resuspend cells in fresh growth media.
6. Count cells using a hemacytometer and seed at appropriate seeding density.

Flask Size	**Cell Density**	**Total Media Volume**
T-25	75,000 - 100,000	5 mL
T-75	225,000 - 300,000	15 mL

Maintenance Procedure

1. Grow cells in incubator at 37ºC, 5% CO_2.
2. Replace media the day after seeding cells.
3. Renew media every 2-3 days.

Passaging Procedure

Passage cells when cell concentration reaches between 2 x 10^4 and 3 x 10^4 cells/cm^2.

1. Aspirate media from flask.
2. Rinse cells using PBS.
3. Add 3 mL 0.25% Trypsin-EDTA solution to the flask. Wait until cells detach from the flask (5-15 minutes).

4. Add 6 mL of complete growth media to the flask to neutralize trypsin.
5. Transfer cells to a 15 mL conical tube.
6. Centrifuge cells at 130 x g for 5 minutes.
7. Discard supernatant and resuspend cells in growth media.
8. Count cells using a hemacytometer and seed at 3 x 10^3 - 4 x 10^3 cells/cm^2.

Flask Size	**PBS Rinse**	**Trypsin**	**Media**
T-25	5 mL	1 mL	2 mL
T-75	10 mL	3 mL	6 mL

Cryopreservation Procedure

1. Complete steps 1-8 of "Passaging Procedure".
2. Determine volume of media and DMSO necessary to cryopreserve cells.
3. Place vials in Mr. Frosty for at least 4 hours but no more than 24 hours.
4. Store in the liquid nitrogen (vapor phase) for long term storage.

Reagent	**Percentage**
Cell Media	95%
DMSO	5%

B2. Human Umbilical Vein Endothelial Cell (HUVEC) Culture Protocol
Protocol adapted from Mai Ngo's cell culture protocol. All subsequent steps are to be performed in a biosafety cabinet using proper sterile technique.

HUVECs

- Lonza Catalog #C2517A: HUVEC Single Donor, in EGM-2
- Have a cobblestone-like morphology

Reagents

- Endothelial Growth Media
    - Endothelial Cell Growth Medium 2 Kit (Phenol Red-Free) (PromoCell, C-22216)
    - SupplementPack (PromoCell, C-39211)
    - 5 mL pen/strep (Invitrogen 15140-122)
- TrypLE Express, no phenol red (ThermoFisher, 12604013)
- Trypsin Neutralizing Solution: 10% FBS in PBS
    - 5 mL Charcoal-Stripped FBS
    - 45 mL PBS without Ca^{2+} and Mg^{2+}
    - Store at 4ºC for up to 1 month.
- PBS without Ca^{2+} and Mg^{2+}
- DMSO (filter sterilized)
- Charcoal-Stripped FBS (Sigma-Aldrich, F6765-500ML, Batch #16M289)
- Trypan Blue

Materials

- Pipettes and pipette tips

- T-25 or T-75 vented flasks, tissue culture treated
- Centrifuge tubes
- Microscope
- Hemocytometer
- 37ºC water bath
- Cell incubators
- Centrifuge
- Mr. Frosty
- Cryopreservation vials

Media Preparation

Thaw SupplementPack and CS-FBS at 15 - 25ºC. Mix the supplement contents by pipetting up and down. Transfer entire content of each supplement (excluding the fetal calf serum) to the Basal Medium bottle. Transfer 10 mL of CS-FBS to the bottle. Add 5 mL of pen/strep. Close the bottle and swirl gently to mix. Store the media at 4 - 8ºC for up to 6 weeks. Do not freeze.
NOTE: This media does not contain enough fetal bovine serum to neutralize trypsin. Make trypsin neutralizing solution and use it instead.

Thawing Procedure

Note: HUVECs can have low viability after freezing. It is normal to observe many dead, floating cells the next day.

1. Thaw cell vial in 37ºC water bath for 1 minute.
2. Resuspend cells using a P1000 pipette.

3. Transfer cell cells to a 15 mL centrifuge tube and add 7 mL of media.
4. Centrifuge cells at 200 x g for 5 minutes.
5. Aspirate the supernatant and resuspend cells in a small amount of media.
6. Count cells using a hemocytometer and seed at the required density.
7. Add media to the flask so that there is 15 mL total in the flask and gently swirl to distribute cells evenly on the flask surface.
8. Change the media the day after seeding.

Flask Size	**Cell Density**	**Total Media Volume**
T-25	116,000	5 mL
T-75	350,000	15 mL

Maintenance Procedure

1. Grow cells in incubator at 37ºC, 5% CO_2.
2. Replace media in flask the day after seeding.
3. Feed cells every other day.
4. Feed cells the day before passaging.

Passaging Procedure

Passage cells at 80% confluence (~6 days). Feed cells the day before passaging.

1. Aspirate media from the flask.
2. Rinse cells with 10 mL PBS.
3. Aspirate PBS from the flask.

4. Add 6 mL TrypLE Express to the flask. Observe cells under microscope and tap the flask gently to help cells detach.
5. Neutralize cells with 9 mL trypsin neutralizing solution.
6. Transfer cells to a 15 mL conical tube.
7. Centrifuge cells at 200 x g for 5 minutes.
8. Aspirate supernatant and resuspend cells in a small amount of media.
9. Count cells using a hemacytometer and seed at appropriate seeding density.
10. Add media to the flask and swirl gently to distribute cells.
11. Change media in the flask the day after passaging.

Flask Size	**PBS Rinse**	**Trypsin**	**Trypsin-Neutralizing Solution**
T-25	5 mL	2 mL	5 mL
T-75	10 mL	6 mL	9 mL

Cryopreservation Procedure

1. Follow steps 1-10 in the "Passaging Procedure."
2. Calculate the volume of cell media, DMSO, and CS-FBS necessary to freeze cells at a density of 750,000 cells/vial.
3. Pipette solution into cryopreservation vials (1.5 mL solution per vial).
4. Place vials in Mr. Frosty in the -80ºC for at least 4 hours and no more than 24 hours.
5. Transfer cells to the liquid nitrogen tank for long term storage.

Reagent	**Percentage**
Cell Media	80%
Serum (CS-FBS)	10%
DMSO	10%

B3. Human Endometrial Microvascular Endothelial Cell (HEMEC) Culture Protocol
This protocol is adapted from the ScienCell protocol for Cat. No. 7010.

1. Prepare a fibronectin-coated culture vessel (2 µg/cm^2). Add 5 ml of sterile Dulbecco's phosphate buffered saline, Ca++- and Mg++-free (Cat. #0303) to a T-75 flask and then add 150 µl of fibronectin stock solution (Cat. #8248). Leave vessel in a 37^{o}C incubator overnight.
2. Prepare complete medium by adding supplements (Endothelial Growth Supplement Cat. No. 1052, Penicillin/Streptomycin Cat. No. 0503, and Fetal Bovine Serum Cat. No. 0025 OR Charcoal-Stripped Fetal Bovine Serum Sigma-Aldrich, F6765-500ML) to phenol red-free Endothelial Cell Medium (Cat. No. 1001).
3. Aspirate the fibronectin solution and add 15 ml of complete medium to the culture vessel. The fibronectin solution can be reused twice.
4. Place the frozen vial in a 37^{o}C water bath. Hold and rotate the vial gently until the contents completely thaw.
5. Carefully remove the cap without touching the interior threads. Gently resuspend and dispense the contents of the vial into the equilibrated, fibronectin-coated culture vessel.
6. Replace the cap or lid of the culture vessel and gently rock the vessel to distribute the cells evenly.
7. Return the culture vessel to the incubator.
8. Do not disturb the culture for at least 16 hours after the culture has been initiated. Refresh culture medium the next day to remove residual DMSO and unattached cells.

Maintaining the culture:

1. Refresh supplemented culture medium the next morning after establishing a culture from cryopreserved cells.
2. Change the medium every two to three days thereafter.

Subculturing:

1. Subculture when the culture reaches 90% confluency.
2. Prepare fibronectin-coated culture vessels (2 μg/cm^2) one day before subculture.
3. Warm complete medium, trypsin/EDTA solution, 0.05% (T/E, Cat. #0183), T/E neutralization solution (TNS, Cat. #0113), and DPBS (Ca++- and Mg++-free, Cat. #0303) to room temperature.
4. Rinse the cells with DPBS.
5. Add 10 ml DPBS and 1 ml 0.05% T/E solution (Cat. #0183) into flask (in the case of a T-75 flask) and place in incubator.
6. During incubation, prepare a 50 ml conical centrifuge tube with 5 ml of fetal bovine serum (FBS, Cat. #0500).
7. Once the cells completely round up, transfer T/E solution from the flask to a 50 ml centrifuge tube (a small percent of cells may detach). Check under a microscope to make sure that all cells detach.
8. Add 5 ml of TNS solution to the flask and transfer detached cells to the 50 ml centrifuge tube. Rinse the flask with another 5 ml of TNS to collect the residual cells.
9. Centrifuge the 50 ml centrifuge tube at 1000 rpm for 5 minutes. Gently resuspend cells in culture medium.

10. Count and plate cells in a new fibronectin-coated culture vessel with the recommended cell density. A seeding density of 5,000-7,000 cells/cm2 is recommended.
11. To freeze cells down, follow this protocol and then freeze cells in CFM (Cat. No. 0133).

B4. Endometrial Epithelial Cell (EEC) Culture Protocol
All subsequent steps are to be performed in a biosafety cabinet using proper sterile technique.

EEC Primary Cells

- Endometrial (Uterine) Epithelial Cells (LifeLine Cell Technology, FC-0078, Lot#03839)
- Donor Info: Caucasian Female, 33 y.o., uterine prolapse, average population doubling time: 45 hours, population doubling time for first passage out of cryopreservation: 24 hours
- Morphology: polygonal, cuboidal, monolayer
- 5 guaranteed population doublings
- Approximate days per passage: 5-8
- Use within 1 to 2 passages

Reagents

Endometrial Epithelial Cell Media

ReproLife Female Reproductive Medium Complete Kit (LifeLine Cell Technology, LL-0068)

Trypsin 0.05% EDTA 0.02% (Phenol Red Free) (LifeLine Cell Technology, CM-0017)

Trypsin-Neutralizing Solution: 10% FBS in PBS

1.5 mL Charcoal-Stripped FBS

13.5 mL PBS without Ca^{2+} and Mg^{2+}

PBS without Ca^{2+} and Mg^{2+}

DMSO

Charcoal-Stripped FBS (Sigma-Aldrich, F6765-500ML, Batch #16M289)

Trypan Blue

Materials

Pipettes and pipette tips

T-25 or T-75 vented flasks, tissue culture treated

Centrifuge tubes

Microscope

Hemocytometer

37ºC water bath

Cell incubators

Centrifuge

Mr. Frosty

Cryopreservation vials

Media Preparation

Basal medium should be stored at 2ºC - 8ºC. LifeFactors should be stored at -20ºC. For long-term storage, LifeFactors should be stored at -80ºC. NOTE: LifeFactors are packaged with extra solution in each vial. Pipette the correct amounts into the media bottle. Thaw LifeFactors and mix by pipetting. L-glutamine should be warmed to 37ºC in a water bath and mixed to dissolve any precipitate. Mix insulin by pipetting the solution until any precipitate dissolves. Add LifeFactors into the ReproLife Basal Medium Bottle. Gently invert the bottle to mix. Store media at 2ºC - 8ºC for up to 2 weeks. Freeze media and store at -20ºC for up to one year. Make small media aliquots to prevent repeated warming of the media. Protect media from light to prevent degradation.

Thawing Procedure

1. Thaw cell vial in 37ºC water bath for 1 minute. Do not allow cap to contact water (contamination risk).
2. Resuspend cells using a P1000 pipette. Do not centrifuge: cells can be plated onto a flask immediately following thawing.
3. Plate cells at proper density (5,000 cells/cm^2) in vented flasks.
4. Add media to cells.
5. Gently rock flask to ensure cells are evenly distributed.
6. Replace media in flask 4 to 36 hours after seeding once cells have attached to remove cryopreservation reagents.

Flask Size	**Cell Density**	**Total Media Volume**
T-25	125,000	5 mL
T-75	375,000	15 mL

Maintenance Procedure

1. Grow cells in an incubator at 37ºC, 5% CO_2.
2. Replace media in flask 4 to 36 hours after seeding once cells have attached.
3. Feed cells every other day.

Passaging Procedure

Passage cells when they reach 85% to 100% confluence but are still actively proliferating.

1. Aspirate media from flask.
2. Rinse cells using PBS.

3. Aspirate PBS from flask.
4. Add 0.05% trypsin/0.02% EDTA to the flask and swirl gently.
5. Allow cells to detach for 2-3 minutes, gently striking the flask to release cells. Do not over trypsinize.
6. Add equal volume of trypsin-neutralizing solution to the flask.
7. Transfer cells to a centrifuge tube (15 mL for T-25, 50 mL for T-75).
8. Centrifuge cells at 150 x *g** for 5 minutes.
9. Aspirate supernatant from the tube. Carefully avoid the cell pellet.
10. Resuspend the cells in media.
11. Count cells using a hemocytometer and re-plate at 5,000 cells/cm^2.

Flask Size	PBS Rinse	Trypsin	Trypsin-Neutralizing Solution
T-25	5 mL	2 mL	2 mL
T-75	10 mL	6 mL	6 mL

Cryopreservation Procedure

Cryopreserve cells at 80% confluence.

1. Complete steps 1-11 of “Passaging Procedure".
2. Determine volume of media, serum, and DMSO or FrostaLife™ (LM-0015) necessary to cryopreserve cells at a density of 500,000 cells per mL to 2,000,000 cells per mL.
3. Add 1.0 mL of total solution to each cryopreservation vial.
4. Place vials in Mr. Frosty for at least 4 hours, but no more than 24 hours.
5. Transfer cells to liquid nitrogen tank (vapor phase) for long-term storage.

B5. HTR-8/SVneo Cell Culture Protocol
All subsequent steps are to be performed in a biosafety cabinet using proper sterile technique.

HTR-8/SVneo

ATCC CRL-3271, lot 70014079, human trophoblast

- From placenta
- Epithelial-like; however, this cell line has been shown to contain both epithelial and mesenchymal-like cell populations
- Derived from transfecting cells from the chorinic villi explants of human first-trimester placenta with gene encoding for simian virus 40 large T antigen
- STR Profile:

Amelogenin: X

CSF1PO: 12

D13S317: 9,12

D16S539: 13

D5S818: 12

D7S820: 12

TH01: 6,9.3

vWA: 13,18

TPOX: 8

- Cite in manuscripts as: HTR-8/SVneo (ATCC® CRL-3271™)

Reagents

- RPMI-1640 Medium (from Cell Culture Facility; based on ATCC 30-2001)

- Charcoal-Stripped Fetal Bovine Serum (CS-FBS) (Sigma-Aldrich, F6765-500ML, Batch #16M289)
- 0.25% Trypsin-EDTA, Phenol Red-Free
    - 25 mL 0.5% Trypsin-EDTA, No Phenol Red (ThermoFisher, 15400054) and 25 mL PBS
- PBS without Ca^{2+} and Mg^{2+}
- DMSO
- Trypan Blue

Materials

- Pipettes and pipette tips
- T-25 or T-75 vented flasks, tissue culture treated
- Centrifuge tubes
- Microscope
- Hemocytometer
- 37ºC water bath
- Cell incubators
- Centrifuge
- Mr. Frosty
- Cryopreservation vials
- 0.22 micron filter

Media Preparation

As per manufacturer's instructions:

"The base medium for this cell line is ATCC-formulated RPMI-1640 Medium, Catalog No. 30-2001. To make the complete growth medium, add the following components to the base medium: fetal bovine serum to a final concentration of 5%"

Combine:

470 ml RPMI-1640 Medium

25 ml CS-FBS

5 ml Penicillin/Streptomycin

Filter sterilize. Store at 4ºC for up to one month.

Thawing Procedure

1. Thaw cell vial in 37ºC water bath by gentle agitation for approximately 2 minutes. Do not allow cap to touch water (contamination risk).
2. Transfer contents from vial into a centrifuge tube with 9 mL of complete culture medium.
3. Centrifuge cell suspension at 130 x g for 5 minutes.
4. Aspirate supernatant.
5. Resuspend cells in fresh growth media.
6. Count cells using a hemacytometer and seed at appropriate seeding density (1.5×10^4 - 3×10^4 viable cells/cm^2).

Flask Size	Cell Density	Total Media Volume
T-25	375,000 - 750,000	5 mL
T-75	1,125,000 - 2,250,000	15 mL

Maintenance Procedure

1. Grow cells in incubator at 37ºC, 5% CO_2.
2. Replace media the day after seeding cells.
3. Renew media every 2-3 days.

Passaging Procedure

1. Aspirate media from flask.
2. Rinse cells using PBS.
3. Add 3 mL 0.25% Trypsin-EDTA solution to the flask. Wait until cells detach from the flask (5-15 minutes).
4. Add 6 mL of complete growth media to the flask to neutralize trypsin.
5. Transfer cells to a 15 mL conical tube.
6. Centrifuge cells at 130 x g for 5 minutes.
7. Discard supernatant and resuspend cells in growth media.
8. Count cells and seed at the appropriate seeding density.

Flask Size	PBS Rinse	Trypsin	Media
T-25	5 mL	1 mL	2 mL
T-75	10 mL	3 mL	6 mL

Cryopreservation Procedure

1. Complete steps 1-8 of “Passaging Procedure”.
2. Determine volume of CS-FBS and DMSO necessary to cryopreserve cells.
3. Place vials in Mr. Frosty for at least 4 hours but no more than 24 hours.
4. Store in the liquid nitrogen (vapor phase) for long term storage.

Reagent	**Percentage**
CS-FBS	92%
DMSO	8%

B6. Swan71 Trophoblast Cell Culture Protocol

Protocol adapted from Dveksler Lab at Uniformed Services University. Original protocol from Straszewski-Chavez et al. "The Isolation and Characterization of a Novel Telomerase Immortalized First Trimester Trophoblast Cell Line, Swan 71," *Placenta*, 2009. All subsequent steps are to be performed in a biosafety cabinet using proper sterile technique. Gifted from Dveksler Lab who was given them by Dr. Mor for PSG work.

Reagents

- DMEM
- FBS
- Puromycin
- TypLE
- PBS without Ca^{2+} and Mg^{2+}
- DMSO
- Trypan Blue

Materials

- Pipettes and pipette tips
- T-25 or T-75 vented flasks, tissue culture treated
- Centrifuge tubes
- Microscope
- Hemacytometer
- 37ºC water bath
- Cell incubators

- Centrifuge
- Mr. Frosty
- Cryopreservation vials
- 0.22 micron filter

Media Preparation

Recommended:

DMEM (Phenol Red-Free for hormone work; From Cell Culture Facility)

10% FBS (CS-FBS for hormone work)

100 µg/mL penicillin/streptomycin

Reagent	**For 500 mL**	**For 100 mL**
DMEM	445 mL	89 mL
10% FBS	50 mL	10 mL
1% P/S	5 mL	1 mL

Filter sterilize. Store at 4ºC for up to one month. Media should be pre-warmed prior to adding to cells. Puromycin (500 ng/mL)→ add directly to flask after first passage from cryopreservation.

Thawing Procedure

1. Thaw vial in 37ºC water bath by gentle agitation for approximately 2 minutes. Do not allow cap to touch water (contamination risk).
2. Transfer full contents of vial to a flask with cell medium.
3. Replace medium the following day.

Notes:

- Do not add puromycin when you take them out of cryopreservation.
- Once passaged, add puromycin at a maintenance dose of 500 ng/mL and add every time to flask, not medium.

Maintenance Procedure

1. Grow cells in incubator at 37ºC, 5% CO_2.
2. Replace media the day after seeding cells.
3. Renew media every 2-3 days.

Notes:

- Add puromycin at a maintenance dose of 500 ng/mL and add every time to flask, not medium.
- Recommended 20,000 to 30,000 cells/cm^2 (1,500,000 to 2,250,000 per T75 or 500,000 to 750,000 per T25)

Passaging Procedure

1. Passage at approximately 80% confluence.
2. Aspirate media from flask.
3. Rinse cells using PBS.
4. Add 5 mL TrypLE solution to the flask. Wait until cells detach from the flask (5-15 minutes).
5. Add 6 mL of complete growth media to the flask to neutralize trypsin.
6. Transfer cells to a 15 mL conical tube.

7. Centrifuge cells at 130 x g for 5 minutes.
8. Discard supernatant and resuspend cells in growth media.
9. Count cells and seed at the appropriate seeding density.

Flask Size	**PBS Rinse**	**TrypLE**	**Media**
T-25	5 mL	2 mL	2 mL
T-75	10 mL	5 mL	6 mL

Cryopreservation Procedure

5. Complete steps 1-8 of "Passaging Procedure".
6. Determine volume of FBS and DMSO necessary to cryopreserve cells. Freeze down at a density equivalent to a confluent T75 flask.
7. Place vials in Mr. Frosty for at least 4 hours but no more than 24 hours.
8. Store in the liquid nitrogen (vapor phase) for long term storage.

Reagent	**Percentage**
Media	80%
FBS	10%
DMSO	10%

B7. Methacrylamide-Functionalized Gelatin Synthesis

This protocol is adapted from Shirahama H, Lee BH, Tan LP, Cho NJ. Precise Tuning of Facile One-Pot Gelatin Methacryloyl (GelMA) Synthesis. *Sci Rep*. 2016;6:31036. doi: 10.1038/srep31036. PubMed PMID: 27503340; PMCID: PMC4977492. The protocol below was adapted from Sara Pedron's protocol.

Reagents:

- Porcine Gelatin type A (Sigma Aldrich G2500)
- Carbonate – bicarbonate (CB) buffer pH 9.4 (Thermo Fisher 28382)
- Methacrylic anhydride (Sigma Aldrich 276685)
- 12-14 kDa dialysis membranes (Fisher Scientific 21-152-8) . Hydrated in DI water at room temperature 20-30 min prior to purification.

Preparation:

Properly clean glassware prior to running experiment: wash with soap and water, rinse with DI water, spray with acetone, spray with ethanol. Make sure all glassware is 100% dry prior to your experiment.

Procedure:

Dissolve 1 g of gelatin in 10 ml of CB buffer at 50ºC. Subsequently, add MAA (0.1 ml for 90%* DOF, 0.04 ml for 50% DOF and 0.015 ml for 25% DOF) dropwise and stirring at 500 rpm. Scale up accordingly for larger batches. Check pH is 9-10 with pH paper. Let reaction proceed for 1 hour for 50% - 25% and 3 hours for 90%, then stop reaction adding 40 ml of warm DI water (scale up for larger batches). Check pH is 6-7 with pH paper, if not add HCl solution (for 90% -

control of pH at this point is not that important because you want high DOF). Then dialyze gelatin solution in 12-14 kDa dialysis membranes against DI water at 50ºC for one week and lyophilize.

* for very high DOF use 20% w/v gelatin solution, instead of 10% w/v.

B8. Cell Laden GelMA Hydrogel Cultures

This protocol has been adapted from Mai Ngo's protocol.

Reagents

- GelMA
- LAP photoinitiator
- PBS
- Cells and cell media

Supplies and equipment

- UV Lamp
- Teflon molds (autoclaved)
- Glass slides (autoclaved)
- Binder clips (autoclaved)
- Syringe needles
- 1.5 mL microcentrifuge tubes (autoclaved)
- Spatula (autoclaved)
- 48 well plates
- Scintillation vials

Procedure

1. UV sterilize GelMA in a scintillation vial for 30 min.

2. Assemble molds by placing Teflon mold on top of glass slide and securing the four sides with binder clips.
3. Add PBS to the GelMA to create a 5% (w/v) solution.
4. Heat the mixture at 37 °C until all the GelMA is dissolved. Add PI to make a 0.1% solution (from a 5% stock solution of LAP) Place in the incubator at 37 °C until further use and protect from light.
5. Passage and count cell types.
6. Form a cell pellet from a suspension containing the desired concentration of cells by centrifuging twice at 200 rcf at 1.5 min each, and then 200 rcf at 2 min. Turn the vial 180° between the first two cycles, then 90° for the last cycle.
7. Remove media from the cell pellet and re-suspend cells in the GelMA solution.
8. Pipette the pre-polymer solution into the wells and place under UV light for 30 seconds (Dial = 2.7 on IGB UV lamp).
9. To remove hydrogels, run a needle around the edge of each hydrogel. Pipette PBS onto each hydrogel. Remove the binder clips and gently separate the mold from the glass slides. Use a spatula to transfer gels to 48 well plates with 0.5-0.8 mL of medium per hydrogel.
10. If creating endometrial tricultures, follow protocol in B9.

B9. Microbial Transglutaminase Enzymatic Gel Coating

Protocol Adapted From: Besser RR, Bowles AC, Alassaf A, Carbonero D, Claure I, Jones E, Reda J, Wubker L, Batchelor W, Ziebarth N, Silvera R, Khan A, Maciel R, Saporta M, Agarwal A. Enzymatically crosslinked gelatin-laminin hydrogels for applications in neuromuscular tissue engineering. Biomater Sci. 2020;8(2):591-606. Epub 2019/12/21. doi: 10.1039/c9bm01430f. PubMed PMID: 31859298; PMCID: PMC7141910.

Reagents

- Recombinant microbial (bacterial) transglutaminase-25 U (Zedira T001)
- ECM biomolecules (See Table Below Adapted from Zambuto et al.)
- Primary and secondary antibodies for biomolecules
- Fluospheres Polystyrene Microspheres 1.0 μm orange fluorescent beads (Invitrogen)
- PBS
- Cell culture grade H_2O

Materials

- Ibidi μ-Slides Angiogenesis Glass Bottom
- Hydrogel samples
- UV lamp
- Microscope
- Incubator

Protocol

Reagent Prep

mTg

Add H_2O to the lyophilized mTg (see COA)

Rotate vial until solid dissolves

If turbid, centrifuge and collect supernatant

Freeze in working aliquots

Coating Gels

1. Prepare hydrogel samples: Add 10 µL of the prepolymer solution to each well of Ibidi µ-Slides Angiogenesis Glass Bottom and then polymerize under UV light.

Note: If making acellular gels, can use fluorescent microbeads ($1x10^{10}$ beads/mL) to visualize hydrogel.

2. Prepare a 1:1 ratio of 0.5 mg/mL mTg and 10 µg/mL ECM biomolecule solution. If making coatings with 2 biomolecules, combine biomolecules in a 1:1 ratio.
3. Pipette 20 µL of this solution onto hydrogels.
4. Incubate hydrogels for 1 hour in 5% CO2 incubators at 37°C.
5. Perform one quick wash using 20 µL of PBS.
6. If making tricultures, passage cells and add them immediately onto the gels.

Visualization of ECM-coating on Hydrogels

1. Block samples for 1 hour in 30 µL of a 2% Abdil solution (2% bovine serum albumin, 0.1% Tween 20, PBS).

2. Stain samples with anti-biomolecule primary antibody diluted in 2% Abdil (30 µL; use vendor recommendation) at 4°C overnight.
3. Perform three PBS washes.
4. Incubate samples with secondary antibody solution diluted in 2% Abdil (1:500, 30 µL) for 2 hours at room temperature.
5. Perform three PBS washes.
6. Store samples in PBS at 4°C until imaged.

Microarray/ECM Biomolecule Information from Underhill Laboratory.

Biomolecule	**Vendor**	**Catalog Number**	**Stock Concentration**
Collagen 1	EMD Millipore	08-115MI	1 mg/mL
Collagen 3	EMD Millipore	CC054	1 mg/mL
Collagen 4	Abcam	ab7536	1 mg/mL
Collagen 5	Abcam	ab7530	1 mg/mL
Fibronectin	EMD Millipore	FC010-10MG	1 mg/mL
Decorin	R&D Systems	143-DE-100	0.5 mg/mL
Lumican	ACROBiosystems	LUM-H5227-100ug	0.5 mg/mL
Laminin	EMD Millipore	CC095	1 mg/mL
Hyaluronic Acid	Lifecore Biomedical	HA60k-1	1 mg/mL
Tenascin C	R&D Systems	3358-TC-050	0.5 mg/mL

B10. 3D Immunofluorescent Staining Protocol for Hydrogels

Original protocol adapted from Mai Ngo's protocol

Materials needed:

- PBS buffer
- Formalin
- PBST: PBS + 0.1% Tween
- PBS + 0.5% Tween
- 2% Abdil: PBS + 0.1% Tween + 2% BSA
    - Store at 4°C. Remake after 1 month.
- Primary and secondary antibodies
- DAPI or Hoechst (Invitrogen H3570)

Day 1 (Approximately 2 hours)

1. Wash the tissue with PBS, 3 quick washes
2. Fix the tissue in formalin for 15 minutes
3. Wash with PBS, 3 quick washes
4. Permeabilize in PBS + 0.5% Tween for at least 15 minutes
5. Wash in PBST for 5 minutes, 3 times
6. Block in 2% abdil for 1 hour
7. Dilute the primary antibody in 2% abdil. Prepare 300 µl solution per well.
8. Add primary antibody, incubate overnight at 4°C. If double staining, you can combine primary antibodies.

Days 2 and 3 performed while protecting samples from light

Day 2 (Approximately 1.5 hours)

1. Wash in PBST for 20 minutes, 4 times. At room temperature on shaker.
2. Dilute the secondary antibody in 2% abdil. Prepare 300 µl solution per well.
3. Add secondary antibody, incubate overnight at 4°C, covered in foil, on shaker.

Day 3 (Approximately 2 hours)

1. Wash in PBST for 20 minutes, 4 times at room temperature.
2. Add DAPI (1:300 diluted in PBS) or Hoescht (1:2000 diluted in PBS) for 30 minutes
3. Wash with PBST.
4. Store in PBST until imaging.

Antibody	**Company/Part #**	**Dilution**	**Species**	**Cell Type**
CD31	Agilent JC70A	1:200	Mouse	HUVEC
Mouse Monoclonal CD10	Agilent R084801-1	1:100	Mouse	HUF/HESC
Anti-Cytokeratin 18	Abcam ab52948	1:250	Rabbit	EEC
Phalloidin-iFluor 488 Reagent CytoPainter	Abcam ab176753	1 µl/1 mL		All
Goat Anti-Mouse IgG (H+L) Cross-Adsorbed Secondary Antibody AlexaFluor 555	Thermo A-21422	1:500	Goat	
Goat Anti-Mouse IgG (H+L) Cross-Adsorbed Secondary Antibody AlexaFluor 488	Thermo A-11001	1:500	Goat	
Goat Anti-Rabbit IgG (H+L) Cross-Adsorbed Secondary Antibody AlexaFluor 555	Thermo A-21428	1:500	Goat	
Goat Anti-Rabbit IgG (H+L) Cross-Adsorbed Secondary Antibody AlexaFluor 488	Thermo A-11008	1:500	Goat	

B11. 2D Immunofluorescent Staining Protocol
Materials needed:

- PBS buffer
- Formalin
- PBST: PBS + 0.1% Tween
- PBS + 0.5% Tween
- 2% Abdil: PBS + 0.1% Tween + 2% BSA
    - Store at 4°C. Remake after 1 month.
- Primary and secondary antibodies
- DAPI or Hoechst (Invitrogen H3570)

Procedure:

1. Wash the tissue with PBS, 3 quick washes
2. Fix the tissue in formalin for 15 minutes
3. Wash with PBS, 3 quick washes
4. Permeabilize in PBS + 0.5% Tween for 15 minutes
5. Wash in PBST for 5 minutes, 3 times
6. Block in 2% abdil for 1 hour
7. Dilute the primary antibody in 2% abdil. Prepare 300 µl solution per well (adjust depending on plate size). Incubate samples in primary antibody overnight at 4°C
8. Perform 5 x 5 minute washes in PBST
9. Dilute the secondary antibody in 2% abdil. Prepare 300 µl solution per well. Incubate samples in secondary antibody overnight at 4°C. Protect samples from light from here onward.
10. Perform 5 x 5 minute washes in PBST

11. Incubate samples in Hoechst for 10 minutes.

12. Perform a quick wash with PBST.

13. Store in PBST until imaging.

Antibody	**Company/Part #**	**Dilution**	**Species**	**Cell Type**
CD31	Agilent JC70A	1:200	Mouse	HUVEC
Mouse Monoclonal CD10	Agilent R084801-1	1:100	Mouse	HUF/HESC
Anti-Cytokeratin 18	Abcam ab52948	1:250	Rabbit	EEC
Phalloidin-iFluor 488 Reagent CytoPainter	Abcam ab176753	1 µl/1 mL		All
Goat Anti-Mouse IgG (H+L) Cross-Adsorbed Secondary Antibody AlexaFluor 555	Thermo A-21422	1:500	Goat	
Goat Anti-Mouse IgG (H+L) Cross-Adsorbed Secondary Antibody AlexaFluor 488	Thermo A-11001	1:500	Goat	
Goat Anti-Rabbit IgG (H+L) Cross-Adsorbed Secondary Antibody AlexaFluor 555	Thermo A-21428	1:500	Goat	
Goat Anti-Rabbit IgG (H+L) Cross-Adsorbed Secondary Antibody AlexaFluor 488	Thermo A-11008	1:500	Goat	

B12. Microarray Immunofluorescent Staining Protocol

Materials needed:

- PBS buffer
- Formalin
- PBST: PBS + 0.1% Tween
- PBS + 0.5% Tween
- 2% Abdil: PBS + 0.1% Tween + 2% BSA
    - Store at 4°C. Remake after 1 month.
- Primary and secondary antibodies
- DAPI Fluoromount

Procedure:

Day 1

1. Wash the tissue with PBS, 3 quick washes
2. Fix the tissue in formalin for 15 minutes
3. Wash with PBS, 3 quick washes
4. Permeabilize in PBS + 0.5% Tween for 15 minutes
5. Wash in PBST for 5 minutes, 3 times
6. Block in 2% abdil for 1 hour at room temperature
7. Dilute the primary antibody in 2% abdil. Prepare 300 µl solution per slide. Incubate samples in primary antibody overnight at 4°C

Day 2

8. Perform 3 x 5 minute washes in PBST

9. Dilute the secondary antibody in 2% abdil. Prepare 300 µl solution per well. Incubate samples in secondary antibody overnight at 4°C. Protect samples from light from here onward.

Day 3

10. Perform 3 x 5 minute washes in PBST
11. Mount using DAPI Fluoromount
12. Image

B13. Nascent Protein Production Staining

Protocol Adapted From:

Loebel C, Kwon MY, Wang C, Han L, Mauck RL, Burdick JA. Metabolic Labeling to Probe the Spatiotemporal Accumulation of Matrix at the Chondrocyte-Hydrogel Interface. Advanced Functional Materials. 2020. doi: 10.1002/adfm.201909802.

Reagents

- Click-iT AHA (Invitrogen, C10102; 100 μM)
- Hanks' Balanced Salt Solution (HBSS)
- Methionine-Free Media (purchased or custom made at the Cell Media Facility)
- AFDye 488 DBCO (Click Chemistry Tools, 1278-1; 30 μM)
- CellMaskTM Deep Red Plasma Membrane Stain (1:1000; Invitrogen, C10046)
- Hoechst or DAPI
- PBS

Materials

- Hydrogel samples
- UV lamp
- Microscope
- Incubator

Protocols

Protocol Using Methionine-Free Media (Short or Long Term)

Note: This protocol can be used for bulk nascent protein production staining (e.g., entire culture period).

1. Starting on day 1 of culture, incubate hydrogels with the methionine analog azidohomoalanine (Click-iT AHA; 100 μM) in methionine-free DMEM supplemented with relevant reagents (e.g., FBS, penicillin/streptomycin, etc.).
2. Replenish the media containing AHA daily.
3. On the final day of culture, wash hydrogels two times with sterile PBS.
4. Incubate hydrogels for 40 min in AFDye 488 DBCO (Click Chemistry Tools, 30 μM) at 37 °C.
5. Wash hydrogels three times with sterile PBS.

Note: Hydrogels are live until this point.

6. Fix hydrogels in 4% formaldehyde (or formalin) for 15 min followed by three PBS washes.
7. Stain or store at 4 °C in PBS until staining.
8. Incubate hydrogels in CellMask™ Deep Red Plasma Membrane Stain (1:1000; Invitrogen) for 40 minutes at 37°C followed by three PBS washes.
9. Incubate hydrogels in Hoechst at room temperature for 30 minutes (1:2000 dilution in PBS) followed by one PBS wash.
10. Store samples at 4°C in PBS until imaged.

Protocol Using HBSS (Short Term)

Note: If your cell media is proprietary and you cannot obtain methionine-free media, you can still use this method using HBSS and short time frames (e.g., scale of hours).

1. On last day of culture, wash hydrogels once with HBSS and incubate in HBSS in the incubator for 30 minutes to deplete the cells of any remaining methionine.
2. Remove HBSS and incubate hydrogels in HBSS containing the methionine analog azidohomoalanine (Click-iT AHA; 100 μM) for 1 hour.
3. Following incubation, perform two HBSS washes.
4. Incubate hydrogels in AFDye 488 DBCO (Click Chemistry Tools; 30 μM) for 40 minutes in the incubator.
5. Following incubation, Wash hydrogels X3 with PBS.

Note: Hydrogels are live until this point.

6. Fix hydrogels for 15 minutes using formalin followed by X3 PBS washes.
7. Stain hydrogels immediately or store at 4°C in PBS until staining.
8. Incubate hydrogels in CellMask™ Deep Red Plasma Membrane Stain (1:1000; Invitrogen, C10046) for 40 minutes at 37°C followed by three PBS
9. Incubate hydrogels in Hoechst at room temperature for 30 minutes (1:2000) followed by one PBS wash.
10. Store at 4°C in PBS until imaged.

B14. CellTiter-Glo 3D Viability Assay
This protocol is adapted from Emily Chen's protocol.

Principle:

CellTiter-Glo is a viability assay. This assay involves lysing cells and generates a luminescent signal proportional to the amount of ATP present. The ATP is proportional to the amount of viable cells in culture.

Advantages:

This assay is simple, fast, robust, and designed specifically for 3D cultures. This assay can be used for low cell numbers (1000s).

Materials and Reagents:

- Day 3 Spheroids in GelMA Hydrogels
- CellTiter Glo 3D Kit
- Opaque 96 well plate (white walled)
- Plate Reader
- Shaker

Procedure:

Preparation:

1. Culture spheroids and image daily for 3 days.
2. Thaw CellTiter Glo overnight at 4C.
3. Equilibrate Reagents and cells to Room Temperature for 30 minutes (at least).
4. Mix reagents gently prior to use by inverting the tube.

Assay:

1. Equilibrate samples and medium to room temperature for 30 minutes.
2. Prepare a stock solution with (1:1) equal amounts of cell medium and CellTiter Glo.
3. Remove medium from each well.
4. Add 400 uL of stock solution to each well.
5. Incubate plate for 1 hour at room temperature on shaker to stabilize signal (8^{th} dot; cover with foil).
6. Transfer 3x100 uL triplicates to an opaque plate for each sample.

Prepare blank triplicates using the CellTiter Stock.

7. Read luminescence on plate reader.
8. Calculate viability by subtracting blank luminescence from sample luminescence.

B15. LDH Assay Protocol

Protocol adapted from Promega LDH-Glo Cytotoxicity Assay Technical Manual TM548.

Assay Principles

Lactate dehydrogenase (LDH) is an enzyme released into cell media when plasma membranes are disrupted. LDH is a cytotoxicity marker. Luminescence signal is generated proportional to the amount of LDH in the sample.

Reagents

- LDH-Glo Cytotoxicity Assay (J2380 or J2381)
    - LDH Detection Enzyme Mix
    - Reductase Substrate
    - Lactate Dehydrogenase
- LDH Storage Buffer (Prepared by User)
    - 200 mM Tris-HCl (pH 7.3), 10% Glycerol, 1% BSA

Materials

- Treated cells
- 96-well opaque, white walled luminescence plates
- Multichannel pipettor
- Plate reader
    - Integration time of 0.5 – 1 second per well

Protocol

Notes:

Do not freeze thaw reagents more than 3 times.

Removal of up to 10% of starting media from the well should be fine as per manufacturer's instructions.

LDH Storage Buffer Preparation

200 mM Tris-HCl (pH 7.3), 10% glycerol, 1% BSA

Filter sterilize using a 0.22 μm filter bottle. Store at 4°C for up to one month.

LDH Detection Reagent Preparation: Immediately before use

1. Thaw LDH Detection Enzyme Mix and Reductase Substrate at room temperature. Keep LDH Detection Enzyme Mix at room temperature and Reductase Substrate on ice once thawed.

2. Immediately before use, prepare LDH Detection Reagent. Each well will use 50 μL sample and 50 μL of LDH Detection Reagent.

Per Reaction (Well): 50 μL LDH Detection Enzyme Mix + 0.25 μL Reductase Substrate

3. Mix by inverting 5 times.

LDH Assay

1. Equilibrate samples to room temperature prior to running assay.

2. Collect samples of culture media: 2-5 μL into 48-95 μL of LDH storage buffer. Mix by pipetting up and down 2-3 times. Proceed with assay or store at -20°C.

3. Dilute samples to recommended dilution in LDH storage buffer.

4. Transfer 50 µL of diluted sample into a 96-well white walled plate.

5. Add 50 µL of LDH Detection Reagent.

6. Incubate at room temperature for 60 minutes. *Protect from light!*

7. Immediately record luminescence.

Controls

- No cell control: Same amount of cell media diluted in LDH Storage Buffer
- Vehicle control: Your standard vehicle control from your experiment
- Maximum LDH release control (optional-use if calculating % cytotoxicity)

Add 2 µl of 10% triton X-100 per 100 µl of vehicle-only cells for 10-15 min or longer (do 30 min for gels)

B16. Matrigel Tube Formation Assay Protocol

Materials

- Phenol Red-Free Matrigel OR Phenol Red-Free Matrigel 96 well plate
- Endothelial cells
- 200 µL pipette tips
- 96-well plate
- Ice

Day before Experiment

- Thaw Matrigel or Matrigel plate overnight in cold room.
- Pre-cool pipette tips and 96-well plate in -80 °C freezer overnight if using Matrigel.

Experiment

Keep Matrigel, pipette tips for dispensing Matrigel, and 96-well plate on ice at all times. For the 96-well plate I have kept it on top of an ice pack while dispensing Matrigel into it.

1. Working quickly, dispense 100 µL of Matrigel into the pre-cooled 96-well plate using the pre-cooled pipette tips.
2. Incubate the plate for 1 hour at 37 °C to let the Matrigel set. Meanwhile, passage endothelial cells.

   NOTE: If using precoated plate, place in incubator for 1 hour and then passage cells.
3. Dispense the following amounts of endothelial cells per well: 5000, 1000, 15000, 20000, 25000. Add media such that there is 100 µL media per well.

4. Incubate the plate for up to 16 hours. Tubes should form between 6 and 16 hours (12 hours recommended). Do not let the cells culture for more than 18 hours without imaging; the tubes will fall apart without any support from stromal cells.
5. Image using a phase microscope.